Investigation of the effects of Anti-Müllerian Hormone on preventing Doxorubicin-induced primordial follicle loss



Xi Wei

St Hugh's College

University of Oxford

A thesis submitted for the degree of

Doctor of Philosophy

Extended Trinity Term

2018

Acknowledgements

Throughout my DPhil journey, I have been fortunate to meet many amazing people who have been my greatest support, and to whom I will be forever grateful for.

First and foremost to my first supervisor Dr Suzannah Williams, I would like to express my sincere appreciation to you for offering me the opportunity to do this DPhil, and thank you for your kindness, constant support and help over the past 3 years. Without your trust and encouragement, I would not have been able to complete my DPhil.

To my secondary supervisor Dr Sheila Lane, thank you for your relentless support and the help that you have dedicated to me. I would be lost without your guidance and direction.

Dr Sairah Sheikh, I could not submit this thesis without your tremendous encouragement and help, especially during those final days when I felt particularly lost. You will be my friend forever.

I would like to sincerely thank Briet, Lindsay and Tomi for all your help, especially before my thesis submission. Also, I would like to thank the rest of Williams group for your support, both past and present members (Belinda, Charlotte, Eleni and Lisa), as this journey would not be the same without you guys.

I would like to thank all technicians from the Oxford Cell and Tissue Biobank for their constant help.

Furthermore, I would like to acknowledge the constant and generous guidance for my project from Ms Celine Jones, Dr Karl Morten, Dr Wei Zhang, Mr Nicolas Ward and Dr Christian Becker. I am very lucky to have known you, and to learn so much from you.

Ms Lesa Levett, thank you for your tremendous help when I met difficulties in my life along this journey, and for keeping me positive!

Thank you Dr Judith Asselin, Mr Simon Lewington and Ms Lesley Cockrem for your help and psychological support.

Thank you Xin and Eszter for being my friends in Oxford who provided me so much encouragements and help.

I would like to express my deepest appreciation to my Mum, Dad and my grandma for their endless love, care and invaluable support for me. Without you, I would not even have been lucky enough to start this unforgettable journey. You are great parents!

Finally to my boyfriend, Chi; I'm so grateful for you because you have never left my side, and have constantly encouraged me. Thank you also being my best friend, and keeping me motivated and inspired. I'm so glad and fortunate that I was able to share this special journey with you!

Abstract

Survival rates from childhood cancer are improving, however chemotherapy can cause ovarian failure and infertility. Doxorubicin (DXR) is a gonadotoxic chemotherapy agent commonly used in childhood cancers. For pre-pubertal girls, ovarian tissue cryopreservation is the only fertility preservation option, however it is invasive and currently experimental. Therefore, non-invasive options need to be developed. A potential strategy utilizing Anti-Müllerian Hormone (AMH) to inhibit primordial follicle activation exists, but needs to be fully investigated.

To determine the effect of AMH on DXR-induced primordial follicle loss *in vitro*, pre-pubertal mouse ovaries were cultured with AMH, DXR or co-treated with AMH and DXR. To determine the effect of AMH on DXR-induced primordial follicle loss *in vivo,* pre-pubertal human ovarian tissue was xenotransplanted into adult female immunocompromised mice administered with AMH, DXR or co-treated with AMH and DXR. Mouse and human ovarian tissues were collected after experiments, fixed, embedded, sectioned and stained with Haematoxylin and Eosin. Primordial follicles (*in vitro* and *in vivo* studies) and growing follicles (*in vivo* studies) were counted.

In this thesis, we showed that DXR induced primordial follicle loss in pre-pubertal mouse ovarian tissue *in vitro,* in a dose-dependent manner. Follicular damage caused by DXR was also demonstrated in adult mouse ovaries *in vivo* but not in human pre-pubertal ovarian tissue xenotransplanted into mice. Although there were trends, there was no significant effect of AMH treatment alone on inhibiting primordial follicle activation in mouse ovarian tissue (*in vitro and in vivo*) or human ovarian tissue (xenotransplanted into mice). There was also no significant evidence of AMH acting to prevent DXR-induced primordial follicle loss in mouse ovaries. Therefore, more studies are warranted to further investigate the effect of AMH on DXR-induced primordial follicle loss.

Content

Acknowledgements 1

Abstract 3

Content 4

List of Figures 14

List of Tables 22

Abbreviation 25

Chapter 1: Introduction 31

1.1 Concept of thesis 32

1.2 Follicle development 32

1.2.1 Primordial follicles 32

1.2.2 Growing follicles 33

1.3 Ovarian reserve and maintenance of primordial follicles 36

1.3.1 Ovarian reserve 36

1.3.2 Balanced primordial follicle activation 36

1.4 Chemotherapy 40

1.4.1 Overview 40

1.4.2 Doxorubicin (Adriamycin®) 40

1.4.2.1 Mechanisms leading to programmed death 42

1.4.2.2 Doxorubicin induced toxicity in the ovary 43

1.4.2.3 Burn-out theory 47

1.4.3 Fertility preservation options 49

1.5 Potential available non-invasive molecules 50

1.6 Anti-Müllerian Hormone 53

1.6.1 Overview 53

1.6.2 AMH receptors and signalling pathways 56

1.6.3 AMH and primordial follicles 57

1.7 Outline of thesis 64

1.8 Hypotheses and Aims 65

Chapter 2: Materials and Methods 66

2.1 Ethical Approval 67

2.1.1 Patient consent 67

2.1.2 Home Office and Research Ethics Committee approval 67

2.2 Mouse colonies 67

2.2.1 Breeding of Mice 68

2.2.2 Mice used for xenotransplantation 68

2.2.3 Mouse identification 68

2.2.4 Post-procedure mouse monitoring 69

2.3 Ovary Dissection 69

2.3.1 Dissection Medium 69

2.3.2 Gross Dissection 69

2.3.3 Fine Dissection 70

2.4 Ovary Culture 70

2.4.1 Culture medium 70

2.4.2 Ovary culture 71

2.5 Human ovarian tissue 71

2.5.1 Tissue collection by OCTB 71

2.5.2 Human ovarian cortical strips freezing and thawing 71

2.6 Histology 72

2.6.1 Fixation 72

2.6.2 Embedding 73

2.6.3 Sectioning 73

2.6.4 Haematoxylin and eosin staining 74

2.6.5 Imaging 75

2.6.6 Assessment of follicle development 75

2.6.6.1 Follicle classification 75

2.6.6.2 Follicle morphology 75

2.6.6.3 Follicle counting 76

2.7 Gel electrophoresis 76

Chapter 3: Production and purification of recombinant Anti-Müllerian Hormone 78

3.1 Introduction 79

3.2 Aim 79

3.3 Materials and Methods 80

3.3.1 Plasmid extraction from filter paper 80

3.3.2 Transformation 81

3.3.3 Purification of plasmid DNA 82

3.3.4 Measurement of plasmid DNA concentration 83

3.3.5 Culturing Human Embryonic Kidney 293T cells 83

3.3.6 Transfection 83

3.3.7 Protein purification 84

3.3.8 Electrophoresis 84

3.3.9 Protein buffer replacement 85

3.3.10 Protein concentration detection 85

3.4 Results 86

3.4.1 Plasmid DNA concentration 86

3.4.2 Purified protein concentration 86

3.4.3 Electrophoresis 87

3.5 Discussion 89

Chapter 4: Investigation into the effect of Anti-Müllerian Hormone administration in pre-pubertal mice *in vivo* 92

4.1 Introduction 93

4.2 Aims 94

4.3 Materials and Methods 95

4.3.1 Mice 95

4.3.2 Reagents 95

4.3.3 Administration 95

4.3.4 Post-injection monitoring 96

4.3.5 Observation of vaginal opening 96

4.3.6 Ovaries collection 96

4.3.7 Statistical Analysis 96

4.4 Results 97

4.4.1 Electrophoresis 97

4.4.2 Body weight changes and clinical signs 97

4.4.3 Age at the onset of puberty (vaginal opening) 98

4.4.4 Morphology and weight of mouse ovaries 99

4.5 Discussion 101

4.6 Conclusion 104

Chapter 5: Investigation into the effects of Doxorubicin on primordial follicles in pre-pubertal mouse ovaries *in vitro* 105

5.1 Introduction 106

5.2 Aims 107

5.3 Materials and Methods 108

5.3.1 Mice 108

5.3.2 Mating 108

5.3.3 Ovarian culture 108

5.3.4 DXR administration 108

5.3.5 Histology 108

5.3.6 Statistical Analysis 109

5.4 Results 110

5.4.1 Histology 110

5.4.2 The effect of DXR on primordial oocyte nuclear diameter.....113

5.4.3 The effect of DXR on primordial follicle numbers 114

5.4.4 The effect of DXR on mouse ovarian volumes 115

5.5 Discussion.....116

5.6 Conclusion 117

Chapter 6: Investigation of the effects of Anti-Müllerian Hormone on prevention of Doxorubicin-induced primordial follicles loss in pre-pubertal mouse ovaries *in vitro*.....118

6.1 Introduction 119

6.2 Aims 120

6.3 Materials and Methods 121

6.3.1 Mice 121

6.3.2 Reagents 121

6.3.3 AMH concentration test 121

6.3.4 Ovarian culture 122

6.3.5 Histological analysis.....122

6.3.6 Statistical analysis 123

6.4 Results 124

6.4.1 The effect of DXR on primordial follicles 124

6.4.2 Ovarian culture with rmAMH 124

6.4.2.1 Histology 124

6.4.2.2 The effect of rmAMH on DXR-induced primordial follicles loss 126

6.4.3 Ovarian culture with rhAMH 127

6.4.3.1 Histology 127

6.4.3.2 The effect of rhAMH on DXR-induced primordial follicle loss 130

6.4.4 Comparisons between rhAMH and rmAMH treated ovarian primordial follicles. 131

6.5 Discussion.....132

6.6 Conclusion.....134

Chapter 7: Development of xenotransplantation protocol.....135

7.1 Introduction 136

7.2 Aims 138

7.3 Materials and Methods 139

7.3.1 Patient inclusion and exclusion criteria.....139

7.3.2 Human ovarian cortical strips.....139

7.3.3 Animals.....140

7.3.4 Surgeries 140

7.3.5 Post-surgical monitoring 143

7.3.6 Xenografts collection.....143

7.3.7 Histology Process 143

7.3.8 Statistical Analysis 144

7.4 Results 145

7.4.1 Patients profiles 145

7.4.2 Xenotransplantation 146

7.4.3 SCID mouse 149

7.4.4 Histological analyses of post-pubertal human ovarian grafts after xenotransplantation 150

7.4.5 Histological analyses of pre-pubertal human ovarian grafts after xenotransplantation 154

7.4.6 Comparisons between pre- and post-pubertal ovarian tissue 160

7.4.7 Uneven follicle distribution 161

7.4.8 Comparisons of follicles at each developmental stage before and after xenotransplantation 162

7.5 Discussion 163

7.6 Conclusion 169

Chapter 8: Investigation of the effects of Anti-Müllerian Hormone on Doxorubicin-induced primordial follicle loss in human ovarian tissue xenotransplanted into mice 170

8.1 Introduction 171

8.2 Aims 172

8.3 Materials and Methods 173

8.3.1 Patient Inclusion and Exclusion Criteria 173

8.3.2 Human ovarian cortical strips 173

8.3.3 Animals 174

8.3.4 Xenotransplantation 175

8.3.5 Post-surgical monitoring 175

8.3.6 Reagent 176

8.3.7 Drug administration 176

8.3.8 Post drug administration monitor 177

8.3.9 Xenografts and mouse tissue collection 177

8.3.10 Histology process and analysis 177

8.3.11 Statistical Analysis 178

8.4 Results 179

8.4.1 Patient profiles 179

8.4.2 Xenotransplantation and graft retrieval 179

8.4.3 DXR effects in mice 180

8.4.4 Effect of Doxorubicin and AMH on mouse ovaries 182

8.4.5 Effect of Doxorubicin and AMH on human ovarian tissue xenotransplanted under the mouse kidney capsule 186

8.4.6 Effect of Doxorubicin and AMH on the subcutaneous xenotransplanted human ovarian tissue 194

8.4.7 Comparison between different xenotransplantation sites 201

8.4.8 Early growing follicles with flattened granulosa cells observed in DXR-treated mouse ovaries *in vivo* 203

8.5 Discussion 204

8.6 Conclusion 209

Chapter 9: Discussion and Conclusion.....211

9.1 Summary of Results 212

9.2 Future Work.....215

9.3 Conclusion.....219

References.....220

List of Figures

Figure 1.1. Summary of follicle development. ……...34

Figure 1.2. Chemical structure of Doxorubicin. ……41

Figure 1.3. Major pathways of DXR induced apoptosis. ……....43

Figure 1.4. The Burn-out theory. ……48

Figure 1.5. A single side of genital ridge including a Müllerian duct. ……...53

Figure 1.6. Alignment of the deduced amino acid sequences of AMH in human and mouse. ……55

Figure 1.7. The signalling pathway of AMH. ……57

Figure 3.1. A pcDNA3.1(+) expression vector containing the modified Flag-tagged human AMH sequence. ……...81

Figure 3.2. Standard curve for the BCA protein assay generated using five concentrations of BSA. ……...87

Figure 3.3. Eluted recombinant AMH and control samples were separated on a NuPAGE Tris-Acetate mini gel and stained with SimplyBlue™ Safe Stain. ……88

Figure 3.4. Purified recombinant AMH was separated and stained on a gel and was compared with the result from a previous publication. ……..90

Figure 4.1. Dissolved rmAMH was ran on a NuPAGE Tris-Acetate mini gel and stained with SimplyBlue™ Safe Stain. ……..97

Figure 4.2. Body weight in mice intraperitoneally injected with normal saline or rmAMH for 28 days. ……...98

Figure 4.3. Age at vaginal opening in mice intraperitoneally injected with normal saline or rmAMH for 28 days. ……98

Figure 4.4. Mouse ovaries collected after 28-day daily intraperitoneal injections of saline or rmAMH. ……...99

Figure 4.5. Left and right ovary weight of mice after 28-day daily intraperitoneal injections of saline or rmAMH. ……100

Figure 5.1. Examples of follicles at the different stages of development in the Day 6 cultured mouse ovaries stained with H and E. ……...110

Figure 5.2. Location of primordial follicles in the Day 6 cultured mouse ovaries stained with H and E. ……110

Figure 5.3. An example of unhealthy follicles in the Day 6 cultured mouse ovaries stained with H and E. ……111

Figure 5.4. Representative images of H and E stained sections from mouse ovaries cultured with different concentrations of DXR. ……...111

Figure 5.5. An example of unhealthy follicles in the Day 6 cultured mouse ovaries stained with H and E. ……112

Figure 5.6. Primordial follicle oocyte nuclear diameters in mouse ovaries treated with different concentrations of DXR. …….113

Figure 5.7. Total number of healthy primordial follicles in mouse ovaries treated with different concentrations of DXR. …….114

Figure 5.8. Volume of mouse ovaries treated with different concentrations of DXR after 6 days of culture. ……..115

Figure 6.1. Standard curve for the BCA protein assay generated using six concentrations of BSA. …….122

Figure 6.2. Primordial follicle numbers in mouse ovaries cultured with DXR at 0 or 50 ng/ml. ……...124

Figure 6.3. Representative ovarian tissue section micrographs of mouse ovaries cultured with different concentrations of rmAMH and with or without exposure to DXR. ……125

Figure 6.4. Primordial follicle oocyte nuclear diameters in mouse ovaries cultured with different concentrations of rmAMH and with or without exposure to DXR. ……...126

Figure 6.5. Primordial follicle numbers in mouse ovaries cultured with different concentrations of rmAMH and with or without exposure to DXR. ……..127

Figure 6.6. Representative ovarian tissue section micrographs of mouse ovaries cultured with different concentrations of rhAMH and with or without exposure to DXR. ……128

Figure 6.7. Primordial follicle oocyte nuclear diameters in mouse ovaries mouse ovaries cultured with different concentrations of rhAMH and with or without exposure to DXR. ……129

Figure 6.8. Primordial follicle numbers in mouse ovaries cultured with different concentrations of rhAMH and with or without exposure to DXR. ……...130

Figure 6.9. Primordial follicle numbers in mouse ovaries cultured with rmAMH or rhAMH at different concentrations. ……..131

Figure 6.10. Primordial follicle numbers in mouse ovaries cultured with rmAMH or rhAMH at different concentrations and exposed to DXR. ……...131

Figure 7.1. Representative images of the process of subcutaneous xenotransplantation of one piece of human ovarian cortical strip into a SCID mouse. …146

Figure 7.2. Representative images of the process of xenotransplantation of one piece of human ovarian cortical strip under the mouse kidney capsule. ……...147

Figure 7.3. Representative images of human ovarian grafts xenotransplanted under the mouse ovarian bursa. ……...148

Figure 7.4. Body weight of immunocompromised mice xenotransplanted with post-pubertal human ovarian tissue for 6 weeks. ……..149

Figure 7.5. Body weight of immunocompromised mice xenotransplanted with pre-pubertal human ovarian tissue for 6 weeks. …….149

Figure 7.6. A representative micrograph of a thawed cryopreserved ovarian tissue section (Patient II) stained with H and E. …….151

Figure 7.7. Follicles at different stages in thawed non-grafted post-pubertal human ovarian tissue fixed in Bouin's and stained with H and E. ……...152

Figure 7.8. A representative ovarian tissue section micrograph of post-pubertal human ovarian graft xenografted under the mouse kidney capsule and stained with H and E. ……...153

Figure 7.9. Follicles at different stages in pre-pubertal human ovarian tissue fixed in 10% neutral buffered formalin and stained with H and E. ……...155

Figure 7.10. A representative thawed non-grafted human pre-pubertal ovarian tissue section (Patient C) stained with H and E. ……...156

Figure 7.11. A representative ovarian tissue section micrograph of pre-pubertal human ovarian graft xenografted under the mouse kidney capsule and stained with H and E. ……...157

Figure 7.12. A representative ovarian tissue section micrograph of pre-pubertal human ovarian graft xenografted under the mouse ovarian bursa and stained with H and E. ……158

Figure 7.13. A representative ovarian tissue section micrograph of pre-pubertal human ovarian graft xenografted inside the mouse subcutaneous pocket and stained with H and E. ……159

Figure 7.14. An example of uneven follicle distribution in the post-pubertal human ovarian tissue. ……...161

Figure 7.15. An example of uneven follicle distribution in the pre-pubertal human ovarian tissue. ……...161

Figure 7.16. Percentage of follicles at the different developmental stages in pre-pubertal human ovarian tissue before and after a 6-week subcutaneous xenotransplantation (Patient A-D). ……162

Figure 8.1. Human ovarian cortical strip division and allocation used in the current study. ……....174

Figure 8.2. SCID mice were intraperitoneally (IP) injected daily with PBS or rhAMH for eight days with a single IP injection of PBS or DXR on the second day. ….176

Figure 8.3. Mouse weight at the time of the surgery and during 8 days of treatment with PBS, AMH, DXR or co-treatment (DXR+AMH) starting 10 days after surgery. …180

Figure 8.4. The spleen weight of the mice after 8 days of treatment with PBS, AMH, DXR or co-treatment (DXR+AMH). …….181

Figure 8.5. The mouse red blood cell counts of the mice after 8 days of treatment with PBS, AMH, DXR or co-treatment (DXR+AMH). ……...181

Figure 8.6. The ovarian volume of the mice after 8 days of treatment with PBS, AMH, DXR or co-treatment (DXR+AMH). …….182

Figure 8.7. Primordial follicle numbers in mouse ovaries after 8 days of treatment with PBS, AMH, DXR or co-treatment (DXR+AMH). ……...183

Figure 8.8. Growing follicle numbers in mouse ovaries from the Control, AMH, DXR and DXR+AMH groups at the end of the experiment. ……183

Figure 8.9. Comparison of percentages of primordial follicles and growing follicles in the mouse ovaries from the Control, AMH, DXR and DXR+AMH groups at the end of the experiment. ……..184

Figure 8.10. Comparison of percentages of healthy and unhealthy growing follicles in mouse ovaries from the Control, AMH, DXR and DXR+AMH groups at the end of the experiment. ……185

Figure 8.11. Follicles at different stages in pre-pubertal human ovarian tissue fixed in 10% neutral buffered formalin and stained with H and E. ……...186

Figure 8.12. Comparison of percentages of primordial follicles and growing follicles between human ovarian tissue before and after xenotransplantation under the kidney capsule. ……..187

Figure 8.13. Comparison of total primordial follicle density and percentages in the human ovarian xenografts retrieved from the mouse kidney capsule from the Control, AMH, DXR and DXR+AMH groups. ……..188

Figure 8.14. Comparison of healthy primordial follicle density and percentages in the human ovarian xenografts retrieved from the mouse kidney capsule from the Control, AMH, DXR and DXR+AMH groups. ……..189

Figure 8.15. Comparison of unhealthy primordial follicle density and percentages in the human ovarian xenografts retrieved from the mouse kidney capsule from the Control, AMH, DXR and DXR+AMH groups. ……190

Figure 8.16. Comparison of total growing follicle density and percentages in the human ovarian xenografts retrieved from the mouse kidney capsule from the Control, AMH, DXR and DXR+AMH groups. ……..191

Figure 8.17. Comparison of healthy growing follicle density and percentages in the human ovarian xenografts retrieved from the mouse kidney capsule from the Control, AMH, DXR and DXR+AMH groups. ……..192

Figure 8.18. Comparison of unhealthy growing human follicle density and percentages in the human ovarian xenografts retrieved from the mouse kidney capsule from the Control, AMH, DXR and DXR+AMH groups. ……193

Figure 8.19. Comparison of primordial follicle percentage and growing follicle percentage between human ovarian tissue before and after subcutaneous xenotransplantation. ……..194

Figure 8.20. Comparison of primordial follicle density and percentages in the human ovarian xenografts retrieved from the mouse subcutaneous pocket from the Control, AMH, DXR and DXR+AMH groups. ……195

Figure 8.21. Comparison of healthy primordial follicle density and percentages in the human ovarian xenografts retrieved from the subcutaneous pocket from the Control, AMH, DXR and DXR+AMH groups. ……..196

Figure 8.22. Comparison of unhealthy primordial follicle density and percentages in the human ovarian xenografts retrieved from the subcutaneous pocket from Control, AMH, DXR and DXR+AMH groups. …….....197

Figure 8.23. Comparison of growing follicle density and percentages in the human ovarian xenografts retrieved from the subcutaneous pocket from the Control, AMH, DXR and DXR+AMH groups. ……...198

Figure 8.24. Comparison of healthy growing follicle density and percentages in the human ovarian xenografts retrieved from the subcutaneous pocket from the Control, AMH, DXR and DXR+AMH groups. …….199

Figure 8.25. Comparison of unhealthy growing follicle percentages in the human ovarian xenografts retrieved from the subcutaneous pocket from the Control, AMH, DXR and DXR+AMH groups. ……...200

Figure 8.26. Comparison of primordial follicle density and percentages in the human ovarian xenografts retrieved from the kidney capsule and subcutaneous pocket. 201

Figure 8.27. Comparison of healthy and unhealthy primordial follicle percentages in the human ovarian xenografts retrieved from the kidney capsule and subcutaneous pocket. ……...202

Figure 8.28. Representative images of healthy and unhealthy early growing follicles surrounded with flattened granulosa cells in mouse ovaries treated with DXR. ……203

List of Tables

Table 1.1. Risk assessment of chemotherapy agents on ovarian function. …….40

Table 1.2. Common childhood cancers treated with DXR. ……41

Table 1.3. Doxorubicin doses used in human and equivalent doses in mouse. 42

Table 1.4. Patient plasma DXR concentrations during the first day after DXR treatment. ……....42

Table 1.5. Mechanisms of DXR-induced cellular death. ……43

Table 1.6. Studies investigating the effects of DXR on ovarian tissue *in vitro*. ….45

Table 1.7. Studies investigating the effects of DXR on ovarian tissue *in vivo*. …..46

Table 1.8. Potential indications for ovarian tissue cryopreservation. …….49

Table 1.9. Promising protective agents against DXR. ……52

Table 1.10. Comparison between mouse and human AMH protein. ……..54

Table 1.11. Studies investigating the effects of AMH on primordial follicle activation in genetically modified mouse models. ……..58

Table 1.12. All studies investigating the effects of AMH on primordial follicle activation *in vitro*. ……...60

Table 1.13. All studies investigating the effects of AMH on primordial follicle activation *in vivo*. ……61

Table 1.14. Effects of AMH on cytokines involved in primordial follicle activation. ……..62

Table 1.15. Summary of current studies investigating the effect of AMH on chemotherapy-induced primordial follicle loss. …….63

Table 2.1. Mouse health status assessment form. ……...69

Table 2.2. Thawing media used for cryopreserved human ovarian cortical strips. ……..72

Table 2.3. Dehydration protocol to prepare fixed tissue for embedding. ……...73

Table 2.4. Protocol of haematoxylin and eosin staining of fixed tissue sections. ..74

Table 2.5. Definition of follicle classification. ……...75

Table 3.1. Buffer formulations for purification of plasmid DNA using the Qiagen HiSpeed Plasmid Midi Kit. …….82

Table 3.2. Average absorbance values of BSA standard samples (A-E) and rhAMH at 562nm from replicates (1-3) based on Blank (PBS) corrected. ……..86

Table 3.3. Concentrations of tested standard samples (BSA) (A-E) and rhAMH samples in µg/ml. ……87

Table 7.1. Summary of patient selection criteria. ……139

Table 7.2. Age and diagnoses of included post-pubertal patients (n=6) in this study. ……145

Table 7.3. Age and diagnoses of included pre-pubertal patients (n=4) in this study. ……145

Table 7.4. Proportion of post-pubertal human ovarian xenografts retrieved from different transplantation sites in SCID mice. ……150

Table 7.5. Number of post-pubertal human ovarian xenografts from different patients retrieved from different transplantation sites in SCID mice. ……...151

Table 7.6. Numbers of follicles at different stages of thawed non-grafted human ovarian tissue from post-pubertal patients. ……...152

Table 7.7. Numbers of follicles at different stages of post-pubertal human ovarian tissue xenografted under the mouse kidney capsule. ……153

Table 7.8. Numbers of follicles at different stages of post-pubertal human ovarian tissue xenografted under the mouse ovarian bursa. ……..154

Table 7.9. Proportion of pre-pubertal human ovarian xenografts retrieved from different transplantation sites in SCID mice. ……154

Table 7.10. Numbers of pre-pubertal human ovarian xenografts of different patients retrieved from different transplantation sites in SCID mice. ……155

Table 7.11. Numbers of follicles at different stages in every 10^{th} ovarian tissue section of thawed non-grafted human ovarian tissue from pre-pubertal patients. ……156

Table 7.12. Follicle numbers and developmental stage in thawed pre-pubertal human ovarian tissue xenografted under the mouse kidney capsule. ……...157

Table 7.13. Follicle numbers and developmental stage in thawed pre-pubertal human ovarian tissue xenografted under the mouse ovarian bursa. ……158

Table 7.14. Follicle numbers and developmental stage in thawed pre-pubertal human ovarian tissue xenografted inside the mouse subcutaneous pocket. …….159

Table 7.15. Mock comparison of the average primordial follicles counted between pre- and post-pubertal human ovarian tissue. ……...160

Table 8.1. Summary of patient inclusion and exclusion criteria. ……..173

Table 8.2. Age and diagnoses of pre-pubertal patient's tissue (n=6) used in this study. …….179

Table 8.3. Proportion of pre-pubertal human ovarian xenografts retrieved from different transplantation sites in SCID mice. ……179

Table 8.4. Number of pre-pubertal human ovarian xenografts used for histological analyses in this study. ……...179

Abbreviation

A

AA	Aplastic anaemia
AAL	Amino acid length
Akt	V-akt murine thymoma viral oncogene homologue 1
ALK2	Activin receptor-like kinase 2
ALK3	Activin receptor-like kinase 3
ALK6	Activin receptor-like kinase 6
AMH	Anti-Müllerian Hormone
AML	Acute myeloid leukaemia
AMHR2	Anti-Müllerian Hormone receptor 2
Apop.	Apoptosis
AT/RT	Atypical teratoid rhabdoid tumor

B

BCA	Bicinchoninic Acid
bFGF	Basic fibroblast growth factor
Blast	Basic Local Alignment Search Tool
BMP	Bone morphogenetic protein
BMS	Biomedical Science
BSA	Bovine serum albumin
β-thal	Beta Thalassemia

C

C-Domain	Carboxy Terminus
$CaPO_4$	Calcium orthophosphates
CC	Cervical cancer

CCSC Childhood Cancer Survivor Study

COCs Cumulus-oocyte complexes

Cy Cyclophosphamide

D

DMEM Dulbecco's Modified Eagle Medium

DNA Deoxyribonucleic acid

DPBS Dulbecco's Phosphate-Buffered Saline

dsDNA Double-stranded DNA

DTT Dithiothreitol

DXR Doxorubicin

E

E13.5 Embryonic day 13.5

E_2 Estrogen

EC Endothelial cells

EDTA Ethylenediaminetetraacetic acid

ES Ewing's Sarcoma

F

FBS Fetal bovine serum

Foxl2 Forkhead box L2

Foxo3a Forkhead box O3a

FSH Follicle-stimulating hormone

FSHR Follicle-stimulating hormone receptor

G

GC Granulosa cells

GDF9 Growth differentiation factor 9

GnRH	Gonadotropin-releasing hormone
GV	Germinal vesicle

H

H & E	Haematoxylin and Eosin
HC	Hilar cholangiocarcinoma
HCL	Hydrogen Chloride
HEK	Human Embryonic Kidney
h-MDS	Hypoplastic Myelodysplasia

I

IP	Intraperitoneal(ly)
IV	Intravenous(ly)

K

KGF	Keratinocyte growth factor
KITL	Kit ligand

L

LH	Luteinising hormone
LHR	Luteinising hormone receptor

M

M2 antibody	Murine IgG1 monoclonal antibody
S.E.M.	Standard error of the mean
MEM	Minimum Essential Medium
MII	Metaphase II
MOPS	3-(N-morpholino)propanesulfonic acid
mTOR	Mammalian target of rapamycin
mTORC1	Mammalian target of rapamycin complex 1 (mTORC1)

N

N/A	Not applicable
N-Domain	Amino Terminus
Na_2HPO_4	Disodium phosphate
NaCl	Sodium chloride
NaOH	Sodium hydroxide
ND	Not described
NGC	Non-grafted control
NHS	National Health Service

O

OD	Optical density
OTC	Ovarian tissue cryopreservation
OCTB	Oxford Cell and Tissue Biobank

P

PAF	Preantral follicle
PBS	Phosphate buffered saline
PCD	Progressive cerebrovascular disease
PCR	Polymerase chain reaction
PDK1	Phosphoinositide-dependent kinase 1
PF	Primary follicle
PGCs	Primordial germ cells
PI3K	Phosphatidylinositol 3-kinase
PIL	Personal licence
PMF	Primordial follicle
PND	Postnatal Day

POI	Premature ovarian insufficiency
PTEN	Phosphatase and tensin homolog

R

R1	type I receptor
R2	type II receptor
rhAMH	recombinant human AMH
rmAMH	recombinant human AMH
rrAMH	recombinant rat AMH
ROS	Reactive oxygen species
rpS6	Ribosomal protein S6
RT	Room temperature

S

S.D.	Standard deviation
SF	Secondary follicle
S6K1	Ribosomal protein S6 kinase β-1
SAA	Severe aplastic anaemia
SCD	Sickle cell disease
SCID	Severe combined immune deficiency
SCN	Severe congenital neutropenia
SDS	Sodium dodecyl sulfate
SMAD	Small mothers against decapentaplegic
SOC	Super Optimal broth with Catabolite repression
Sub-cut	Subcutaneous

T

TF	Transitional follicles

TGF-β	Transforming Growth Factor-β
Tris-Cl	Tris(hydroxymethyl)aminomethane chloride
TS	Thoracic sarcoma
TUNEL	Terminal deoxynucleotidyl transferase dUTP nick end labelling

V

v/v	Volume/volume

W

w/v	Weight/volume

Y

Y/N	Yes or No

Chapter 1: Introduction

1.1 Concept of thesis

Substantial progress in chemotherapy treatment over the past four decades has contributed to the increased long-term survival of cancer patients (Hudson, 2010; Smith *et al*., 2010). However, several distressing side effects induced by chemotherapy, such as premature ovarian insufficiency (POI), impact on quality-of-life for ~8% of childhood cancer survivors both physically and psychologically (Sklar *et al*., 2006). This therefore warrants further strategies to be developed to prevent chemotherapy-induced POI.

1.2 Follicle development

1.2.1 Primordial follicles

The ovary is the female reproductive organ which originates from the embryonic genital ridge (Wilhelm *et al.*, 2007). Primordial follicles are the basic functional units within the ovary, each of which is composed of an oocyte and a layer of pre-granulosa cells. The oocytes arise from the primordial germ cells (PGCs) that develop from the cells within the extra-embryonic proximal epiblast (Lawson and Hage, 1994).

At approximately 5 weeks of gestation in humans, the PGCs migrate to the genital ridges via the hindgut epithelium and dorsal mesentery (Wartenberg, 1981). Up until 12 weeks of gestation, the PGCs remain undifferentiated; after which germ cell differentiation is initiated. Germ cell differentiation occurs at different stages due to the asynchronous development nature of the human foetal PGCs. PGCs form germ cell nests at around 14 weeks of gestation with meiosis occurring in some germ cells (Childs *et al*., 2012). The germ cell nests are surrounded by somatic cells, which are thought to arise from the ovarian surface epithelium (Sawyer *et al.*, 2002). Beyond 17 weeks of gestation in humans, and at the time of birth in mice, the germ cell nests begin to breakdown, at which point

somatic cells invade the nests and surround the oocytes, forming individual primordial follicles (Maheshwari and Fowler, 2008; Pepling and Spradling, 2001). Each primordial follicle is encapsulated by a basal lamina, which separates the follicle from surrounding stromal cells (Juengel *et al*., 2002). Only one third of the germ cells survive the germ cell breakdown, while others are lost via programmed cell death (Pepling and Spradling, 2001).

1.2.2 Growing follicles

The primordial follicles in human and mouse remain meiotically quiescent until they are either recruited to grow from the pool, or undergo atresia (Pangas and Rajkovic, 2015). Once recruited, some of the activated primordial follicles will grow through the various stages of development, eventually resulting in the ovulation of a mature fertilisable egg (Figure 1.1) (McGee and Hsueh, 2000). This process is known as follicle development.

In brief, follicle development (Figure 1.1) starts with the transition of the primordial follicle into a primary follicle. This transition involves the differentiation of the surrounding squamous pregranulosa cells into cuboidal granulosa cells, and recruitment of theca cells from the stroma (Williams and Erickson, 2012). Continuous proliferation of the granulosa and theca cells and growth of the oocyte results in transition of a primary follicle into a secondary follicle. The development of small antral spaces between the granulosa cells marks the transition of the secondary follicle into an antral follicle. Finally, the small antral spaces fuse into a large antral cavity resulting in the formation of the preovulatory follicle, which will eventually ovulate to release the mature egg (Williams and Erickson, 2012).

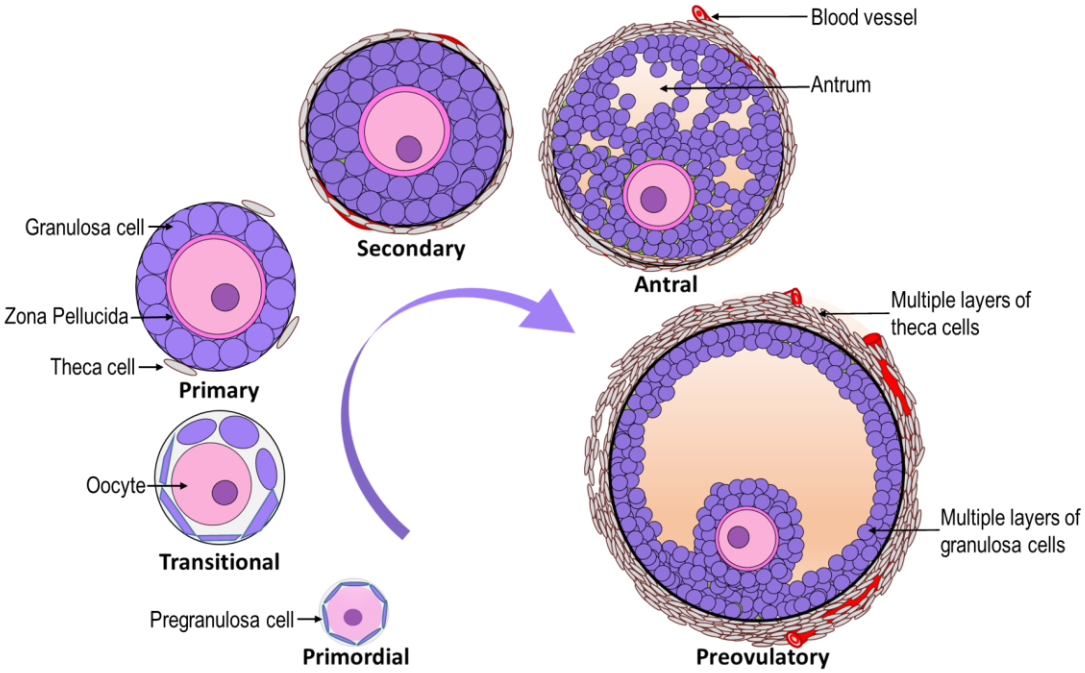


Figure 1.1. Summary of follicle development. The development of ovarian follicles begins with primordial follicles that contain a non-growing oocyte surrounded by a single layer of pre-granulosa cells. These follicles will develop through primary, secondary and antral stages to become preovulatory follicles which contain a fully grown oocyte and multiple layers of granulosa and theca cells. All follicles are not at the same scale.

Normally, only a single follicle in monovulatory species, such as humans, will achieve dominance in each menstrual cycle and mature into a preovulatory follicle that will undergo ovulation. The remaining recruited follicles will then undergo atresia (Williams and Erickson, 2012). In polyovulatory species, such as rodents, several follicles will be selected synchronously during an oestrous cycle and develop to the preovulatory stage (Sirotkin *et al*., 2017).

In order to achieve successful follicular development, this process is regulated by tightly coordinated hormones and intra-ovarian factors (Hsueh *et al*., 2015).

The main hormonal regulator, gonadotropin-releasing hormone (GnRH) is released from the hypothalamus in a pulsatile manner (Tsutsumi and Webster, 2009). In response to the GnRH pulses, gonadotrophins follicle-stimulating hormone (FSH) and luteinising hormone (LH) are secreted into circulation from the anterior pituitary gland (Tsutsumi and Webster, 2009). These two gonadotrophins exert an array of effects, either directly by stimulating follicle growth, or via the production of hormones such as oestrogen and progesterone. Levels of these gonadotrophins are regulated either by direct positive feedback or by negative feedback in response to oestrogen and progesterone levels (Messinis, 2006). At lower levels, increased estrogen levels inhibit the release of FSH and LH from the anterior pituitary gland via negative feedback. Once estrogen levels reach a high peak, estrogen feedback on LH and FSH production changes from negative to positive resulting in a LH and FSH surge that stimulates ovulation. Corpora lutea also produce progesterone and estrogen which inhibit the production of FSH and LH. Without the occurrence of fertilisation, the corpus luteum will degenerate and decreased progesterone and estrogen levels will then stop suppressing the release of FSH and LH (Richards and Pangas, 2010).

In addition to the regulation from the hypothalamus and pituitary, hormones and cytokines generated within the ovary also play a role in follicular development through an autocrine or paracrine manner (Knight and Glister, 2006). Most of these locally produced hormones and proteins belong to the transforming growth factor-β (TGF-β) superfamily and include molecules such as AMH, bone morphogenetic proteins (BMPs), growth differentiation factors (GDFs), activins and inhibins (Knight and Glister, 2001; Shimasaki *et al.*, 2004; Drummond, 2005). These inhibitors and promoters coordinate in order to promote and maintain normal follicle development (Knight and Glister, 2006). For the purpose of this thesis I will be focusing on AMH and will discuss further in Section 1.6.

1.3 Ovarian reserve and maintenance of primordial follicles

1.3.1 Ovarian reserve

The ovarian reserve refers to the potential of female ovarian function and is typically reflected by the population of resting primordial follicles (Richardson *et al.*, 2013). The primordial follicle pool has been considered to be finite, and to date, there is no robust evidence to indicate that the primordial follicle pool is renewable in mammals (Notarianni, 2011; Lei and Spradling, 2013; Yuan *et al*., 2013). Primordial follicles reach their maximum population of ~6-7 million at approximately mid-gestation, at which time it then declines to ~2 million population at birth, ~300 thousand at the onset of puberty, and then continuously declines throughout female reproductive life (Baker *et al*., 1963; Faddy *et al*., 1992; Pepling, 2006). When the number of primordial follicles decreases to ~1000 at approximately 51 years of age, this starts the onset of menopause (Faddy and Gosden, 1996). Given that the process of primordial follicle activation is irreversible, it is vital for the majority of primordial follicles to maintain quiescent in order to retain fertility throughout the whole female reproductive lifespan.

1.3.2 Balanced primordial follicle activation

As previously discussed, the activation of primordial follicles is marked by the growth of the oocyte and the differentiation of squamous pre-granulosa cells into cuboidal granulosa cells (Hirshfield, 1991). The mechanisms that maintain the primordial follicle pool in a quiescent state and cause primordial follicle activation remain unclear, although they have been widely investigated.

Several mechanisms and pathways have been proposed to play a role in maintaining the balance of primordial follicle activation, such as phosphatidylinositol 3-

kinase (PI3K) and the mammalian target of rapamycin (mTOR) pathways (Reddy *et al*., 2010; Adhikari and Liu, 2010).

Role of the PI3K pathway in primordial follicle activation

The PI3K pathway is a signalling pathway involved in the regulation of cell growth, movement, survival and metabolism (Cantley, 2002). There are many key molecules involved in the PI3K pathway, such as serine-threonine protein kinase B (Akt), phosphoinositide-dependent kinase 1 (PDK1) and phosphatase and tensin homolog (PTEN) (Engelman *et al*., 2006). A number of studies have demonstrated that components of this pathway play a role in determining the fate of primordial follicles (Troussard *et al*., 2003; Reddy *et al*., 2008; Reddy *et al*., 2009; Jagarlamudi *et al*., 2009).

PTEN is a tumour suppressor protein that suppresses the activation of the PI3K pathway through inactivation of a vital component of the pathway, phosphatidylinositol-3, 4, 5-triphosphate (Cantley and Neel, 1999; Kim, 2012). The role of PTEN in mouse oocytes was elucidated by its deletion in oocytes specifically (Reddy *et al*., 2008). Loss of PTEN from the oocytes of primordial follicles resulted in their premature activation leading to POI (Reddy *et al*., 2008). Furthermore, when human ovarian cortical strips were cultured with PTEN inhibitor, there was a marked increase in primordial follicle activation (Li *et al*., 2010). Thus, these studies demonstrate that PTEN plays an important role in the activation of primordial follicles from their quiescent state.

PDK1 is crucial for the phosphorylation and activation of Akt, which is the hallmark of activation of PI3K pathway. In a mutant mouse model with oocyte-specific deletion of PDK1 (Reddy *et al*., 2009), mice develop POI. This therefore indicates that the PI3K pathway plays a role in primordial follicle activation and survival (Reddy *et al*., 2009).

Role of the mTOR pathway in primordial follicle activation

In addition to phosphorylating Akt, PDK1 is also responsible for the activation of ribosomal protein S6 (rpS6) via rpS6 kinase β-1 (S6K1) activation (Reddy *et al*., 2009). rpS6 is a protein required for translation, and is part of the mTOR signalling pathway. rpS6 also plays the crucial role of the survival and activation of primordial follicles via both the mTORC1-S6K1-rpS6 and PI3K/PTEN-PDK1 pathways (Adhikari *et al*., 2009; Reddy *et al.*, 2009). Inadequate activation of rpS6 by deletion of PDK1 or S6K1 in oocytes results in accelerated loss of primordial follicles in mice, whereas elevated expression and phosphorylation of rpS6 as a result of the absence of PTEN in oocytes is correlated with enhanced primordial follicle activation (Reddy *et al*., 2008; Reddy *et al*., 2009).

Role of Foxo3a in primordial follicle activation

Forkhead box O3a (Foxo3a) is expressed in the nucleus of the primordial follicle oocyte, and has been shown to suppress primordial follicle activation (Castrillon *et al*., 2003). Interestingly, there is a nucleo-cytoplasmic shuttling of Foxo3a that coincides with primordial follicle formation and activation (John *et al*., 2008). Initially, Foxo3a is expressed inside the cytoplasm of most of the oogonia prior to primordial follicle formation, whereas during primordial follicle assembly, the expression is detected both in the nucleus and cytoplasm, indicating that a translocation of this protein has occurred. After primordial follicle assembly, expression of Foxo3a was observed within the oocyte nuclei in primordial follicles, however, in primary follicles, a nuclear to cytoplasmic shuttling occurs within the oocyte (John *et al*., 2008).

In Foxo3a deficient mice, there is over activation and complete depletion of primordial follicles just two weeks after birth, demonstrating that Foxo3a plays a role in suppressing primordial follicle activation and maintaining quiescence (Castrillon *et al*.,

2003). Furthermore, Foxo3a has been suggested to exert its role in primordial follicle activation via a linear pathway, PTEN/PI3K-Akt-Foxo3 (John *et al.,* 2008).

Role of Foxl2 in primordial follicle activation

Another Forkhead factor, Forkhead box L2 (Foxl2), is expressed in granulosa cells and has also been suggested to regulate primordial follicle activation (Schmidt *et al.*, 2004; Uda *et al*., 2004). In Foxl2 deficient mice, squamous pre-granulosa cells failed to differentiate into cuboidal granulosa cells during primordial follicle activation. Furthermore, these follicles contained abnormally large oocytes surrounded by squamous granulosa cells that failed to develop into secondary follicles. Eventually loss of these follicles via atresia resulted in the mice undergoing POI (Schmidt *et al*., 2004; Uda *et al*., 2004).

There are several other pathways involved in the primordial follicle activation such as Hippo signalling pathway (Grosbois and Demeestere, 2018) and SMAD2/3 pathways (Hardy *et al*., 2018), which act as either positive or negative regulators of primordial follicle activation. During normal follicular development, primordial follicle recruitment is maintained by a balance of these regulators. However, if this balance is disturbed, for example by exposure to gonadal toxic chemotherapy agent, this would cause the finite primordial follicle pool to be depleted prematurely and result in POI (De Vos *et al*., 2010).

1.4 Chemotherapy

1.4.1 Overview

The rate of survival has reached as high as 83% for childhood cancers (Siegel *et al*., 2015). However, the incidence of childhood cancer continues to steadilly increase by approximately 0.6% per year (Siegel *et al*., 2015). According to the results from the Childhood Cancer Survivor Study (CCSC), approximately 6.3% of childhood cancer survivors develop acute ovarian failure, and 8% of patients demonstrate premature non-surgical menopause (Green *et al*., 2009). Thus, with the increasing population of cancer survivors, preventing cancer treatment-induced side effects such as loss of ovarian function and infertility has become increasingly important.

Research has shown that different chemotherapy agents have different levels of risk of developing ovarian failure post-treatment (Fleischer *et al.*, 2011; Blumenfeld, 2012) (Table 1.1). For the purpose of this thesis I will be focusing on Doxorubicin (DXR) and will discuss this in detail.

Table 1.1. Risk assessment of chemotherapy agents on ovarian function.

Risk level	Families	Agents
High	Alkylating agents	Cyclophosphamide, procarbazine, busulphan, chlorambucil, melphalan, ifosfamide, chlormethamine
Medium	Platinum agents	Cisplatin, carboplatin
	Anthracycline antibiotics	Doxorubicin
	Taxoids	Docetaxel, paclitaxel
Low	vinca plant alkaloids	Vincristine, vinblastine
	anthracycline antibiotics	Bleomycin
	Antimetabolites	methotrexate, 5-fluorouracil, mercaptopurine

1.4.2 Doxorubicin (Adriamycin®)

Doxorubicin (DXR), also named as Adriamycin, is one of the anti-tumor antibiotics belonging to the antracyline family produced from *Streptomyces peucetius* subsp. *caesius* since the 1960's (Bonadonna *et al*., 1970). Chemically, DXR is composed of a water-

insoluble tetracyclic quinoid aglycone (adriamycinone) and a linked water-soluble aminosugar (daunosamine) (Arcamone *et al*., 1969) (Figure 1.2). Due to the water-insoluble nature of the adriamycinone, DXR is typically used as the hydrochloride salt form, doxorubicin hydrochloride, so that it may be conveniently administered either clinically or experimentally in a water-based vehicle (*e.g.* saline) (Wong *et al*., 2007).

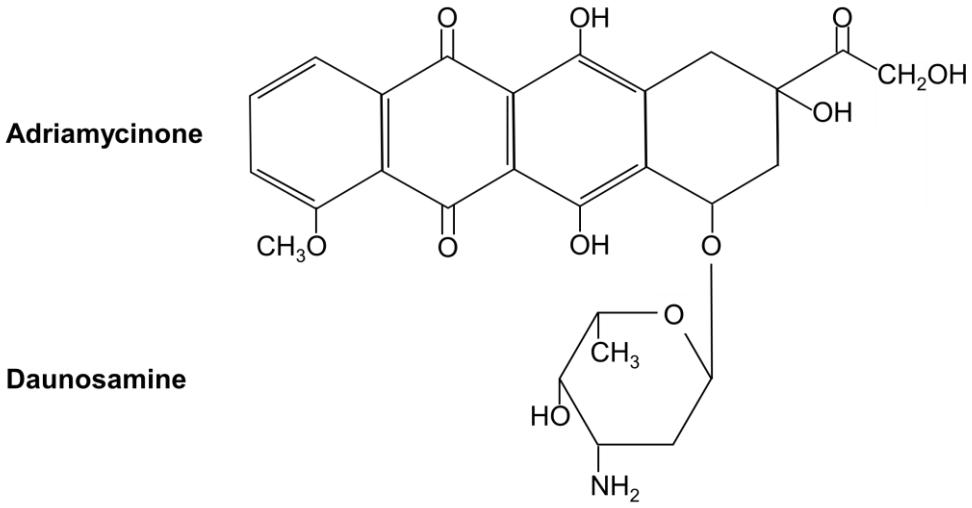


Figure 1.2. Chemical structure of Doxorubicin.

DXR is used either alone or in combination with other chemotherapeutic agents for a wide variety of cancer types, including nearly 50% of all childhood cancers (Table 1.2) and other common cancers in adults such as gastric carcinoma, breast and ovarian cancers (Roti *et al*., 2014).

Table 1.2. Common childhood cancers treated with DXR.

Cancers	Percentage of all childhood cancers
Leukaemia	29%
Lymphoma	9%
Neuroblastoma	6%
Wilm's tumors	5%

Clinically, DXR is administered intravenously (IV) at a dose of 40-75mg/m^2/3wks for adult patients; or at a dose of 35-75mg/m^2/3wks or 20-30mg/m^2/week for childhood patients (data available at https://reference.medscape.com/drug/doxorubicin-342120). The

specific dose can vary by cancer type and patient age (Lichtman and Villani, 2000). Since we planned to administer DXR into mice in this project, the dose range used in humans was converted to equivalent mouse dose (Table 1.3) by the candidate according to formula developed by Shin *et al*., 2010.

Table 1.3. Doxorubicin doses used in human and equivalent doses in mouse.

	Human	Mouse
Childhood	35-75mg/m^2	12-25mg/kg
	20-30mg/m^2	7-10mg/kg
Adults	40-75mg/m^2	13-25mg/kg

Plasma DXR concentrations in patients during the first day after intravenous administration of DXR are listed in Table 1.4. Children diagnosed with acute lymphoblastic leukaemia who received DXR treatment had a medium plasma concentration of DXR at 62.8 ng/ml (Frost *et al*., 2002).

Table 1.4. Patient plasma DXR concentrations during the first day after DXR treatment.

Patients	Cancer	Dose	Plasma concentration	Reference
Children	Leukaemia	40mg/m^2	22.6-334.0 ng/ml	Frost *et al*., 2002
Adults	Breast cancer	60mg/m^2	39.8-630.4 ng/ml	Barpe *et al*., 2010

DXR has a short half-life of 8 minutes in the distribution phase, and a long half-life of 30 hours in the elimination phase (Greene *et al*., 1983).

1.4.2.1 Mechanisms leading to programmed death

DXR is considered as a cell-cycle dependent chemotherapy agent which targets cancer cells through the Synthesis and Gap2/Mitotic phase (Ling *et al*., 1996). Primordial follicles are in a quiescent state, containing an oocyte arrested at meiosis prophase I, and surrounded by pre-granulosa cells mitotically arrested at the G0/G1 stage (Cordeiro *et al*., 2015). Hence, theoretically, doxorubicin should not directly kill primordial follicles.

Currently, there are two main mechanisms involved in DXR-induced cell death (Gewirtz, 1999). It can either be directly intercalated into the DNA or it can cause the generation of reactive oxygen species. This causes the DNA to break, and eventually induce apoptosis via the P53-mediated pathway (Magnelli *et al*., 1995; Kaur *et al*., 2012). Alternatively, DXR can damage the DNA of mitochondria, resulting in the release of mitochondrial cytochrome C and eventually induce apoptosis (Clementi *et al*., 2003) (Figure 1.3 and Table 1.5).

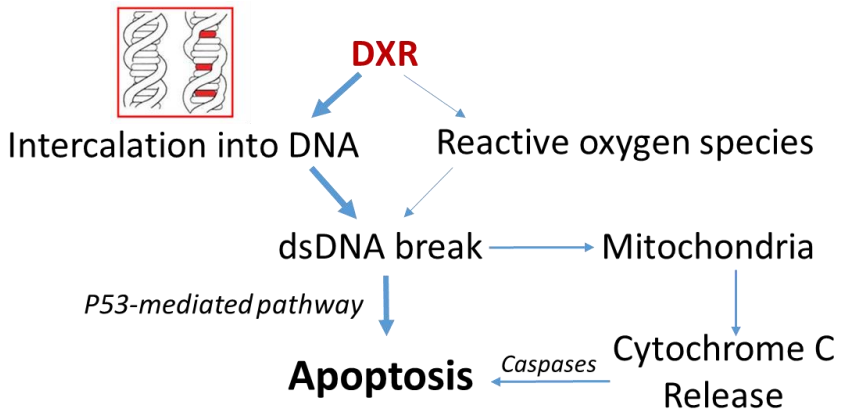


Figure 1.3. Major pathways of DXR induced apoptosis.

Table 1.5. Mechanisms of DXR-induced cellular death.

Mechanisms	References
Inhibit topoisomerase II	Tewey *et al.*, 1984
Inhibition of DNA synthesis	Schott and Robert, 1989
DNA intercalation and crosslinking	Chen *et al.*, 2012
Free radical generation; increased oxidative stress	Lahoti *et al.*, 2012
Break cell plasma membrane and mitochondrial membrane	Praet *et al.*, 1984

1.4.2.2 Doxorubicin induced toxicity in the ovary

Numerous studies have investigated the effects of DXR on ovarian tissue using animal models. However, very few have tested its effects on human ovarian tissue (Table 1.6 and 1.7). According to *in vitro* and *in vivo* studies, we found that DXR has dose-dependent toxicity on ovarian tissue, and that it was more damaging to growing follicles

than primordial follicles (Table 1.6 and 1.7). Roti *et al*., 2012 showed that DXR damages both the oocytes and granulosa cells in the growing follicles in mice. However, many studies investigating the effects of DXR *in vitro* use concentrations of DXR which are much higher than patient plasma levels (Table 1.6), and thus do not provide an accurate clinical representation of the exposure of human ovarian tissue to DXR.

Furthermore, DXR-induced primordial follicle loss can be found in several studies, whereas DXR-induced primordial follicle apoptosis was rarely reported (Table 1.6 and 1.7). In an *in vivo* study using a mouse model, no apoptosis of primordial follicles was detected until 48 hour after injection of DXR, although DXR was found to accumulate around primordial follicles 4 hours after injection (Roti *et al*., 2012). However, in the same study, apoptosis was detected in the stroma and the granulosa cells of growing follicles as early as 2 and 4 hours respectively (Roti *et al*., 2012). This indicates that the toxicity of DXR on ovarian tissue is cell-type and follicle type-dependent (as revealed in the Table 1.7) and that primordial follicle loss or apoptosis after DXR administration might not be a direct effect of DXR, but due to an indirect mechanism on primordial follicles which remains unclear. Currently, one such theory has been proposed depicting this indirect mechanism of primordial follicle loss, named the “burn-out theory” (discussed in Section 1.4.2.3).

Table 1.6. Studies investigating the effects of DXR on ovarian tissue *in vitro*.

Research Groups	Type	Dose	Culture		PMF loss	Growing follicles	Other main findings
			Total	DXR			
Polyovular species (Mouse)							
Perez *et al*., 1997	Mouse Oocyte	200nM	24 h		N/A	MII oocyte apoptosis	ND
Bar-Joseph *et al*., 2010	Mouse Oocyte	200nM	0.5 h		N/A	GV, MII oocytes apoptosis	GV more vulnerable than MII
Roti Roti and Salih, 2012	Mouse GCs cell line	50 or 500nM	4h	3 h	ND	PF GCs dsDNA	Dose dependent
Morgan *et al*., 2013	Mouse Ovaries (PND 0)	10ng/ml	6 d	24 h (D1)	N	0	Dose dependent; No apoptosis detected in PMFs
		50ng/ml			N	↓Trans and PF	
		100ng/ml			Y	↓Trans and PF	
		200ng/ml			Y	↓Trans and PF	
Xiao *et al*., 2017	Mouse secondary follicles	2 or 20nM	8 d		N/A	0	0
		100 or 200nM				↓Secondary follicle survival	↓E_2
Zhang *et al*., 2017	Mouse GCs	400ng/ml	24 h		N/A	0	0
		0.8 or 1.6µg/ml				↓GCs survival	↑ROS
Monovular species							
Soleimani *et al.*, 2011	Human ovarian cortex	1 or 10µg/ml	24 h		N	ND	Ovarian vascular damage
		100µg/ml			Apop.		
Guerreiro *et al*., 2016	Goat ovarian cortex	3ng/ml	1 or 7d		N	0	DNA damage in pre-GCs, growing follicle oocytes, stroma (30ng/ml)
		30ng/ml			Y	↓growing follicles after 7 d	
		300ng/ml			Y	↓growing follicles	

PMF: Primordial follicle. TF: Transitional follicles. PF: Primary follicle. GCs: Granulosa cells. Y/N: Yes/No. N/A: Not applicable (not containing PMF). ND: Not described. 0: no effects. ↓: Decrease. ↑: Increase. Apop. : Apoptosis. MII: Metaphase II. GV: Germinal vesicle. ROS: Reactive oxygen species. E_2: Oestrogen. PND: Postnatal Day.

Table 1.7. Studies investigating the effects of DXR on ovarian tissue *in vivo*.

Research Groups	Type	Dose and route		Collected after DXR.	PMF loss	Growing follicles	Other main findings
Polyovular species							
Ben-Aharon *et al.*, 2010	Mouse (4-8wk)	7.5 mg/kg	IP	1 d	ND	ND	↓ovarian size
				7 d	ND	ND	↓ovarian weight
				1 month	N	↓SF	↓ovarian weight and size
		10 mg/kg		2 d	ND	ND	↓ovulation rate
				7 d			↓↓ovulation rate
				1 month			↓ovulation rate
Soleimani *et al.*, 2011	Mouse (7wk)	10 mg/kg	IP	1 d	Y	PAF GCs DNA damage	GV oocyte DNA damage Apop. at all stages
Roti *et al.*, 2012	Mouse (4wk)	20 mg/kg	IP	2 h	N	0	Stroma cell DNA damage
				4 h	N	GCs DNA damage	Stroma cell DNA damage
				10 or 24 h	N	Oocytes and GCs damage	Oocytes and GCs damage
				48 h	Apop.		
Kropp *et al.*, 2015	Mouse (4wk)	20 mg/kg	IP	2 h	N	0	Stroma cell DNA damage
				4 h	N	GCs DNA damage	Stroma cell DNA damage
				12 h	N	Oocytes and GCs damage	Oocytes and GCs damage
				24 h	ND		
		10 mg/kg		4-7 month	ND	ND	↓Litter size
Xiao *et al.*, 2017	Mouse (3wk)	0.4 mg/kg	IP	8 d	ND	0	Dose-dependent
		2 or 10 mg/kg				↓oocyte maturation	
Kano *et al.*, 2017	Mouse (6-7wk)	7.5mg/ml 6.5mg/ml	2-IP	7-14 d	Y	↓PF	0
Monovular species							
Soleimani *et al.*, 2011	2-37 yr Human Xenograft $1mm^3$ →mice	10 mg/kg	I V	1 d	Apop.	ND	Stromal and vascular damage (same research group)
Li *et al.*, 2013	16-37 yr Human Xenograft $3mm^3$→mice			3 d			

IP: Intraperitoneal. IV: Intravenously. PMF: Primordial follicle. PF: Primary follicle. SF: Secondary follicle. PAF: Preantral follicle. GCs: granulosa cells. Y/N: Yes/No. ND: Not described. 0: no effects. ↓: Decrease. Apop. : Apoptosis. GV: Germinal vesicle.

1.4.2.3 Burn-out theory

Most chemotherapy preferentially kills cells that are rapidly proliferating by disrupting necessary metabolic pathways such as deoxyribonucleic acid (DNA) replication (Choy *et al*., 2008). Currently, the mechanisms of chemotherapy induced-dormant primordial follicle loss have not been deciphered yet. Both *in vivo* and *in vitro* studies have indicated that the dormant primordial follicle loss induced by the most commonly used chemotherapy agents was most likely due to the overactivation and growth initiation of the dormant primordial follicles rather than directly destroying them by inducing apoptotic cell death (Morgan *et al*., 2012; Kalich-Philosoph *et al*., 2013). The destruction of growing follicles stimulates the activation of quiescent primordial follicles into irreversible growth and development. As the primordial follicles pool is finite, with each cycle of chemotherapy and the subsequent cycle of destruction and replenishment of growing follicles, the pool becomes prematurely exhausted resulting in POI; this phenomenon is known as the burn-out theory (Figure 1.4) (Kalich-Philosoph *et al*., 2013).

Therefore, theoretically if primordial follicle activation could be prevented during chemotherapy, the ovary would retain its primordial follicle pool and childhood cancer survivors would retain lifelong fertility.

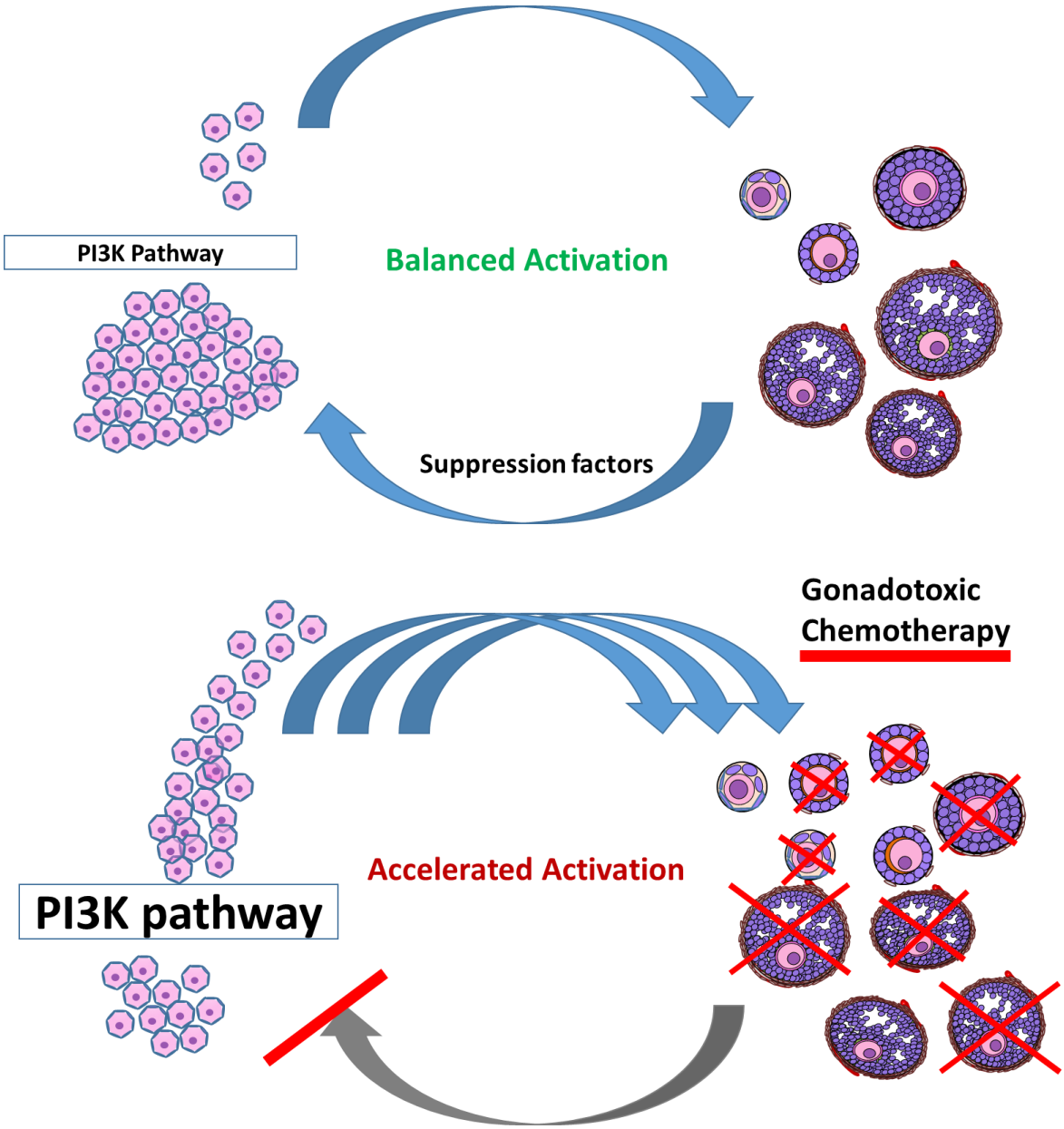


Figure 1.4. The Burn-out theory (Roness *et al*., 2013)**.** During normal follicular development, primordial follicle recruitment is under balanced regulation by the PI3K pathway. Suppressive factors produced by growing follicles assure that the majority of primordial follicles are maintained in a quiescent state and only a few are activated into growth; exposure to gonadotoxic chemotherapy breaks this balance by killing growing follicles resulting in loss of the negative suppression of primordial follicles and acceleration of recruitment of primordial follicles entering into the growing follicle pool. Thus, the finite primordial follicle pool becomes prematurely burned out.

1.4.3 Fertility preservation options

Currently, the most common options for female fertility preservation are oocyte, embryo or ovarian tissue cryopreservation (OTC).

Although it is still considered an experimental technique, OTC is the only fertility preservation option available (Table 1.8) for a number of patient cohorts including pre-pubertal girls, patients who cannot postpone chemotherapy treatment for ovulatory induction and oocyte retrieval, cancer patients whose malignancies are hormone sensitive, and women with benign hematologic diseases who have undergone hematopoietic stem cell transplantation (Donnez *et al*., 2010; Albani *et al*., 2012; Rodriguez-Wallberg and Oktay, 2012).

Table 1.8. Potential indications for ovarian tissue cryopreservation (Sonmezer *et al*., 2005; Donnez and Dolmans, 2010; Albani *et al*., 2012).

Sort	Diagnosis
Diseases	Extra-pelvic diseases: bone cancer, thyroid cancer, kidney cancer, breast cancer, melanoma, neuroblastoma;
	Pelvic diseases: non-gynaecological malignancy, gynaecological malignancy;
	Systemic diseases: Hodgkin's disease, non-Hodgkin's lymphoma, leukaemia, melanoblastoma
Benign Hematologic Diseases	sickle cell anaemia, thalassemia, aplastic anaemia, recurrent ovarian cysts

OTC followed by ovarian tissue auto-transplantation has been shown to resume endocrine function and initiate puberty in recipients and more recently, live births following cryopreservation of pre-pubertal ovarian tissue have been reported (Demeestere *et al*., 2015). However, despite this success, there remains a number of concerns and risks associated with the cryopreservation technique.

In a case report by Oktay and his colleagues, over 50 percent of follicles were lost during the freezing and thawing process (Oktay *et al*., 2016). Furthermore, human ovarian

tissue after cryopreservation and thawing showed a higher percentage of degenerated follicles, lower estrogen and progesterone production and a lower glucose uptake than the fresh ovarian tissue, all of which indicate reduced ovarian function (Bastings *et al*., 2014). Another main concern is the possibility of reintroducing malignant cells into cancer survivors when auto-transplanting the cryopreserved ovarian tissue (Akar and Oktay, 2005). Malignant cells were found in a graft of a patient diagnosed with chronic myelogenous leukaemia using highly sensitive real-time polymerase chain reaction (PCR) (Meirow *et al*., 2008). Moreover, for patients who have a significant risk of metastasis within ovary, ovarian tissue transplantation is not advised (Akar and Oktay, 2005).

Thus, in order to avoid OTC related risks, further research is warranted in order to develop more non-invasive fertility preservation options for patients undergoing chemotherapy.

1.5 Potential available non-invasive molecules

Several potential protective molecules have so far been investigated to protect against chemotherapy-induced ovarian damage. However, most of them (such as imatinib, rapamycin, melatonin and sphingosine-1-phosphate) are involved in the cell death programmes (*e.g.* apoptosis), which have the possibility of interfering with the positive chemotherapy effects in cancer patients (Roness *et al*., 2014; Zhou *et al*., 2017). GnRH analogs do not affect apoptosis mechanisms; however, clinical trials so far have not able to reach an agreement about its efficacy on fertility preservation (Del Mastro *et al*., 2011; Munster *et al*., 2012).

All investigated protective molecules against DXR-induced primordial follicle loss investigated thus far are summarised in Table 1.9. Although some of them have been approved for other clinical uses, such as Dexazoxane that is used to prevent DXR-induced

cardiotoxicity (Swain *et al*., 1997), none of these promising protective agents has been implemented in clinical practice yet to block DXR-induced gonadotoxity.

Of these candidate protective molecules, AMH is the only natural hormone generated within human body and has only become a fertility protector candidate in oncofertility in recent years (Roness *et al*., 2015). It is important to note that AMH had not been studied to protect the ovary against DXR before we planned this current project.

Table 1.9. Promising protective agents against DXR.

Research group	Protector	Potential mechanisms	Prevent PMF loss	Model	Type
Against DXR					
Roti Roti and Salih, 2012 Kropp *et al*., 2015	Dexrazoxane	Inhibit topoisomerase II	ND	Mice	*In vitro; in vivo*
Sanchez *et al*., 2013	Lithium chloride	Restoration of β-catenin signalling	N/A	Human luteinized GCs	*In vitro*
Jafarian *et al*., 2013	Papaver bracteatum Lindl. Extract	Antioxidant	ND	Mouse oocytes and embryos	*In vivo*
Salih, 2011	Multidrug resistance gene	Drug resistance	N/A	Mouse immortalized GCs	*In vitro*
Li *et al*., 2013	S1P	Inhibit the ceramide-induced death pathway	Yes	Mice+human xenograft	*In vivo*
Roti *et al*., 2014	Bortezomib	Prevent DXR nuclear accumulation	Yes	Mice	*In vitro; In vivo*
Protect Ovary					
Imai *et al*., 2007	GnRHa	Unclear	N/A	Human mature GCs	*In vitro*
Kano *et al*., 2017	AMH	Unclear	Yes	Mouse	*In vivo*

GnRHa: gonadotropin-releasing hormone analog. S1P: sphingosine-1-phosphate. PMF: Primordial follicle. GCs: granulosa cells. N/A: Not applicable (not containing PMF). ND: Not described.

1.6 Anti-Müllerian Hormone

1.6.1 Overview

Anti Müllerian Hormone (AMH), also named as Müllerian Inhibiting Substance, is a protein which results in the regression of the Müllerian ducts during male gonadal differentiation and was first discovered following a series of experiments using castrated fetal rabbits in 1947 (Jost, 1953). Müllerian ducts, also known as Paramesonephric ducts, are paired ducts located within the mesonephros of the genital ridges which are present during the early prenatal development in foetuses of both sexes (Rey, 2005) (Figure 1.5). In the absence of AMH, the Müllerian ducts develop into the upper vagina, uterus and fallopian tubes as occurs in a normal female embryo (Mullen and Behringer, 2004).

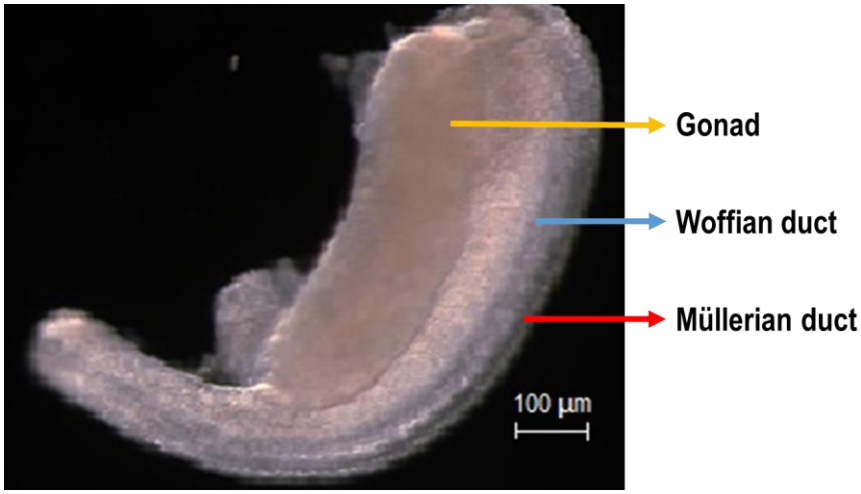


Figure 1.5. A single side of genital ridge including a Müllerian duct. This genital ridge was dissected from embryonic day 13.5 female mouse embryos by the candidate.

Although AMH was discovered in the 1940s, its glycoprotein dimeric nature was not identified until 1978 (Picard *et al.*, 1978), and the AMH gene was identified and sequenced in 1986 (Cate *et al.*, 1986; Picard *et al.*, 1986). The human AMH gene is located on the short arm of chromosome 19 and mouse AMH gene is located in

chromosome 10, both are comprised of five exons and four introns (Cohen-Haguenauer *et al.*, 1987; King *et al.*, 1991). The AMH gene transcribes a 140-kDa glycoprotein consisting of a 110-kDa amino-terminus and a 25-kDa carboxy-terminus which is the bioactive domain (MacLaughlin and Donahoe, 2010). The 140-kDa AMH is composed of two 70kDa homodimers; each homodimer of the pro-AMH was then cleaved to produce activity.

The sequence of AMH carboxy-terminus is highly conserved. After running a Basic Local Alignment Search Tool (Blast) search at the National Centre for Biotechnology Information Genomes database using a compositional matrix adjustment method, 73% alignment in the entire protein and 92% alignment in the carboxy terminus between human and mouse origin AMH were shown. This confirms the fact that AMH is a highly conserved protein (Table 1.10, Figure 1.6).

Table 1.10. Comparison between mouse and human AMH protein.

AMH	GenBank NO.	AAL	Alignment Identity		
			Entire	**N-Domain***	**C-Domain***
Mus musculus	CAA44912.1	555	72%	69%	92%
Homo sapiens	AAH49194.1	560			

*N-Domain: Amino Terminus; C-Domain: Carboxy Terminus. AAL: Amino acid length.

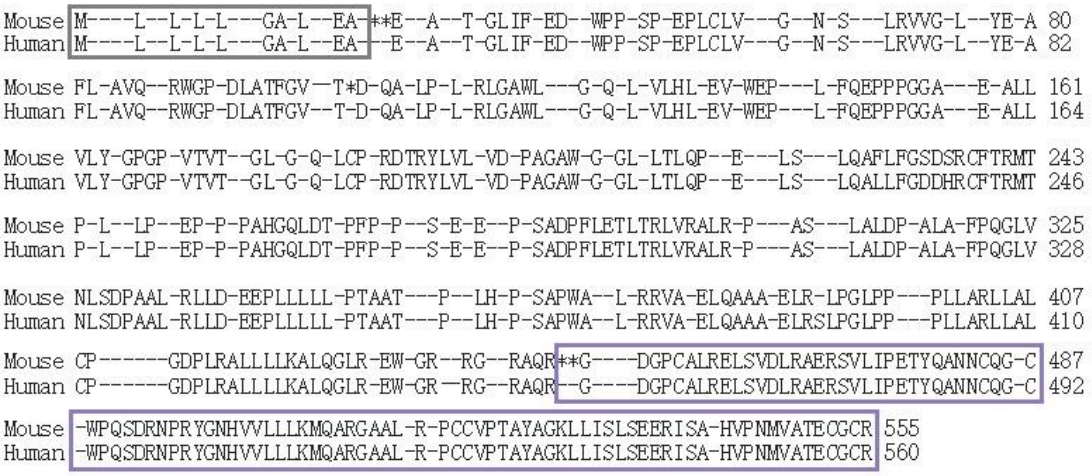


Figure 1.6. Alignment of the deduced amino acid sequences of AMH in human and mouse. First 25 amino acids (leader sequence) in the grey box of both human and mouse AMH sequences make up a secretion specific signal peptide. The carboxy terminus shown in the purple box is the bioactive domain of AMH.

AMH is produced by the sertoli cells of the testes in males and in females, AMH is believed to be generated by the granulosa cells of growing follicles at the pre-antral or early antral stages (Blanchard and Josso, 1974; Weenen *et al*., 2004). AMH has been shown to have a similar pattern of expression in the granulosa cells of both rodents and humans (Durlinger *et al.*, 2002). It has been shown that the highest expression of AMH is in the granulosa cells and those closest to the oocyte (Nilsson *et al*., 2007). Two studies have reported localisation of AMH in primordial follicle oocytes, however, this is most likely due to a non-specific binding of antibodies, as other stages of follicles also expressed AMH in oocytes in these studies (Stubbs *et al*., 2005; Almeida *et al*., 2018). Thus far, there is no robust evidence demonstrating AMH in primordial follicles.

Aside from its expression in the testes and ovaries, AMH has also been detected in other organs such as the brain (Bédécarrats *et al*., 2003). Furthermore, despite AMH also being expressed in other organs, the absence of detectable AMH in serum after bilateral

oophorectomy indicates that the ovary is the primary source of circulating AMH (La Marca *et al.*, 2005).

1.6.2 AMH receptors and signalling pathways

AMH belongs to the transforming growth factor-β (TGF-β) family and therefore shares the general characteristics of this family (Kumar *et al.*, 2010). Similar to other TGF-β family members, the bioactive carboxy-terminal domain of AMH initiates its signalling pathway through interaction with two types of transmembrane serine/threonine kinase receptors: type I and type II (Josso and di Clemente, 2003).

The TGF-β family has five type II receptors that can activate type-I receptors (Di Clemente *et al*., 2003). AMH receptor II is one of the type II receptors, however it specifically binds only AMH, different to other type II receptors shared by other TGF-β family members. AMH shares three type I receptors, activin receptor-like kinase 3 (ALK3), ALK6 and ALK2, with other TGF-β family members such as bone morphogenetic proteins (BMPs) (Di Clemente *et al*., 2003). The ligand binds first to the type II receptor, subsequently activating the type I receptors which initiates the SMAD 1/5/8 intracellular pathway, targeting the intracellular gene expression (Figure 1.7).

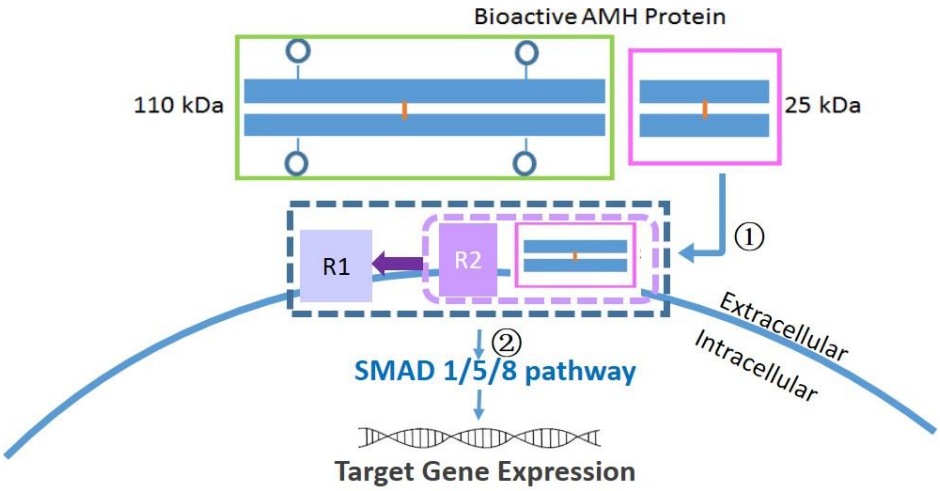


Figure 1.7. The signalling pathway of AMH. ①The active moiety of AMH (pink box) first binds to AMH type II receptor (R2) and subsequently activates type I receptors (ALK2, 3 and 6) (R1). ②After AMH binds with R1, the SMAD 1/5/8 intracellular pathway will then be activated and subsequently target intracellular gene expression (Josso and di Clemente, 2003; McLennan and Pankhurst, 2015).

AMH has been suggested for use as a therapeutic agent for Müllerian duct origin cancers (Marca and Volpe, 2007). Its downstream signalling pathway is different to most chemotherapy agents (Pieretti-Vanmarcke *et al*., 2006) and thus, it should not affect the functional pathway of chemotherapy agents to kill cancer cells.

Although the presence of AMHR2 has been reported in pre-granulosa cells of the adult mouse (n=1) (Kano *et al*., 2017), it was mostly concluded to be expressed in the same pattern as AMH in growing follicles.

1.6.3 AMH and primordial follicles

In women, AMH is generated by the granulosa cells of growing follicles. Studies have confirmed that AMH attenuates primordial follicle activation in both human and

mouse ovarian tissue *in vitro* (Durlinger *et al*., 2002; Carlsson *et al*., 2006). Recently these results have been confirmed *in vivo* by Hayes *et al*. who reported an increased percentage of primordial follicles in AMH treated mice (Hayes *et al*., 2016). The most robust evidence of the effect of AMH on primordial follicle activation is from the AMH or AMHR2 knock-out models that are summarised in Table 1.11. The general trend amongst AMH or AMHR2-knockdown mice is the presence of a normal follicular pool size at puberty, followed by accelerated activation of primordial follicles.

Table 1.11. Studies investigating the effects of AMH on primordial follicle activation in genetically modified mouse models.

Research Group	Model	Main finding
Durlinger *et al*., 1999	AMH-knockout mice	At 25 days: No effect; 4 months: Inhibin levels were higher, FSH levels were lower; 13-month: Inhibin levels were lower, FSH levels were unchanged compared to wild-type mice.
Gigli *et al*., 2005	AMHR2-null mice	AMHR2-null ovaries had more growing follicles compared to wild-type mice xenografted into chick embryo from PND0 to PND4.
Visser *et al*., 2007	AMH-null mice	Increased oocyte degeneration and follicular atresia; Increased initial and cyclic recruitment in AMH-null mice with normal number of preovulatory follicles
Park *et al*, 2014	AMH-knockdown mice	*In vivo* mouse gene delivery experiments revealed that AMH-knockdown accelerated follicle recruitment

PND: Postnatal day. FSH: Follicle stimulation hormone.

In addition to these gene knock-out models, numerous studies have tested the effect of AMH on ovarian function, as summarised in Table 1.12 and 1.13. Interestingly, there is no dose-dependent effect of AMH detected *in vitro.* Studies using AMH suggest that a dose of 50 ng/ml seems the minimum optimal concentration to have an effect on the activation of primordial follicles (Table 1.12). According to Table 1.12, most studies showed AMH has no detrimental effects on follicle viability.

Commercial AMH from R&D systems (USA) was the mostly used product *in vitro*, whilst another AMH preparation from Cusabio (China) showed an effect *in vivo* (Table 1.12 and 1.13). Therefore, both of them would be suitable products for use in our study. However, Kano *et al.* (2017) reported concerns about the bioactivity of the commercial AMH products since the R&D systems AMH failed to regress Müllerian ducts *in vitro* in their experiments. However, a paper recently published by a Japanese group demonstrated that the R&D systems AMH was able to regress mouse Müllerian ducts (Yamamoto *et al*., 2018).

Table 1.12. All studies investigating the effects of AMH on primordial follicle activation *in vitro*.

Research Groups	Ovarian tissue	AMH	Source	Dose	Period	PMF activation +ve/-ve	Other main findings
Polyovular species							
Durlinger *et al.*, 2002	Mice (PND2)	rrAMH	Home-made	900 ng/ml	2 or 4 d	-ve	↓Inhibin α-subunit expression
Nilsson *et al.*, 2007	Rat (PND4)	rhAMH	Biogen*	50 ng/ml	10 d	-ve	No dose-dependent effect; ↓Follicle development: ↑Inhibitory factors expression; ↓Stimulatory factors expression.
				250 ng/ml		-ve	
Mark-Kappeler *et al*., 2010	Rat (PND4)	rhAMH	R&D	100 ng/ml	8 d	0	No dose-dependent effect
				200 ng/ml		-ve	
				400 ng/ml		-ve	
Monovular species							
Schmidt *et al.*, 2005	Human 30 yrs (n=2) 9-19 yrs (n=4)	rhAMH	Biogen	300 ng/ml	28 d	+ve	↑Follicular development; ↑Diameter of PFs
Carlsson *et al.*, 2006	Human 33.7 ± 3.6 yrs	rrAMH	Home-made	10 ng/ml	7 d	0	No effect on follicle viability
				30 ng/ml		0	
				100 ng/ml		-ve	
Bertoldo *et al.*, 2016	Sheep (pre-pubertal)	rhAMH	R&D	5/50/100 ng/ml	2 d	0	0
				5 ng/ml	5 d	0	0
				50 ng/ml		-ve	↑TUNEL positive follicles*
				100 ng/ml		-ve	
				5 ng/ml	9 d	0	↓ TUNEL positive follicles
				50 ng/ml		-ve	
				100 ng/ml		-ve	↑TUNEL positive follicles
Rocha *et al.*, 2016	Goat (adult)	rhAMH	R&D	50 ng/ml	1 or 7 d	-ve	No effect on follicle viability
				150 ng/ml		-ve	
Yang *et al.*, 2017	Bovine (fetal)	rhAMH	Not Described	100, 200, 500 ng/ml	12 d	-ve	In response to Insulin only: Dose-dependent inhibitory effects on the diameters of PFs
				1000 ng/ml		0	0

PMF: Primordial follicles. PND: Postnatal day. -ve/+ve: negative/positive effect. 0: no effect. TUNEL: terminal deoxynucleotidyl transferase dUTP nick end labelling *Not classified the stages of TUNEL positive follicles. Biogen has ended drug production by 2016. rrAMH: recombinant rat AMH. rh: recombinant human AMH. PFs: Primary follicles.

Table 1.13. All studies investigating the effects of AMH on primordial follicle activation *in vivo*.

Research Groups	Model	AMH	Source	Route	Dose	Period	PMF activation +ve/-ve	Other main findings
Administrations of AMH without ovarian tissue transplantation								
Hayes *et al*., 2016	Mice (3wk;8wk)	rmAMH	Cusabio	IP	120 ng/d	28 d	-ve	0
					300 ng/d			
Kano *et al*., 2017	Mice (6-7wk)	Aav9 vector	Homemade	Sub-cut	3e11 particles/d	39 d	0	↓Ovarian size ↓Growing follicles
		rhAMH		IP	1.5mg/kg(30µg)/d	40 d	0	
		rhAMH		Pump	14.4µg/d	15 d	0	↓Primary follicles
Sonigo *et al*., 2019	Mice (6wk)	rmAMH	Cusabio	IP	5mg/kg(100µg)	1 d	ND	↓Foxo3a phosphorylation
						8 d	-ve	↓Primary and Secondary
					0.5mg/kg(10µg)/wk	(Once/wk) 4wks	ND	↓Cycles
Administrations of AMH with ovarian issue transplantation								
Kong *et al*., 2016	Mice (5wk)	rhAMH	Biorbyt	IP	5, 25, and 125 µg/48 h	7 or 28 d	0	0
Man *et al*., 2016	Human (Not mention age) To mice	rhAMH	Endothelial cells that were engineered to ectopically express AMH		N/A	14 d	-ve	0
Man *et al*., 2017	Human (Not mention age) To mice	rhAMH			N/A	98 d	-ve	↓ primary follicle
Detti *et al*., 2018	Human pre-pubertal girl To mice	rhAMH	R&D	Pump	1.23 µg 0.25 µL/h AMH	14 d	0	↓ apoptosis↓ apoptosis ↓ cellular activation

IP: Intraperitoneal. IV: Intravenously. Sub-cut: Subcutaneous. PMF: Primordial follicle. PF: Primary follicle. ND: Not described. 0: no effects. ↓: Decrease. -ve/+ve: negative/positive effect. 0: no effect. rrAMH: recombinant rat AMH. rh: recombinant human AMH. PFs: Primary follicles.

In addition to these experiments, a mathematical model has been generated indicating that the administration of exogenous AMH is potentially able to slow primordial follicle activation, thus prolonging the fertility life for females (Margolskee and Selgrade, 2013).

In order to gain an insight into the effects of AMH on primordial follicle activation, the studies of the effect of AMH on cytokines involved in primordial follicle activation were also reviewed (Table 1.14). According to Table 1.14, we found an overall inhibitory effect of AMH on cytokines that promote primordial follicle development and a stimulatory effect on cytokines that inhibit primordial follicle activation.

Table 1.14. Effects of AMH on cytokines involved in primordial follicle activation.

Cytokines	Functions in PMF activation	Tissue	AMH effects	References
Oocytes derived				
GDF9	Potential to facilitate PMF activation	Human ovarian cortex grafts; Rat ovary	Suppress	Detti *et al*., 2018; Nilsson *et al*., 2007
BMP15	Stimulate of the proliferation of undifferentiated GCs	Rat ovary	Suppress	Nilsson *et al*., 2007
bFGF	Induce PMF development	Rat ovary	Suppress	Nilsson *et al*., 2007
Foxo3a	Inhibitor for the PI3K pathway (phosphorylation of Foxo3a leading to PMF activation)	Mouse ovary	Decrease Foxo3a phosphorylation	Sonigo *et al*., 2019
Pre-granulosa cell derived				
Foxl2	Inhibiting the initiation of PMF growth	Human GCs	Positive loop	Park *et al*, 2014; Sacchi *et al*., 2017
KITL	Induce PMF development	Rat ovary	Suppress	Nilsson *et al*., 2007
Stroma/theca cell derived				
BMP4	Promote primordial to primary follicle transition	Rat ovary	Suppress	Nilsson *et al*., 2007
KGF	Induce PMF development	Rat ovary	Suppress	Nilsson *et al*., 2007

GDF9: Growth differentiation factor 9. BMP4/15: Bone morphogenetic protein 4/15. Foxl2: Forkhead box L2. Foxo3a: Forkhead box O3a. PFs: Primary follicles. SFs: Secondary follicles. PAFs: Preantral follicles. PMF: Primordial follicle. GCs: granulosa cells. KITL: Kit ligand. bFGF: basic fibroblast growth factor. KGF: Keratinocyte growth factor.

Role of AMH to protect primordial follicles against Chemotherapy

Until recently, AMH had not been investigated as an onco-fertility protector. A study published in 2015 demonstrated the effect of AMH against Cyclophosphamide induced primordial follicle loss (Roness *et al*., 2015). However, whether AMH can prevent primordial follicle loss in conjunction with DXR *in vivo* has not been determined before this experiment was planned.

Table 1.15. Summary of current studies investigating the effect of AMH on chemotherapy-induced primordial follicle loss.

Research Groups	Age	AMH	Route	Dose	Period	PMF loss	Regimen
In vitro							
Roness *et al*., 2015	Pre-pubertal Mice	N/A	N/A	100 ng/ml	2 hours	-ve	Single Cy
In vivo							
Kano *et al*., 2017	Adult Mice	Aav9 vector	Sub-cut	3e11 particles /d	0-12 d	-ve	(on d1 d7) DXR IV 3mg/kg
		rhAMH Homemade	Pump	14.4µg/d	0-15 d	-ve	(on d1) DXR IP 7.5mg/kg (on d2) DXR IP 6mg/kg
Sonigo *et al*., 2019	Adult Mice	rmAMH Cusabio	IP	5mg/kg (100µg)	8 d	-ve	Single Cy

Cy: Cyclophosphamide. IP: Intra-peritoneal. IV: Intra-venous. PMF: Primordial follicles. Sub-cut: Subcutaneous. -ve: negative.

In an *in vitro* study, AMH rescued Cyclophosphamide-induced primordial follicle loss in mouse ovarian tissue after cotreatment with Cyclophosphamide metabolite (phosphoramide mustard) and AMH at 100ng/ml for 2 hours followed by 7 days of culture (Roness *et al*., 2015). Cyclophosphamide has been proposed to reduce primordial follicle numbers via over activating the PI3K pathway (burn-out theory). However, in this study, 24 hours after the AMH treatment, there was no change in the expression of Akt and rpS6 which belong to the PI3K pathway (Roness *et al*., 2015). A more recent study by Sonigo *et al.* (2019) demonstrated a significant reduction of Foxo3a phosphorylation 24 hours after

AMH injection, indicating that AMH might mediate the PI3K pathway by regulating Foxo3a phosphorylation.

1.7 Outline of thesis

Since previous studies used a variety of DXR doses (Section 1.4.2.2, Table 1.6), we first wanted to establish the optimal dose by conducting an *in vitro* study to investigate whether AMH has an effect on DXR-induced primordial follicle loss in pre-pubertal mouse ovaries in a dose-dependent manner. In order to do this, recombinant AMH would need to be generated. We also needed to determine whether AMH is safe to be administered into mice and exerted an effect on ovarian function. Once this was determined, an optimum dose of DXR that can induce primordial follicle loss would need to be established and whether the co-administration of AMH with DXR can prevent the DXR-induced primordial follicle loss in mice *in vitro* would be investigated.

Our main interest was whether AMH has an effect on DXR-induced primordial follicle loss on human ovarian tissue; this has not been investigated. Therefore we aimed to determine the effects of AMH on DXR-induced primordial follicle loss in human ovarian tissue *in vivo* by using a mouse xenograft model.

Since xenotransplantation has not been conducted in the Williams lab before, a xenotransplantation protocol needed to be established. For example, different transplantation sites would be compared since research indicates that the speed of follicular development of transplanted ovarian tissue might be affected by the site of transplantation (Terada *et al*., 2008; Dath *et al*., 2010). Dath *et al*. (2010) stated that human ovarian tissue transplanted under the mouse ovarian bursa can cause antral follicles to develop in just three weeks, whereas tissue transplanted subcutaneously can take up to 3 months (Terada *et al*., 2008) and up to 5 months under the kidney capsule (Soleimani *et*

al., 2010). Comparing follicle development between ovarian tissues transplanted in these different sites would be important to establish the optimal location for transplantation and allow verification of this published data from our experiments.

1.8 Hypotheses and Aims

Hypothesis 1: AMH can be safely administered into pre-pubertal mice.

Aim 1 - Generate recombinant AMH (Chapter 3).

Aim 2 - To determine if the administration of commercial AMH adversely affects health, ovarian function, and the onset of puberty in mice *in vivo* (Chapter 4).

Hypothesis 2: AMH can prevent DXR-induced primordial follicle loss in mouse ovaries *in vitro*.

Aim 3 - To determine if DXR induces primordial follicle loss in pre-pubertal mice *in vitro* (Chapter 5).

Aim 4 - To determine if the administration of rmAMH and rhAMH can prevent DXR-induced primordial follicle loss in mice *in vitro* (Chapter 6).

Hypothesis 3: AMH can prevent DXR-induced primordial follicle loss in human ovarian tissue xenotransplanted into mice and in mouse ovaries *in vivo*.

Aim 5 - To compare different transplantation sites and establish xenotransplantation protocols using post- and pre-pubertal human ovarian tissue (Chapter 7).

Aim 6 - To determine if the administration of AMH can prevent DXR-induced primordial follicle loss in xenografted pre-pubertal human ovarian tissue (Chapter 8).

Chapter 2: Materials and Methods

2.1 Ethical Approval

2.1.1 Patient consent

All human ovarian tissue used was donated to research by the patients during informed consent by the Oxford Cell and Tissue Biobank (OCTB). Patients were given the option to donate excess tissue (if over 50 ovarian cortical strips were collected) to (i) research and/or (ii) research involving animal models.

2.1.2 Home Office and Research Ethics Committee approval

The work carried out in this thesis was approval by the Home Office and the Local Ethical Review Panel at the University of Oxford under a project licence held by Dr. Williams (Project Licence number 30/3352) in accordance with the UK Animals (Scientific Procedures) Act 1986, and the Health Research Authority South Central - Oxford B Research Ethics Committee (REC reference: 14/SC/0041) and registered with the Oxford University Hospitals NHS Foundation Trust (R&D reference: 8825).

In order for the candidate to perform drug administration and surgery on animals, a personal license (PIL) was required. To gain the license, training courses (PIL category A, B and PIL category C additional training) provided by Oxford University Veterinary Services were attended and following practical and written assessments were passed. The candidate was trained to and assessed in performing animal injections and surgeries.

2.2 Mouse colonies

All mice used in this project were housed in ventilated cages with a 12-hour light/12-hour dark cycle. Mice were fed with food and clean water, *ad libitum*. Two management systems were used to manage the colonies used in this project, Excel sheets

used in the Williams's group and the Sanger system used by Biomedical Services (University of Oxford, UK).

2.2.1 Breeding of Mice

Breeding cages to generate CD1xC57BL/6 female pups (F1) were set up with one male (C57BL/6) (Biomedical Services, University of Oxford, UK) paired with two females (CD1) (Charles River Laboratories, Kent, UK) at 8 weeks of age. CD1 mice were used due to their large litter size. The day after mating (day 0), females were checked daily for a copulatory plug. Females with a plug visible at the entrance of vagina indicated that mating had occurred and they were likely to be pregnant. As soon as a plug was found, females were removed from the mating cage to a fresh cage.

Litters were born on gestation days 20-21. The day of birth was considered as postnatal day 0. Before or by the age of postnatal day 6, sex was determined based on the anogenital distance, prominent genitalia and the presence of a pigment spot on the scrotum (Wolterink-Donselaar *et al*., 2009).

2.2.2 Mice used for xenotransplantation

Female mice with severe combined immune deficiency (SCID) (CB17/Icr-*Prkdc*^{SCID}/IcrIcoCrl) (Charles River, UK) aged at 9-10 weeks were used as hosts for human ovarian cortical tissue. After arrival at the animal facility, mice were given at least one week for acclimatisation before their use in experiments.

2.2.3 Mouse identification

In order to identify mice, all mice were ear clipped with a different number using the ear clipping tool (Vet-tech, Congleton, UK).

2.2.4 Post-procedure mouse monitoring

Mouse health, condition and behaviour was assessed routinely after any procedures such as surgeries or drug injections. Assessment was carried out by remote observation and handling (Table 2.1).

Table 2.1. Mouse health status assessment form.

From a distance	**On handling**
Unhealthy signs	
Inactive	Vocalisation
Isolated	Discharge eyes or nose
Hunched posture	Wet or soiled coat
Starey coat	Stiches missing
Lethargy	Wound open/infected
Rigidity	Weight loss
Healthy signs	
Grooming	Inquisitive
Eating and drinking well	Weight gain
Nest building	Normal urine and faeces

2.3 Ovary Dissection

2.3.1 Dissection Medium

Dulbecco's phosphate buffered saline (DPBS, Sigma, Gillingham, UK) was supplemented with bovine serum albumin (BSA, Factor V Heat Shock Treated; Fisher Scientific, Loughborough, UK) at 1mg/ml. The dissection medium was filtered with a vacuum bottle-top filter (pore size 0.2μm) (Corning, New York, USA) and stored at 4°C. Before dissection, the medium was added to four Petri dishes (Corning Falcon, Fisher Scientific, UK) and pre-warmed at 37°C in the incubator.

2.3.2 Gross Dissection

Mice were culled by cervical dislocation. The fat pad beside the ovaries was held by forceps and scissors were used to cut the fallopian tubes. Ovaries were dissected into a

Petri dish containing pre-warmed DPBS supplemented with 1mg/ml BSA. This Petri-dish was then wiped with 70% ethanol and transferred into a Class II hood.

2.3.3 Fine Dissection

The ovarian bursa and surrounding fat tissue were removed from the mouse ovaries using sterile spring scissors and forceps under a microscope located inside a sterile laminar flow hood on a heated stage at 37°C.

After dissection, all ovaries were transferred into the second Petri dish containing pre-warmed dissection medium and went through two further washing stages to prepare them for culture.

2.4 Ovary Culture

2.4.1 Culture medium

Alpha Minimum Essential Medium (α-MEM) (1X) (Sigma, UK) was used as the basal medium for all ovary culture in this thesis. The osmolality in the actual product is higher than the osmolality in mice which is around 285 mOsm/kg. Sterile water was therefore added to the α-MEM medium to adjust the osmolality according to the following formula:

$$H_2O_{volume}\ (ml) = \frac{\text{Actual mOsm/kg} - 285\ \text{mOsm/kg}}{\text{Actual mOsm/kg}} \text{ x Medium volume (ml)}$$

After the osmolality had been adjusted, the medium was aliquotted into 50ml sterile Falcon tubes, sealed with parafilm and stored at 4°C. Before culture, the medium was supplemented with 3mg/ml BSA, 100 IU/ml penicillin and 0.1mg/ml streptomycin and filtered using 0.22μm filter units (Millex-GP Syringe Filter Unit, Merck, UK) in a

sterile hood. The culture medium was pre-incubated at 37°C and 5%CO_2 in the incubator for at least one hour before culture.

2.4.2 Ovary culture

Culture media were transferred to a 24-well tissue culture plate (Corning Costar, UK) at a final volume of 1ml/well. A Whatman Nucleopore polycarbonate membrane (Sigma, UK) was placed on the top of the culture medium. Each ovary was transferred into the centre of a membrane using a P200 pipette with a round-bore tip. During ovary transfer, the plate was kept on a heated stage at 37°C in the sterile Class II flow hood. After adding the ovaries, the culture plate was placed into the incubator and cultured for six days at 37°C and 5% CO_2. The medium (50%) was changed every two days.

2.5 Human ovarian tissue

2.5.1 Tissue collection by OCTB

Ovarian cortical tissue was obtained from patients following a planned unilateral oophorectomy for fertility preservation purposes. The ovarian cortical tissue were cut into strips (1x1x5 mm pieces), processed and frozen by the OCTB technicians following an established protocol (Revel *et al*., 2003) and stored in liquid nitrogen (-196°C) until use.

2.5.2 Human ovarian cortical strips freezing and thawing

Tissue was requested from the OCTB using a form stating tissue requirements. Tissue was selected by OCTB and collected by the candidate. Thawing was carried out based on the OCTB protocol.

The cryovials containing ovarian cortical strips were firstly thawed in a water bath at 30°C for 3 minutes. In order to wash the cryoprotectant agents, ovarian cortical strips were washed in three different pre-made sterile solutions (5 minutes/wash on the rocker) (Table 2.2).

Table 2.2. Thawing media used for cryopreserved human ovarian cortical strips.

Constituents*	**Solution**		
	I	**II**	**III**
Ethylene glycol	0.28ml	0.14ml	
1M Sucrose	0.5ml	0.5ml	0.5ml
Serum Substitute Supplement	0.5ml	0.5ml	0.5ml
Leibovitz's L-15 media	3.72ml	3.86ml	4ml
Total	5ml	5ml	5ml

* Serum Substitute Supplement was from Irvine Scientific. Ethylene glycol, sucrose and L-15 media were all from Sigma.

2.6 Histology

2.6.1 Fixation

After six days of culture, whole ovaries from postnatal day 6 (PND6) female mouse pups were fixed in 10% neutral buffered formalin (Sigma, UK) for six hours on a rocker at ~40 rpm. Adult mouse ovaries were fixed in 10% neutral buffered formalin for eight hours on a rocker at ~40 rpm. Human tissue xenografts were either fixed in Bouin's (Sigma, UK) or 10% neutral buffered formalin for eight hours. After fixation, tissue was transferred into 70% ethanol (Sigma, UK) and stored at 4°C.

2.6.2 Embedding

Tissue was transferred into fresh 70% ethanol and dehydrated through increasing concentrations of ethanol, followed by three changes of xylene (as described in Table 2.3).

Table 2.3. Dehydration protocol to prepare fixed tissue for embedding.

Reagents	Duration	Volume - Small*	Volume - Large*
70% Ethanol	15 min	200µl	800µl
80% Ethanol	15 min	200µl	800µl
95% Ethanol	15 min	200µl	800µl
100% Ethanol	15 min	200µl	800µl
100% Ethanol	15 min	200µl	800µl
100% Ethanol	15 min	200µl	800µl
Xylene	15 min	200µl	800µl
Xylene	15 min	200µl	800µl
Xylene	15 min	200µl	800µl

*Small: small piece of tissue (<1mm^3); Large: large piece of tissue (>1mm^3).

After dehydration, tissue was transferred into a plastic mold containing melted paraffin wax in the oven at 62°C and covered with a pre-warmed cassette. The tissue was immersed in the paraffin wax for three and half hours, to allow the paraffin wax to thoroughly penetrate the tissue. After embedding, the oven was turned off and the paraffin blocks containing the tissue were left to cool. The blocks were then put into the fridge at 4°C for at least one hour.

2.6.3 Sectioning

The paraffin embedded tissues were serially cut at 5µm using a microtome (Leica, Nussloch, Germany). The sections were floated on a water bath at 42°C and then loaded onto positively charged microscope slides (VWR International, Leuven, Belgium). After drying the slides at room temperature, the slides were baked at 62°C for an hour and then put into slide boxes. Every 10th section was collected onto the same slide.

2.6.4 Haematoxylin and eosin staining

The slides were dewaxed in xylene and rehydrated through decreasing concentrations of ethanol (Table 2.4). Haematoxylin (Shandon Gill 2 Haematoxylin; Fisher Scientific, UK) was used for nuclear staining. The counterstaining was done using eosin (Sigma-Aldrich) which stains the cytoplasm pink. The slides were then dehydrated and mounted with coverslips using Depex (Fisher Scientific, Loughborough, UK) and left to dry overnight.

Table 2.4. Protocol of haematoxylin and eosin staining of fixed tissue sections.

Reagents	Duration
Dewax	
Xylene I	8 min
Xylene II	4 min
Xylene III	4 min
Rehydration	
100% ethanol	3 min
100% ethanol	3 min
90% ethanol	2 min
70% ethanol	2 min
50% ethanol	3 min
Tap water	3 min
Staining	
Haematoxylin	2 min
Running water	5 min
Acid alcohol*	5 sec
Running water	5 min
80% ethanol	1 min
Eosin alcoholic	1 sec
Dehydration	
95% ethanol	30 sec
100% ethanol	45 sec
100% ethanol	1 min
100% ethanol	2 min
Xylene I	8 min
Xylene II	8 min

*Acid alcohol was made of 1% hydrogen chloride in 70% ethanol to remove excessive haematoxylin stain.

2.6.5 Imaging

Sections were visualised using a DM2500 Leica microscope (Microscope services Ltd, Woodstock, UK) and imaged using a MicroPublisher 5.0 Real-Time Viewing camera (Qimaging, Microscope services Ltd, Canada).

2.6.6 Assessment of follicle development

2.6.6.1 Follicle classification

Only follicles with a visible nucleus were staged. Follicles containing an oocyte and surrounded by flattened pre-granulosa cells were classified as primordial follicles which are the main interest of this project (Table 2.5). If the follicle was composed of an oocyte with a layer of mixed flattened pre-granulosa cells and cuboidal granulosa cells, it was classified as transitional. Follicles were defined as primary follicles if they contained one complete layer of cuboidal granulosa cells, and secondary follicles if they contained more than one layer of granulosa cells (Van den Hurk *et al.*, 1997). Follicles with an antrum present were defined as antral follicles.

Table 2.5. Definition of follicle classification (Van den Hurk *et al.*, 1997).

Stage	Definitions
Primordial	Flattened pre-granulosa cells
Transitional	At least one cuboidal granulosa cell
Primary	One layer of cuboidal granulosa cells
Secondary	Two layer of granulosa cells
Antral	Presence of an antrum

2.6.6.2 Follicle morphology

Follicles stained with haematoxylin and eosin were classified as healthy or atretic according to their morphology. A healthy follicles was defined as an intact oocyte with a normal nucleus and cytoplasm, and less than 10% of pyknotic granulosa cells (Tomic *et al.*, 2006).

Follicles were considered atretic if they had an oocyte with a pyknotic nucleus and condensed cytoplasm or more than 10% of the granulosa cells contained pyknotic bodies (Tomic *et al*., 2006). While the total number of granulosa cells was less than 10 in transitional and primordial follicles, follicles were considered atretic if there was one pyknotic granulosa cell present.

2.6.6.3 Follicle counting

Follicles with a visible nucleus were counted after follicle stage classification. With the exception of one specific study in Chapter 7 where follicles in every single section were counted, follicles were counted in every 10th section and the total number of follicles was calculated using the Abercrombie correction factor (Abercrombie, 1946):

$$\textbf{Total number of follicles} = \frac{number\ of}{follicles\ counted} \times sampling\ number \times \frac{Abercrombie}{correction\ factor}$$

$$\textbf{Abercrombie correction factor} = \frac{Thickness\ of\ sections\ (\mu m)}{Average\ nuclear\ diameter\ (\mu m) + Thickness\ of\ sections\ (\mu m)}$$

$$\textbf{Nuclear diameter } (\boldsymbol{\mu m}) = \sqrt{\frac{Area\ of\ nucleus}{\pi}} \times 2$$

Nuclear area and diameter was measured using ImageJ software (National Institute of Health, USA).

2.7 Gel electrophoresis

Gel electrophoresis was used to analyse the purified recombinant AMH and to determine whether the supernatant of the dissolved commercial AMH contained the correct protein according to molecular weight of the protein bands.

Samples (18µl) of reconstituted protein were separately mixed with 2.5µl Novex NuPAGE sample reducing agent and 6µl Novex NuPAGE LDS sample buffer (Life technologies, UK). All samples including the protein stain standard were incubated in a dry block heating system (Grant QBD, UK) at 101°C for 5 min to denature the proteins.

New NuPAGE Tris-Acetate mini gel (Life technologies, UK) was loaded into an XCell SureLock Mini-Cell gel running tank. Novex sharp pre-stained protein standard (10µl) was first loaded into one well of the gel followed by the samples. The gel was run at 160V for 40 minutes.

After running, the mini gel was rinsed twice for 5 minutes in ultrapure water and subsequently stained with SimplyBlue Safe Stain (Invitrogen, UK) overnight on a rocker at ~35 rpm.

The gel was distained in distilled H_2O for an hour and then imaged using a GelDoc-It®TS3Imager (Ultra-Violet Products Ltd., Cambridge, UK).

Chapter 3: Production and purification of recombinant Anti-Müllerian Hormone

3.1 Introduction

Advanced chemotherapy regimens contribute to an improving long-term survival rate for childhood cancer patients whereas it also brings side effects such as premature ovarian insufficiency (POI) and infertility (Green *et al*., 2009). Current fertility preservation options such as oocyte cryopreservation are not possible for pre-pubertal children and adolescents. Ovarian tissue cryopreservation is the only option available for pre-pubertal girls. However it is an invasive, experimental procedure and in patients with blood or ovarian cancers, transplantation of tissue back carries a risk of reintroducing cancer cells. Therefore, alternative non-invasive options need to be developed.

Anti-Müllerian Hormone (AMH) is a glycoprotein belonging to the transforming growth factors (TGF-β) family and has been shown to prevent primordial follicle activation *in vitro* and *in vivo*. Furthermore, AMH has been show to prevent chemotherapy (cyclophosphamide) induced primordial follicle loss *in vitro*. However, whether AMH can prevent Doxorubicin (DXR) induced primordial follicle loss had not been determined before we started this study. In order to investigate this, recombinant human AMH (rhAMH) would need to be generated.

3.2 Aim

To generate and purify recombinant human AMH (rhAMH).

3.3 Materials and Methods

3.3.1 Plasmid extraction from filter paper

A pcDNA3.1(+) expression vector containing a Human Albumin Leader and AMH with a Flag tag (Figure 3.1) attached after a modified cleavage site (position 428; RARR/S) was received on filter paper (a gift from Dr Demetrios Vavvas's group, Harvard Medical School, USA).

The original leader sequence (25aa) of AMH (see Chapter 1, Figure 1.6) was replaced by human albumin (24aa) in order to increase protein secretion since albumin has a much higher endogenous secretion rate than AMH (Rothschild *et al*., 1988; Pépin *et al*., 2013). The human albumin was removed during protein processing as the Flag tag was only incorporated in AMH (Pépin *et al*., 2013).

Half a sample spot was cut from the plasmid-containing filter paper, placed in an Eppendorf tube and 110µl Nuclease-Free water (Life Technologies, USA) added. The tube was then centrifuged at 12800 x g for 1.5 minutes, and the water containing the plasmid was collected.

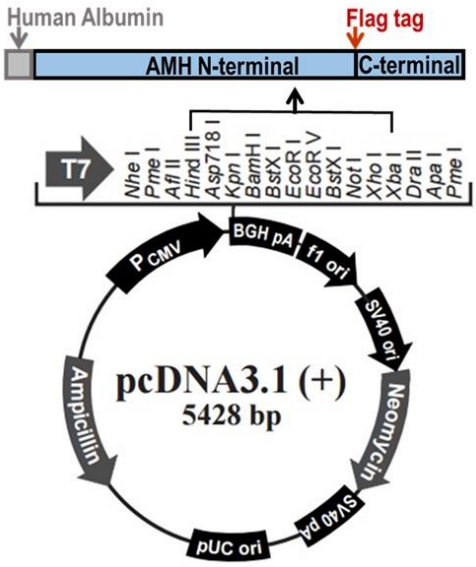


Figure 3.1. A pcDNA3.1(+) expression vector containing the modified Flag-tagged human AMH sequence. Ampicillin resistance gene and pUC origin are for selection and maintenance in *E.* coli cells. Image modified from Invitrogen, UK.

3.3.2 Transformation

The pcDNA3.1(+) expression vector (1µl) containing the HumanAlbuminLeader/RARR/S-modified AMH was added into a tube containing 50 µl of TOP10 *E.coli* competent cells (Invitrogen, UK) and incubated on ice for half an hour. The tube was then placed in the water bath for 45 seconds at 42°C. Super optimal broth with catabolite repression (SOC) medium (600µl) (Invitrogen) was then added into the tube and the tube was incubated in a shaking incubator at 37°C for one hour. After incubation, 200µl of the transformant was spread onto a prewarmed agar plate containing 100 µg/ml Ampicillin (sodium salt) (Sigma, UK) and grown for 18 hours at 37°C. A single colony was chosen and grown in a flask containing 100ml Luria-Bertani (supplemented with Ampicillin) (Sigma), and incubated in a shaking incubator at 37°C (shaking, speed: 220rpm) for 22-24 hours.

3.3.3 Purification of plasmid DNA

The plasmid DNA was purified using a Qiagen HiSpeed Plasmid Midi Kit (QIAGEN, UK) which was based on a modified alkaline lysis protocol. After 15 minutes of centrifugation at 4500 x g at 4°C, the supernatant was discarded. The bacterial pellet was resuspended in 6ml resuspension buffer (Buffer P1, Table 3.1) containing RNase A solution. The cells were lysed with 6ml lysis buffer (Buffer P2) and following 5 minutes at room temperature (RT), 6ml of prechilled neutralization buffer (Buffer P3) was added into the tube. The lysate was transferred into a QIAfilter Cartridge and incubated for 10 minutes at RT. The cell lysate was filtered and added into a Hispeed Tip which had been pre-equilibrated with 4ml Equilibration Buffer (Buffer QBT). The Hispeed Tip resin containing the DNA was then washed with 20ml wash buffer (Buffer QC). The plasmid DNA was eluted in 5ml elution buffer (Buffer QF). The plasmid DNA was then concentrated and desalted by adding 3.5ml isopropanol (70% of the volume of Buffer QF), followed by filtration through a QIAprecipitator. In order to wash the DNA, 2ml of 70% ethanol was pressed through the QIAprecipitator. Finally, 1ml of Nuclease-Free water (Life technologies, UK) was added into the syringe and pressed through the QIAprecipitator to elute DNA.

Table 3.1. Buffer formulations for purification of plasmid DNA using the Qiagen HiSpeed Plasmid Midi Kit.

Name	Function	Components & Condition
Buffer P1	Resuspension	50mM Tris-Cl, PH 8.0, 10mM EDTA; 100ug/ml RNase A, 2-8°C
Buffer P2	Lysis	200mM NaOH, 1% SDS (w/v), 20°C
Buffer P3	Neutralization	3.0M potassium acetate, PH 5.0, pre-chilled at 4°C
Buffer QBT	Equilibration	750mM NaCl, 50mM MOPS, PH 7.0, 15% isopropanol (v/v) 20°C
Buffer QF	Elution	1.25M NaCl, 50mM Tris-Cl, PH 8.5, 15% isopropanol (v/v) 20°C

Tris-C: Tris(hydroxymethyl)aminomethane chloride. EDTA: Ethylenediaminetetraacetic acid. NaOH: Sodium hydroxide. SDS: Sodium dodecyl sulfate. MOPS: 3-(N-morpholino) propanesulfonic acid. NaCl: Sodium chloride. w/v: weight/volume. v/v: volume /volume.

3.3.4 Measurement of plasmid DNA concentration

The concentration of plasmid DNA was measured using a spectrophotometer (Eppendorf, UK). Eluate (4µl) and Nuclease-Free water (96µl) was added into one 1.5ml tube and centrifuged for 1 minute (12800 x g). 100µl of Nuclease-Free water was added into a corresponding control tube. The concentration of the plasmid DNA sample was calculated using a formula: DNA concentration (µg/ml) = Absorbance (at 260nm) x 50(ds DNA) x 25(Dilution factor). The rest of the plasmid DNA sample was stored at -20°C.

3.3.5 Culturing Human Embryonic Kidney 293T cells

A cryovial containing frozen Human Embryonic Kidney (HEK) 293T cells was thawed and transferred into a tube containing 10ml pre-warmed Dulbecco's Modified Eagle Medium (DMEM) (Gibco, UK) supplemented with 10% fetal bovine serum (FBS) (Sigma), 2mM glutamine, 1% v/v 5000U penicillin and 5mg/ml streptomycin and sodium pyruvate (Sigma). The thawed cells in DMEM were centrifuged for 10 minutes at 1200rpm. The supernatant was then discarded and the cell pellet resuspended in 25ml of DMEM supplemented with 10% FBS, 2mM glutamine, 1% v/v 5000U penicillin and 5mg/ml streptomycin and sodium pyruvate before transfer into a 175cm^2 tissue culture flask (Appleton Woods, UK). This flask containing HEK293T cells was incubated in a humidified chamber at 37°C in 5% CO_2 in air for 3 days. Cells were grown to 70% confluency before transfection.

3.3.6 Transfection

The cells were transfected using the calcium phosphate transfection method. Plasmid DNA/$CaPO_4$ precipitate (21ml) was prepared by adding 10.5ml DNA/$CaCl_2$ mixture (1.085ml 2M $CaCl_2$, 970.9µl of purified plasmid DNA and 8.4441ml Nuclease-

Free water) dropwise into 10.5ml 2xHepes-buffered saline (pH 7.12) made of 1.6% NaCl (w/v), 1.2% Hepes sodium salt (w/v) (Sigma) and 0.04% Na_2HPO_4 (w/v) (Sigma). After 5-min incubation, 3ml of plasmid DNA/$CaPO_4$ precipitate was transfected into each prepared flask containing HEK293T cells (7 flasks in total).

The DNA/$CaPO_4$ precipitate was incubated on the cells overnight at 37°C in 5% CO_2 in air. The next day, 25 ml pre-warmed serum free DMEM media (supplemented with 2mM glutamine, 1% v/v 5000U penicillin and 5mg/ml streptomycin and sodium pyruvate) were added to each flask. After 4 days in culture, media containing secreted AMH was collected into four 50ml Falcon tubes and stored in the -80°C freezer.

3.3.7 Protein purification

Anti-flag M2 affinity Gel (300µl) (Sigma) was added into a Poly-Prep® Chromatography Column (Bio-Rad, UK) and washed with 5ml PBS. Four tubes of collected culture media were defrosted and loaded onto the Chromatography Column (Bio-Rad) and passed through under gravity. The samples were passed through the column multiple times to enhance binding efficiency. Flag-tagged protein was bound by the anti-FLAG affinity gel within the column. The samples were then eluted by competitive elution with 200µl of 3X FLAG® Peptide (Sigma) three times (600µl in total).

3.3.8 Electrophoresis

The eluted samples and the affinity gel (18µl of each) were separately mixed with 2.5µl Novex NuPAGE sample reducing agent (Dithiothreitol, DTT) and 6µl Novex NuPAGE LDS sample buffer (Life technologies, UK). After 5 minutes incubation at 101°C, all samples were loaded on a NuPAGE Tris-Acetate mini gel (Life technologies) which was then placed in an XCell SureLock Mini-Cell gel running tank. Novex sharp pre-

stained protein standards (10µl) (Invitrogen) were also loaded into the gel and run at 150V for 50 minutes. The mini gel was rinsed three times for 5 minutes in ultrapure water and subsequently stained with SimplyBlue Safe Stain (Invitrogen) for one hour on a shaker. It was imaged using a GelDoc-It®TS3 Imager (UVP, UK). The results were compared with published publications.

3.3.9 Protein buffer replacement

In order to make the recombinant protein safe for administration in mice, the buffer containing the AMH was replaced by sterile 1X PBS (Sigma). All samples were put into a BioDesignDialysis TubingTM (BioDesign Inc., USA) (MWCO, 8000Da) with a closure clamp and placed in a 2L beaker containing pre-chilled 1X PBS and a magnetic bar. This beaker stayed on a magnetic stirrer over night at 4°C. The next day, the buffer was replaced with fresh pre-chilled sterile 1X PBS for one further hour stirring.

3.3.10 Protein concentration detection

The concentration of sample collected was detected using a Pierce Bicinchoninic Acid (BCA) Protein Assay Kit (Life Technologies), and confirmed using an Eppendorf BioPhotometer plus (Eppendorf).

3.4 Results

3.4.1 Plasmid DNA concentration

After plasmid DNA transformation and purification, the spectrophotometer measured the absorbance at 260nm of purified plasmid DNA as 0.346. The concentration of our sample was 432.5 µg/ml, calculated using the formula: DNA concentration (µg/ml) = Absorbance (at 260nm) x 50(ds DNA) x 25(Dilution factor).

3.4.2 Purified protein concentration

The absorbance value of the purified AMH protein sample at 562nm is 0.036, displayed as optical density (OD) (Table 3.2). The standard curve generated using bovine serum albumin (BSA) standards is shown in Figure 3.2. The final concentration of the recombinant AMH protein is approximately 80µg/ml (Table 3.3).

Table 3.2. Average absorbance values of BSA standard samples (A-E) and rhAMH at 562nm from replicates (1-3) based on Blank (PBS) corrected.

NO.	Standard					rhAMH
	A	B	C	D	E	
1	0.176	0.066	0.019	0.005	-0.001	0.036
2	0.176	0.066	0.019	0.005	-0.001	0.037
3	0.176	0.066	0.019	0.005	-0.001	0.037

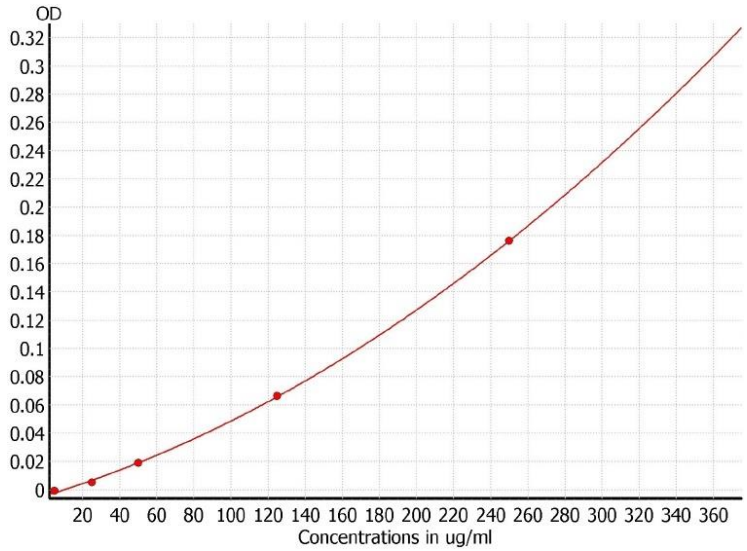


Figure 3.2. Standard curve for the BCA protein assay generated using five concentrations of BSA. Absorbance values are displayed as OD.

Table 3.3. Concentrations of tested standard samples (BSA) (A-E) and rhAMH samples in µg/ml.

NO.	Standard					rhAMH
	A	B	C	D	E	
1	249.905	125.634	49.929	21.839	7.722	80.5
2	249.905	125.634	49.929	21.839	7.722	80.994
3	249.905	125.634	49.929	21.839	7.722	82.143

The concentration of the purified AMH protein was re-tested using the spectrophotometer (Eppendorf) with the help of Ms Celine Jones at the Institute of Reproductive Sciences (University of Oxford), giving a result of approximately 90 µg/ml. The average of these two results was then calculated as the final concentration which is 85 µg/ml. The total purified protein yield was 130µl which contained 11.05µg of rhAMH protein.

3.4.3 Electrophoresis

After electrophoresis, the stained gel revealed a 70kDa band, a 55kDa band and a very wide band at 12.5kDa in the eluted protein columns (Figure 3.3). This indicates that

the majority of recombinant AMH was cleaved endogenously at the cleavage site 427 (total length 560). After elution of the purified recombinant protein, the columns containing the 'affinity gel after elution' samples revealed a heavy chain (50 kDa band) and a light chain (25kDa band) (Figure 3.3). This is because the disulfide bridges of the covalently attached murine IgG_1 monoclonal antibody (within the affinity gel) was dissociated by DTT. The 'affinity gel after elution' samples also contained a light band at 12.5 kDa, indicating very little recombinant protein was not being eluted from the gel. In the same column, there is also a very light band at around 2.8kDa which is possibly the 3XFlag peptide.

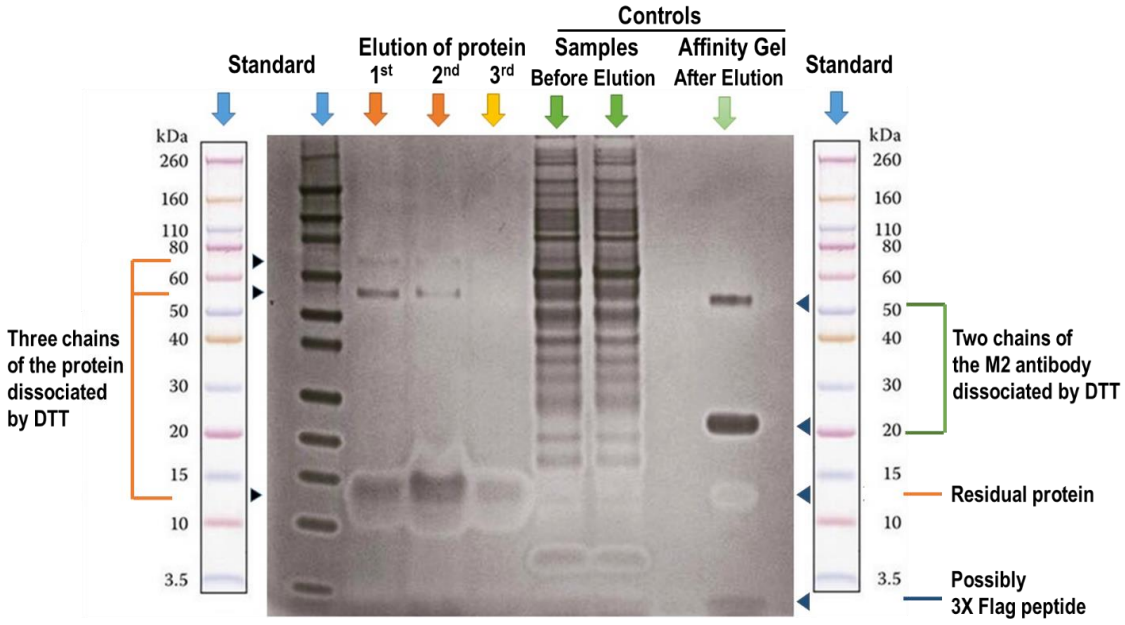


Figure 3.3. Eluted recombinant AMH and control samples were separated on a NuPAGE Tris-Acetate mini gel and stained with SimplyBlue™ Safe Stain. Standard: The Novex® Sharp Pre-Stained Protein Standard. DTT: Dithiothreitol. M2 antibody: purified murine IgG1 monoclonal antibody.

3.5 Discussion

Currently, availability of commercial recombinant AMH proteins are limited. Also, most commercial recombinant AMH is the carboxy terminal dimer part which is the bioactive domain. However, bioactivity might be influenced by the absence of the amino terminal part since the amino-terminal domain of AMH might enhance the serum half-life of the carboxy terminal domain and subsequently increase bioactivity (Wilson *et al*., 1993). Furthermore, successful production of full-length recombinant human AMH has been reported (Papakostas *et al.,* 2010). Therefore, in order to investigate the effect of AMH on primordial follicle activation in mice and human, we generated full-length rhAMH.

Different concentrations of rhAMH measured by the BCA assay and spectrophotometer may be due to the fact that the BCA assay method is not a true end-point method. While we were assessing the protein concentration, the color continued to develop.

The purified protein bands revealed by the stained gel are consistent with results from previous publications (Figure 3.4). This suggests that the protein we obtained is rhAMH.

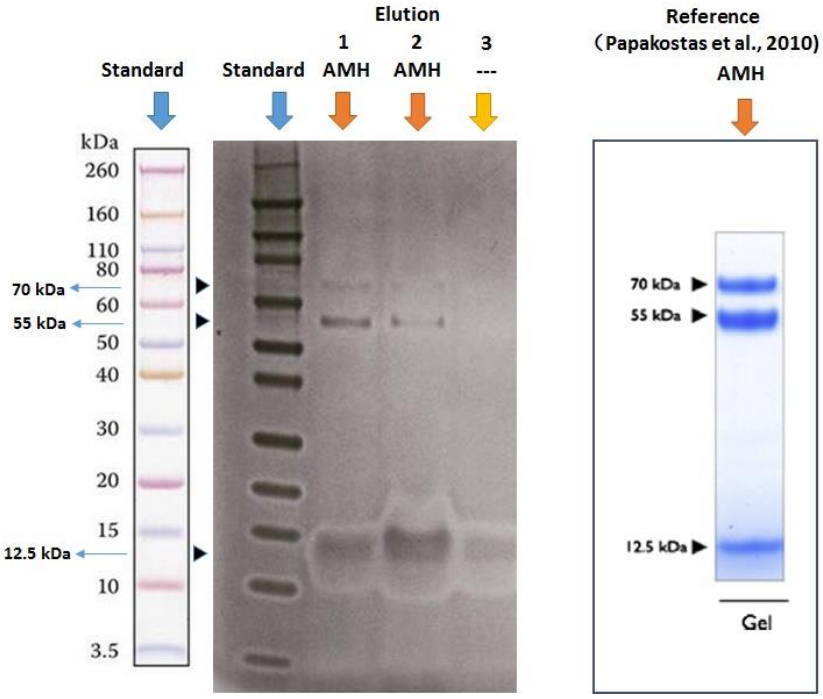


Figure 3.4. Purified recombinant AMH was separated and stained on a gel and was compared with the result from a previous publication. Standard: The Novex® Sharp Pre-Stained Protein Standard.

AMH is a glycoprotein dimer composed of two monomers linked by disulfide bridges (Belville *et al*., 2004). The separated chains of the protein revealed in the stained gel were dissociated by DTT. The N-terminal part and the C-terminal part of the protein which associate in a non-covalent fashion were separated by endogenous cleavage. The two darker bands at 12.5kDa and 55kDa compared to the 70kDa band indicates the majority of our recombinant AMH was cleaved endogenously. This is in line with a previous study, reporting over 60% of AMH being cleaved when expressed in HEK cells (Papakostas *et al*., 2010).

AMH, a protein containing 560 amino acids, consists of a secretion specific signal peptide of 25 amino acids and a monomeric protein of 535 amino acids. A cleavage motif has been reported presenting at residue 427 which might explain the appearance of the two

major bands (12.5kDa and 55kDa AMH fragments) appearing on the gel (Kim *et al.*, 2014).

However, as the total yield of generated rhAMH was calculated to be only approximately around 11 µg, which was only enough for 4-week AMH administration for one mouse, we did not continue to produce AMH. In consideration of the long generation time and the insufficient amount produced, we decided to purchase commercial recombinant mouse AMH (rmAMH) (Cusabio, China) used by Hayes *et al*. (2016) and commercial rhAMH (R&D systems, UK) for subsequent experiments.

Chapter 4: Investigation into the effect of Anti-Müllerian Hormone administration in pre-pubertal mice *in vivo*

4.1 Introduction

Cancer survivors may suffer long-term distressing sequelae induced by chemotherapy such as premature ovarian insufficiency (POI) and infertility. Protection of ovarian function before or at the time of cancer treatment has become particularly important. Chemotherapy-induced POI results from the accelerated demise of the finite primordial follicle pool, which is likely due to overactivation of the dormant primordial follicles rather than directly destroying them (Kalich-Philosoph *et al*., 2013); known as burnout as discussed in Section 1.4.2.3.

Treatment with Anti-Müllerian Hormone (AMH), a molecule produced by the granulosa cells of growing follicles, can preserve primordial follicle numbers by inhibiting primordial follicle activation in human ovarian tissue *in vitro* and in mouse ovarian tissue *in vitro* and *in vivo* (Durlinger *et al*., 2002; Carlsson *et al.*, 2006; Hayes *et al.*, 2016). Therefore, administration of AMH during chemotherapy treatment *in vivo* is likely to suppress primordial follicle activation and thus preserve the pool and subsequent fertility for cancer patients. Therefore we aimed to investigate the effect of AMH on preventing chemotherapy-induced primordial follicle loss using recombinant AMH.

However, the commercial recombinant mouse AMH (rmAMH) used by Hayes *et al*. (2016) was not prescribed for *in vivo* use. Although the research group administered this commercial AMH in mice *in vivo* for up to 28 days, they were the only research group to report using it *in vivo* at the time of this experiment (Hayes *et al*., 2016). For Gold Standard Practise, a pilot study was required in order to evaluate the safety of administrating a product not specified for *in vivo* use with repeated daily intra-peritoneal injections of 28 days in mice.

In an *in vivo* study (Hayes *et al.*, 2016), AMH treatment resulted in a significant decrease in the level of estrogen in pre-pubertal female mice which is possibly due to the

decreased percentage of growing follicles. However, estrogen deficiency might influence the onset of puberty since estrogen plays an important role in the onset of puberty in rats and humans (Ramirez and Sawyer, 1965; Ankarberg-Lindgren *et al.*, 2014). Therefore, the time to puberty in mice following exogenous AMH treatment would be assessed in our experiment. To our knowledge, this is the first study to investigate whether the administration of AMH perturbs the timing of the onset of puberty in mammals.

4.2 Aims

- To determine if repeated intra-peritoneal (IP) injections for 28 days adversely affect mouse behaviour and growth.
- To investigate the effect of rmAMH on ovarian function in mice *in vivo*.
- To investigate the effect of rmAMH on the onset of puberty in mice *in vivo*.

4.3 Materials and Methods

4.3.1 Mice

Female C57BL/6 mice (Biomedical Services, Oxford) aged 21 days were housed as described in Chapter 2 Section 2.2.

In order to identify the mice, each was ear-clipped from No.1 to No.12, and allocated into two groups according to body weight: Control group and AMH-treated group on Day 0.

4.3.2 Reagents

Normal saline (0.9% NaCl) was made using 0.9g sodium chloride (Fisher Scientific, UK) in 100ml H_2O. It was then sterile filtered using a vacuum unit filter (Corning, USA) in a Class II hood.

Lyophilized rmAMH (Cusabio, China) was reconstituted with sterile-filtered H_2O and stored at 0.1 mg/ml. For injection, the stock was further diluted with normal saline.

To confirm the dissolved lyophilized rmAMH contained the rmAMH. The protein was analysed using electrophoresis (described in Chapter 2 Section 2.7).

4.3.3 Administration

Mice were administered daily with rmAMH (300ng) in 200µl saline or saline only by IP injection for 28 days. The IP injection site was alternated daily between the left and right side to minimise repeated trauma to the injection sites.

4.3.4 Post-injection monitoring

Mouse behaviour and growth rate were assessed before and after each injection. Assessment of general condition and behaviours were carried out daily by observation and handling as described in Chapter 2 Section 2.2.4.

4.3.5 Observation of vaginal opening

The onset of puberty was assessed by a visual examination of the mouse vaginal opening from Day 0. The first date of vaginal opening was recorded and represented the age of the onset of puberty.

4.3.6 Ovaries collection

At the end of this experiment (28 days of IP injections of Saline or AMH), the mouse ovaries were collected and fixed as described in Section 2.5.1. After fixation, they were weighed using an electronic scale (Sartorius, German) and imaged under a microscope (Leica, German). They were delivered to the Oxford Centre for Histopathology Research for processing and embedding. However, all ovarian samples were damaged due to unexpected issues during processing by the facility.

4.3.7 Statistical Analysis

All data was analysed using GraphPad Prism version 7.00 (GraphPad Software, USA). Data was tested for normality using Shapiro-Wilk normality test. Results were presented as mean ± standard deviation (S.D.), with $P<0.05$ considered significant. A Mann-Whitney test was used if the data was not normality distributed. A T-test was used if the data passed the Shapiro-Wilk normality test. Two-way ANOVA was used to compare mouse body weight between the control and AMH groups during 28 days.

4.4 Results

4.4.1 Electrophoresis

According to the protein stain standard, the protein from the supernatant was 13 kDa. This is in line with the datasheet provided by the manufacturer, confirming that the supernatant contained rmAMH.

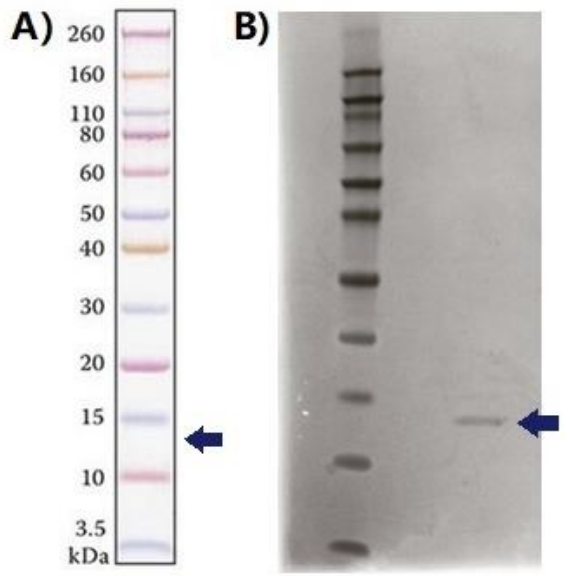


Figure 4.1. Dissolved rmAMH was ran on a NuPAGE Tris-Acetate mini gel and stained with SimplyBlue™ Safe Stain. A) The Novex® Sharp Pre-Stained Protein Standard; B) The stained gel of dissolved rmAMH (Cusabio).

4.4.2 Body weight changes and clinical signs

There were no differences between the two groups when comparing body weights during treatment and at sacrifice (Figure 4.2). The mouse body weights steadily increased in both groups.

Furthermore, daily pre- and post-injection health assessment showed that all mice were healthy during both treatments. They were active, curious with healthy coat and without any discharge from the eyes or nose.

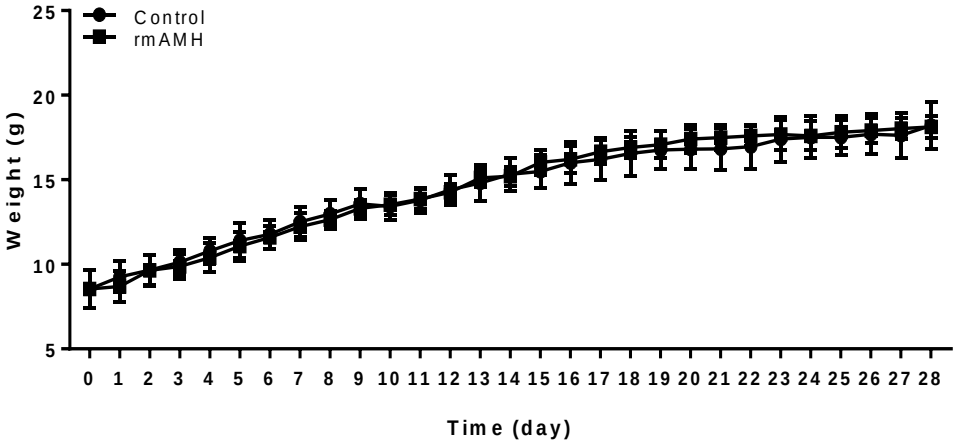


Figure 4.2. Body weight in mice intraperitoneally injected with normal saline or rmAMH for 28 days. Data were presented as Mean ± S.D. N=6 for each group.

4.4.3 Age at the onset of puberty (vaginal opening)

In mice treated with normal saline, vaginal opening was observed at post-natal Day 29±4.73. Vaginal opening of mice treated with rmAMH occurred at Day 32±0.52 (Figure 4.3). There is no difference between the two groups.

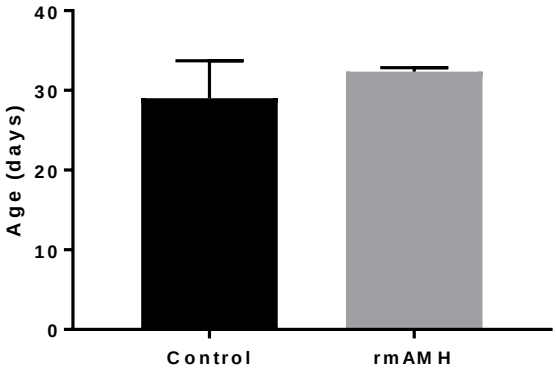


Figure 4.3. Age at vaginal opening in mice intraperitoneally injected with normal saline or rmAMH for 28 days. Data were present as Mean ± S.D. n=6 per group.

4.4.4 Morphology and weight of mouse ovaries

Upon collection, gross ovarian morphology was assessed by examination of the individual ovaries using the stereomicroscope. No difference was observed between the two groups regarding ovarian morphology, and developing follicles were observed in all ovaries (Figure 4.4 A-B).

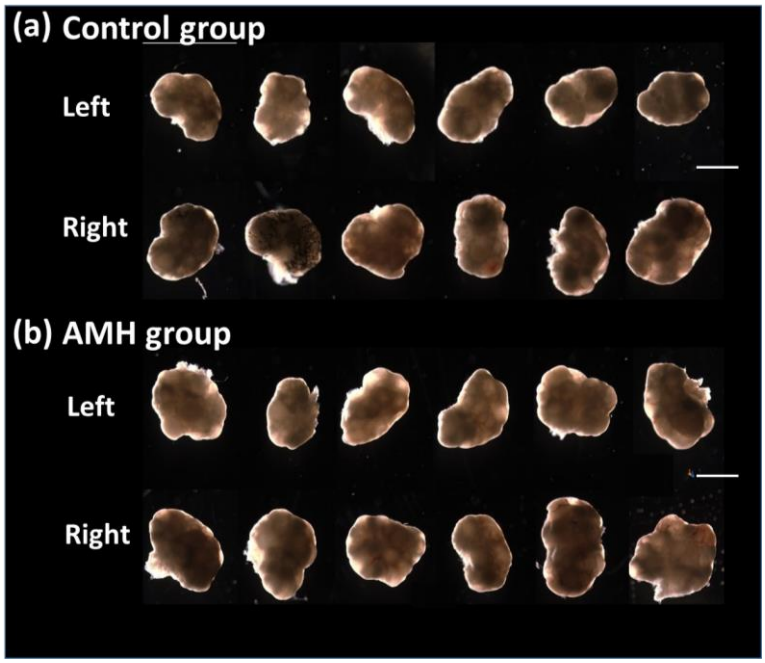


Figure 4.4. Mouse ovaries collected after 28-day daily intraperitoneal injections of saline or rmAMH. Representative images of ovaries from mice in the (a) control and (b) AMH groups. Scale bars represent 1mm.

There is no difference in weight between the left ovaries of the control mice (1.88±0.29mg, n=6), and the mice treated with rmAMH (2.03±0.6mg, n=6) at the time of sacrifice (Figure 4.5a), and similarly, with right ovary weight (2.5±0.47mg and 2.71±0.45mg, respectively, n=6) (Figure 4.5b). Interestingly, the right ovaries were found to be heavier in both groups compared to the left ovaries (Figure 4.5c-d).

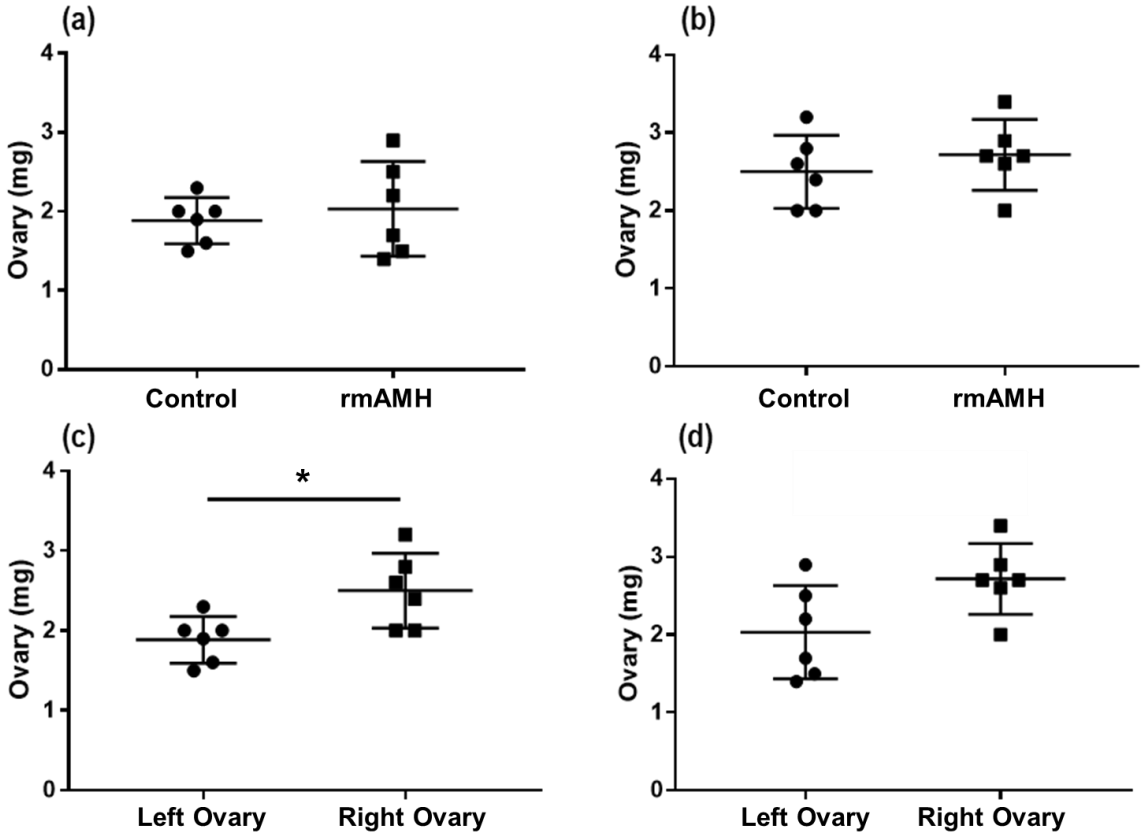


Figure 4.5. Left and right ovary weight of mice after 28-day daily intraperitoneal injections of saline or rmAMH. (a) Left ovary weight of mice treated with normal saline (n=6) or rmAMH (n=6). (b) Right ovary weight of mice treated with normal saline or rmAMH. (c) In mice treated with saline, a comparison of the left and right ovarian weights. (d) In mice administrated with rmAMH, comparisons between left and right ovarian weights. Data were present as Mean ± S.D. * $P<0.05$.

4.5 Discussion

In this study, we determined whether it is safe to administer the commercial AMH in mice *in vivo* for up to 28 days. Based on the assessment of mouse health, ovarian function and the onset of puberty after the AMH treatment, there was no adverse impact detected.

Effect of administrations of rmAMH on mouse health

It is well known that a health evaluation of research mice is included in screening potential toxic drugs *in vivo* (Karl *et al*., 2003). Changes in body weight and careful observation of mouse behaviour usually provide valuable information to assess health status. Using a range of tests, the safety of administration of AMH was therefore studied in this experiment.

Based on the data presented on body weight, administration of rmAMH in mice *in vivo* has no adverse effects. The mean mouse body weight was 18.2±1.4g in the control group (n=6) and 18.1±0.7g in the rmAMH treated group (n=6) at 7 weeks of age. These weights are consistent with reference body weights (18.2±1.1g at 7 weeks) of the same strain of female mice at The Jackson Laboratory (data available at https://www.jax.org/jax-mice-and-services/strain-data-sheet-pages/body-weight-chart-000664).

Similarly, the accumulated results of behavioural observations indicate that administration of rmAMH has no negative effects on mouse health. There is no difference found between mice treated with rmAMH or saline. AMH is a naturally generated hormone and it has been suggested to be used as a therapeutic agent for Müllerian duct origin cancers (Marca and Volpe, 2007). In addition, long-term AMH administration has been shown to be non-toxic and actually anti-carcinogenic (Meirelles *et al.*, 2012). Recombinant human AMH (home-made) was given IP in female mice for 5 days per week for 10 weeks (20 μg/animal/day) to examine whether AMH can inhibit tumor growth *in vivo* with no

detrimental effects reported (Pieretti-Vanmarcke *et al*., 2006). Therefore it could be concluded that rmAMH (Cusabio) administration in mice is safe.

Effect of repeated daily IP injections on mouse health

The accumulated results of the general health assessments, including body weight test and observations of mouse behaviour, indicate that daily IP injections up to 28 days have no adverse effects on mouse health. This is in line with previous study, where there were no adverse effects observed after daily injections of saline in female mice for 30 days (Davis *et al*., 2014).

Effect of administrations of AMH on the age of the onset of puberty

The onset of puberty represents the maturation of the hypothalamo-pituitary-gonadal axis, which can be characterized by increased levels of sex steroids and changes in circulating gonadotropins. However, it can be influenced both by genetic and external factors. Variation in the timing of onset of puberty is disadvantageous to health and is associated with increased risk of breast cancer (Day *et al*., 2015) or cardiovascular diseases (Prentice and Viner, 2013). In this experiment we determined the age at the onset of puberty in mice treated with saline and rmAMH by observation of the time of vaginal opening.

Vaginal opening is a reliable marker as it signifies the onset of puberty and is a non-invasive and quick method of assessment (Ojeda *et al*., 2006). The literature documented the mean age at vaginal opening of the C57BL/6 female mice is post natal day 31.7 ± 2.6 (n=298) (Rzeczkowska, 2012). In our experiment, the average age at vaginal opening detected has no difference between two groups and is in line with above publication at day 32±0.52, indicating that the administration of rmAMH does not influence the onset of puberty.

Effect of administration of rmAMH on ovarian function

Ovarian weight is an essential component for evaluation of ovarian function, and the ovary changes in size and activity throughout female reproductive life (Lass and Brinsden, 1999). In humans, there is continuous growth of the ovaries throughout childhood (Griffin *et al*., 1995). Ovarian volume and weight decreases in menstruating women from 40 years of age, and is further reduced in postmenopausal women (Lass and Brinsden, 1999).

Assessment of ovarian weight can reflect ovarian function. In some toxicity tests in rodents *in vivo*, degeneration of follicles were found in ovaries with deceased ovarian weight. In humans, ovarian weight is usually positively correlated with ovarian volume (Rosendahl *et al*., 2010). Changes in ovarian weight and volume provide valuable information for diagnosis and treatment in gynaecological and reproductive disorders.

In this experiment, no difference regarding ovarian weight was found between the rmAMH-treated group and the control group. The data presented therefore indicates that AMH administration has no adverse effects on ovarian function.

Right ovaries were heavier than left ovaries in mice

Interestingly, regardless of different treatment, right ovaries had higher ovarian weight than left ovaries, suggesting that an inequality exists between both sides. The inequality in reproductive function of the left and right ovaries in mice, sheep and dogs has been investigated in previous studies (Casida *et al*., 1966; Wiebold and Becker, 1987; Hayer *et al*., 1993); which showed that right ovaries were larger in size and contained more corpora lutea than left ovaries. This left-right difference in ovarian volume has also been observed in humans (Korsholm *et al*., 2017). The difference between left and right ovaries highlights the importance to analyse ovaries from the same side when comparing different individuals.

In addition, while designing experiments using IP injections, the importance of rotating injecting sites should not be neglected.

4.6 Conclusion

According to the assessment of mouse health, ovarian weight and the onset of puberty, we conclude that there is no adverse effect of administration of commercial rmAMH in pre-pubertal mice for up to 28 days. The commercial rmAMH was therefore used in the following studies.

Chapter 5: Investigation into the effects of Doxorubicin on primordial follicles in pre-pubertal mouse ovaries *in vitro*

5.1 Introduction

Chemotherapy induced premature ovarian insufficiency (POI) affects around 8 percent of female childhood cancer survivors both physically and psychologically (Sklar *et al*., 2006). One of the most commonly used gonadotoxic chemotherapeutic agents is doxorubicin (DXR). DXR is an anthracycline antitumor antibiotic either used alone or involved in combination with other chemotherapeutic agents for up to 50% of all cancers, including childhood cancers such as thyroid cancer, leukaemia, lymphoma, neuroblastoma and Wilm's tumors (Roti *et al*., 2014). The wide usage of DXR has led to an increased demand for research to prevent DXR-induced POI.

DXR kills cells by inducing double strand DNA breaks and oxidative stress as discussed in Chapter 1. Clinical studies have shown that up to 80% of women treated with a regimen that included DXR, developed permanent amenorrhea with various incidences depending on age (Lee *et al*., 2006). In animal studies, there is a significant reduction in the population of ovarian follicles including primordial follicles following DXR treatment *in vitro* and *in vivo* (Morgan *et al*., 2013; Roti *et al*., 2012). However, there is no robust evidence to show any direct action on primordial follicles as discussed in Chapter 1. The decrease of primordial follicle numbers might be due to replenishment of the diminished numbers of growing follicles in the growing follicle pool. Therefore, if primordial follicles could be preserved during DXR treatment, patients treated with DXR would be prevented from developing POI.

In order to establish an appropriate dose for DXR-induced primordial follicle loss *in vitro*, a preliminary experiment was performed. Pre-pubertal mouse ovaries were used as the research model due to the high proportions of primordial follicles. Previous publications have cultured neonatal mouse ovaries to investigate the effects DXR on primordial follicles (Morgan *et al*., 2013). However, germ cell nests have not all completed their transition to

individual primordial follicles until postnatal day 6 (PND 6) in mice (Pepling and Spradling, 2001; Bristol-Gould *et al*., 2006). In order to investigate the effect of DXR on primordial follicles in pre-pubertal mice, ovaries from PND 6 pups were used. To our knowledge, this is the first study to investigate the effects of DXR on pre-pubertal mouse ovaries after primordial follicle assembly.

5.2 Aims

- To determine the effect of DXR on primordial follicle loss in postnatal day 6 mice *in vitro*.
- To compare three different dosages of DXR on postnatal day 6 ovaries *in vitro*.

5.3 Materials and Methods

5.3.1 Mice

Postnatal day 6 female pups were generated from CD1 x C57BL6 matings (described in Section 2.2.1).

5.3.2 Mating

Mating was confirmed by the presence of a vaginal plug (described in Section 2.2.1).

5.3.3 Ovarian culture

Postnatal day 6 ovaries (n=14) from 7 female pups were dissected and cultured for 6 days (described in Section 2.4).

5.3.4 DXR administration

DXR (Sigma) was dissolved in sterile water and filtered using a 0.22 µm filter unit. The DXR was added on the second day of culture for 24 hours at concentrations of 0, 50, 100 and 200 ng/ml (in 20 µl sterile water). Same amount of sterile water was added into the control group. On day 3, all ovaries were transferred to a new well containing pre-equilibrated control culture medium with a new membrane for the remaining 4 days of culture to ensure complete removal of DXR.

5.3.5 Histology

Following culture, ovaries were fixed in 10% neutral buffered formalin (Sigma) for 6 hours and stored at 4°C in 70% ethanol overnight. The tissue was then processed and

embedded in paraffin (described in Section 2.6.2). All tissues were serially sectioned at 5µm, and every 10th section was stained with haematoxylin and eosin (described in Section 2.6.4).

Within healthy follicles (intact oocyte with no pyknotic bodies in granulosa cells), primordial follicles were recognised as an oocyte surrounded by a single layer of flattened pre-granulosa cells. Primordial follicles with a visible nuclear were counted in every 10th section. The total number of healthy primordial follicles was calculated using the Abercrombie correction factor (Abercrombie, 1946) as described in Section 2.6.6.3. Follicles with a visible nucleus in the middle section of each ovary were selected for oocyte nucleus area measurement using Image J, as these measurements were required for Abercrombie correction.

The ovarian area of every 10th section was measured using Image J. Ovarian volume was calculated using total ovarian area multiplied by the thickness of section and the interval number. All ovaries were analysed blindly.

5.3.6 Statistical Analysis

All data was analysed using GraphPad Prism version 7.00 (GraphPad Software, USA). Data was tested for normality using a Shapiro-Wilk normality test. One-way ANOVA was applied to determine whether differences were present across different dosage treatments. Results are presented as Mean ± S.E.M. Significance was considered when $P<0.05$.

5.4 Results

5.4.1 Histology

In all groups, only follicles at primordial (Figure 5.1A), transitional (Figure 5.1B), primary (Figure 5.1C) and secondary stages (Figure 5.1D) were observed. There were no antral follicles observed in the Day 6 cultured ovaries.

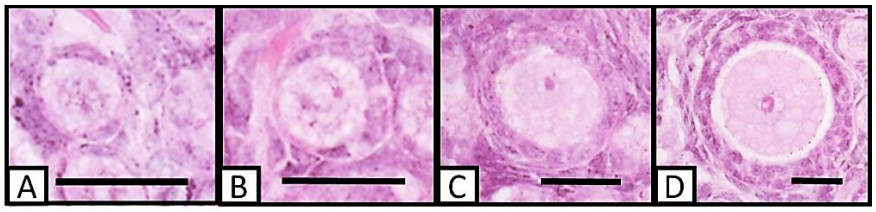


Figure 5.1. Examples of follicles at the different stages of development in the Day 6 cultured mouse ovaries stained with H and E. A) Primordial follicle: an oocyte surrounded by flattened pre-granulosa cells. B) Transitional: one or more of the surrounding granulosa cells are cuboidal. C) Primary: one complete layer of cuboidal granulosa cells around the oocyte. D) Secondary: more than one layer of granulosa cells. Scale bars represent 25μm.

Primordial follicles were mostly located at the edge of ovaries in clusters (Figure 5.2).

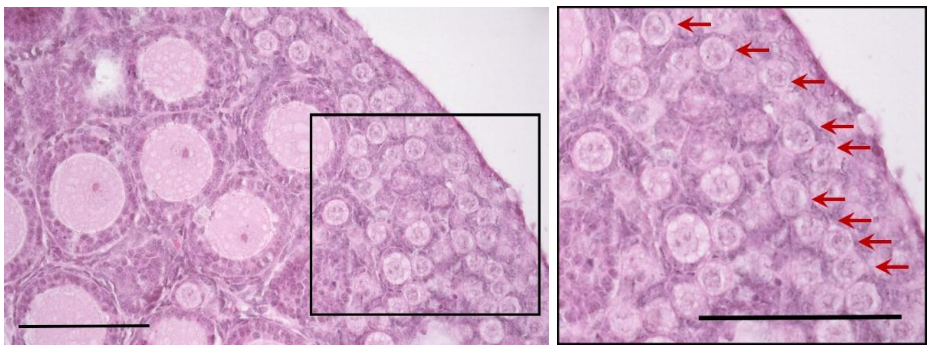


Figure 5.2. Location of primordial follicles in the Day 6 cultured mouse ovaries stained with H and E. Red arrows indicate primordial follicles. Scale bars represent 100μm.

Based on H and E stain, unhealthy follicles showed a significant altered morphology as illustrated in Figure 5.3.

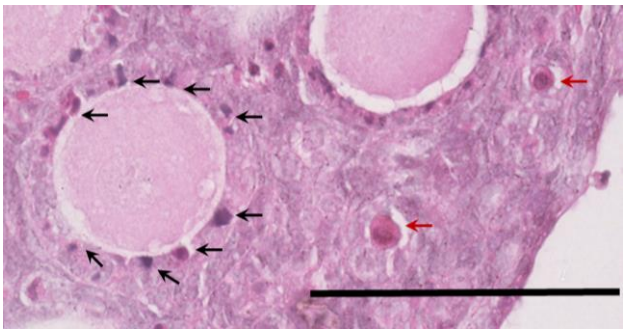


Figure 5.3. An example of unhealthy follicles in the Day 6 cultured mouse ovaries stained with H and E. The secondary follicle contains a healthy oocyte but is surrounded with numerous pyknotic granulosa cells (black arrows). Two transitional follicles with atretic oocytes (pyknotic nuclear with shrunken cytoplasm) (red arrows). Scale bar represents 100μm.

Unhealthy follicles were most frequently found in DXR cultured ovaries (Figure 5.4).

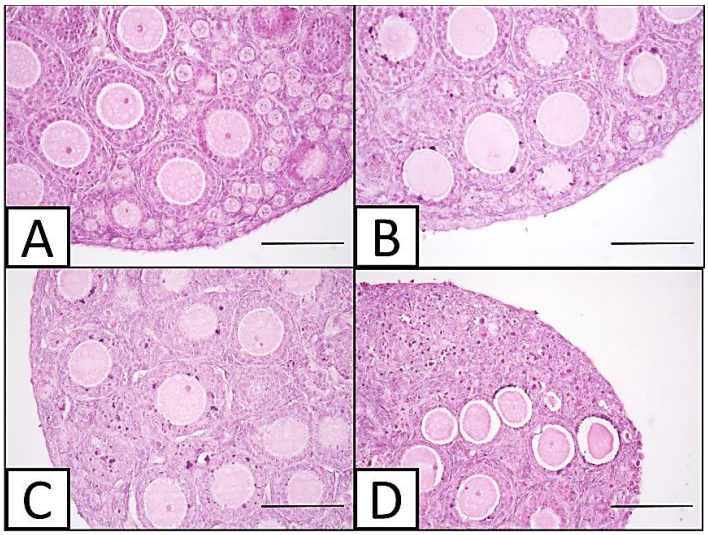


Figure 5.4. Representative images of H and E stained sections from mouse ovaries cultured with different concentrations of DXR. (A) 0ng/ml DXR (Control). (B) 50ng/ml DXR. (C) 100ng/ml DXR. (D) 200ng/ml DXR. Scale bars represent 100μm.

Unhealthy follicles were found at the transitional, primary and secondary stages. It could not be concluded whether primordial follicles were influenced, as in atretic follicles, it was often difficult to distinguish whether the small unhealthy follicle was at the transitional or primordial stage. However, healthy primordial follicles were observed in DXR-cultured ovaries (Figure 5.5).

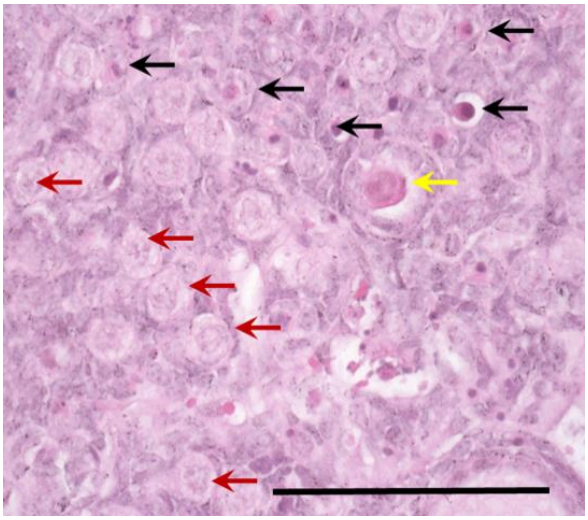


Figure 5.5. An example of unhealthy follicles in the Day 6 cultured mouse ovaries stained with H and E. Red arrows point to healthy primordial follicles, black arrows point to either transitional or primordial. Yellow arrow points to a primary follicle with a pyknotic oocyte. Scale bar represents 100μm.

5.4.2 The effect of DXR on primordial oocyte nuclear diameter

There was no difference observed in oocyte nuclear diameter of healthy primordial follicles between the different concentrations of DXR (Figure 5.6).

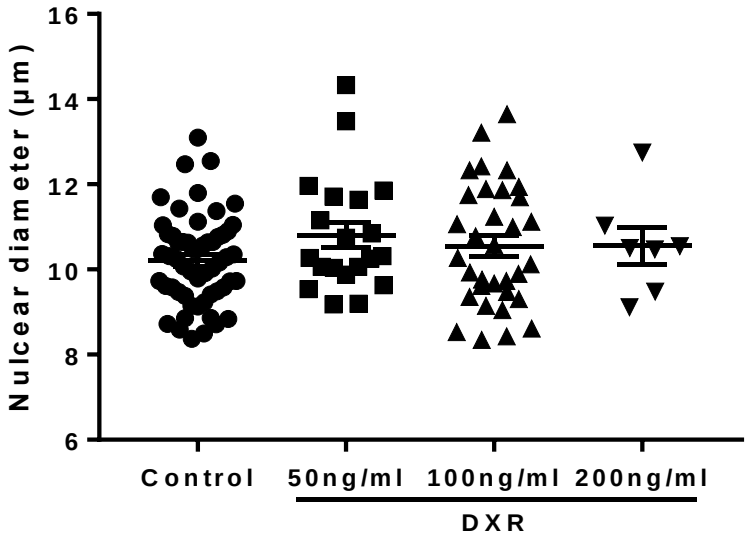


Figure 5.6. Primordial follicle oocyte nuclear diameters in mouse ovaries treated with different concentrations of DXR. There was no difference between each group. Data was presented as Mean ± S.E.M. Control n=3; N=56 follicles. 50ng/ml DXR n=3; N=20 follicles. 100ng/ml DXR n=5; N=33 follicles. 200ng/ml DXR n=3; N=7 follicles.

5.4.3 The effect of DXR on primordial follicle numbers

Comparisons of primordial follicle numbers were made between the control group ovaries and those exposed to varying DXR concentrations. Compared to the control group, ovaries cultured with DXR at the three different dosages had decreased numbers of primordial follicles (Figure 5.7).

Furthermore, within the DXR treated groups, ovaries cultured with DXR at 50ng/ml had significantly more primordial follicles than ovaries cultured with 100ng/ml and 200ng/ml of DXR (Figure 5.7). No further differences were observed when comparing primordial follicles in ovaries cultured with 100ng/ml and 200ng/ml of DXR.

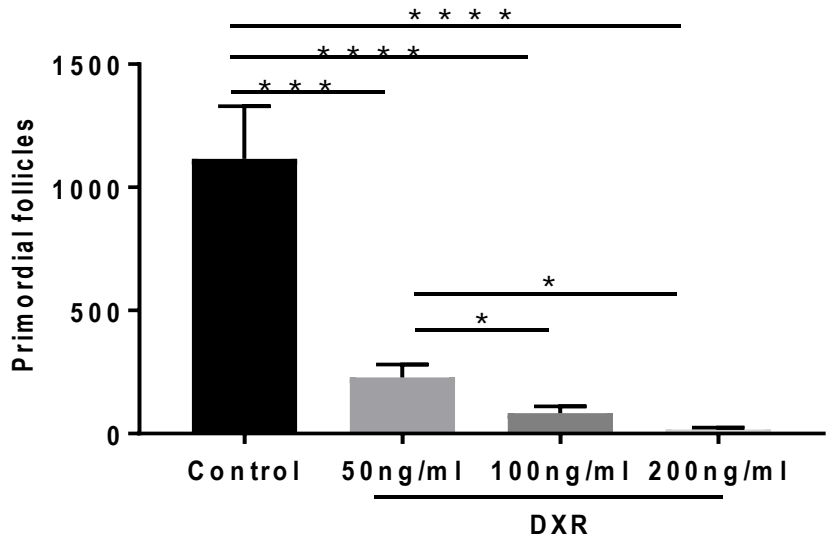


Figure 5.7. Total number of healthy primordial follicles in mouse ovaries treated with different concentrations of DXR. Values are presented as Mean ± S.E.M. *P<0.5. ***P<0.001. ****P<0.0001. Control n=3; 50ng/ml DXR n=3; 100ng/ml DXR n=5; 200ng/ml DXR n=3.

5.4.4 The effect of DXR on mouse ovarian volumes

The volumes of control group ovaries and those exposed to varying DXR concentrations were compared. First, when compared to the control group, ovaries exposed to DXR at 200ng/ml in the second day of culture were much smaller (Figure 5.8). When comparing ovary volumes within the DXR treated groups, ovaries cultured with DXR at 200ng/ml were smaller than those treated at 50ng/ml of DXR.

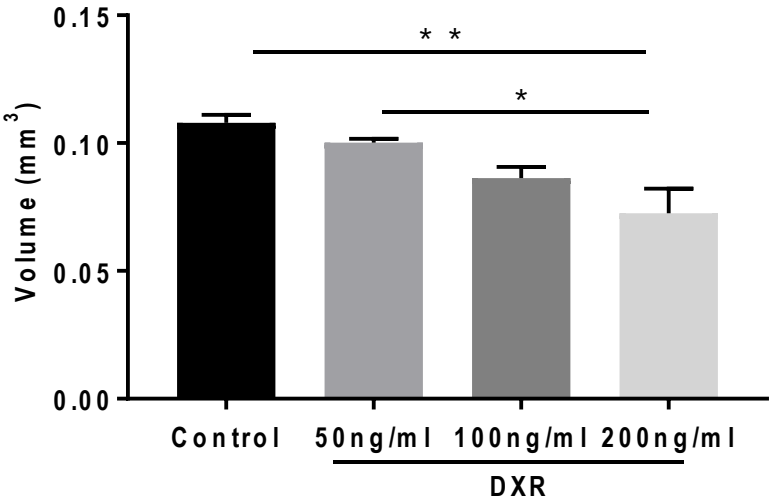


Figure 5.8. **Volume of mouse ovaries treated with different concentrations of DXR after 6 days of culture.** Values are present as Mean ± S.E.M. *$P<0.05$ **$P<0.01$. Control n=3; 50ng/ml DXR n=3; 100ng/ml DXR n=5; 200ng/ml DXR n=3.

5.5 Discussion

In this experiment, we determined the effect of DXR on pre-pubertal mouse ovarian tissue *in vitro*. Based on the results, we observed that DXR resulted in primordial follicle loss in a dose dependent manner.

Effect of DXR on primordial follicles

DXR has been linked to inducing POI due to a decreased ovarian reserve after treatment. Dosage of chemotherapy treatments are known to influence the risk of developing POI following chemotherapy (Chiarelli *et al.*, 1999). In our experiment, ovaries cultured with DXR showed a significant reduction in primordial follicle population in a dose-dependent manner. Dose-dependent effects of chemotherapy on primordial follicle loss in mice are also in line with previous publications (Meirow *et al.*, 1999; Morgan *et al*., 2013). The concentration of DXR used in this experiment (50, 100 and 200ng/ml) are within the plasma range for cancer patients (20-600ng/ml) (Table 1.4; Chapter 1) (Barpe *et al.*, 2010).

Morphologically, in some very small follicles prior to the primary stage, classification of unhealthy follicles between primordial and transitional stages was not possible. However, unhealthy follicles at primary and secondary stages were clearly found in DXR treated ovaries. Additionally, despite a significant loss of primordial follicles, morphological healthy primordial follicles were observed in DXR treated ovaries with no difference in primordial oocyte nuclear diameters compared to control ovaries.

The mechanisms of chemotherapy-induced primordial follicle loss have not been precisely defined. So far, there is no robust evidence to show any direct action of DXR on primordial follicles. In human ovarian tissue treated with DXR *in vitro* and xenografted into mice, apoptosis and DNA damage were reported in primordial follicles (Soleimani *et al.*, 2011). However, in their study, a much higher concentration of DXR (100µg/ml) was used

compared to patient plasma levels, and no follicles were classified as transitional. According to the pictures illustrated in their paper, transitional follicles seem to be counted as primordial follicles.

Although there was a significant reduction in primordial follicle numbers in all DXR groups, there were still some healthy primordial follicles remaining after the exposure to DXR in the present experiment. This indicates the possibility of an indirect damage caused by DXR on primordial follicles, which might be due to the up-regulating activation of the primordial follicles to replace those growing follicles killed by chemotherapy (Morgan *et al*., 2012; Kalich-Philosoph *et al*., 2013). This is known as the burn-out hypothesis (discussed in Chapter 1).

Effect of DXR on ovarian volume

Changes in ovarian volume with DXR treatment *in vitro* was in line with a previous publication in mice *in vivo* (Ben-Aharon *et al*., 2010). There was a sharp decline in ovarian size after DXR treatment observed by *in vivo* imaging which was supported by a decline in ovarian weight. The ovarian volume changes observed in this experiment are consistent with the dose-dependent toxicity of DXR on ovarian reserve.

5.6 Conclusion

In this study, DXR induced a significant reduction of primordial follicle numbers and ovarian volume in pre-pubertal mouse ovarian tissue in a dose-dependent manner. Based on the results in this experiment, a dosage of 50ng/mg was chosen for next experiment (Chapter 6) as it is the lowest concentration to show an effect on primordial follicle numbers. In addition, it is within the plasma range of cancer patients during the first day after DXR treatment (Table 1.4; Chapter 1).

Chapter 6: Investigation of the effects of Anti-Müllerian Hormone on prevention of Doxorubicin-induced primordial follicles loss in pre-pubertal mouse ovaries *in vitro*

6.1 Introduction

Gonadotoxic chemotherapeutic agents such as doxorubicin (DXR) contribute to an increased long-term survival rate of childhood cancer patients whereas they also bring side effects such as premature ovarian insufficiency (POI). Anti-Müllerian Hormone (AMH) has been shown to attenuate primordial follicle loss *in vitro* and *in vivo*, possibly through the prevention of primordial follicle activation (Durlinger *et al*., 2002; Carlsson *et al*., 2006, Hayes *et al*., 2016). The signalling pathway of AMH is initiated when it binds to its specific receptor (AMH receptor II), a mechanism which differs from chemotherapy agents. Thus, AMH should not affect the functional pathway of chemotherapy agents to kill cancer cells (McLennan and Pankhurst, 2015).

AMH has been used in conjunction with chemotherapy *in vitro*, where it has been reported that 2h co-treatment of mouse ovaries with AMH and Cyclophosphamide metabolite (phosphoramide mustard) results in less primordial follicle loss than use of Cyclophosphamide metabolite only (Roness *et al*., 2015; Roness *et al*., 2016). However, whether AMH can prevent primordial follicle loss in conjunction with DXR had not been determined prior to this investigation.

DXR is widely used for the treatment of common childhood cancers such as leukaemia and Wilm's tumour (Roti *et al*., 2014). DXR-induced diminished ovarian reserve at the lowest dose of 50 ng/ml has been verified in Chapter 5. Therefore, it is important to determine whether or not AMH has an inhibitory effect on DXR-induced primordial follicle loss in pre-pubertal mouse ovaries, which has not been investigated so far.

Currently, only a few sources of commercial AMH are available. In order to investigate the effect of AMH on ***human*** ovarian tissue in the future, recombinant human AMH (rhAMH) from R&D system was used in addition to the recombinant mouse AMH (rmAMH) (Cusabio) used in Chapter 4. The bioactivity of rmAMH (Cusabio) has been

demonstrated in a previous publication (Hayes *et al*., 2016) whereas previous studies of rhAMH (R&D systems) have conflicting descriptions of its bioactivity (Nilsson *et al*., 2011; Xu *et al*., 2016; Kano *et al*., 2017). Thus, testing the bioactivity of commercial rhAMH was also an aim of this experiment.

6.2 Aims

- To determine the effects of rmAMH and rhAMH at different doses on attenuating primordial follicle decline and preventing DXR-induced primordial follicle loss in pre-pubertal mouse ovaries *in vitro*.
- To compare the efficacy of rmAMH and rhAMH on attenuating primordial follicle decline and DXR-induced primordial follicle loss in pre-pubertal mouse ovaries *in vitro*.
- To determine the bioactivity of rhAMH (R&D Systems).

6.3 Materials and Methods

6.3.1 Mice

F1 postnatal day 6 female mice (CD1 x C57BL6), were used in this experiment (described in Section 2.2.1).

6.3.2 Reagents

Lyophilized rmAMH (Cusabio, China) and rhAMH (R&D systems) were reconstituted in 10% 4mM hydrochloric acid (Sigma) with 90% Dulbecco's Phosphate-Buffered Saline (DPBS) within a class II fume hood to produce stock solutions at 100µg/ml.

6.3.3 AMH concentration test

Since there were small amounts of what appeared to be unreconstituted protein after rmAMH (Cusabio) had been dissolved, a BCA assay was performed in order to determine the concentration of protein in the reconstituted rmAMH and rhAMH using a NanoDrop ND-1000 spectrophotometer (Thermo fisher scientific, UK). The mini-BCA assay (which is capable of detecting protein concentrations within a range of 0.01-20mg/ml) is ideal for concentration tests of the reconstituted rmAMH and rhAMH, with an estimated concentration at 0.1mg/ml.

A set of standards with a range of 0.01-0.016mg/ml was made using serial dilutions of Bovine Serum Albumin (Fisher Scientific, UK) in 10% 4mM HCL with 90% PBS. An example of a generated standard curve is illustrated in Figure 6.1.

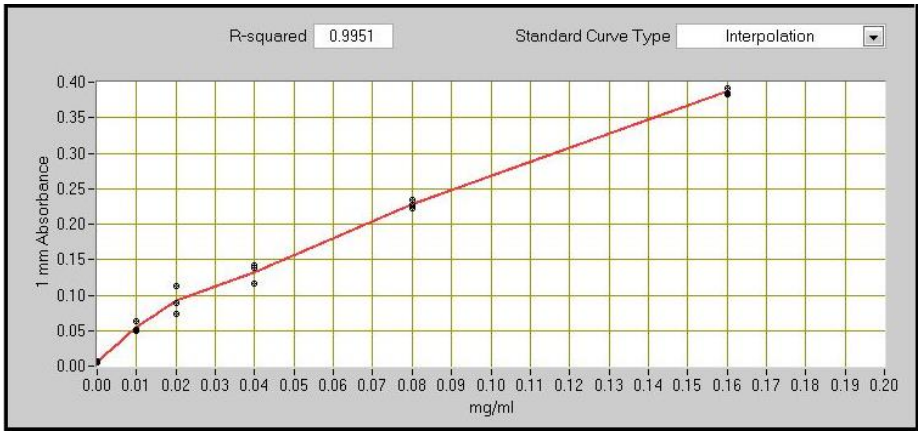


Figure 6.1. Standard curve for the BCA protein assay generated using six concentrations of BSA. This is an example of the standard curve generated with a high correlation coefficient (R^2>0.99). The average concentrations of assayed rmAMH and rhAMH were 0.089mg/ml and 0.097mg/ml respectively.

6.3.4 Ovarian culture

Postnatal day 6 ovaries were dissected and cultured for 6 days as described in Chapter 2. From the beginning of the culture (Day 0), either rmAMH or rhAMH was added to the media at concentrations of 50, 100 or 200ng/ml (in 20µl DPBS). Same amount of DPBS was added into the Control and DXR groups. At Day 2 of culture, DXR was added to produce a concentration of 50ng/ml for 24 hours only and replaced entirely after 24 hours with tissue moved into a new well containing fresh media to eliminate all trace of DXR. The culture media was changed every two days.

6.3.5 Histological analysis

Ovaries were collected at the end of culture and fixed in 10% buffered formalin solution. They were processed, embedded and sectioned serially at 5µm as described in Section 2.6.1-3. Every 10th section of ovarian tissue was stained with haematoxylin and eosin (Section 2.6.4). Follicle health status was assessed as described in Section 2.6.6.2.

Primordial follicles were recognised as an oocyte surrounded by a single layer of flattened pre-granulosa cells. Primordial follicles with a visible nucleus were then counted in every 10^{th} section, and the number per ovary were determined using the Abercrombie correction factor (Section 2.6.6.3). Primordial follicle oocyte nuclear area was measured using Image J software. All analyses were carried out blind.

6.3.6 Statistical analysis

All data was analysed using GraphPad Prism version 7.00. Data was tested for normality using the Shapiro-Wilk normality test. One-way ANOVA was applied to determine if there were differences across different treatments groups or the different dosage treatments for groups generated normally distributed data. If the data of groups were not normally distributed, the Kruskal Wallis test and the Dunn's multiple comparisons test were used. When comparing two groups, the Mann-Whitney U test was used if the data was not normally distributed.

These results are presented as mean ± S.E.M. for multiple comparisons and as mean ± S.D. for a comparison between two independent groups. Significance was considered when $P<0.05$.

6.4 Results

6.4.1 The effect of DXR on primordial follicles

First, the effect of DXR on the total number of healthy primordial follicles was established. Comparisons between the two groups revealed that the total number of healthy primordial follicles was lower in DXR-treated ovaries when compared to ovaries in the control group (Figure 6.2).

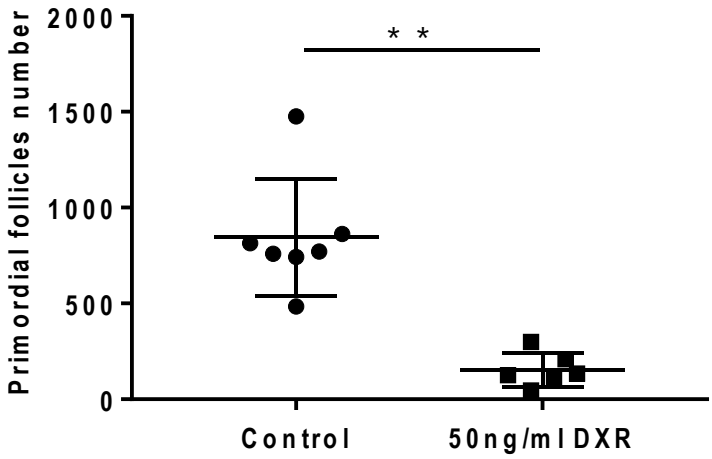


Figure 6.2. Primordial follicle numbers in mouse ovaries cultured with DXR at 0 or 50 ng/ml. Values represent Mean ± S.D. ***P*<0.01. Control n=7; DXR n=6.

6.4.2 Ovarian culture with rmAMH

6.4.2.1 Histology

First, ovarian histology was assessed in the ovaries that had been treated with rmAMH +/- DXR. Representative pictures of ovarian tissue sections stained with haematoxylin and eosin from each group are shown in Figure 6.3. Unhealthy follicles were frequently observed in the ovaries that were exposed to DXR, regardless of rmAMH concentration used (Figure 6.3).

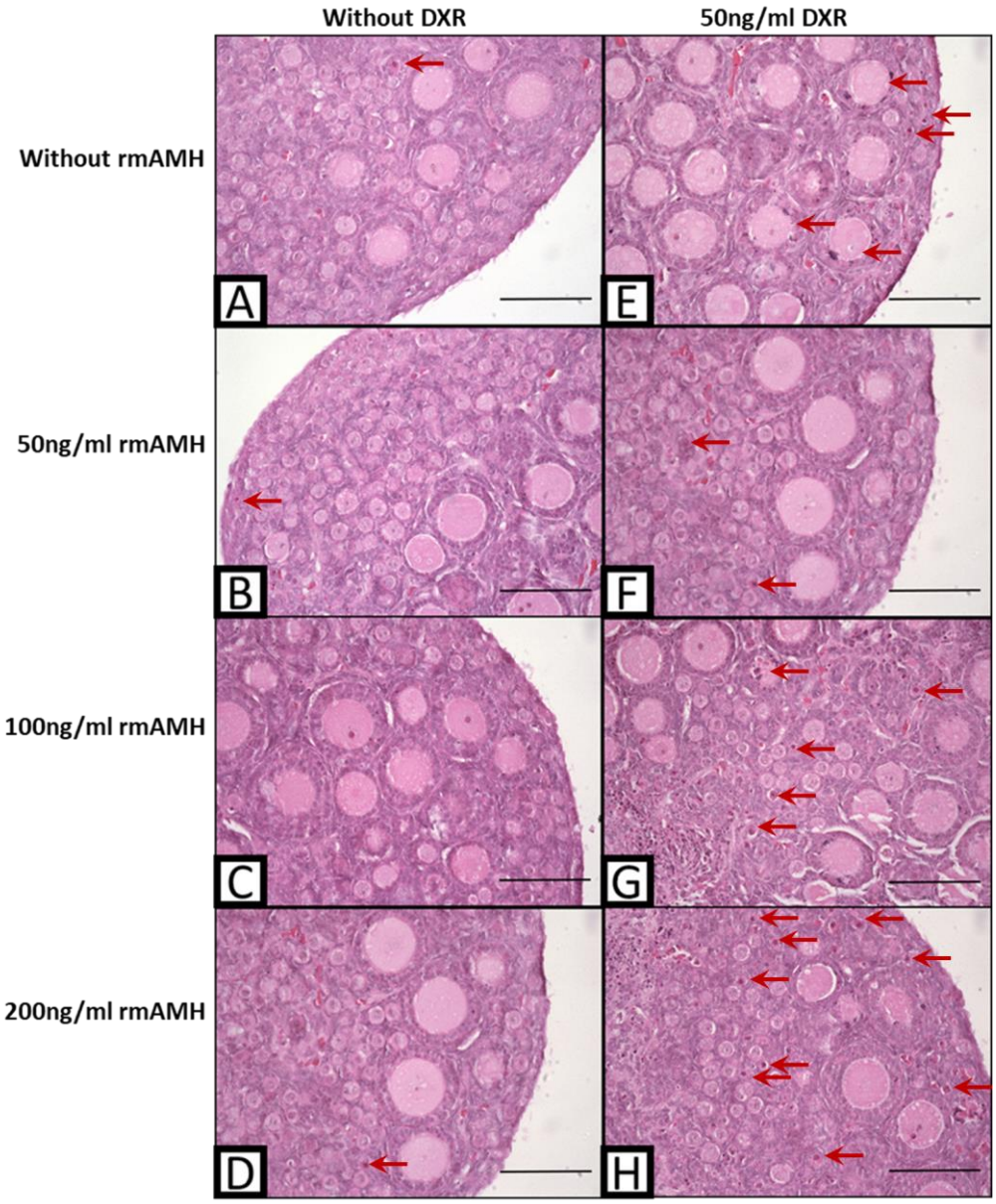


Figure 6.3. Representative ovarian tissue section micrographs of mouse ovaries cultured with different concentrations of rmAMH and with or without exposure to DXR. A) Control ovaries n=7. B-D) Ovaries cultured with rmAMH at concentrations of 50ng/ml (n=6), 100ng/ml (n=7) and 200ng/ml (n=7). E) Ovaries treated with 50ng/ml DXR (n=6). F-H) Ovaries co-treated with DXR and rmAMH at 50ng/ml (n=4), 100ng/ml (n=5) and 200ng/ml (n=4). Sections stained with H and E. Red arrows denote unhealthy follicles as indicated by a pyknotic oocytes or more than 10% pyknotic granulosa cells. Bars represent 100μm.

Primordial oocyte nuclear area was measured for each different treatment group. No differences were found either between the control and treatment groups, or within each of the groups themselves (Figure 6.4).

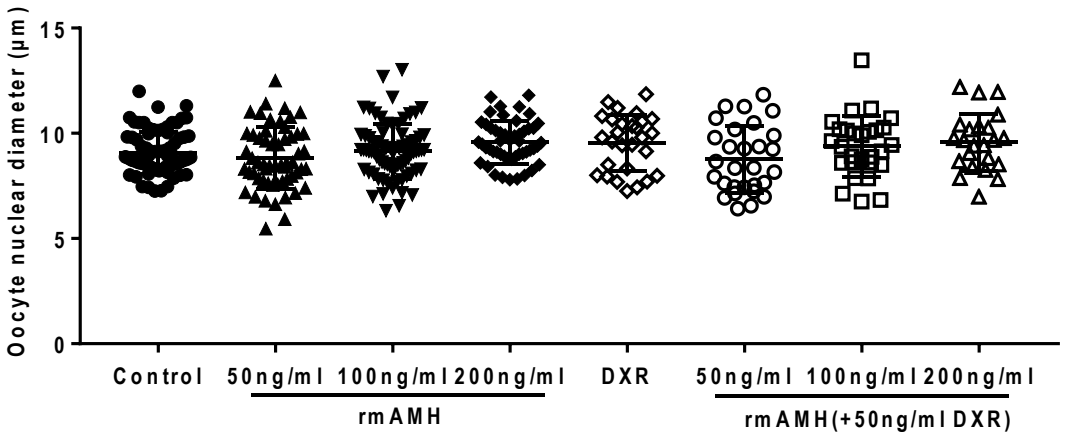


Figure 6.4. Primordial follicle oocyte nuclear diameters in mouse ovaries cultured with different concentrations of rmAMH and with or without exposure to DXR. There was no difference between each group. Data was presented as Mean ± S.E.M. Control ovaries n=7. Ovaries cultured with rmAMH at 50ng/ml (n=6), 100ng/ml (n=7) and 200ng/ml (n=7). Ovaries treated with 50ng/ml DXR (n=6). Ovaries co-treated with DXR and rmAMH at 50ng/ml (n=4), 100ng/ml (n=5) and 200ng/ml (n=4).

6.4.2.2 The effect of rmAMH on DXR-induced primordial follicles loss

Total number of primordial follicles were counted and corrected using the Abercrombie correction. No difference in the total number of primordial follicles was observed in rmAMH-treated ovaries in comparison with the ovaries in the control group (Figure 6.5).

Similarly, no differences in the total number of primordial follicles were observed in the rmAMH and DXR cotreated ovaries, in comparison with the ovaries in the DXR group.

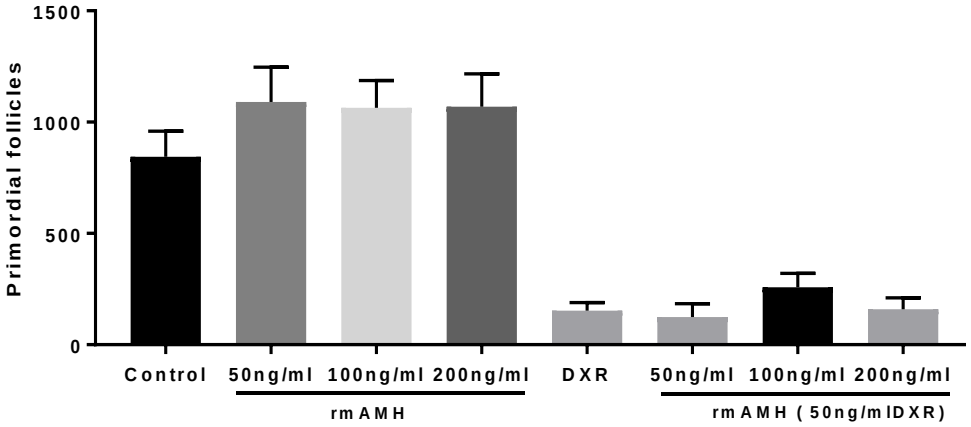


Figure 6.5. Primordial follicle numbers in mouse ovaries cultured with different concentrations of rmAMH and with or without exposure to DXR. Data was presented as Mean ± S.E.M. Control ovaries (n=7). Ovaries cultured with rmAMH at 50ng/ml (n=6), 100ng/ml (n=7) and 200ng/ml (n=7). Ovaries treated with 50ng/ml DXR (n=6). Ovaries co-treated with DXR and rmAMH at 50ng/ml (n=4), 100ng/ml (n=5) and 200ng/ml (n=4).

6.4.3 Ovarian culture with rhAMH

6.4.3.1 Histology

The analysis conducted in the experiment using the rmAMH was then repeated using the rhAMH. Representative pictures of ovarian tissue sections stained with haematoxylin and eosin from each group are shown in Figure 6.6. Once again, unhealthy follicles were frequently observed in ovaries that had been exposed to DXR, regardless of the rhAMH concentration used (Figure 6.6).

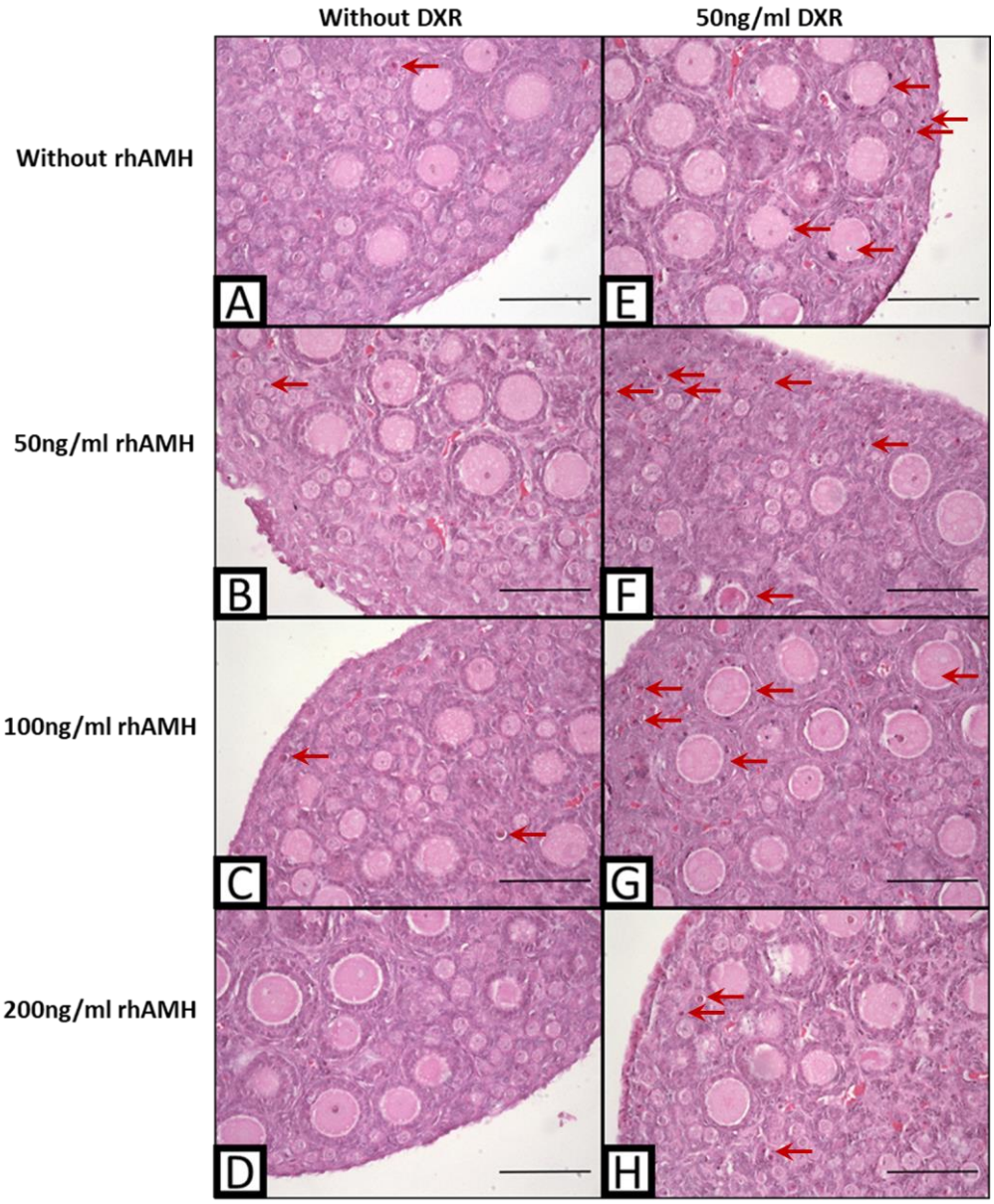


Figure 6.6. Representative ovarian tissue section micrographs of mouse ovaries cultured with different concentrations of rhAMH and with or without exposure to DXR. A) Control ovaries n=7. B-D) Ovaries cultured with rhAMH at concentrations of 50ng/ml (n=4), 100ng/ml (n=5) and 200ng/ml (n=5). E) Ovaries treated with 50ng/ml DXR (n=6). F-H) Ovaries co-treated with DXR and rhAMH at 50ng/ml (n=5), 100ng/ml (n=3) and 200ng/ml (n=3). Sections stained with H & E. Red arrows denote unhealthy follicles as indicated by a pyknotic oocytes or more than 10% pyknotic granulosa cells. Bars represent 100μm.

Similarly, no differences in the primordial oocyte nuclear area were found either between the control and treatment groups, or within each of the groups (Figure 6.7).

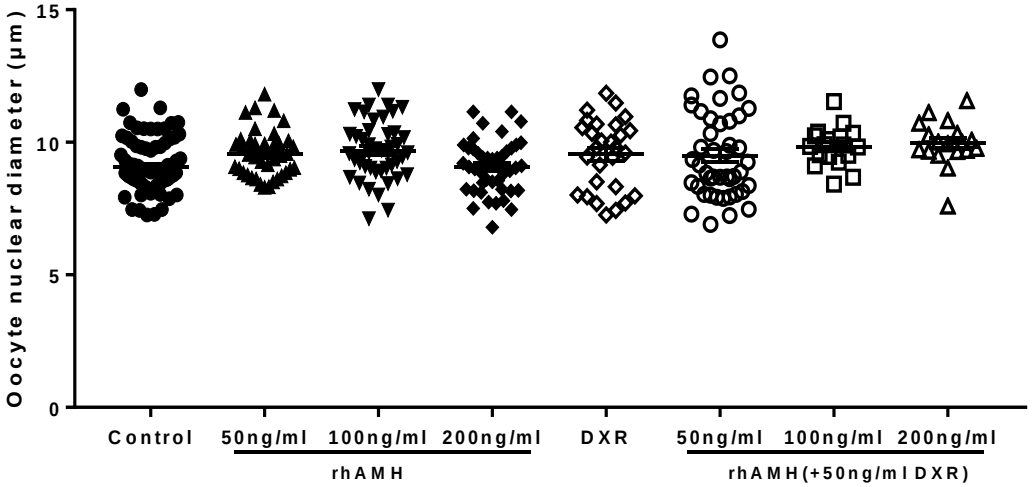


Figure 6.7. Primordial follicle oocyte nuclear diameters in mouse ovaries mouse ovaries cultured with different concentrations of rhAMH and with or without exposure to DXR. Data was presented as Mean ± S.E.M. Control ovaries n=7. Ovaries cultured with rhAMH at concentrations of 50ng/ml (n=4), 100ng/ml (n=5) and 200ng/ml (n=5). Ovaries treated with 50ng/ml DXR (n=6). Ovaries co-treated with DXR and rhAMH at 50ng/ml (n=5), 100ng/ml (n=3) and 200ng/ml (n=3).

6.4.3.2 The effect of rhAMH on DXR-induced primordial follicle loss

The total number of healthy primordial follicles determined after Abercrombie correction in each group are shown in Figure 6.8.

Although rhAMH treatment resulted in a small increase in primordial follicle numbers, this was not statistically significant. There was no difference in the number of primordial follicles between the rhAMH-treated groups at three different concentrations. Similarly, no differences in the total number of primordial follicles were observed in rhAMH and DXR cotreated ovaries, in comparison with the ovaries in the DXR group.

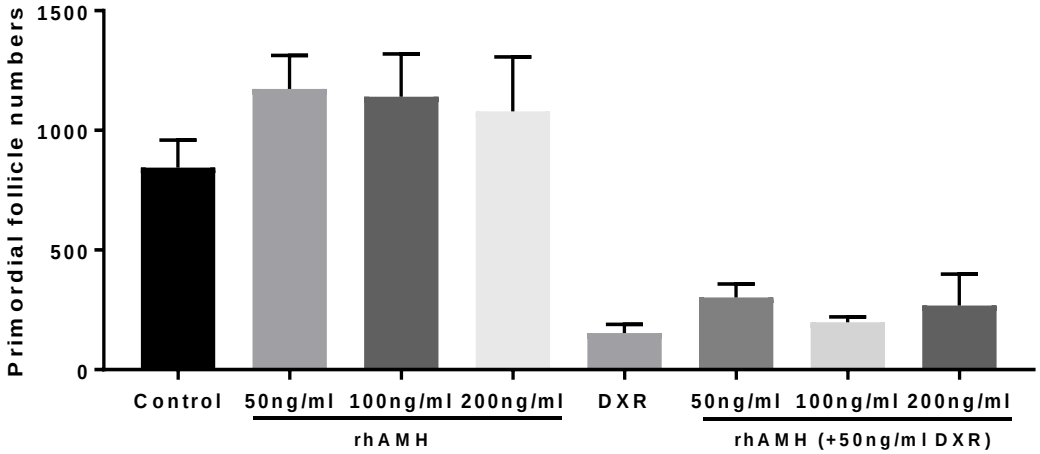


Figure 6.8. Primordial follicle numbers in mouse ovaries cultured with different concentrations of rhAMH and with or without exposure to DXR. Data was presented as Mean ± S.E.M. Control ovaries n=7. Ovaries cultured with rhAMH at concentrations of 50ng/ml (n=4), 100ng/ml (n=5) and 200ng/ml (n=5). Ovaries treated with 50ng/ml DXR (n=6). Ovaries co-treated with DXR and rhAMH at 50ng/ml (n=5), 100ng/ml (n=3) and 200ng/ml (n=3).

6.4.4 Comparisons between rhAMH and rmAMH treated ovarian primordial follicles.

There was no difference detected between the effects of rmAMH and rhAMH supplemented with or without DXR on primordial follicle numbers (Figure 6.9 and 6.10). This indicates that AMH is a highly conserved protein.

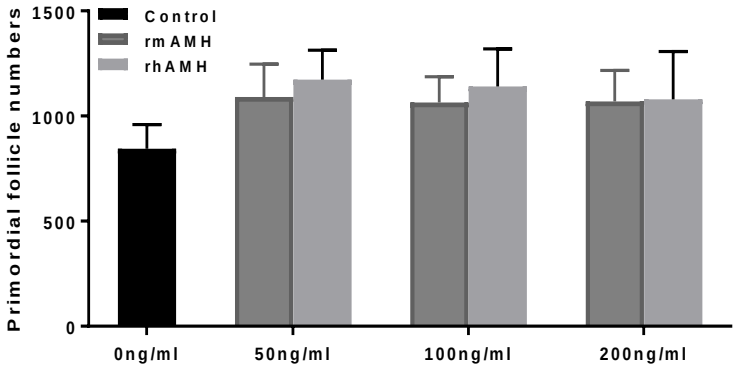


Figure 6.9. Primordial follicle numbers in mouse ovaries cultured with rmAMH or rhAMH at different concentrations. Data were present as mean ± S.E.M. Control ovaries (0ng/ml): n=7. Ovaries cultured with rmAMH at 50ng/ml (n=6), 100ng/ml (n=7) and 200ng/ml (n=7). Ovaries cultured with rhAMH at concentrations of 50ng/ml (n=4), 100ng/ml (n=5) and 200ng/ml (n=5).

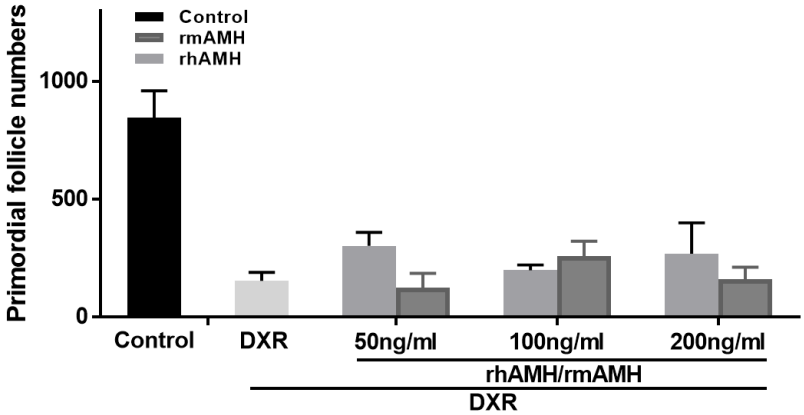


Figure 6.10. Primordial follicle numbers in mouse ovaries cultured with rmAMH or rhAMH at different concentrations and exposed to DXR. Data were present as Mean±S.E.M. Ovaries co-treated with DXR and rmAMH at 50ng/ml (n=4), 100ng/ml (n=5) and 200ng/ml (n=4). Ovaries co-treated with DXR and rhAMH at 50ng/ml (n=5), 100ng/ml (n=3) and 200ng/ml (n=3).

6.5 Discussion

In this experiment, rmAMH and rhAMH were administrated to pre-pubertal mouse ovaries *in vitro*, co-treated with or without DXR, in order to determine if AMH could attenuate DXR-induced primordial follicle loss. Treatment with both rmAMH and rhAMH at all concentrations had no significant effect on primordial follicle loss although they led to a numerical increase in primordial follicle numbers. Similarly, there was no significant effect observed of rmAMH or rhAMH on DXR-induced primordial follicle loss. Hence, this does not support the hypothesis 2 in Chapter 1, Section 1.8.

Effect of AMH alone on attenuating primordial follicle loss

Previous research has suggested that AMH can preserve follicle numbers not only in rodents *in vitro* and *in vivo*, but also in bovine and human ovaries *in vitro* (Durlinger *et al*., 2002; Carlsson *et al*., 2006; Hayes *et al*., 2016; Yang *et al*., 2017). However, in our study, AMH had no significant effect, although data present here showed a trend towards an increase in primordial follicle numbers in both rmAMH and rhAMH treated ovaries irrespective of concentrations. This would potentially be due to the insufficient amount of AMH used, short culture period with AMH or small number of samples. In a previous study using the rhAMH (R&D systems), rat ovaries were cultured with 200 ng/ml and 400 ng/ml of AMH for 8 days resulting a suppression of primordial follicle activation, whereas no effect was observed with AMH used at a concentration of 100 ng/ml (Mark-Kappeler *et al*., 2010). Durlinger *et al*., 2002, cultured mouse ovaries with home-made recombinant rat AMH (rrAMH) at a high concentration of 900 ng/ml for only 2 days, which resulted in a suppression of primordial follicle activation.

In addition, morphologically unhealthy follicles were rarely seen in rmAMH or rhAMH treated ovaries in this experiment. A study reported more atretic follicles found in

AMH gene knockout mice, which indirectly suggests that AMH might act as a protective factor of follicle survival (Durlinger *et al*., 1999).

Effect of AMH on DXR-induced primordial follicle loss

DXR kills cancer cells mainly by interfering with DNA replication, and therefore the dividing granulosa cells of secondary and antral follicles are more preferably damaged (Morgan *et al*., 2013). DXR-treated ovaries are thus ideal to investigate the AMH intervention on preventing primordial follicle loss. However, in our experiment, no protective effect of AMH on preventing DXR-induced primordial follicle loss was observed, although ovaries treated with DXR supplemented with rhAMH contained numerically more primordial follicles at all concentrations than ovaries cultured with DXR alone. This might have been due to insufficient time in culture with AMH, before initiating chemotherapy. In our study, we added DXR 24 hours after the AMH administration. However, DXR has a smaller molecular weight at 0.543 kDa whereas the molecular weight of commercial AMH protein we used is around 13 kDa. We therefore speculated that AMH did not penetrate the mouse ovaries in time to inhibit primordial follicle activation before DXR exerted its toxic effect *in vitro*. Thus DXR might have initiated damage on the ovarian tissue before AMH could exert a protective effect. In future experiments, we could potentially pre-treat the ovarian tissue for longer with the AMH before culturing with DXR.

Differences between the efficacy of rmAMH and rhAMH

According to the data described in this Chapter, there is no difference found between rmAMH and rhAMH treatments, either alone or in conjunction with DXR.

New publications

While we were planning on further investigating the effects of AMH in preventing DXR induced follicle loss in mice *in vivo*, a new publication demonstrated the ovarian protective efficacy of AMH against DXR-induced primordial follicle loss in mouse ovaries *in vivo* (Kano *et al*., 2017). The bioactivity of rhAMH (R&D) was also confirmed using a mouse urogenital bridge assay (Yamamoto *et al*., 2018), where Müllerian ducts regressed after exposure to rhAMH.

6.6 Conclusion

DXR-induced ovarian reserve damage was confirmed again in pre-pubertal mice (Chapter 5-6). Thus, investigation of methods to protect the fertility of childhood cancer patients who would receive DXR is critically important. rhAMH was proven to be bioactive (Yamamoto *et al*., 2018) and thus can be used in further studies.

Ovaries cultured with rhAMH (at all concentrations) and DXR contained numerically more primordial follicles than those cultured with DXR alone. However the difference was not statistically significant which might be due to an insufficient dose of AMH, an insufficient culture duration before exposure to DXR, and a small sample size. Taking the recently updated literature (Kano *et al*., 2017) into consideration, AMH administration shows promise to offer fertility protection for cancer patients treated with DXR. However, more research is required to further investigate if AMH exerts the same effect on human ovarian tissue *in vivo*.

Chapter 7: Development of xenotransplantation protocol

7.1 Introduction

Chemotherapy induced POI affects the quality of life of approximately 8 percent of female cancer survivors. One of the commonly used gonadotoxic chemotherapeutic agents is Doxorubicin (DXR) resulting in loss of primordial follicles, as revealed in Chapter 5 and confirmed in Chapter 6. It is therefore important to prevent DXR-induced diminished ovarian reserve for cancer patients. Anti-Müllerian Hormone (AMH) has been shown to have a protective effect on the ovarian reserve against DXR in mice *in vivo* (Kano *et al*., 2017). However, whether AMH can prevent DXR-induced primordial follicle loss in human ovarian tissue has not been investigated yet. In order to investigate the effect of AMH on human ovarian tissue, xenotransplantation of cryopreserved human ovarian tissue into a mouse model was planned. However, xenotransplantation of human ovarian tissue into mouse had not been carried out at the University of Oxford before. Preliminary experiments were therefore required to establish effective xenotransplantation protocols and to test the survival and development potential of the cryopreserved human ovarian tissue stored in the Oxford Cell and Tissue Biobank (OCTB).

In order to establish effective xenotransplantation protocols, post-pubertal human ovarian tissue was used due to the lack of data regarding survival and growth of pre-pubertal human ovarian tissue. Research has shown that there are many abnormal primordial follicles in pre-pubertal human ovarian tissue, verified by their reduced ability to grow *in vitro* (Anderson *et al*., 2014). Therefore, to optimise establishing xenotransplantation, we used post-pubertal human ovarian tissue rather than pre-pubertal human ovarian tissue. Once an effective protocol is established using post-pubertal human ovarian tissue, the growth and survival potential of pre-pubertal human ovarian tissue will be investigated.

In addition to the age of ovarian tissue, xenotransplantation sites were also investigated and compared. Clinically, ovarian tissue can be transplanted back to either

anatomical or non-anatomical sites, named as orthotopic or heterotopic transplantation, respectively (Sonmezer and Oktay, 2010). In a mouse, there are many sites that can be used for transplantation such as under the kidney capsule, into a subcutaneous pocket, under the ovarian bursa and into the peritoneal cavity (Gook *et al*., 2005; Schubert *et al*., 2008; Dolmans *et al*., 2007; Nottola *et al*., 2008). Furthermore, research indicates that the follicular development of transplanted ovarian tissue can be influenced by the different sites (Hernandez-Fonseca *et al*., 2004; Terada *et al*., 2008; Dath *et al*., 2010).

A comparison of follicle development in human ovarian grafts at two sites was carried out and revealed a larger proportion of growing follicles under the kidney capsule whereas grafts in the subcutaneous space had a larger proportion of primordial follicles after 6 months of xenotransplantation (Hernandez-Fonseca *et al*., 2004). Dath *et al*. (2010) compared four sites for human ovarian tissue xenotransplantation (ovarian bursa, subcutaneous space, intraperitoneal and intra muscle) and found that only grafts under ovarian bursa had follicular development to the antral stage after 3 weeks of xenotransplantation. Terada *et al*. (2008) grafted human ovarian tissue to three different sites (kidney capsule, ovarian bursa and subcutaneous space) of ovariectomised mice for 12 weeks and also provided 14 days of human menopausal gonadotrophin treatment (10 weeks after transplantation). After 12 weeks, only the grafts transplanted under the ovarian bursa had large graafian follicles present. Therefore, considering the limited data, to confirm the most effective protocol to facilitate future studies, the effect of different xenotransplantation sites on xenografted ovarian tissue survival and follicular development was assessed in this preliminary experiment.

Human ovarian tissue xenotransplanted under the ovarian bursa has been carried out either with the absence (Terada *et al*., 2008) or presence of hosts' ovaries (Dath *et al*., 2010). The removal of host ovary not only facilitates the growth and development of graft but also

provides space for human ovarian graft since there is very limit space under mouse ovarian bursa. However, ovariectomy induced estrogen deficiency results in high levels of FSH and FSH has been suggested to stimulate the PI3K pathway (Huang *et al.*, 2008) which might influence the effect of AMH on primordial follicles. Therefore, since follicles can grow in xenografted tissues without ovariectomy (Dath *et al.*, 2010), we decided not to carry out ovariectomy in our study.

Tissue cryopreserved by OCTB technicians use the same cryopreservation protocol as Revel's group (Revel *et al.*, 2003). Although live births following ovarian tissue transplantation of cryopreserved human ovarian tissue have been reported using this protocol in Israel (Revel *et al.*, 2011), it is important to evaluate the function of the ovarian tissue stored by OCTB to determine if it retains the potential to survival and grow. Thus clarifying that ovarian tissue cryopreserved by the OCTB maintains follicular developmental competence was also an aim of this experiment.

7.2 Aims

- To investigate whether OCTB cryopreserved human pre-pubertal and post-pubertal ovarian tissue can survive and grow in mice after xenotransplantation;
- To compare the effect of different xenotransplantation sites on human ovarian follicle survival and development;
- To compare the difference between post- and pre-pubertal cryopreserved human ovarian tissue.

7.3 Materials and Methods

7.3.1 Patient inclusion and exclusion criteria

All patients included in this study were selected based on: 1) informed consent for research; 2) more than 50 ovarian cortical strips stored; 3) informed consent for animal studies. Donated ovarian tissue from the patients that fulfilled the above requirements were selected according to pubertal status, cancer treatment history prior to ovarian tissue cryopreservation and specific diagnoses (summarised in Table 7.1). Puberty status was determined at the time of ovarian tissue cryopreservation (OTC) based on the doctors' diagnoses and recorded in the database by the OCTB group.

Table 7.1. Summary of patient selection criteria.

Criteria	Post-puberty patients	Pre-puberty patients
Inclusion	Post-puberty	Pre-puberty
	Surgery and OTC on the same day	Surgery and OTC within 24 hours
	Consent to research and animal studies	
	Cortical strips total number > 50 strips	
Exclusion	Received anti-cancer treatments before OTC	
	Diagnosed with diseases involving ovarian tissues	

OTC: ovarian tissue cryopreservation.

7.3.2 Human ovarian cortical strips

Human ovarian cortical strips were frozen by OCTB and thawed by the candidate as described in Section 2.5. A single strip of ovarian cortical tissue was used from each patient.

The thawed single strip of ovarian cortical tissue was put into a sterile glass petri dish containing L-15 media at 4°C and then cut into 1x1x1 mm pieces under a microscope in a class II fume hood. At least one piece of 1 mm^3 ovarian cortical tissue was fixed in Bouin's solution for post-pubertal human ovarian tissue and in 10% neutral buffered formalin for pre-pubertal human ovarian tissue for 8 hours to serve as a control for the

transplanted ovarian tissue. Pieces of ovarian tissue for xenotransplantation were transported to the animal facility in sterile L-15 at 4°C. Before the anaesthesia induction and initial preparations of surgeries, the Bijou tube containing the ovarian tissue was placed outside to allow the tissue to warm to room temperature.

7.3.3 Animals

Immunocompromised SCID mice were used as hosts for human grafts as described in Section 2.2.2. For post-pubertal human ovarian tissue xenotransplantation, host SCID mice (n=12) received one piece of ovarian tissue each. Xenotransplantation sites in use were under the kidney capsule (n=6) and under the ovarian bursa (n=6).

For pre-pubertal human ovarian tissue xenotransplantation, host SCID mice (n=12) received one piece of ovarian tissue each. Xenotransplantation sites in use were under the kidney capsule (n=4), under the ovarian bursa (n=4) and into the subcutaneous pocket (n=4).

7.3.4 Surgeries

The surgery protocol for transplantation of mouse ovarian tissue under the kidney capsule was established in the Williams' group. The protocol of murine xenotransplantation beneath the ovarian bursa was established by the candidate based on the protocol reported by Dolmans *et al*., 2007. The protocol of the transplantation into the left lateral skin was established by the candidate.

7.3.4.1 Anaesthesia induction and initial preparations

Anaesthesia was induced in a chamber containing 4% isoflurane (Zoetis, UK) and 2.5L/min of oxygen. Once the animal was fully anaesthetised, the animal was transferred to

a face-mask with 2.5% isoflurane and oxygen with a flow rate at 1.5L/min on a heat pat (37°C) for fur clipping and initial preparations. Eye lubricant (Allergan, UK) was put on the mouse eyes to prevent them from drying out during surgery. Analgesic agents, Vetergesic (10% in 100µl injectable water, Ceva Animal Health, UK) and Matacam (10% in 100µl injectable water, Boehringer Ingelheim, Germany), were administered subcutaneously. Left dorsal and lateral areas of mice were shaved and the exposed skin was antiseptically cleaned three times using sterile gauze soaked in 4% chlorhexidine (Hibiscrub, Mölnlycke Health Care, UK) in warm water. A sterile surgical drape covered the animal with a hole exposing the surgical area. All surgical procedures were carried out by the candidate under a microscope in a clean surgery room at the BMS, Oxford.

7.3.4.2 Xenotransplantation under the kidney capsule

A small flank incision of the skin and a further small incision of the body wall were made to access the left kidney. Under the microscope, the left kidney was exteriorised and a small pocket was made under the kidney capsule using two pairs of fine forceps. A piece of human ovarian tissue was inserted into the pocket under the kidney capsule. The kidney was then put back into the anatomical site and the body wall and the skin were closed with interrupted sutures using 4-0 Vicryl sutures (Ethicon, USA). After the surgery was completed, the position of the graft inside the kidney capsule was drawn on the surgical sheet for recording purposes.

7.3.4.3 Xenotransplantation under the ovarian bursa

A small incision of the skin and a further incision of the body wall were made to expose the left ovary. A small opening on the ovarian bursa was opened by two pairs of fine forceps under the microscope. A piece of human ovarian tissue was grafted under the ovarian

bursa. In the experiment of xenotransplanting post-pubertal human ovarian tissue, grafts were placed under the ovarian bursa without stitches (Dolmans *et al*., 2007). However, grafts were lost as described later in the results. In the experiment of xenotransplantation of pre-pubertal human ovarian tissue, the ovarian bursa was closed using vicryl 0.7(6/0) sutures (Ethicon, USA) after placing the ovarian graft.

The left ovary was then placed back inside the body wall and the body wall and skin were closed by interrupted sutures as above.

7.3.4.4 Subcutaneous xenotransplantation

A small skin incision was made in the left lateral flank of the mouse. Holding one side of the open skin using a pair of blunt forceps or a bulldog clamp, a small pocket under the skin was made using fine forceps from the inside of the skin. All pockets were at least 0.5cm far away from the edge of the skin incisions. A graft was inserted into the sub-cut pocket. The pocket was closed using a vicryl 0.7(6/0) suture. Skin incisions were closed by interrupted sutures.

7.3.4.5 Recovery

Once xenotransplantation was completed and the isoflurane was switched off, mice were ear-clipped for identification and maintained at 1.5L/min oxygen until spontaneous movements happened. Mice were then transferred into pre-warmed cages with soft bedding for recovery from anaesthesia. Mice were given soft food (normal food soaked in water) in a petri dish, normal food and water inside the recovery cages.

7.3.5 Post-surgical monitoring

Each mouse was housed singly on the first day after surgery and housed together with other mice from the second day. Mice were weighed, monitored and evaluated based on a post-procedure assessment form (as described in Section 2.2.4) daily during the first two weeks and twice a week for the following period until the experiments were completed.

7.3.6 Xenografts collection

For post-pubertal human ovarian tissue xenotransplantation, ovarian grafts were retrieved after 3 weeks from the ovarian bursa (n=3). The rest of post-pubertal human ovarian grafts under ovarian bursa (n=3) and under the kidney capsule (n=6) were recovered 6 weeks following xenotransplantation.

For pre-pubertal human ovarian tissue xenotransplantation, human ovarian grafts under the kidney capsule (n=4), under the ovarian bursa (n=4) and from the subcutaneous pocket (n=4) were recovered 6 weeks following xenotransplantation. All mice were sacrificed by cervical dislocation.

7.3.7 Histology Process

Recovered post-pubertal xenografts were fixed in Bouin's solution overnight. Recovered pre-pubertal xenografts were fixed in 10% neutral buffered formalin for 8 hours. They were processed, embedded and sectioned as described in Chapter 2. For post-pubertal ovarian xenografts, every single ovarian section was stained with haematoxylin and eosin and analysed. For the embedded pre-pubertal ovarian tissue grafts, every 10^{th} ovarian section was stained with haematoxylin and eosin and analysed. Follicles with a visible nucleus were counted at the different stages as described in Chapter 2.

7.3.8 Statistical Analysis

All data was analysed using GraphPad Prism version 7.00 (GraphPad Software, USA). Data was tested for normality using Shapiro-Wilk normality test. One-way ANOVA was applied to determine if there were differences present in mouse body weight across different xenotransplantation protocols. Results are presented as mean ± S.E.M. for multiple comparisons. Significance were considered when $P<0.05$.

7.4 Results

7.4.1 Patients profiles

Following the inclusion and exclusion criteria summarised in Table 7.1, ovarian cortical strips from six post-pubertal and four pre-pubertal patients were collected from the OCTB. Patient information is listed in Tables 7.2 and 7.3. All the cryopreserved ovarian tissue samples were dissected from the right ovaries following a planned unilateral oophorectomy.

Table 7.2. Age and diagnoses of included post-pubertal patients (n=6) in this study.

Patient No.	Age	Diagnoses
I	18	Hilar cholangiocarcinoma (HC)
II	25	Cervical cancer (CC)
III	14	Thoracic sarcoma (TS)
IV	16	Hypoplastic Myelodysplasia (h-MDS)
V	13	Ewing's Sarcoma (ES)
VI	22	Atypical teratoid rhabdoid tumor (AT/RT)

Table 7.3. Age and diagnoses of included pre-pubertal patients (n=4) in this study.

Patient No.	Age	Diagnoses
A	10	Severe congenital neutropenia (SCN)
B	12	Severe aplastic anaemia (SAA)
C	5	Aplastic anaemia (AA)
D	6	Sickle cell disease; progressive cerebrovascular disease (SCD;PCD)

7.4.2 Xenotransplantation

A series of representative photographs taken by the candidate illustrate the process of subcutaneous xenotransplantation (Figure 7.1).

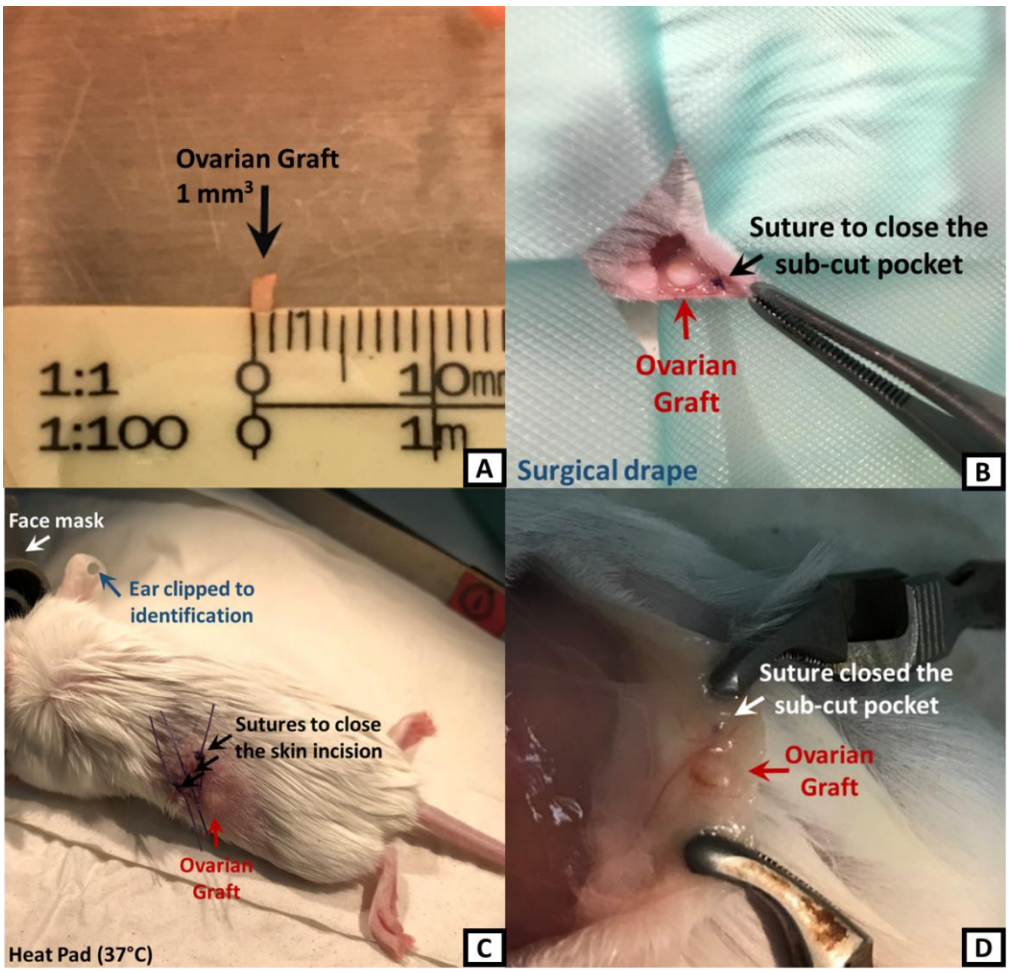


Figure 7.1. Representative images of the process of subcutaneous xenotransplantation of one piece of human ovarian cortical strip into a SCID mouse. A) A piece of human ovarian cortical tissue (1mm^3) was cut from a single ovarian cortical strip in L-15 media. B) The graft was xenografted into a subcutaneous pocket in a SCID mouse under anaesthesia and closed by a suture. C) The skin incision was closed by three interrupted sutures. The ovarian graft position could be observed from outside the skin. D) After six weeks, the mouse was sacrificed and the ovarian graft recovered. Blood vessels were observed around and above the graft.

A series of representative graphs illustrated a piece of human ovarian tissue before, by the time of surgery and 6 weeks after xenotransplantation under the mouse kidney capsule (Figure 7.2).

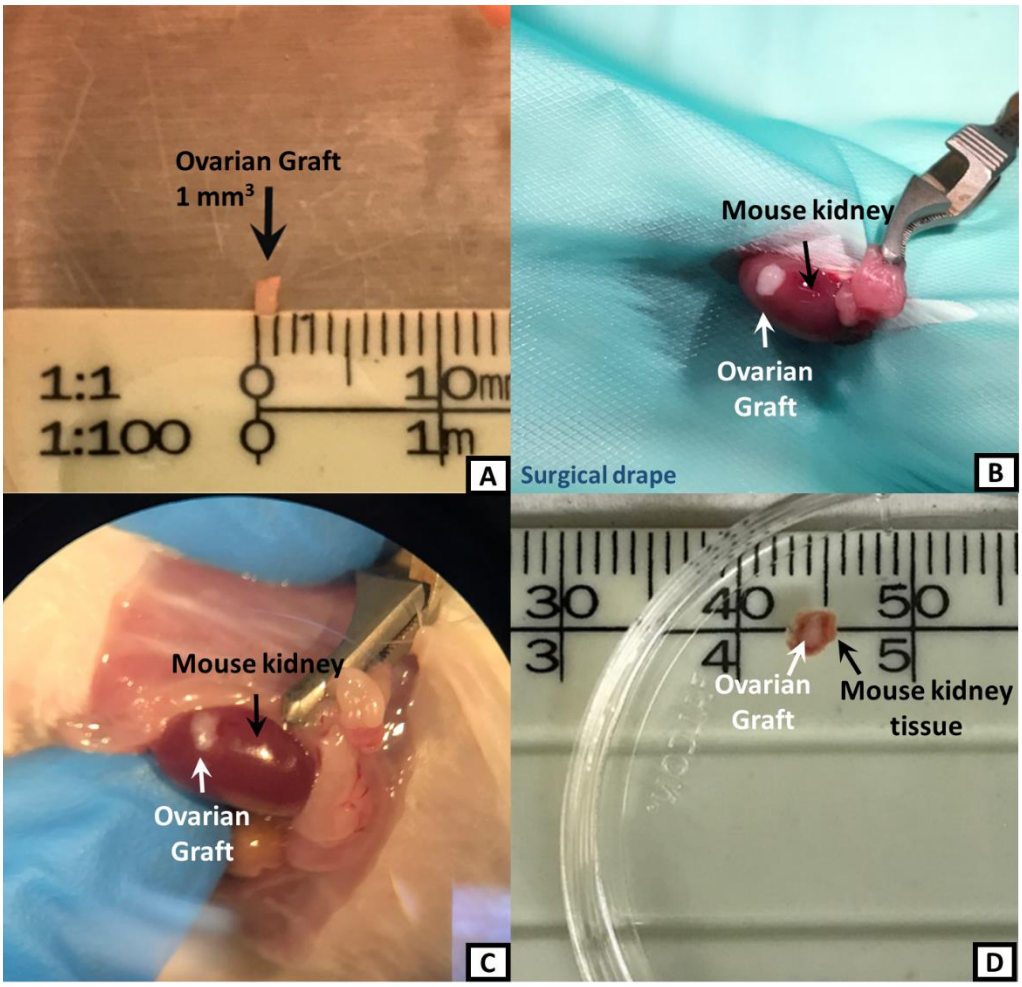


Figure 7.2. Representative images of the process of xenotransplantation of one piece of human ovarian cortical strip under the mouse kidney capsule. A) A piece of human ovarian cortical tissue (1mm^3) was cut from a single ovarian cortical strip in L-15 media. B) The graft was xenografted under the kidney capsule in a SCID mouse under anaesthesia. C) After six weeks, the mouse was sacrificed and the ovarian graft recovered. D) The graft and surrounding attached kidney tissue were dissected and fixed together. Minimum interval of the ruler is 1 mm.

Representative images of xenografted human ovarian tissue recovered under mouse ovarian bursa are shown in Figure 7.3.

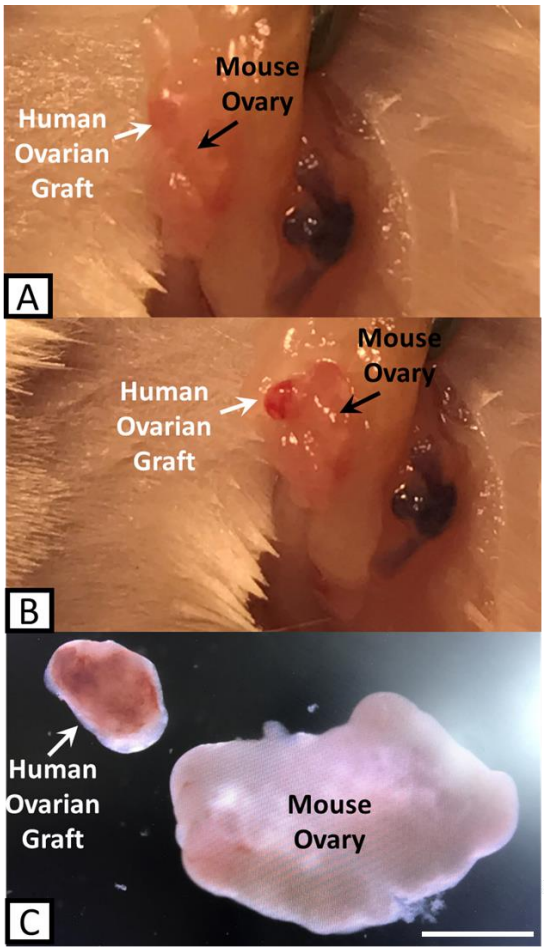


Figure 7.3. Representative images of human ovarian grafts xenotransplanted under the mouse ovarian bursa. A) After six weeks of xenotransplantation, the mouse was sacrificed and the ovarian graft recovered from under the ovarian bursa. B) The ovarian bursa was opened to reveal the human ovarian graft. C) The human ovarian graft and the mouse ovary under the microscope. Bar represents 1mm.

Dissolvable sutures (vicryl 6/0, Ethicon) were added to close the ovarian bursa when xenotransplanting pre-pubertal human ovarian tissue; none of the sutures were found by the time of graft collection.

7.4.3 SCID mouse

The mouse survival rate in this study was 100% (n=24) with all mice gaining weight through the study (Figure 7.4-5). There was no wound opening, unexpected bleeding or immunological rejection symptoms observed following surgeries. There was no abnormal behaviour observed during the entire study.

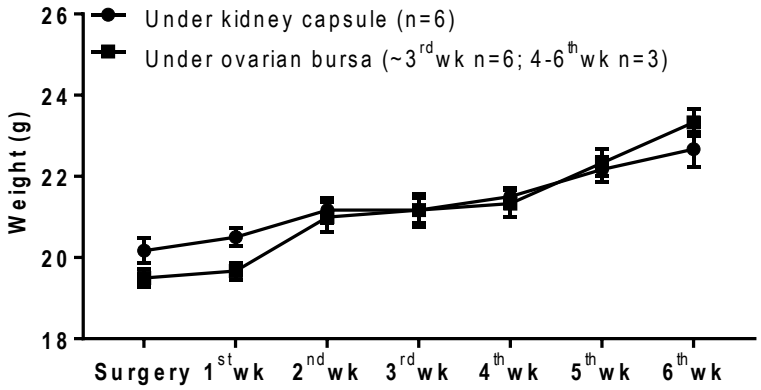


Figure 7.4. Body weight of immunocompromised mice xenotransplanted with post-pubertal human ovarian tissue for 6 weeks. Mice hosting post-pubertal human ovarian tissue under the ovarian bursa were sacrificed at 3 weeks (n=3) or 6 weeks (n=3) separately. Mice hosting pre-pubertal human ovarian tissue under the kidney capsule were sacrificed at 6 weeks (n=6).

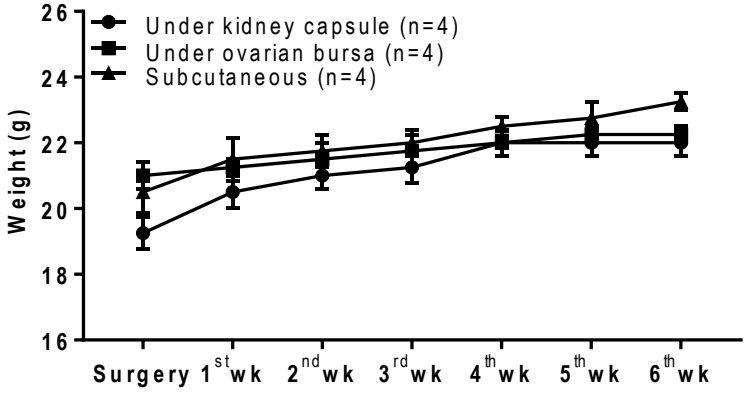


Figure 7.5. Body weight of immunocompromised mice xenotransplanted with pre-pubertal human ovarian tissue for 6 weeks. Mice hosting post-pubertal human ovarian tissue under the kidney capsule (n=4), the ovarian bursa (n=4) and subcutaneous (n=4) were all sacrificed at 6 weeks post surgeries.

7.4.4 Histological analyses of post-pubertal human ovarian grafts after xenotransplantation

For the post-pubertal human ovarian tissue xenotransplantation experiment, three weeks after surgery, three pieces of human ovarian tissue xenografted under the ovarian bursa were collected (n=3 mice), however, none of them had follicles present (Table 7.4-5). After six weeks of xenotransplantation, human ovarian grafts were collected from under the mouse kidney capsule (n=6) and under the ovarian bursa (n=2) (Table 7.4-5). One piece of human ovarian tissue xenografted under the ovarian bursa was lost six weeks after xenotransplantation. Another graft originally xenografted under the mouse ovarian bursa was found inside the abdominal cavity at the time of collection.

All xenografts under the kidney capsule (n=6) and most of the xenografts originally grafted under the mouse ovarian bursa (n=5) were vascularised, revealed by the presence of blood vessels containing red blood. One human xenograft collected beneath the ovarian bursa was not vascularised (Patient I).

Table 7.4. Proportion of post-pubertal human ovarian xenografts retrieved from different transplantation sites in SCID mice.

Sites under	Duration	Grafts collected	Follicles present
Kidney capsule	6 weeks	6 of 6	2 of 6
Ovarian bursa	3 weeks	3 of 3	0 of 3
	6 weeks	2 of 3	1 of 3

Table 7.5. Number of post-pubertal human ovarian xenografts from different patients retrieved from different transplantation sites in SCID mice.

Patient No.	Age	Diagnoses	Thawed	Grafts collected			Follicles Present		
				KC 6 wks	OB 3wks	OB 6wks	KC 6 wks	OB 3wks	OB 6wks
I	18	HC	✓	✓	✓		✗	✗	
II	25	CC	✗	✓	✓		✓	✗	
III	14	TS	✓	✓	✓		✗	✗	
IV	16	h-MDS	✓	✓		✗	✗		✗
V	13	ES	✓	✓		✓	✗		✗
VI	22	AT/RT	✓	✓		✓*	✓		✓*
✓/Total			5/6	6/6	5/6		2/6	1/6	

**This graft was found in the abdominal cavity at the time of retrieval.* HC: Hilar cholangiocarcinoma. KC: Kidney capsule. OB: Ovarian bursa. CC: Cervical cancer. Thoracic sarcoma. TS: Thoracic sarcoma. h-MDS: Hypoplastic Myelodysplasia. ES: Ewing's Sarcoma AT/RT: Atypical teratoid rhabdoid tumor.

Patient II had no follicles in the thawed cryopreserved ovarian tissue (Table 7.6). Instead, this piece of tissue contained many vessels which is indicative of the ovarian medulla (Figure 7.6).

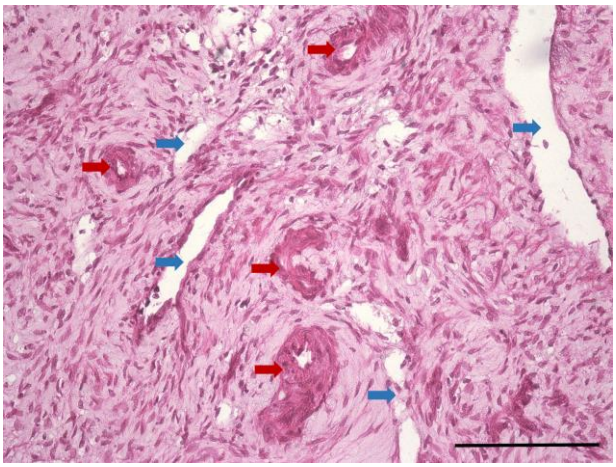


Figure 7.6. A representative micrograph of a thawed cryopreserved ovarian tissue section (Patient II) stained with H and E. The red arrows point to the muscular arteries. The blue arrows point to the veins. The bar represents 100µm.

Follicles in thawed non-grafted post-pubertal human ovarian tissue at different stages are illustrated in Figure 7.7.

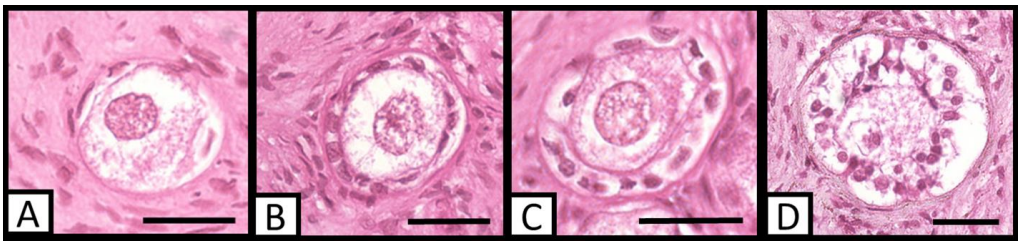


Figure 7.7. Follicles at different stages in thawed non-grafted post-pubertal human ovarian tissue fixed in Bouin's and stained with H and E. A) Primordial follicle: an oocyte surrounded by flattened pre-granulosa cells. B) Transitional: one or more of the surrounding granulosa cells are cuboidal (with at least one pre-granulosa cell). C) Primary: one complete layer of granulosa cells around the oocyte. D) Secondary: more than one layer of granulosa cells. Scale bars represent 25μm.

Follicles at the different developmental stages in the thawed cryopreserved post-pubertal human ovarian tissue were counted (Table 7.6).

Table 7.6. Numbers of follicles at different stages of thawed non-grafted human ovarian tissue from post-pubertal patients.

Patient No.	Age	Diagnoses	Follicle stages				Total
			PMF	Trans	PF	SF	
I	18	HC	10	7	1	4	22
II	25	CC	0	0	0	0	0
III	14	TS	31	19	2	0	52
IV	16	h-MDS	12	4	0	0	16
V	13	ES	10	1	0	0	11
VI	22	AT/RT	108	34	3	0	145

Follicle numbers were counted in a piece of 1 mm^3 ovarian cortical tissue. PMF: Primordial follicle. Trans: Transitional follicle. PF: Primary follicle. SF: Secondary follicle. HC: Hilar cholangiocarcinoma. CC: Cervical cancer. Thoracic sarcoma. TS: Thoracic sarcoma. h-MDS: Hypoplastic Myelodysplasia. ES: Ewing's Sarcoma AT/RT: Atypical teratoid rhabdoid tumor.

Histological analyses of human ovarian grafts under the kidney capsule

A representative picture of post-pubertal human ovarian graft recover from the mouse kidney capsule is illustrated in Figure 7.8.

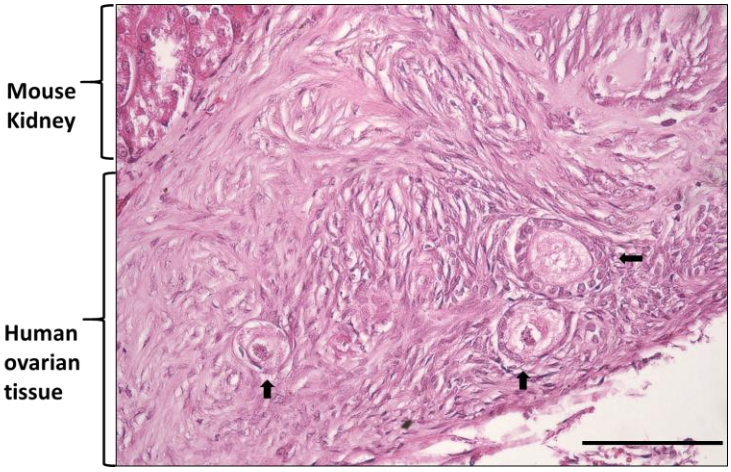


Figure 7.8. A representative ovarian tissue section micrograph of post-pubertal human ovarian graft xenografted under the mouse kidney capsule and stained with H and E. This xenografted human ovarian tissue closely attached to the mouse kidney tissue after 6-week xenotransplantation. Black arrows point to follicles. Bar represents 100µm.

The follicle numbers at the different developmental stages in xenografts from under the mouse kidney capsule are shown in Table 7.7.

Table 7.7. Numbers of follicles at different stages of post-pubertal human ovarian tissue xenografted under the mouse kidney capsule.

Patient No.	Age	Diagnoses	Follicle stages				Total
			PMF	Trans	PF	SF	
I	18	HC	0	0	0	0	0
II	25	CC	4	10	7	4	25
III	14	TS	0	0	0	0	0
IV	16	h-MDS	0	0	0	0	0
V	13	ES	0	0	0	0	0
VI	22	AT/RT	5	1	2	0	8

PMF: Primordial follicle. Trans: Transitional follicle. PF: Primary follicle. SF: Secondary follicle. HC: Hilar cholangiocarcinoma. CC: Cervical cancer. Thoracic sarcoma. TS: Thoracic sarcoma. h-MDS: Hypoplastic Myelodysplasia. ES: Ewing's Sarcoma AT/RT: Atypical teratoid rhabdoid tumor.

Histological analyses of human ovarian grafts under the ovarian bursa

None of the xenografts retrieved (n=5 of 6) under the mouse ovarian bursa had any follicles present whereas the one found in the abdominal cavity contained 3 follicles (Table 7.8). However, most of the xenografts (Patient II-VI) had vascularisation established.

Table 7.8. Numbers of follicles at different stages of post-pubertal human ovarian tissue xenografted under the mouse ovarian bursa.

Patient No.	Age	Diagnoses	Follicle stages				Total
			PMF	Trans	PF	SF	
3 weeks following xenotransplantation							
I	18	HC	0	0	0	0	0
II	25	CC	0	0	0	0	0
III	14	TS	0	0	0	0	0
6 weeks following xenotransplantation							
IV	16	h-MDS	Missing				
V	13	ES	0	0	0	0	0
VI*	22	AT/RT	0	1	1	1	3

**Graft was found in the mouse abdomen cavity.* PMF: Primordial follicle. Trans: Transitional follicle. PF: Primary follicle. SF: Secondary follicle. HC: Hilar cholangiocarcinoma. CC: Cervical cancer. Thoracic sarcoma. TS: Thoracic sarcoma. h-MDS: Hypoplastic Myelodysplasia. ES: Ewing's Sarcoma AT/RT: Atypical teratoid rhabdoid tumor.

7.4.5 Histological analyses of pre-pubertal human ovarian grafts after xenotransplantation

Pre-pubertal ovarian xenografts were recovered from the mouse kidney capsule (n=4), under the mouse ovarian bursa (n=3) and in the subcutaneous pocket (n=4) after six weeks of xenotransplantation (Table 7.9-7.10). There was one piece of human ovarian tissue transplanted under the mouse ovarian bursa that was not recovered (Patient D). Revascularization was established in 75% of the collected xenografts (3/4) (Patient B-D).

Table 7.9. Proportion of pre-pubertal human ovarian xenografts retrieved from different transplantation sites in SCID mice.

Sites under	Duration	Grafts collected	Follicles present
Kidney capsule	6 weeks	4 of 4	1 of 4
Ovarian bursa	6 weeks	3 of 4	1 of 4
Subcutaneous	6 weeks	4 of 4	4 of 4

Table 7.10. Numbers of pre-pubertal human ovarian xenografts of different patients retrieved from different transplantation sites in SCID mice.

Patient No.	Age	Diagnoses	Thawed	Graft collected			Follicle present		
				KC	**OB**	**SC**	**KC**	**OB**	**SC**
A	10	SCN	✓	✓	✓	✓	✗	✗	✓
B	12	SAA	✓	✓	✓	✓	✗	✓	✓
C	5	AA	✓	✓	✓	✓	✓	✗	✓
D	6	SCD; PCD	✓	✓	✗	✓	✗	✗	✓
✓/Total			4/4	4/4	3/4	4/4	1/4	1/4	4/4

SCN: Severe congenital neutropenia. SAA: Severe aplastic anaemia. AA: Aplastic anaemia. SCD: Sickle cell disease. PCD: progressive cerebrovascular disease. KC: Kidney capsule. OB: Ovarian bursa. SC: Subcutaneously.

Follicles at different stages in the pre-pubertal human ovarian tissue are illustrated in Figure 7.9.

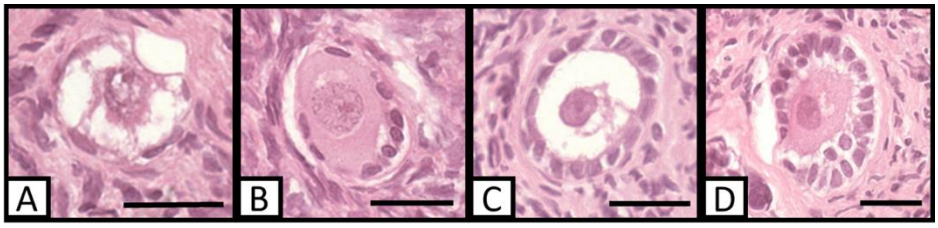


Figure 7.9. Follicles at different stages in pre-pubertal human ovarian tissue fixed in 10% neutral buffered formalin and stained with H and E. A) Primordial follicle: an oocyte surrounded by flattened pre-granulosa cells. B) Transitional: one or more of the surrounding granulosa cells are cuboidal. C) Primary: one complete layer of granulosa cells around the oocyte. D) Secondary: more than one layer of granulosa cells. Scale bars represent 25μm.

Follicle numbers at different stages in the thawed cryopreserved pre-pubertal human ovarian tissue were counted in every 10th ovarian sections (Table 7.11).

Table 7.11. Numbers of follicles at different stages in every 10th ovarian tissue section of thawed non-grafted human ovarian tissue from pre-pubertal patients.

Patient No.	Age	Diagnoses	*No.*	Follicle stages				Total
				PMF	Trans	PF	SF	
A	10	SCN	1st	64	23	10	2	99
			2nd	75	11	4	2	92
B	12	SAA	1st	1	2	1	2	6
			2nd*	25	3	0	1	29
C	5	AA	1st	0	0	0	0	0
			2nd	3	0	0	0	3
D	6	SCD; PCD	1st	33	5	11	2	51
			2nd	67	3	4	3	77

**Not enough as a 1 mm^3 (approximately 0.3 mm^3), in case there are follicles, this tissue was collected and embedded. Except this piece, others are around 1 mm^3.* PMF: Primordial follicle. Trans: Transitional follicle. PF: Primary follicle. SF: Secondary follicle. SCN: Severe congenital neutropenia. SAA: Severe aplastic anaemia. AA: Aplastic anaemia. SCD: Sickle cell disease. PCD: progressive cerebrovascular disease.

In one piece of the thawed ovarian tissue of patient C, there are no follicles present. However, the tissue contained many blood vessels as shown in Figure 7.10, which is a sign of the ovarian medulla.

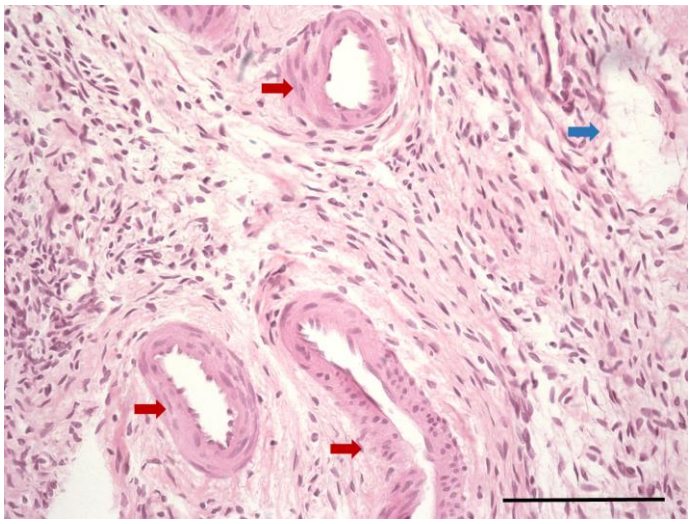


Figure 7.10. A representative thawed non-grafted human pre-pubertal ovarian tissue section (Patient C) stained with H and E. The red arrows point to muscular arteries and the blue arrow points to a vein. Bar represents 100µm.

Histological analyses of human ovarian grafts under the kidney capsule

The follicle numbers at the different developmental stages in human pre-pubertal xenografts transplanted under the mouse kidney capsule are shown in Table 7.12. Only one xenograft under the kidney capsule had follicles that survived, a representative picture is illustrated (Figure 7.11). There were blood vessels containing red blood cells within the ovarian xenograft near the border of the mouse kidney tissue.

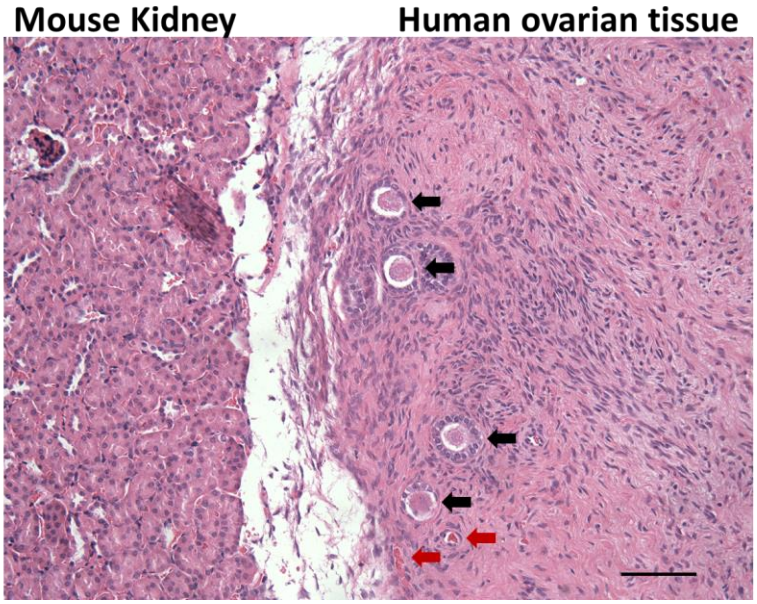


Figure 7.11. A representative ovarian tissue section micrograph of pre-pubertal human ovarian graft xenografted under the mouse kidney capsule and stained with H and E. Section was stained with H & E. Black arrows point to follicles. Red arrows point to blood vessels. Bar represents 100µm.

Table 7.12. Follicle numbers and developmental stage in thawed pre-pubertal human ovarian tissue xenografted under the mouse kidney capsule.

Patient No.	Age	Diagnoses	Follicle stages				Total
			PMF	Trans	PF	SF	
A	10	SCN	0	0	0	0	0
B	12	SAA	0	0	0	0	0
C	5	AA	1	4	1	2	8
D	6	SCD;PCD	0	0	0	0	0

PMF: Primordial follicle. Trans: Transitional follicle. PF: Primary follicle. SF: Secondary follicle. SCN: Severe congenital neutropenia. SAA: Severe aplastic anaemia. AA: Aplastic anaemia. SCD: Sickle cell disease. PCD: progressive cerebrovascular disease.

Histological analyses of pre-pubertal human ovarian grafts under the ovarian bursa

The follicle numbers at different stages in human pre-pubertal xenografts transplanted under the mouse ovarian bursa are shown in Table 7.13. Only one piece of xenograft under the mouse ovarian bursa contained follicles (Figure 7.12).

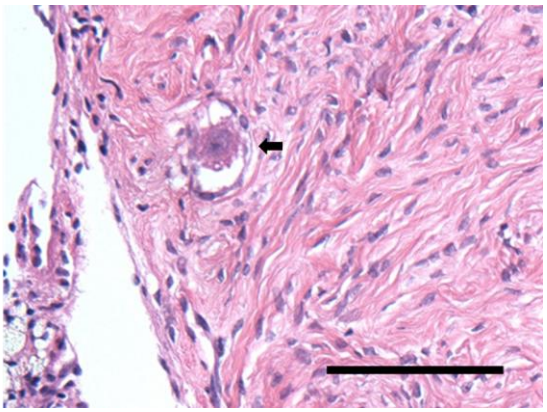


Figure 7.12. A representative ovarian tissue section micrograph of pre-pubertal human ovarian graft xenografted under the mouse ovarian bursa and stained with H and E. The black arrow points to a transitional follicle. Bar represents 50µm.

Table 7.13. Follicle numbers and developmental stage in thawed pre-pubertal human ovarian tissue xenografted under the mouse ovarian bursa.

Patient No.	Age	Diagnoses	Follicle stages				Total
			PMF	Trans	PF	SF	
A	10	SCN	0	0	0	0	0
B	12	SAA	1	2	0	0	3
C	5	AA	0	0	0	0	0
D	6	SCD; PCD	Graft not present				

PMF: Primordial follicle. Trans: Transitional follicle. PF: Primary follicle. SF: Secondary follicle. SCN: Severe congenital neutropenia. SAA: Severe aplastic anaemia. AA: Aplastic anaemia. SCD: Sickle cell disease. PCD: progressive cerebrovascular disease.

Histological analyses of pre-pubertal human ovarian grafts inside the mouse subcutaneous pocket

The follicle numbers at different stages in human pre-pubertal ovarian tissue xenografted subcutaneously in mice is shown in Table 7.14. All xenografts had follicles that survived xenotransplantation. A representative picture is illustrated as Figure 7.13.

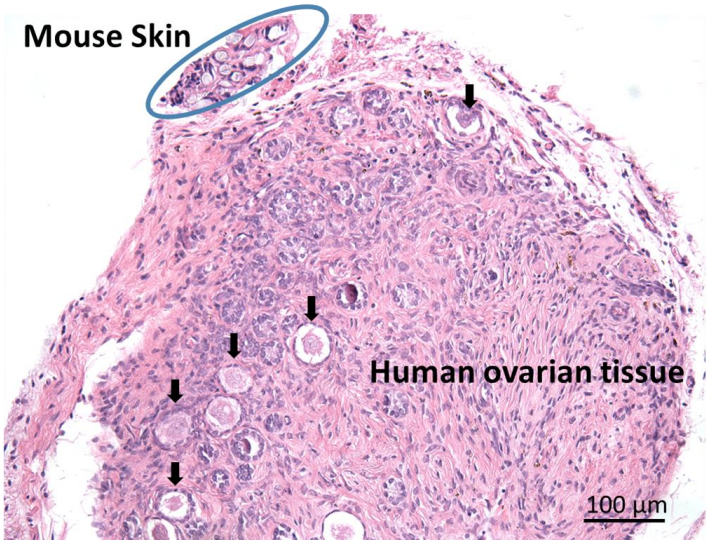


Figure 7.13. A representative ovarian tissue section micrograph of pre-pubertal human ovarian graft xenografted inside the mouse subcutaneous pocket and stained with H and E. Section was stained with H & E. Black arrows point to follicles. Blue circle denotes mouse skin. Bar represents 100µm.

Table 7.14. Follicle numbers and developmental stage in thawed pre-pubertal human ovarian tissue xenografted inside the mouse subcutaneous pocket.

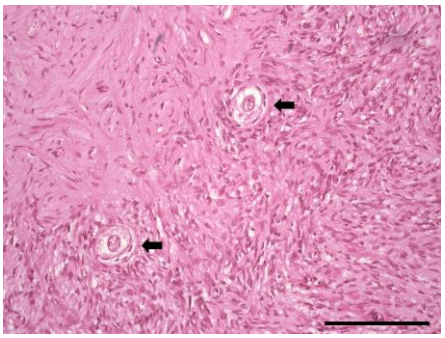
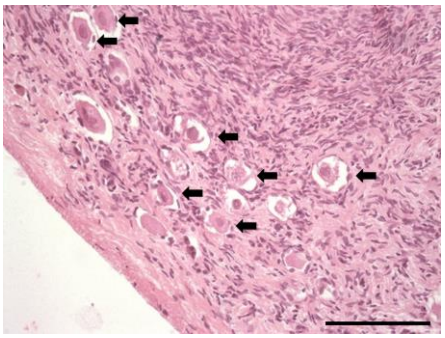
Patient No.	Age	Diagnoses	Follicle stages				Total
			PMF	Trans	PF	SF	
A	10	SCN	0	1	1	1	3
B	12	SAA	1	5	0	0	6
C	5	AA	2	0	1	0	3
D	6	SCD;PCD	27	17	2	1	47

PMF: Primordial follicle. Trans: Transitional follicle. PF: Primary follicle. SF: Secondary follicle. SCN: Severe congenital neutropenia. SAA: Severe aplastic anaemia. AA: Aplastic anaemia. SCD: Sickle cell disease. PCD: progressive cerebrovascular disease.

7.4.6 Comparisons between pre- and post-pubertal ovarian tissue

Due to different follicle counting and tissue fixation methods, pre- and post-pubertal ovarian tissue could not be directly compared. However, even after the follicle counting was performed in every 10^{th} section of the pre-pubertal ovarian tissue, the average number of primordial follicles was still higher than the average primordial follicle count in every single section of similar tissue size ($1mm^3$) for post-pubertal ovarian tissue (Table 7.15). This confirms that primordial follicles, which is our main focus, has a higher density in the pre-pubertal human ovarian tissue compared to the post-pubertal human ovarian tissue as would be expected.

Table 7.15. Mock comparison of the average primordial follicles counted between pre- and post-pubertal human ovarian tissue.

Ovarian tissue	Average follicles	Representative pictures
Post-pubertal	28.5 primordial follicles in $1mm^3$ (N=6)	
Pre-pubertal	40.7 primordial follicles in **1/10** of $1mm^3$ (N=4)	

Data is based on Table 7.7 and 7.11.
Black arrows point to the primordial follicles. Bars represent 100µm.

7.4.7 Uneven follicle distribution

In our study, follicles were found distributed non-homogeneously in both pre- and post-pubertal human ovarian tissue (Figure 7.14 and 7.15).

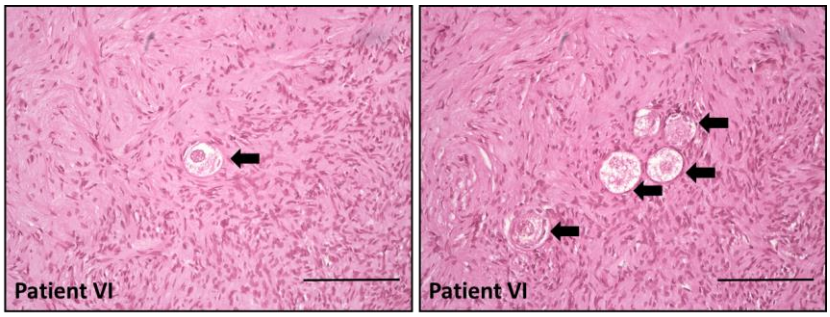


Figure 7.14. An example of uneven follicle distribution in the post-pubertal human ovarian tissue. This figure illustrated two ovarian tissue sections (left and right pictures) from the same post-pubertal patient (Patient VI) containing different numbers of follicles. Sections were stained with H & E. Black arrows point to follicles. Bars represent 100µm.

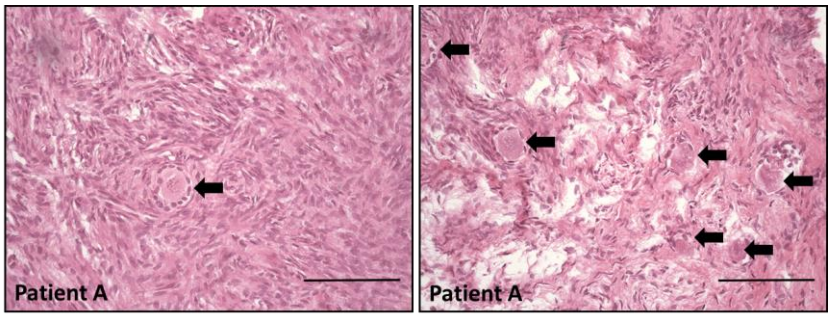


Figure 7.15. An example of uneven follicle distribution in the pre-pubertal human ovarian tissue. This figure illustrated two ovarian tissue sections (left and right pictures) from the same pre-pubertal patient (Patient A) containing different numbers of follicles. Sections were stained with H and E. Black arrows point to follicles. Bars represent 100µm.

7.4.8 Comparisons of follicles at each developmental stage before and after xenotransplantation

Within the post-pubertal human ovarian xenografts and the pre-pubertal human ovarian xenografts collected from under the kidney capsule and the ovarian bursa, there were not enough follicles to be analysed before and after xenotransplantation. However, in subcutaneous human pre-pubertal ovarian xenografts, a decreased proportion of primordial follicles and an increased proportion of growing follicles (transitional, primary and secondary follicles) were observed compared to the thawed non-grafted human ovarian tissue (Figure 7.16).

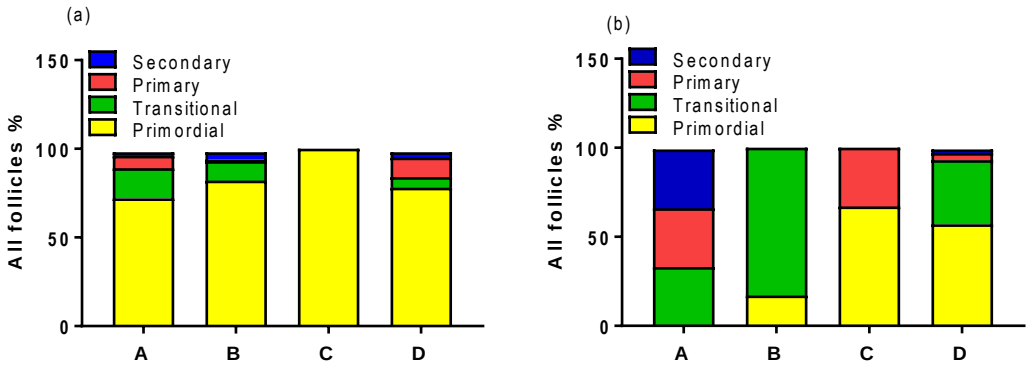


Figure 7.16. Percentage of follicles at the different developmental stages in pre-pubertal human ovarian tissue before and after a 6-week subcutaneous xenotransplantation (Patient A-D). (a) Percentage of follicles at the different developmental stages in thawed non-grafted pre-pubertal ovarian tissue. (b) Percentage of follicles at the different developmental stages in pre-pubertal ovarian xenografts after a 6-week subcutaneous xenotransplantation.

7.5 Discussion

In order to investigate the effects of AMH on preventing DXR-induced primordial follicle loss in human ovarian tissue xenotransplanted in mice, the present study was performed to establish effective xenotransplantation protocols. The survival and growth potential of both post- and pre-pubertal cryopreserved human ovarian tissue have been revealed, indicating that the cryopreservation protocol used by the OCTB team is effective. Among different xenotransplantation sites, all pre-pubertal human ovarian tissue xenografted subcutaneously in mice had follicles that survived 6 weeks after xenotransplantation.

Histological analysis of non-grafted pre- and post-pubertal human ovarian tissue

In this study, ovarian medulla and uneven follicle distribution was observed in the thawed human ovarian tissue.

As the only fertility preservation option for childhood cancer patients, ovarian tissue cryopreservation involves freezing ovarian cortical tissue (Donnez *et al*., 2013). The ovarian cortex is the outer layer of the ovary containing the majority of primordial follicles but is poorly vascularized, while the centre portion of the ovary known as the ovarian medulla, contains a large number of blood vessels and loose connective tissue. There is no distinct borderline between the ovarian cortex and medulla. In one piece of ovarian tissue ($1mm^3$) of Patient II and Patient B, there were no follicles found in the thawed ovarian tissue. However, the haematoxylin and eosin stained ovarian tissue sections from these two samples showed the presence of many blood vessels and loose connective tissue, indicating that these two pieces of ovarian tissue are from, or are very close to, the ovarian medulla (Figure 7.6 and 7.10). From the ovarian cortex to the medulla region, follicular density reduces (Kristensen *et al*., 2010).

Uneven distribution of follicles was observed in the current study. In ovarian tissue sections from the same patient, follicles were distributed non-homogeneously (Figure 7.14-15). Uneven follicular distribution has also been previously reported in human ovaries (Schmidt *et al*., 2003). It highlights the importance for transplanting multiple ovarian cortical strips back to cancer survivors to increase the chance of follicles to exist in the transplanted ovarian tissue. In subsequent studies, xenotransplantation of multiple pieces of human ovarian tissue would be used. Even though there was an uneven distribution of follicles, a higher follicular density was observed in the pre-pubertal ovarian tissue (Table 7.15). Consistent with previous work, a study investigating the follicle density of 17 cancer patients indicated a significant positive correlation between follicular density and age despite the variation within individual pieces of ovarian cortex (Kristensen *et al*., 2010).

Xenotransplantation and grafts retrieval

Mouse xenotransplantation has been used as a research model for numerous purposes such as the examination of the viability of cryopreserved ovarian tissue or the investigation of the effects of hormonal treatments on human ovarian tissue (Maltaris *et al*., 2007). SCID mice possess dysfunctional B and T lymphocytes offering a desirable condition for the development of a xenograft. However, there is no consensus on the optimal site for xenotransplantation. Studies indicate that different transplantation sites affect the follicular development of xenotransplanted human ovarian tissue (Terada *et al*., 2008, Dath *et al*., 2010). To compare the effect of different xenotransplantation sites, human ovarian tissues were placed under the mouse kidney capsule, ovarian bursa and into a subcutaneous pocket. We were able to retrieve the grafts from all mice hosting human ovarian tissue under the kidney capsule (10/10) and inside the subcutaneous pocket (4/4). However, under the mouse ovarian bursa, one piece of post-pubertal human ovarian graft was missing and another piece

was found inside the mouse abdominal cavity (2/6). In order to prevent losing grafts under the mouse ovarian bursa, sutures were added to close the ovarian bursa after xenografting the pre-pubertal human ovarian tissue. However, one piece of human pre-pubertal ovarian graft (1/4) was still lost. It is therefore concluded that there is a risk of losing grafts from under the mouse ovarian bursa.

Regarding the grafted tissue survival rate, all of the pre-pubertal human ovarian tissue subcutaneously xenografted in mice (4/4) survived xenotransplantation after 6 weeks. This is consistent with previous work; ovarian subcutaneous graft recovery was more than 90% in another study (Weissman *et al*., 1999). The mouse subcutaneous site has been previously described as giving poorly vascularized grafts. However, the xenografts in the current study were all revascularised as revealed by the presence of blood vessels containing red blood cells (4/4). Compared to the xenografts in other sites, more follicles were present in the mouse subcutaneous pocket grafts and this might be due to quicker revascularization. Revascularization of subcutaneous allotransplantation was detected as early as 2 days after surgery in rats (Dissen *et al*., 1994). However, further experiments to determine the revascularization time in subcutaneous xenotransplanted human ovarian tissue are required. In general, subcutaneous tissue grafting has several advantages compared to the other sites such as a less complicated surgical procedure, more follicles present post xenotransplantation and the ability to conduct external assessment as showed in Figure 7.1C.

Transplantation under the kidney capsule is one of the most frequently used xenotransplantation sites. It has been reported that 98% of human ovarian tissue xenografts survived under the kidney capsule in immunodeficient mice (Newton *et al*., 1996). The renal site has been thought to result in better survival rate, possibly due to an increase in vascularization (Sherwood, 1989). It also has the advantage of securing the graft by the kidney capsule membrane without additional sutures (Gosden *et al*., 1994). However, there

were not many follicles present after xenotransplantation in our study potentially due to the heterogeneous nature of follicle distribution in human ovaries.

The mouse ovarian bursa is a thin membrane that encapsulates the mouse ovary and the end of the oviduct and has been used as a site for xenotransplantation (Zhang *et al*., 2013). Compared to the ovarian grafts transplanted subcutaneously and beneath the kidney capsule, a previous study demonstrated that only grafts under the ovarian bursa had mature Graafian follicles within 12 weeks of xenotransplantation (Terada *et al*., 2008). This has been suggested to be due to blood flow and exogenous gonadotropins administered (Terada *et al*., 2008). In the Terada *et al.* study, bilateral ovariectomy was performed and human menopausal gonadotropin was intraperitoneally injected into the hosts for 2 weeks after 10 weeks of the xenotransplantation.

In contrast to published studies, none of the post-pubertal human ovarian tissue xenografted under the mouse ovarian bursa had follicles 3 weeks after the xenotransplantation and only a few grafts had follicles 6 weeks after xenotransplantation (2/10). This is potentially due to the presence of the hosts' own ovaries, which resulted in too limited space to secure the graft in place and less success in establishing revascularisation of the human ovarian grafts (2/10). Limited space under ovarian bursa can be optimised by performing ovariectomy. However, as discussed in Section 7.1, ovariectomy will not be performed in order to avoid us investigating the effect of AMH. Therefore, in our study, compared to under the mouse kidney capsule and the subcutaneous pocket, grafts under the mouse ovarian bursa were more likely to be lost, which was in agreement with previous researchers (Dath *et al*., 2010).

Based on the above results, xenotransplantation site under the mouse ovarian bursa would not be used in our following experiments.

Less primordial follicles and more growing follicles in the subcutaneous xenografts

According to Figure 7.16, there is a reduced proportion of primordial follicles and a higher percentage of growing follicles in subcutaneous xenografted human ovarian tissue. This is in line with previous publications (Hernandez-Fonseca *et al*., 2004) and is possibly due to reduced expression of the phosphatase and tensin homologue (PTEN) (Ayuandari *et al*., 2016) which has been shown after subcutaneous xenotransplantation. PTEN negatively regulates the PI3K pathway and plays a vital role in primordial follicle activation.

Ovarian fragmentation might also contribute to the activation of primordial follicles which is possibly due to reduced pressure from the dense ovarian tissue (Silber, 2016). Hippo signalling might also be involved in fragmentation-induced primordial follicle activation (Kawamura *et al*., 2013). Therefore, in future studies, larger piece of human ovarian tissue would be used to avoid excess fragmentation-induced primordial follicle activation.

The reason for the absence of antral follicles in our studies might be due to the short term of xenotransplantation. Lotz *et al*., (2014) indicated that, without exogenous gonadotropin stimulation, pre-pubertal ovarian tissue had antral follicles and mature oocytes after 4-month xenotransplantation.

Massive follicle loss in human ovarian grafts after xenotransplantation

In the present study, compared to the thawed non-grafted human ovarian tissue, the majority of the human ovarian xenografts had significantly less follicle numbers. Ischemic reperfusion injury has been thought of as one of the primary reasons resulting in failed transplantation (Jassem and Heaton, 2004). A sufficient blood supply has been suggested to play an important role in primordial follicle survival (Soleimani *et al*., 2008). In our study, the human ovarian grafts that contained no blood vessels or red blood cells had no follicles

present. However, the grafts with blood vessels but no follicles, may be due to uneven distribution of follicles but might also be due to ischemia induced follicle loss which takes place before revascularisation is established. It has been shown that in intraperitoneal xenotransplanted grafts in nude mice, hypoxia was identified during the first five days with a significant increase in oxygenation in the following five days (Van Eyck *et al*., 2009). Quick establishment of an effective blood supply would likely contribute to the survival of ovarian follicles in transplanted ovarian tissues. The profuse blood supply has been thought of as the main reason to select graft placements under the mouse kidney capsule and ovarian bursa (Weissman *et al*., 1999).

Follicles can survive xenotransplantation without hormone stimulation

External hormonal stimulation was commonly used to support graft growth. FSH has been reported to protect the transplanted tissue from ischemic damage by accelerating revascularization (Ma *et al.,* 2017). In addition to external hormone stimulation, it has been shown that the absence of the host ovaries contributed to an enhanced follicular development in the xenografted human ovarian tissue (Maltaris *et al*., 2006). This is because removal of the hosts' ovaries removes negative feedback thus providing a high FSH environment. The potential mechanism behind this is possibly due to the FSH-induced increase in expression of the vascular endothelial growth factor, stimulation of the PI3K/AKT pathway and a subsequent increase in the expression of survivin (Huang *et al.,* 2008). However, the PI3K/AKT pathway plays a key role in primordial follicle activation. The present study was primarily done to establish the best model to determine the effect of AMH on DXR-induced primordial follicle loss in human ovarian tissue *in vivo*. Therefore the use of FSH was avoided since it might affect the effect of AMH on primordial follicles.

In previous work, very few papers reported xenotransplantation of human ovarian tissue without hormonal stimulations (Dolmans *et al.*, 2007; Dath *et al*., 2010). Consistent with these studies, our data provide evidence that follicles in xenografted post- and pre-pubertal human ovarian tissue can develop and survive in mice with intact ovaries.

7.6 Conclusion

In this study, both the post- and pre-pubertal cryopreserved human ovarian tissue obtained from the OCTB retained the ability to survive and develop. Due to the variation in follicle density and distribution of follicles within human ovaries, transplantation of multiple pieces of human ovarian tissue was particularly important both experimentally and clinically. Subcutaneous and renal sites of xenotransplantation will be used for our following experiments primarily due to the high graft recovery rate. In addition, larger pieces of human ovarian tissue are planned to be transplanted to avoid excess fragmentation induced primordial follicle activation. Pre-pubertal ovarian tissue will also be used for the following experiment mainly because of higher follicle density compared to post-pubertal tissue. The established xenotransplantation protocols in this chapter allowed us to progress to conduct experiments using transplanted human ovarian tissue.

Chapter 8: Investigation of the effects of Anti-Müllerian Hormone on Doxorubicin-induced primordial follicle loss in human ovarian tissue xenotransplanted into mice

8.1 Introduction

Doxorubicin (DXR), a commonly used chemotherapy agent in childhood cancers, results in a significant loss of primordial follicles (as described in Chapter 5 and 6). AMH has been shown to exert a protective effect on primordial follicle loss with DXR in mice *in vivo* (Kano *et al*., 2017), and this warranted further investigation in order to determine if AMH exerts the same effect against DXR on human ovarian tissue *in vivo*.

In order to investigate the effect of AMH on DXR-induced primordial follicle loss in xenotransplanted human ovarian tissue, an experimental protocol of xenotransplantation of pre-pubertal human ovarian tissue into SCID mice was established (described in Chapter 7).

The most frequently used method of administration of DXR into mice was by intra-peritoneal (IP) injections as referred to in Chapter 1 (Table 1.7). Different strains of mice tolerate different doses of chemotherapy (Aston *et al*., 2017). The administration of DXR in SCID mice had not previously been carried out at the University of Oxford and therefore, we selected a dose of DXR based on the literature. DXR appears to be more toxic in mice than in humans since a single dose of 5mg/kg (IP injection) which is lower than equivalent dose used in patients (Chapter 1; Table 1.3) killed mice within one week (Denard *et al*., 2015). There are no deaths reported following a single injection of DXR at a dose of 4mg/kg so far (Sonowal *et al*., 2017). Therefore, a dose of DXR at 4mg/kg was used in our experiment.

Due to uneven follicle distribution in human ovarian tissue (as illustrated in Chapter 7), two pieces of pre-pubertal human ovarian tissue from the same patient would be xenografted into each host mouse in order to maximise the chance of follicles being present. One piece would be placed under the mouse kidney capsule, and the other would be placed into the mouse subcutaneous pocket, based on results obtained in Chapter 7. The piece of

human ovarian tissue placed inside the mouse subcutaneous pocket would be larger to avoid the risk of excessive fragmentation-induced primordial follicle activation.

We hypothesized that AMH could prevent DXR-induced primordial follicle loss in pre-pubertal human ovarian tissue when xenotransplanted into mice. Since the mouse ovaries would also remain *in situ*, we also hypothesized that AMH could prevent DXR-induced primordial follicle loss in mouse ovaries.

8.2 Aims

- To determine if AMH can attenuate primordial follicle loss in pre-pubertal human ovarian tissue xenotransplanted into mice and in the mouse ovaries;
- To evaluate the effects of DXR on pre-pubertal human ovarian tissue xenotransplanted into mice and mouse ovaries;
- To determine if AMH can prevent DXR-induced primordial follicle loss in human ovarian xenografts and mouse ovaries;
- To compare follicular development, and the effects of AMH and DXR treatment on the human ovarian grafts in different xenotransplantation sites.

8.3 Materials and Methods

8.3.1 Patient Inclusion and Exclusion Criteria

All patients included in this study were selected through the anonymised OCTB database as described in Chapter 7 and summarised in Table 8.1.

Table 8.1. Summary of patient inclusion and exclusion criteria.

Criteria	Pre-pubertal patients
Inclusion	Pre-puberty
	Surgery and OTC within 24 hours
	Consent to research and animal studies
	Cortical strips total number > 50 strips
Exclusion	Received anti-cancer treatments before OTC
	Diagnosed with diseases involving ovarian tissues

OTC: ovarian tissue cryopreservation.

8.3.2 Human ovarian cortical strips

Four strips of ovarian cortical tissue were used from each patient; one for each treatment. Thawing was carried out based on the OCTB protocol as described in Section 2.5. Each single strip of ovarian cortical tissue (1x1x5 mm) was put into a sterile glass petri dish containing L-15 media at 4°C in order to slow down tissue degeneration after thawing. Each strip was cut into two 1x1x1 mm pieces (one for post-thawed non-grafting histological analysis, and the other one for kidney capsule transplantation) and one large (1x1x3 mm) piece for subcutaneous transplantation (Figure 8.1).

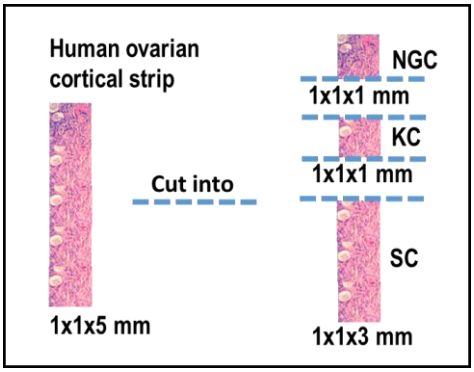


Figure 8.1. Human ovarian cortical strip division and allocation used in the current study. NGC: non-grafted human ovarian tissue. KC: kidney capsule. SC: subcutaneous pocket.

The piece of ovarian tissue (1x1x1 mm) as a non-grafting control was fixed in 10% neutral buffered formalin for 8 hours. The fragments of human ovarian tissue that were used for xenotransplantation were transported to the animal facilities as described in Chapter 7.

8.3.3 Animals

Severe combined immune deficiency (SCID) female mice aged between 9 to 10 weeks were used as hosts for pre-pubertal human ovarian cortical tissue. The mice were housed and acclimatised as described in Section 2.2.

SCID mice were weighed, ear-clipped and divided into four groups by weight, the Control (PBS-treated) group (n=6), AMH treated group (n=6), DXR-treated group (n=6) and AMH+DXR (co-treatment) group (n=6). Every SCID mouse received one piece of human ovarian tissue in each transplantation site; under the kidney capsule and into a subcutaneous pocket.

8.3.4 Xenotransplantation

Anaesthesia induction and initial preparations were performed as described in Section 7.3.4.1. Once the mice were anaesthetised, xenotransplantation under the mouse kidney capsule was performed followed by xenotransplantation into a mouse subcutaneous pocket. The specific surgical procedures are described in Section 7.3.4.2 and 7.3.4.4. Mice were transferred back to the cage after they had fully recovered from the anaesthesia as described in 7.3.4.5.

All four strips of human ovarian cortical strips from the same patient were thawed at the same time. To avoid any potential adverse effects caused by the different duration before surgery and after tissue thawing on our experimental results, the sequence of each group was rotated. Additionally, this was the first time we performed two xenotransplantations within one surgery and four surgeries per patient's ovarian tissue. In order to shorten the duration between human ovarian tissue thawing and surgery, when I was approaching completion of one surgery, Dr Sairah Sheikh would have the next anaesthetized mouse ready for surgery. Dr Sheikh would then monitor recovery of the mouse that had undergone surgery. All surgeries were performed by the candidate.

8.3.5 Post-surgical monitoring

The mice were singly housed for 24 hours after surgery, after one day, they were then housed together with other mice in the same treatment group. Mice were weighed, monitored and evaluated based on post-surgical assessment form (as described in Chapter 2) daily for the first two days post surgery and every three days before the PBS/AMH treatment began 10 days later.

8.3.6 Reagent

Lyophilized rhAMH (R&D systems, UK) was reconstituted as described in Chapter 6. In order to make sure the dissolved solution contained protein, Mini BCA assay was performed before the experiment started to determine protein concentrations as described in Chapter 6. DXR (Sigma) was dissolved in sterile water at 10mg/ml and further diluted with DPBS to 4mg/ml for injection.

8.3.7 Drug administration

Ten days after the surgery, mice were given a single IP injection of either 200µl of PBS in the Control and DXR groups or rhAMH (300ng rhAMH in 200µl of PBS) in the AMH and the co-treatment groups (Day 0) in the morning for eight days (Figure 8.2). Mice were given additional soft food inside the mouse cage (i.e. normal food soaked in clean water) which was changed daily until the end of this experiment to facilitate feeding in the case of chemotherapy-induced loss of appetite. On the afternoon of Day 1 (after two injections of the rhAMH and PBS) DXR was IP injected into the mice at a dose of 4mg/kg (based on each individual mouse weight) in the DXR and co-treatment groups and PBS was injected into mice in the Control and AMH groups. From this stage, all mice that received DXR were housed in a new cage to avoid any risk of contaminations of the DXR from their urine or bedding to the mice in the non-DXR groups.

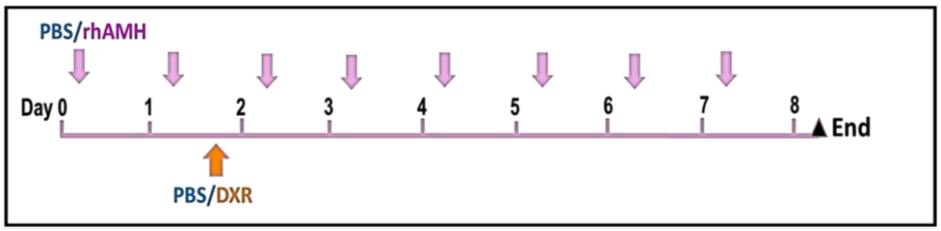


Figure 8.2. SCID mice were intraperitoneally (IP) injected daily with PBS or rhAMH for eight days with a single IP injection of PBS or DXR on the second day.

8.3.8 Post drug administration monitor

The mice were weighed and behaviour assessed before and after each injection. In this particular study, mouse appetite was monitored by observing the presence of the normal food left inside the cage and the soft food in the petri dish.

One mouse was found dead on Day 7 (as described in the result section), and thus mouse monitoring was increased to twice a day after this point.

8.3.9 Xenografts and mouse tissue collection

At the end of this experiment, mouse blood was collected via cardiac puncture by Dr Suzannah Williams, whilst under anaesthesia established by the candidate. All mice were then sacrificed by cervical dislocation. Xenotransplanted human ovarian tissue were then retrieved from the mouse subcutaneous pocket and from the mouse kidney capsule. All tissues were immediately placed into fixative upon retrieval. Mouse ovaries were also collected. The spleen was collected by Dr Suzannah Williams.

Mouse blood (100µl/mouse) was put into EDTA blood collection tubes (Starstedt, Germany) and sent to the Molecular Haematology Unit at the John Radcliffe Hospital, Oxford. Mouse red blood counts were measured using the Scil Vet abc Plus™ hematology analyser (Horiba ABX, Warsaw, Poland).

8.3.10 Histology process and analysis

Human xenografts and mouse ovaries were fixed, processed and sectioned as described in Chapter 2. Every 10^{th} human and mouse ovarian section was stained with haematoxylin and eosin, and analysed. Follicles containing a nucleus were counted at different stages classified as described in Chapter 2. The mouse spleens were fixed, weighed and stored in 70% ethanol at 4°C.

The total number of follicles at each developmental stage was calculated using the Abercrombie correction factor (Abercrombie, 1946) (Section 2.6.6.3). Oocyte nuclear diameters were measured in 10 follicles (if >10 follicles, only measure 10) located in the top, middle and bottom of each human ovarian graft. The mouse ovarian sections were imaged and the nucleus area measured using image J. All mouse ovaries and human ovarian grafts were analysed blind. In this study, we specifically focused on primordial follicles, and therefore all follicles beyond the primordial stage were presented as combined data named "growing follicles". Healthy follicles were defined as described in Section 2.6.6.2. The follicles were considered unhealthy and atretic if the oocyte was degenerating, the oocyte nucleus was pyknotic or fragmented, or if more than 10% of granulosa cells were pyknotic.

8.3.11 Statistical Analysis

All data was analysed using GraphPad Prism version 7.00 (GraphPad Software, USA). Data was tested for normality using a Shapiro-Wilk normality test. One-way ANOVA was applied to determine if there were any differences present across different treatments for groups which had normally distributed data. If the data were not normally distributed, the Kruskal Wallis test and the Dunn's multiple comparisons test were then used. Results are presented as mean ± S.E.M. Significance was considered when $P<0.05$.

8.4 Results

8.4.1 Patient profiles

Based on the inclusion and exclusion criteria as summarised in Table 8.1, ovarian cortical strips from pre-pubertal patients (n=6) were collected from the OCTB. Patient information is listed in Table 8.2.

Table 8.2. Age and diagnoses of pre-pubertal patient's tissue (n=6) used in this study.

Patient No.	Age	Diagnoses
A	12	Severe aplastic anaemia (SAA)
B	5	Aplastic anaemia (AA)
C	12	Sickle Cell Disease (SCD)
D	10	Severe congenital neutropenia (SCN)
E	6	Sickle cell disease; progressive cerebrovascular disease (SCD;PCD)
F	4	Beta Thalassemia (β-thal)

8.4.2 Xenotransplantation and graft retrieval

Pre-pubertal ovarian xenografts were recovered from the mouse kidney capsule and the subcutaneous pocket in Control, AMH, DXR and cotreatment groups as described in Table 8.3-4.

Table 8.3. Proportion of pre-pubertal human ovarian xenografts retrieved from different transplantation sites in SCID mice.

Sites	Control	AMH	DXR	DXR+AMH
Kidney capsule	6/6	6/6	6/6	4/5
Subcutaneous	6/6	6/6	6/6	5/5

One mouse was found dead in the DXR+AMH group and the collected xenografts from that mouse were excluded. One kidney capsule graft xenografted was lost.

Table 8.4. Number of pre-pubertal human ovarian xenografts used for histological analyses in this study.

Sites	Control	AMH*	DXR	DXR+AMH
Kidney capsule	6	4	6	4
Subcutaneous	6	4	6	5

**Two pieces of tissue from two patients in this group together with the non-grafted ovarian tissue looked abnormal (no nuclear was stained after H & E staining), so they were excluded.*

8.4.3 DXR effects in mice

The mouse weight in the Control and AMH groups were steady during the entire study. In the DXR and co-treated group, mice lost weight after the administration of DXR (4mg/kg) (Figure 8.3).

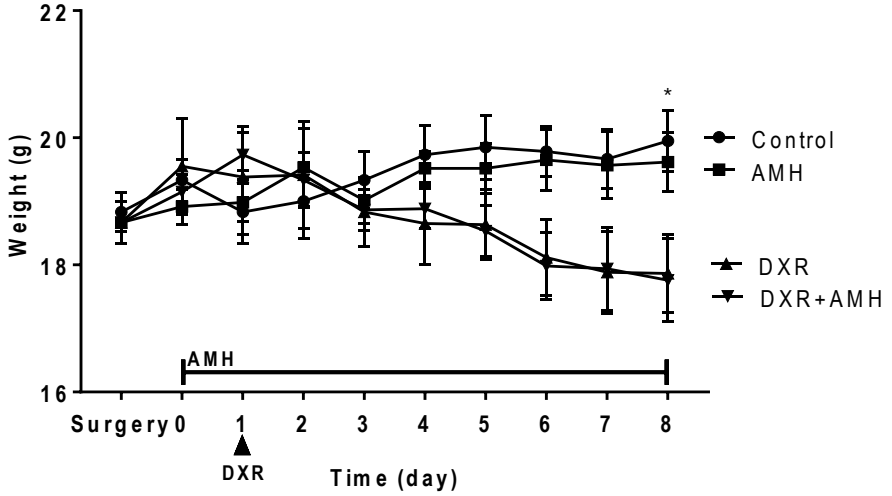


Figure 8.3. Mouse weight at the time of the surgery and during 8 days of treatment with PBS, AMH, DXR or co-treatment (DXR+AMH) starting 10 days after surgery. Data was presented as Mean ± S.E.M. Control group: n=6. AMH group: n=6. DXR group: n=6. Co-treatment group: n=6 until day 6; n=5 from day 7 to the end of the experiment). *P<0.05.

The soft food in the petri dish and normal food left inside the cage was eaten by the host mice in the Control and AMH groups daily during the entire experiment. In the DXR and co-treated groups, although the normal food left in the cage was found partially eaten, the soft food in the petri dish was not eaten from the second day after the chemotherapy administration, indicating a loss of appetite. In the DXR and co-treatment group, there was red urine found 2 days following the DXR administration.

Compared to mice in the Control and AMH groups, mice in the DXR and co-treatment groups had a reduced spleen weight at the end of the experiment (Figure 8.4).

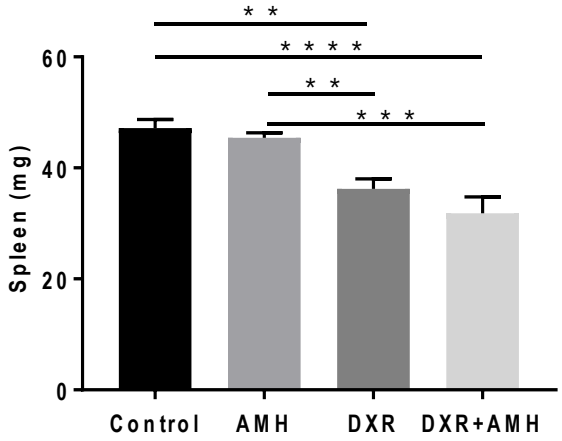


Figure 8.4. The spleen weight of the mice after 8 days of treatment with PBS, AMH, DXR or co-treatment (DXR+AMH). Data are presented as Mean ± S.E.M. Control group: n=6. AMH group: n=6. DXR group: n=6. Co-treatment group: n=5. **P<0.01. ***P<0.001. ****P<0.0001.

According to the haematological analysis results, there was no difference found in mouse red blood cells at the end of this experiment between the different treatment groups (Figure 8.5).

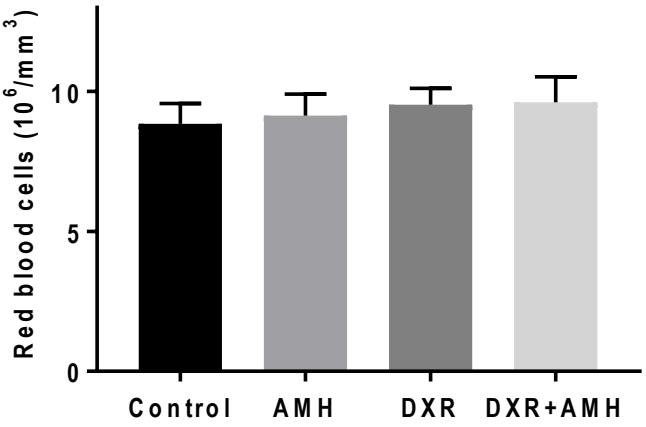


Figure 8.5. The mouse red blood cell counts of the mice after 8 days of treatment with PBS, AMH, DXR or co-treatment (DXR+AMH). Data are presented as Mean ± S.E.M. Control group: n=5. AMH group: n=6. DXR group: n=6. Co-treatment group: n=5.

8.4.4 Effect of Doxorubicin and AMH on mouse ovaries

8.4.4.1 Ovarian volume of SCID host mouse

At the end of the experiment, ovarian volume in mice treated with DXR was ~50% of the size of ovaries in control and AMH groups (Figure 8.6).

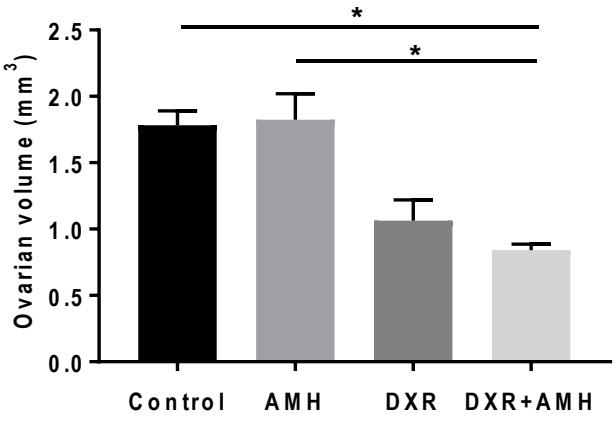


Figure 8.6. The ovarian volume of the mice after 8 days of treatment with PBS, AMH, DXR or co-treatment (DXR+AMH). Data is presented as Mean ± S.E.M. Control group: n=6. AMH group: n=6. DXR group: n=6. Co-treatment group: n=5. *P<0.05.

8.4.4.2 Primordial follicle numbers in SCID host mouse ovaries

The total number of primordial follicles was significantly lower in mice in the DXR group compared to Control and AMH groups (Figure 8.7). In addition, the mice co-treated with DXR and AMH had less primordial follicle numbers compared to the mice in the AMH group.

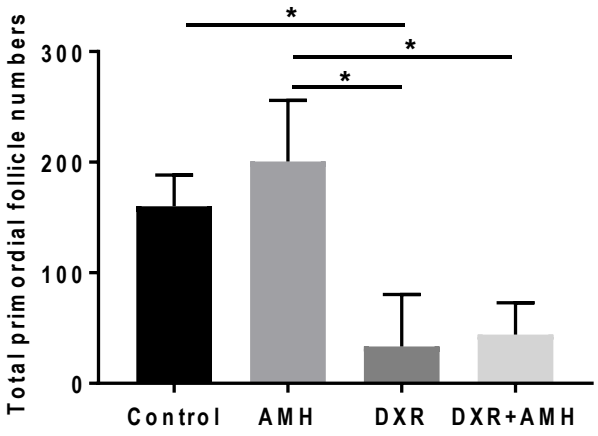


Figure 8.7. Primordial follicle numbers in mouse ovaries after 8 days of treatment with PBS, AMH, DXR or co-treatment (DXR+AMH). Data are presented as Mean ± S.E.M. Control group: n=6. AMH group: n=6. DXR group: n=6. Co-treatment group: n=5. *P<0.05.

Regarding the numbers of growing follicles, mice treated with DXR had lower growing follicle numbers compared to mice without any DXR treatment (Figure 8.8).

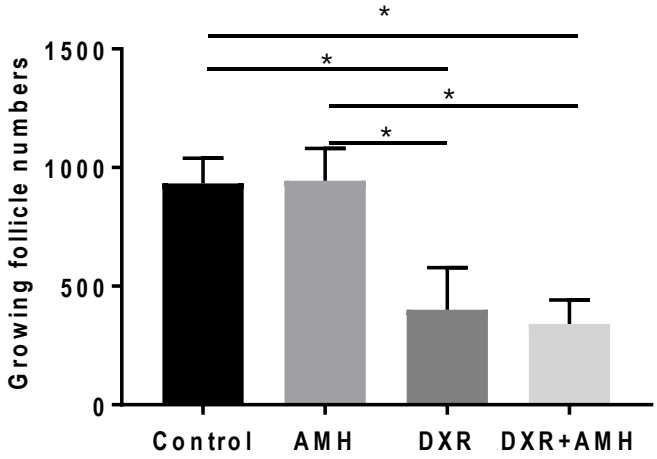


Figure 8.8. Growing follicle numbers in mouse ovaries from the Control, AMH, DXR and DXR+AMH groups at the end of the experiment. Data is presented as Mean ± S.E.M. Control group: n=6. AMH group: n=6. DXR group: n=6. Co-treatment group: n=5. *P<0.05.

When follicle numbers were expressed as a percentage, DXR-treated mice had a lower proportion of primordial follicles compared to the AMH group (Figure 8.9). Equally, DXR treatment resulted in significantly higher percentages of growing follicles in the DXR and co-treatment group in comparison with the AMH-treated mice.

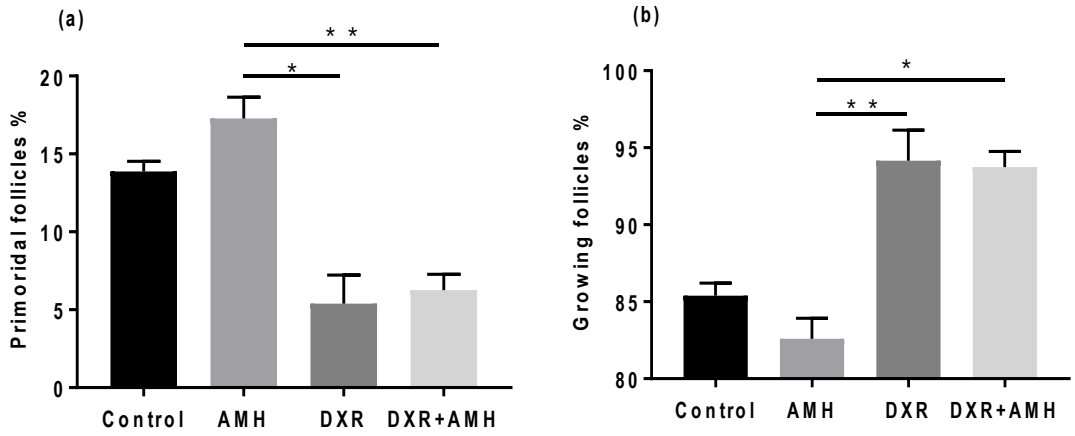


Figure 8.9. Comparison of percentages of primordial follicles and growing follicles in the mouse ovaries from the Control, AMH, DXR and DXR+AMH groups at the end of the experiment. (a) Primordial follicle percentages in the mouse ovaries from different groups. (b) Growing follicle percentages in the mouse ovaries from different groups. The data are presented as Mean ± S.E.M. Control group: n=6. AMH group: n=6. DXR group: n=6. Co-treatment group: n=5. *P<0.05. **P<0.01.

The health of the mouse primordial follicles was not easily determined. Based on analyses of the mouse growing follicles, the majority of growing follicles in the DXR and co-treatment groups were unhealthy (Figure 8.10).

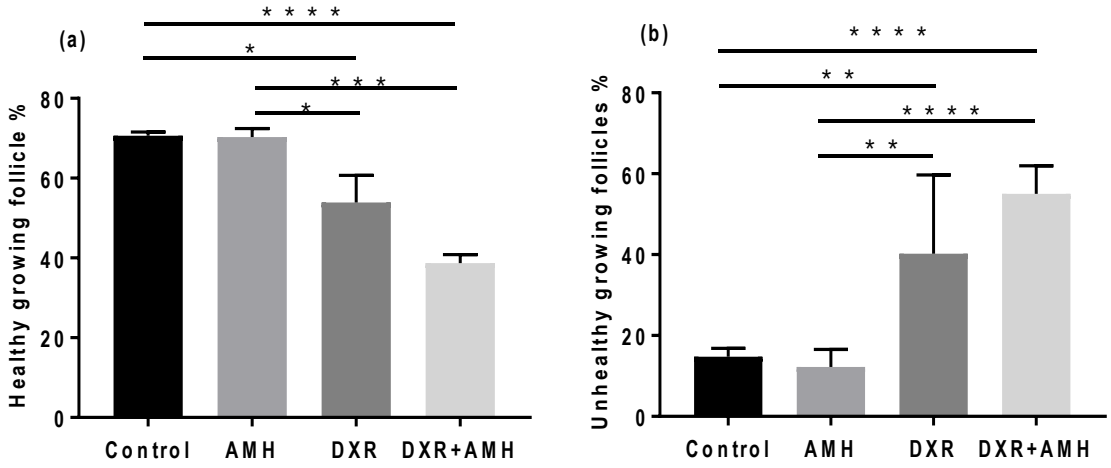


Figure 8.10. Comparison of percentages of healthy and unhealthy growing follicles in mouse ovaries from the Control, AMH, DXR and DXR+AMH groups at the end of the experiment. (a) Healthy growing follicle percentages in mouse ovaries from different groups. (b) Unhealthy growing follicle percentages in mouse ovaries from different groups. The data are presented as Mean ± S.E.M. Control group: n=6. AMH group: n=6. DXR group: n=6. Co-treatment group: n=5. *P<0.05. **P<0.01. ***P<0.001. ****P<0.0001.

8.4.5 Effect of Doxorubicin and AMH on human ovarian tissue xenotransplanted under the mouse kidney capsule

8.4.5.1 Human ovarian follicle stage classification

Follicles at different stages in the pre-pubertal human ovarian tissue are illustrated in Figure 8.11.

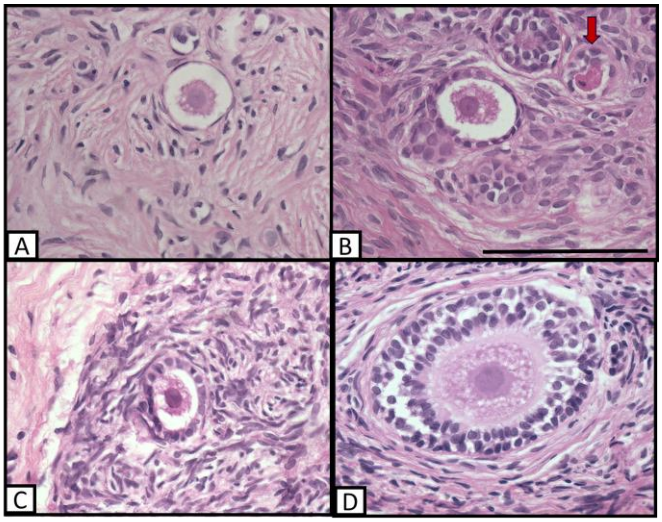


Figure 8.11. Follicles at different stages in pre-pubertal human ovarian tissue fixed in 10% neutral buffered formalin and stained with H and E. A: Primordial follicle. B-D: Growing follicles (B: Transitional follicle. C: Primary follicle. D: Secondary follicle). Red arrow denotes an unhealthy follicle. Bar represents 100μm.

8.4.5.2 Human follicle development after xenotransplantation

After xenotransplantation, there is a decrease in the percentage of primordial follicles and an increase in the proportion of growing follicles, indicating good survival and development of transplanted human ovarian tissue (Figure 8.12).

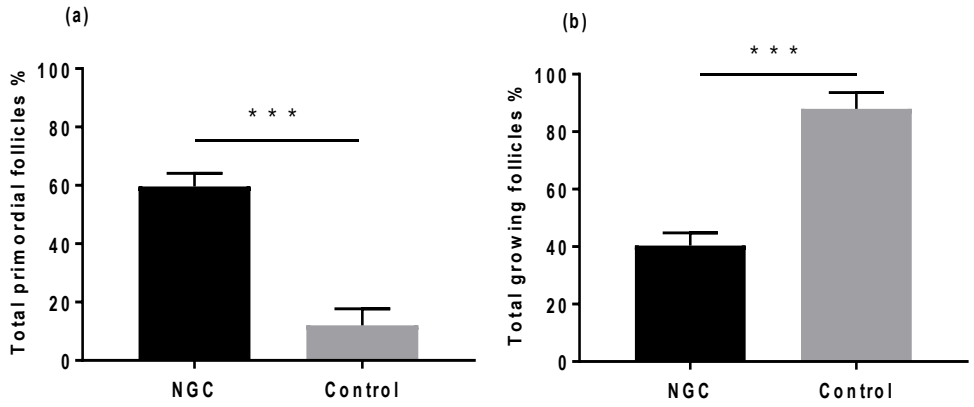


Figure 8.12. Comparison of percentages of primordial follicles and growing follicles between human ovarian tissue before and after xenotransplantation under the kidney capsule. (a) Primordial follicle percentages in non-grafted human ovarian tissue and xenografts after xenotransplantation. (b) Growing follicle percentages in non-grafted human ovarian tissue and xenografts after xenotransplantation. The data is presented as Mean ± S.D. NGC: Non-grafted control. NGC group: n=20. Control: n=5. ***P<0.001.

8.4.5.3 Comparison of human primordial follicles in DXR and AMH treated groups

There was no difference in the primordial follicle density of the human ovarian grafts in mice from the control, AMH, DXR and cotreatment groups (Figure 8.13).

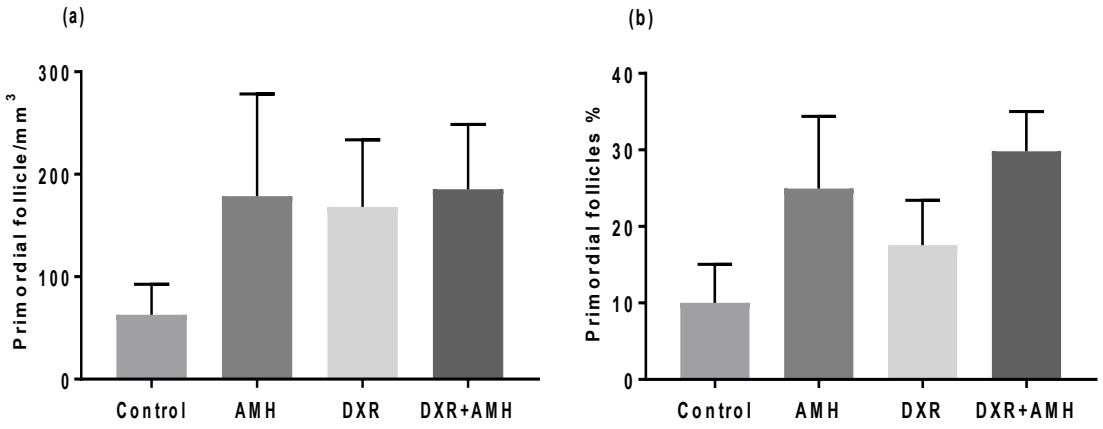


Figure 8.13. Comparison of total primordial follicle density and percentages in the human ovarian xenografts retrieved from the mouse kidney capsule from the Control, AMH, DXR and DXR+AMH groups. (a) Primordial follicle density in the human ovarian xenografts retrieved from the kidney capsule from different groups. (b) Primordial follicle percentages in the human ovarian xenografts retrieved from the kidney capsule from different groups. The data are presented as Mean ± S.E.M. Control group: n=6. AMH group: n=4. DXR group: n=6. DXR+AMH group: n=4.

Compared to control group, significantly lower percentages of healthy primordial follicles were observed in the xenografts retrieved from the kidney capsule of the DXR+AMH treated group (Figure 8.14).

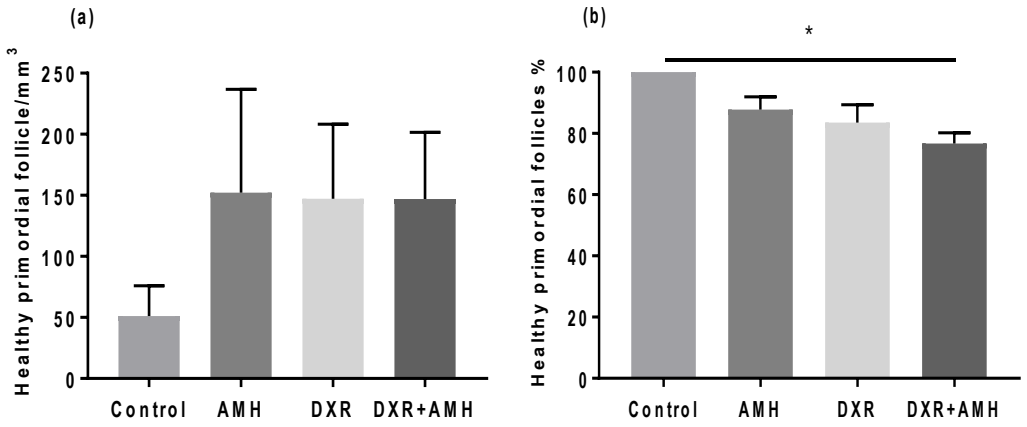


Figure 8.14. Comparison of healthy primordial follicle density and percentages in the human ovarian xenografts retrieved from the mouse kidney capsule from the Control, AMH, DXR and DXR+AMH groups. The data are presented as Mean ± S.E.M. (a) Healthy primordial follicle density in the human ovarian xenografts retrieved from the kidney capsule from different groups. Control group: n=6. AMH group: n=4. DXR group: n=6. DXR+AMH group: n=4. (b) Healthy primordial follicle percentages in the human ovarian xenografts retrieved from the kidney capsule from different groups. Control group: n=3. AMH group: n=4. DXR group: n=4. DXR+AMH group: n=4. *P<0.05.

Considering the decline in healthy primordial follicles in the co-treatment group, significantly higher percentages of unhealthy primordial follicles were detected also in the co-treatment group in comparison with the control group (Figure 8.15).

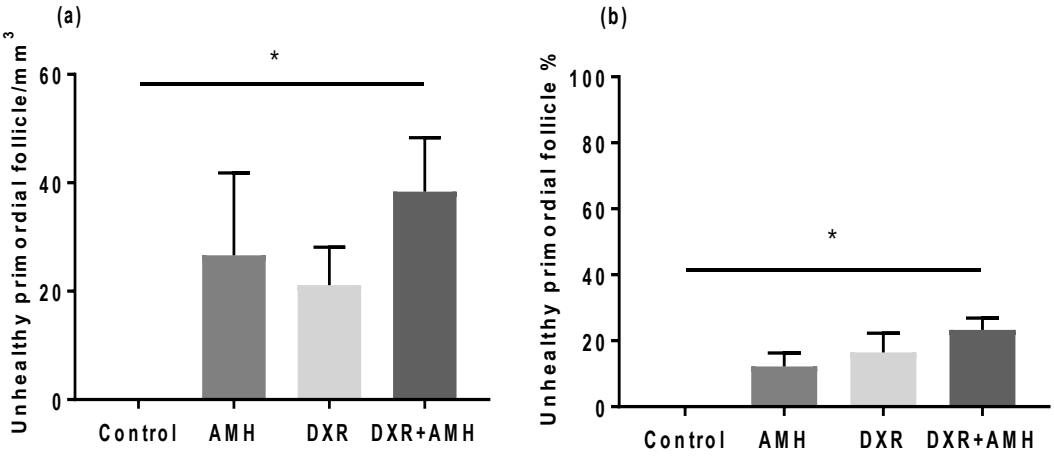


Figure 8.15. Comparison of unhealthy primordial follicle density and percentages in the human ovarian xenografts retrieved from the mouse kidney capsule from the Control, AMH, DXR and DXR+AMH groups. The data are presented as Mean ± S.E.M. (a) Unhealthy primordial follicle density in the human ovarian xenografts retrieved from the kidney capsule from different groups. Control group: n=6. AMH group: n=4 DXR group: n=6. DXR+AMH group: n=4. (b) Unhealthy primordial follicle percentages in the human ovarian xenografts retrieved from the kidney capsule from different groups. Control group: n=3. AMH group: n=4. DXR group: n=4. DXR+AMH group: n=4. *P<0.05.

There was no difference in the total growing follicle density in the human ovarian tissue between the different groups (Figure 8.16).

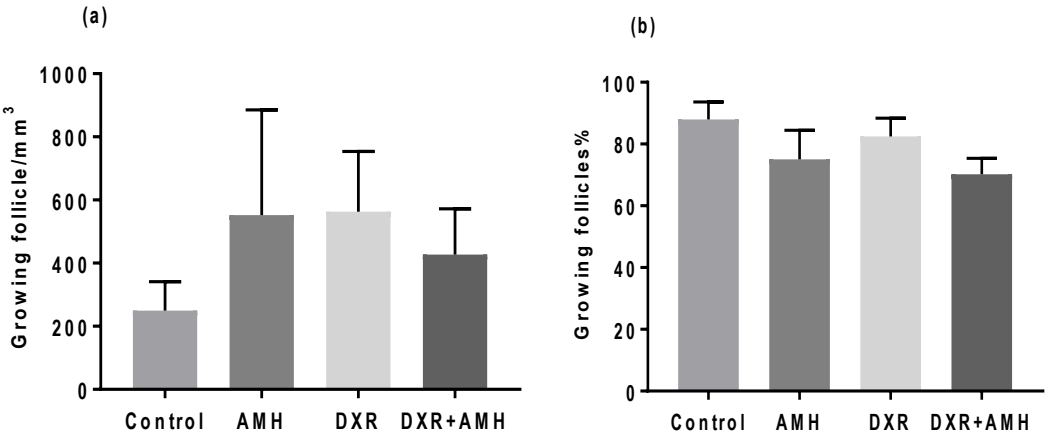


Figure 8.16. Comparison of total growing follicle density and percentages in the human ovarian xenografts retrieved from the mouse kidney capsule from the Control, AMH, DXR and DXR+AMH groups. The data are presented as Mean ± S.E.M. (a) Growing follicle density in the human ovarian xenografts retrieved from the kidney capsule from different groups. Control group: n=6. AMH group: n=4. DXR group: n=6. DXR+AMH group: n=4. (b) Growing follicle percentages in the human ovarian xenografts retrieved from the kidney capsule from different groups. Control group: n=5. AMH group: n=4. DXR group: n=6. DXR+AMH group: n=4.

There was also no difference observed in the density or percentages of healthy growing follicles between the different groups (Figure 8.17).

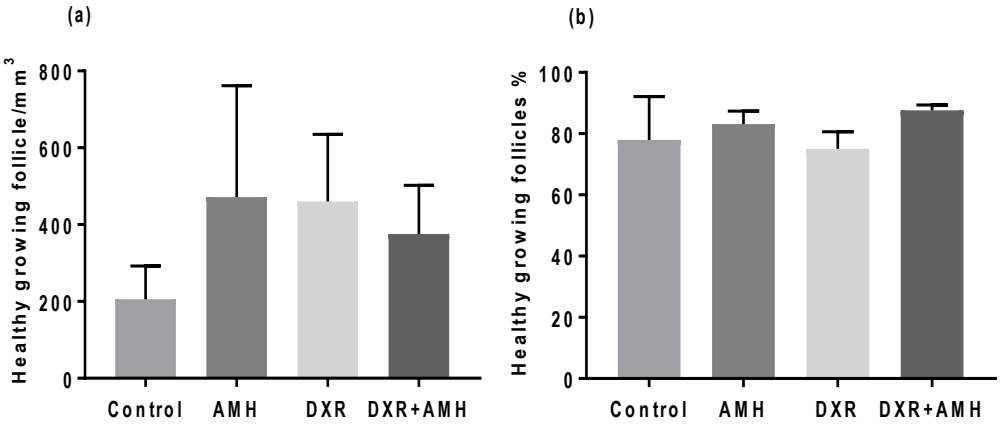


Figure 8.17. Comparison of healthy growing follicle density and percentages in the human ovarian xenografts retrieved from the mouse kidney capsule from the Control, AMH, DXR and DXR+AMH groups. The data are presented as Mean±S.E.M. (a) Healthy growing follicle density in the human ovarian xenografts retrieved from the kidney capsule from different groups. Control group: n=6. AMH group: n=4. DXR group: n=6. DXR+AMH group: n=4. (b) Healthy growing follicle percentages in the human ovarian xenografts retrieved from the kidney capsule from different groups. Control group: n=5. AMH group: n=4. DXR group: n=6. DXR+AMH group: n=4.

Similarly, there was no difference observed in the density or percentages of unhealthy growing follicles between different groups (Figure 8.18).

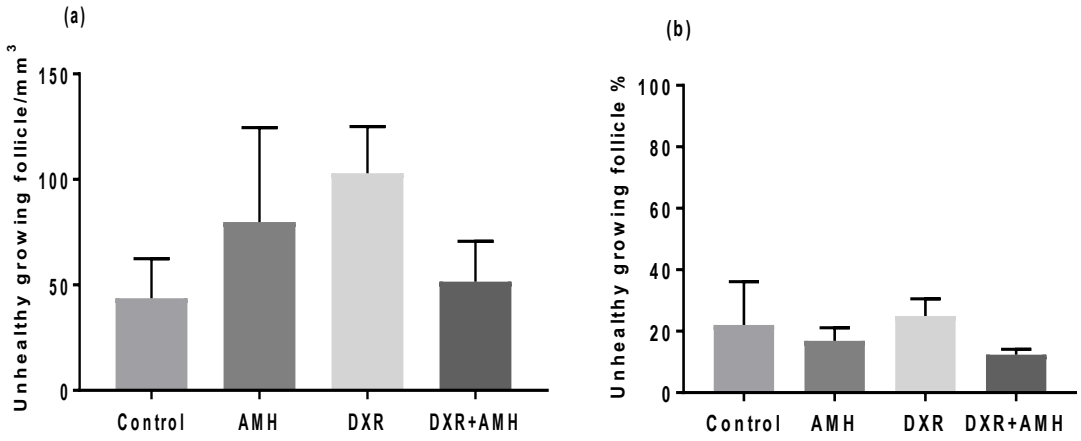


Figure 8.18. Comparison of unhealthy growing human follicle density and percentages in the human ovarian xenografts retrieved from the mouse kidney capsule from the Control, AMH, DXR and DXR+AMH groups. The data are presented as Mean ± S.E.M. (a) Unhealthy growing follicle density in the human ovarian xenografts retrieved from the kidney capsule from different groups. Control group: n=6. AMH group: n=4. DXR group: n=6. DXR+AMH group: n=4. (b) Unhealthy growing follicle density in the human ovarian xenografts retrieved from the kidney capsule from different groups. Control group: n=5. AMH group: n=4. DXR group: n=6. DXR+AMH group: n=4.

8.4.6 Effect of Doxorubicin and AMH on the subcutaneous xenotransplanted human ovarian tissue

8.4.6.1 Follicle development after xenotransplantation

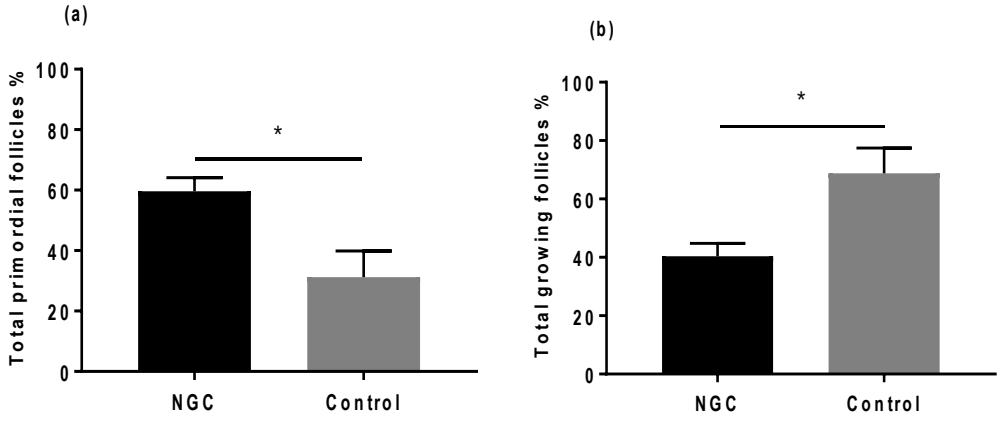


Figure 8.19. Comparison of primordial follicle percentage and growing follicle percentage between human ovarian tissue before and after subcutaneous xenotransplantation. (a) Primordial follicle percentages in non-grafted human ovarian tissue and xenografts after xenotransplantation. (b) Growing follicle percentages in non-grafted human ovarian tissue and xenografts after xenotransplantation. The data are presented as Mean ± S.D. NGC: Non-grafted control. NGC group: n=20. Control group: n=6. *P<0.05.

After xenotransplantation, there is a decrease in the proportion of primordial follicles and an increase in proportion of growing follicles, indicating survival and development of transplanted human ovarian tissue (Figure 8.19).

8.4.6.2 Comparison of human primordial follicles in DXR and AMH treated groups

There was no difference in the primordial follicle density in human ovarian xenografts between different groups (Figure 8.20).

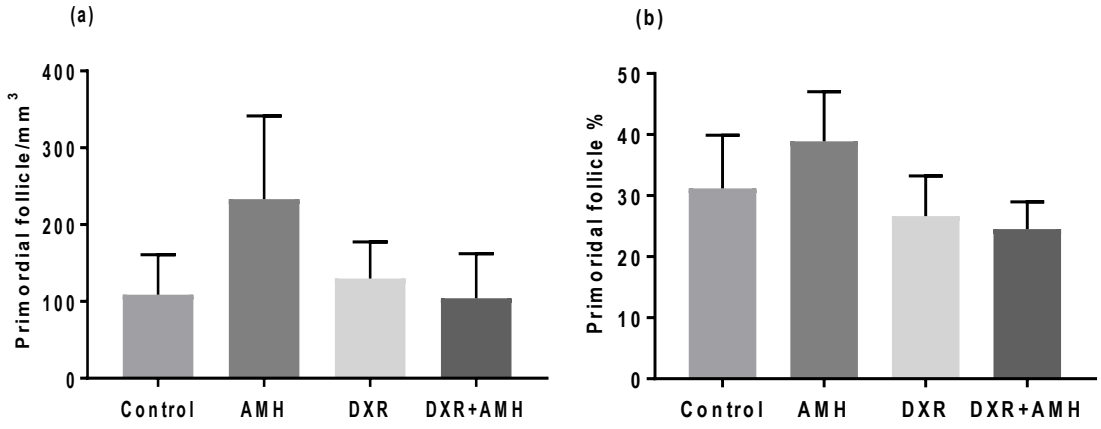


Figure 8.20. Comparison of primordial follicle density and percentages in the human ovarian xenografts retrieved from the mouse subcutaneous pocket from the Control, AMH, DXR and DXR+AMH groups. The data are presented as Mean ± S.E.M. (a) Primordial follicle density in the human ovarian xenografts retrieved from the subcutaneous pocket from different groups. (b) Primordial follicle percentages in the human ovarian xenografts retrieved from the subcutaneous pocket from different groups. Control group: n=6. AMH group: n=4. DXR group: n=6. Co-treatment group: n=5.

Unlike the healthy primordial follicle percentages in the human ovarian xenografts retrieved from the kidney capsule (Figure 8.14), there was no difference observed between the co-treatment group and other groups in human ovarian xenografts retrieved from the subcutaneous pocket (Figure 8.21).

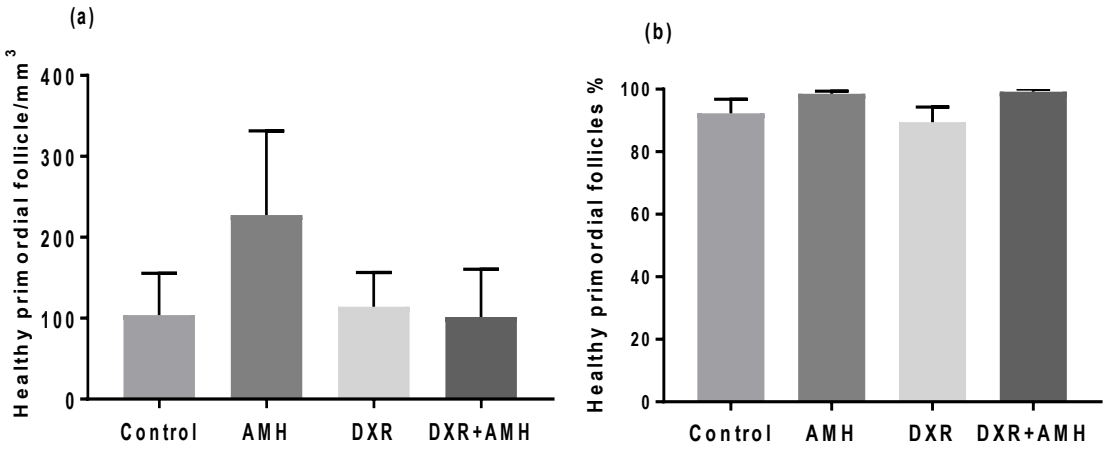


Figure 8.21. Comparison of healthy primordial follicle density and percentages in the human ovarian xenografts retrieved from the subcutaneous pocket from the Control, AMH, DXR and DXR+AMH groups. The data are presented as Mean ± S.E.M. (a) Healthy primordial follicle numbers in the human ovarian xenografts retrieved from the subcutaneous pocket from different groups. (b) Healthy primordial follicle percentages in the human ovarian xenografts retrieved from the subcutaneous pocket from different groups. Control group: n=6. AMH group: n=4. DXR group: n=6. Co-treatment group: n=5.

There was no difference found in the unhealthy primordial follicle density and percentages between different treatment groups (Figure 8.22).

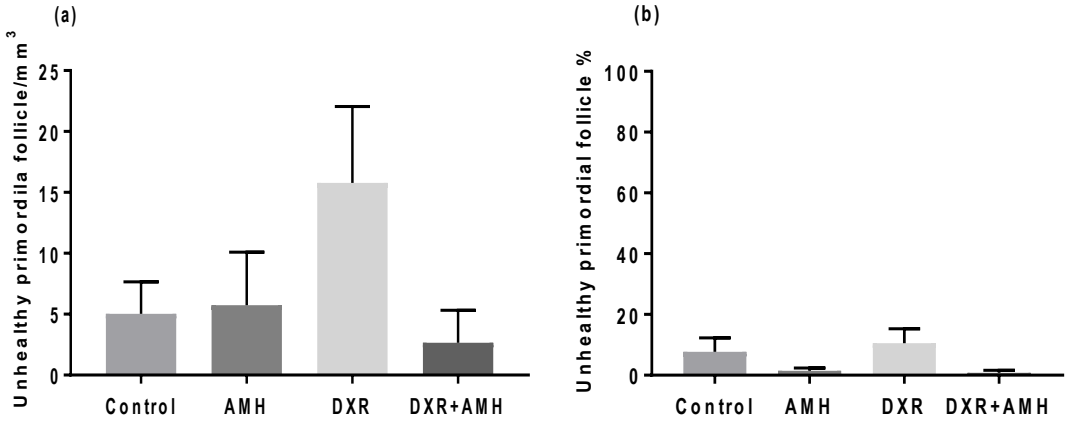


Figure 8.22. Comparison of unhealthy primordial follicle density and percentages in the human ovarian xenografts retrieved from the subcutaneous pocket from Control, AMH, DXR and DXR+AMH groups. The data are presented as Mean ± S.E.M. (a) Unhealthy primordial follicle numbers in the human ovarian xenografts retrieved from the subcutaneous pocket from different groups. (b) Unhealthy primordial follicle percentages in the human ovarian xenografts retrieved from the subcutaneous pocket from different groups. Control group: n=6. AMH group: n=4. DXR group: n=6. Co-treatment group: n=5.

There was no difference found in the growing follicle density and percentages between different treatment groups (Figure 8.23).

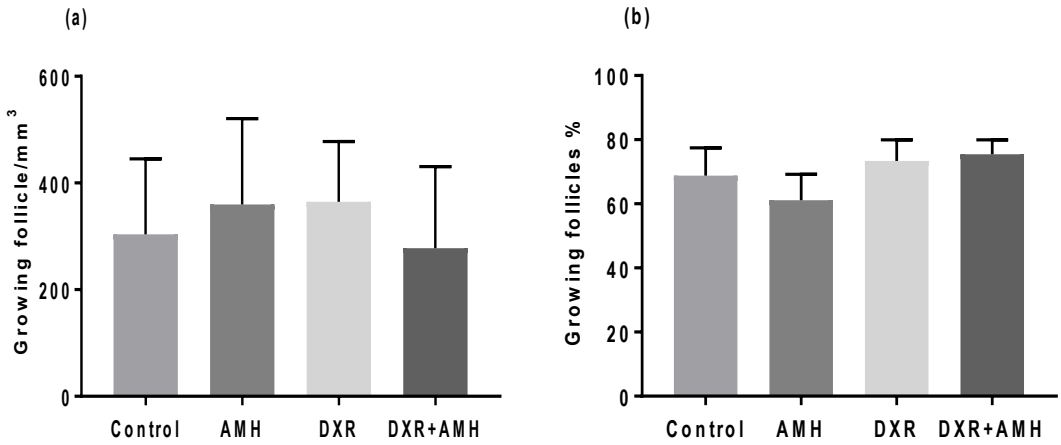


Figure 8.23. Comparison of growing follicle density and percentages in the human ovarian xenografts retrieved from the subcutaneous pocket from the Control, AMH, DXR and DXR+AMH groups. The data are presented as Mean ± S.E.M. (a) Growing follicle density in the human ovarian xenografts retrieved from the subcutaneous pocket from different groups. (b) Growing follicle percentages in the human ovarian xenografts retrieved from the subcutaneous pocket from different groups. Control group: n=6. AMH group: n=4. DXR group: n=6. Co-treatment group: n=5.

There was no difference observed regarding the density or percentages of the healthy growing follicles within different treatment groups (Figure 8.24).

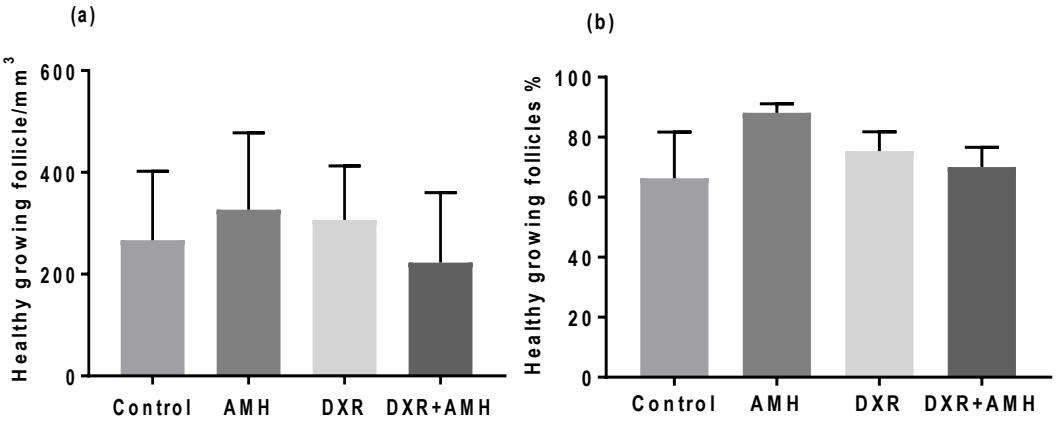


Figure 8.24. Comparison of healthy growing follicle density and percentages in the human ovarian xenografts retrieved from the subcutaneous pocket from the Control, AMH, DXR and DXR+AMH groups. The data are presented as Mean ± S.E.M. (a) Healthy growing follicle density in the human ovarian xenografts retrieved from the subcutaneous pocket from different groups. (b) Healthy growing follicle percentages in the human ovarian xenografts retrieved from the subcutaneous pocket from different groups. Control group: n=6. AMH group: n=4. DXR group: n=6. Co-treatment group: n=5.

There was no difference observed regarding the density or percentages of the unhealthy growing follicles within different treatment groups (Figure 8.25).

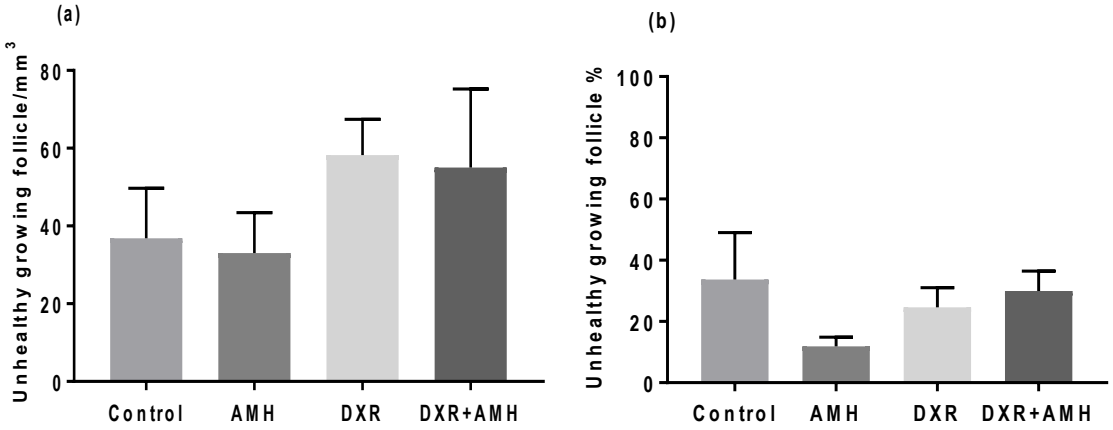


Figure 8.25. Comparison of unhealthy growing follicle percentages in the human ovarian xenografts retrieved from the subcutaneous pocket from the Control, AMH, DXR and DXR+AMH groups. The data are presented as Mean ± S.E.M. (a) Unhealthy growing follicle density in the human ovarian xenografts retrieved from the subcutaneous pocket from different groups. (b) Unhealthy growing follicle percentages in the human ovarian xenografts retrieved from the subcutaneous pocket from different groups. Control group: n=6. AMH group: n=4. DXR group: n=6. Co-treatment group: n=5.

8.4.7 Comparison between different xenotransplantation sites

There was no difference in the total primordial follicle density and percentages between the two different xenotransplantation sites in response to different treatments (Figure 8.26). In the co-treatment group, there was a significantly lower percentage of healthy primordial follicles and a higher percentage of unhealthy primordial follicles detected in the xenografts transplanted under the mouse kidney capsule (Figure 8.27).

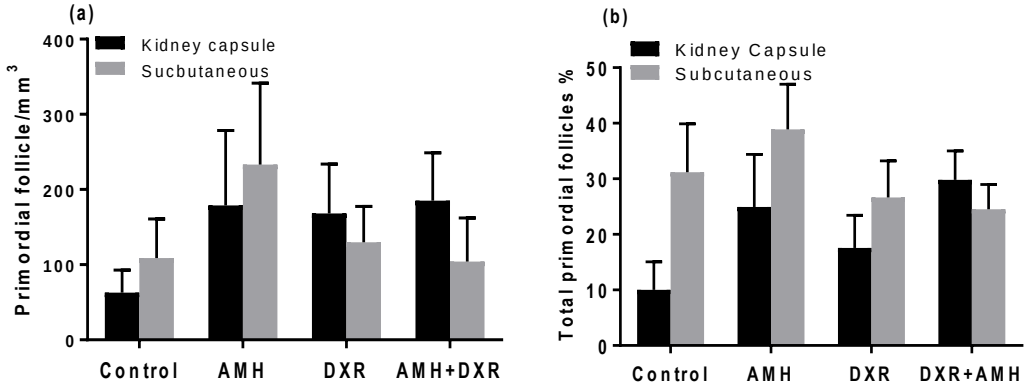


Figure 8.26. Comparison of primordial follicle density and percentages in the human ovarian xenografts retrieved from the kidney capsule and subcutaneous pocket. The data are presented as Mean ± S.E.M. (a) Primordial follicle density in the human ovarian xenografts retrieved from the kidney capsule and subcutaneous pocket from different groups. Control group: n=6. AMH group: n=4. DXR group: n=6. DXR+AMH group: n=4 (kidney capsule), n=5 (sub-cut). (b) Primordial follicle percentages in the human ovarian xenografts retrieved from the kidney capsule and subcutaneous pocket from different groups. Control group: n=5 (kidney capsule), n=6 (sub-cut). AMH group: n=4. DXR group: n=6. DXR+AMH group: n=4 (kidney capsule), n=5 (sub-cut). Sub-cut: Subcutaneous.

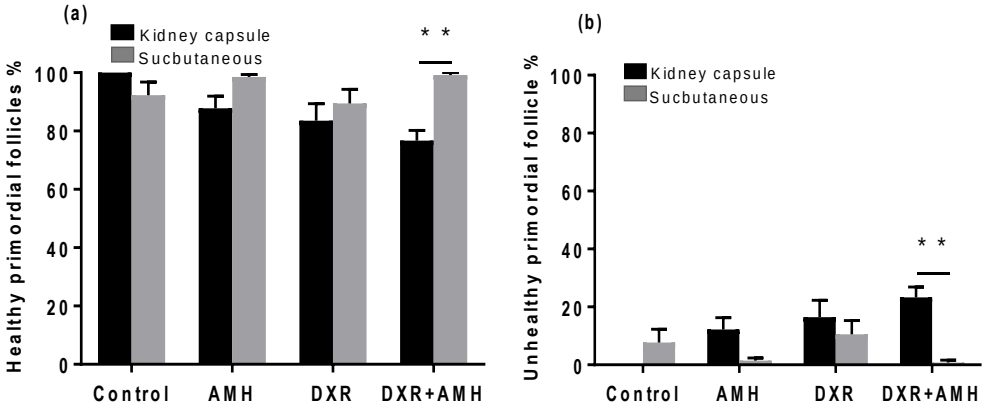


Figure 8.27. Comparison of healthy and unhealthy primordial follicle percentages in the human ovarian xenografts retrieved from the kidney capsule and subcutaneous pocket. The data are presented as Mean ± S.E.M. (a) Healthy primordial follicle percentages in the human ovarian xenografts retrieved from the kidney capsule and subcutaneous pocket from different groups. (b) Unhealthy primordial follicle percentages in the human ovarian xenografts retrieved from the kidney capsule and subcutaneous pocket from different groups. Control group: n=3 (kidney capsule), n=6 (sub-cut). AMH group: n=4. DXR group: n=4 (kidney capsule), n=6 (sub-cut). DXR+AMH group: n=4 (kidney capsule), n=5 (sub-cut). **P<0.01. Sub-cut: Subcutaneous.

8.4.8 Early growing follicles with flattened granulosa cells observed in DXR-treated mouse ovaries *in vivo*

In this study, we found an interesting difference when comparing the DXR-treated ovaries and the non-DXR treated ovaries. There were several early growing follicles that were only seen in the DXR-treated ovaries (including DXR+AMH group) surrounded with few layers of flattened granulosa cells. This altered morphology seems to be cell-type and follicle-type dependent, given that we only found it at early stages (Figure 8.28).

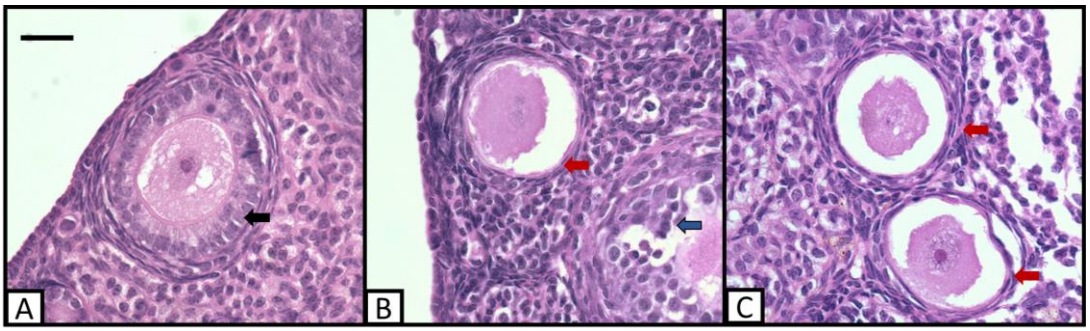


Figure 8.28. Representative images of healthy and unhealthy early growing follicles surrounded with flattened granulosa cells in mouse ovaries treated with DXR. Sections were stained with H and E. (A) Healthy secondary follicle surrounded with cuboidal granulosa cells (black arrow). (B) Unhealthy follicle surrounded with flattened granulosa cells (red arrow). Blue arrow represents the granulosa cells (cuboidal) in an atretic antral follicle. (C) Unhealthy follicles surrounded with flattened granulosa cells (red arrows). Bar represents 25μm.

8.5 Discussion

For this study, pre-pubertal human ovarian tissue was xenotransplanted into mice to determine if AMH could prevent DXR-induced primordial follicle loss in human ovarian xenografts, and in mouse ovaries *in vivo*. Simultaneously, we determined the effects of DXR and AMH individually on follicular development of these samples. Our results indicate that a single dose of DXR at 4mg/kg induces primordial follicle loss in mouse ovaries, but not in human ovarian xenografts. Additionally, more unhealthy growing follicles were observed in the DXR group in mouse ovaries (Figure 8.10). We found no protective effect of AMH on DXR-induced primordial follicle loss in mouse ovaries in our study.

Effect of AMH treatment on attenuating primordial follicle loss in mouse ovary

Compared to the Control group, there was no significant effect of AMH on the number of primordial follicles in mouse ovaries. This is consistent with Kano *et al.* 2017, who reported that AMH treatment alone for up to 15 days has no effect on the primordial follicle numbers in mouse ovaries *in vivo*. However, in their study, fewer growing follicles were found in the AMH-treated group when AMH administration was extended for 40 days, suggesting a blocking effect of AMH on primordial follicle activation (Kano *et al*., 2017). However, a decline in growing follicles was not demonstrated in our experiment. This could be attributed to a lower dose used and/or shorter time of AMH administration. Hayes *et al.* (2016) used the same dose of AMH as we used (300ng AMH/day/mouse) for daily IP injections in mice (n=5) for 28 days, which resulted in a higher percentage of primordial follicles in the AMH group compared to controls.

Effect of AMH treatment on attenuating primordial follicle loss in human ovarian xenografts

In the human ovarian xenografts, AMH did not preserve primordial follicle numbers compared to the control group. This might be due to the fact that the majority of primordial follicles may have been activated following the xenotransplantation before AMH administration. Therefore, in future studies, it might be worth initiating AMH administration at a higher dose prior to xenotransplantation and for a longer period.

In a very recent study (Detti *et al*., 2018), no difference was found in primordial follicle numbers between the AMH group and control group (n=6) after 14 days of AMH administration with 7 days recovery after human ovarian tissue xenotransplantation. However, similarly to Kano's study of mouse ovaries (Kano *et al*., 2017), they observed a decrease in growing follicle numbers in the human ovarian graft following AMH treatment, suggesting a suppressive effect of AMH on primordial follicle activation (Detti *et al.*, 2018). Additionally, decreased apoptosis and reduced cellular proliferation were observed in the human ovarian grafts following AMH treatment. This is consistent with Kong *et al*. (2016), where decreased apoptosis was detected after AMH treatment in mouse ovarian tissue auto-transplanted. In the future, it may be useful to analyse apoptosis to determine if AMH has an effect on the health of the xenografts.

Effect of DXR on primordial follicles and growing follicles in mouse ovary

DXR is a widely used chemotherapeutic agent in common childhood cancers. In chapter 5 and 6, we demonstrated its gonadotoxic side effects in pre-pubertal mouse ovaries *in vitro*. The functionality of DXR was confirmed by a loss of mouse body weight and spleen weight following DXR treatment, which is consistent with a previous study (Molyneux *et al*., 2011).

In our study, we confirmed the negative impact of DXR on the mouse primordial and growing follicle populations *in vivo*. Similar to previous studies (Morgan *et al*., 2013; Guerreiro *et al*., 2016; Kano *et al*., 2017), DXR treatment resulted in primordial follicle loss in mouse ovaries. Additionally, there was a higher percentage of growing follicles observed in the DXR group in mouse ovary (Figure 8.9), suggesting that the total follicle loss may be due to acceleration of primordial follicle activation, which is known as burn-out theory discussed in Section 1.4.2.3 (Kalich-Philosoph *et al*., 2013).

In our study, morphological analyses of DXR-treated mouse ovaries revealed increased numbers/proportions of unhealthy follicles, which is consistent with previous research (Morgan *et al*., 2013). The existence of healthy primordial follicles following DXR treatment in our experiment supports burn-out theory (indirectly induced primordial follicle loss). However, even though DXR administration results in higher proportions of growing follicles, the majority of these follicles were unhealthy. Therefore, these results indicate that activated growing follicles might be unhealthy.

There was also one mouse found dead in the co-treatment group. However, in consideration of the high prevalence of spontaneous thymic lymphomas in SCID mice which could induce the premature death (Huang *et al*., 2011), the reason for the death of the mouse cannot be concluded.

Interestingly, in DXR-treated mouse ovaries, we observed a type of early growing follicle with only few layers of flattened granulosa cells. To our knowledge, there are no other reports of similar descriptions of follicular morphology in ovaries after DXR treatment. One study reported similar growing follicles with flattened granulosa cells in Foxl2 mutant mice (Schmidt *et al*., 2004). In this mouse model with a complete deletion of Foxl2, the differentiation and proliferation of pre-granulosa cells was blocked, with growing follicles surrounded by flattened cells in adult mice (Uda *et al*., 2004). We therefore propose

that DXR might adversely impact primordial follicle pre-granulosa cells via Foxl2 involved mechanisms. The results generated from this study contribute to further insight into the effects of DXR on human ovarian follicular development, and shed light on future studies to develop protective methods to protect ovaries from DXR-induced ovarian damage.

Effect of DXR on primordial follicles in human ovarian xenografts

Our study did not show DXR-induced primordial follicle loss in pre-pubertal human ovarian tissue xenotransplanted into mice. This might be because the dose of DXR we used was lower than the concentration of DXR that human ovaries are exposed to clinically. Currently, there is no robust evidence demonstrating that DXR has a direct effect on primordial follicles. Soleimani *et al*. 2010 used patients aged from 2-37, and found DXR-induced apoptosis in primordial follicles. In our study, we did not find a DXR-induced effect on unhealthy primordial follicle numbers.

The effect of AMH in DXR-induced primordial follicle loss in mouse ovary

There was no effect of AMH on prevention of DXR-induced primordial follicle loss that was detected in mouse ovaries in this study. In mouse ovaries, DXR-induced primordial follicle loss. However, in contrast to previous work (Kano *et al*., 2017), we did not observe any effect of AMH on prevention of DXR-induced primordial follicle loss in adult mice *in vivo*. This might have been due to an insufficient dose of both AMH and DXR. Kano *et al*., (2017) used a much higher dose of AMH (home-made) (14.4µg/day via a mini-pump) for longer administration period (14 days) and gave two injections of DXR at higher doses (7.5mg/kg and 6.0mg/kg) in adult mice (n=5) than our experiment, which might explain why we did not observe an effect of AMH on the prevention of DXR-induced primordial follicle loss. Similarly, a recent paper has shown that administrating commercial AMH (Cusabio) in

adult mice at the same accumulative dose as the Kano's group (10μg/single injection/wk) for 4 weeks rescued cyclophosphamide-induced primordial follicle loss in mice *in vivo* (Sonigo *et al*., 2019).

The effects of DXR and AMH on primordial follicle numbers in human ovarian xenografts

Regarding the human ovarian xenografts, because there was no effect of DXR on primordial follicle numbers, the effect of AMH on the prevention of DXR-induced primordial follicle loss was not able to be elucidated in our study.

The only difference we observed between the DXR and co-treatment groups was that in the human ovarian grafts xenografted under mouse kidney capsule rather than the subcutaneous pocket, more unhealthy primordial follicles were observed in the co-treatment group. However, due to the fact that DXR itself failed to show a detrimental effect on primordial follicles, the difference described above might be due to the different transplantation sites used. Therefore, it was not possible to test our hypothesis that AMH could prevent DXR-induced primordial follicle loss in pre-pubertal human ovarian tissue when xenotransplanted into mice.

Comparison between different transplantation sites

There were more primordial follicles observed in the subcutaneous human ovarian xenografts with a lower percentages of growing follicles compared to the human ovarian xenografts under the mouse kidney capsule. This might be due to the fact that the kidney has increased vascularization to support follicle development.

Another potential reason might be the size of the transplanted tissue and the times of fragmentation. Unlike Chapter 7, which 1x1x1 mm pieces of tissue were randomly selected,

we cut the strip into 1x1x1 mm, 1x1x1 mm and 1x1x3 mm for this experiment as illustrated in Figure 8.1. Therefore, all human ovarian grafts xenotransplanted into the subcutaneous pocket had only been fragmented once whereas the ovarian grafts xenotransplanted under the kidney capsule had undergone two fragmentations. According to previously published studies, tissue fragmentation disrupts the Hippo signalling pathway leading to an acceleration of primordial follicle activation (Kawamura *et al*., 2013; Grosbois and Demeestere, 2018). Therefore a larger piece of tissue with fewer fragmentations transplanted into the mouse subcutaneous pocket may have led to less disruptions of the Hippo signalling pathway. This might have preserved some primordial follicles though the reduction of primordial follicle activation. If this is the reason, it highlights the importance of ensuring consistency in fragmentation for each piece of tissue for any future experiment.

8.6 Conclusion

Our results did not that show AMH attenuated primordial follicle loss in mice *in vivo* or in human ovarian xenografts. Our results also demonstrated DXR-induced ovarian damage in mouse ovaries, but not in human ovarian xenografts. Consequently, the hypothesis that AMH treatment affords protection against DXR-induced primordial follicle loss in human ovarian xenografts could not be tested. However, we did not observe any 'rescuing' effect of AMH on DXR induced-primordial follicle loss in mouse ovaries.

Additionally, our results demonstrated that xenotransplantation of human ovarian tissue with fewer fragmentations into a mouse subcutaneous pocket resulted in more primordial follicles remaining after xenotransplantation, suggesting this could be used as a useful experimental model in future fertility preservation studies.

We are also the first group to demonstrate that, in DXR-treated mice, there are a small number of early growing follicles surrounded with flattened granulosa cells with large

oocyte. We speculate that these follicles are the wave of primordial follicles exposed to DXR, and grow with impaired pre-granulosa cells, mimicking the morphology of ovarian follicles in Foxl2 mutant mice. This finding will hopefully contribute to future studies analysing the mechanisms of DXR on mouse ovarian follicles.

Chapter 9: Discussion and Conclusion

9.1 Summary of Results

Childhood cancer survivors may suffer long-term distressing sequelae induced by chemotherapy such as premature ovarian insufficiency (POI) and infertility. Protection of the ovarian function of childhood patients before or during cancer treatments has become particularly important. Since the 1990s, AMH has emerged as a potential molecule for preserving fertility in mammals. However, the role of AMH in onco-fertility has not been explored until recent years (Roness *et al*., 2015). One of the most widely used gonadotoxic chemotherapeutic agents for the treatment of common childhood cancers is doxorubicin (DXR). This thesis primarily aimed to examine AMH treatment as a possible non-invasive treatment for childhood cancer patients to preserve fertility. In this project, we focused mainly on primordial follicles which represent the ovarian reserve and determine life-long fertility in females.

Doxorubicin induced ovarian reserve damage

Initial experiments set out to compare different doses of doxorubicin using a mouse model. Our results demonstrated that pre-pubertal mouse ovaries cultured with DXR had a significant reduction in primordial follicle population, which is consistent with previous studies (Morgan *et al*., 2013). Subsequent experiments confirmed that DXR treatment resulted in primordial follicle loss in mice *in vivo*. Additionally, increased proportions of growing follicles were observed in mice *in vivo* one week after DXR treatment (Chapter 8), suggesting an acceleration in primordial follicle recruitment, supporting the burn-out theory (Kalich-Philosoph *et al*., 2013).

In mice treated with DXR *in vivo*, the majority of growing follicles remaining after DXR treatment were unhealthy (Chapter 8). These results provide robust evidence for DXR-

induced follicular damage in mouse, which are in agreement with that of previous studies summarised in Table 1.6 and 1.7.

We observed that in early growing follicles (primary-secondary stage) there were normally sized oocytes surrounded by a few flattened granulosa cells, which is highly similar to Foxl2 mutant mouse ovaries (Schmidt *et al*., 2004). However, none of the other studies using DXR (as reviewed in Chapter 1) reported similar results or similar description of follicles).

In our study, there is no effect of DXR on human ovarian tissue follicles. This could be due to the lower dose we used compared to the clinical doses used in humans.

Effect of AMH treatment on ovarian function

The work conducted in this thesis determined that AMH administration up to 28 days did not perturb the onset of puberty in pre-pubertal mice (Chapter 4). In the rmAMH and rhAMH-treated pre-pubertal mouse ovaries *in vitro,* AMH did not demonstrate prevention of primordial follicle loss. This is possibly due to the insufficient dose of AMH we used or the short culture period of AMH as discussed in Chapter 6.

Regarding the human ovarian grafts, there was no effect of AMH on primordial follicle numbers, potentially because the majority of the primordial follicles have been activated following xenotransplantation before the administration of AMH. Therefore, in future work, it might be better to initiate the AMH administration at a higher dose before xenotransplantation, and administrate it for a longer period of time. This notion is supported by a recent publication, in which AMH administration was started one week before human ovarian tissue xenotransplantation. Fewer growing follicles were observed after 14 days of AMH administration, and 7 days after undergoing human ovarian tissue

xenotransplantation, suggesting a suppressive effect of AMH on primordial follicle activation (Detti *et al*., 2018).

Effect of AMH on DXR-induced primordial follicle loss

In contrast to a previous study (Kano *et al*., 2017), we did not observe AMH effects on rescuing DXR-induced primordial follicle loss in mouse ovaries *in vitro* and *in vivo* (Chapter 8). However, Kano *et al*. (2017) used a much higher dose of AMH (1.4μg/d versus 300ng/d) for a longer period of culture than in our experiment, and they used higher doses of DXR injected into mice than out experiment (7.5mg/kg and 6mg/kg versus 4mg/kg) in mice. This might be a reason as to why we did not observe an effect of AMH on preventing DXR-induced primordial follicle loss, as specifically discussed in Chapter 8.

Regarding the human ovarian grafts, there was no effect of AMH on preventing DXR-induced primordial follicle loss potentially due to the fact that DXR at a single dose of 4mg/ml did not lead to primordial follicle loss in the transplanted human ovarian xenografts. Therefore, we cannot draw any conclusions from this based on our current results.

As shown in the Detti *et al*. study (2018), there was less apoptosis detected in human ovarian xenografts following AMH treatment. Therefore, it is important to use other methods such as TUNEL to investigate whether AMH is able to reduce DXR-induce apoptosis in ovarian tissue.

The influence of fragmentation and size of human ovarian fragments for xenotransplantation

One result from this project is the establishment of a subcutaneous xenotransplantation model to investigate the effect of AMH and DXR in human ovarian

xenografts. Xenotransplantation of a larger piece of human ovarian tissue (which had undergone only one fragmentation) into the mouse subcutaneous pocket resulted in less primordial follicle loss compared to xenotransplantation of the smaller pieces of ovarian tissue (which had undergone two fragmentations) under the mouse kidney capsule. Therefore, xenotransplantation of a larger piece of human ovarian tissue with fewer fragmentations is a better model to investigate primordial follicle activation, in comparison to smaller pieces of ovarian tissue as specifically discussed in Chapter 8.

9.2 Future Work

9.2.1 Experiments to investigate the effect of AMH on DXR-induce primordial follicle loss with optimised protocol

The most important next step following the work conducted by the candidate in this thesis would be to determine whether or not AMH exerts any effect in human ovarian xenografts with or without DXR. This could involve but not limited to: 1) an increased dose of AMH; 2) initiation of the AMH treatment before xenotransplantation; 3) a prolonged administration period; 4) use of other methods than histological analysis such as TUNEL; 5) an increased dose of DXR; 6) more replicates for each experiment.

If multiple transplantation sites are used and compared again, it would be optimal to ensure that the fragmentation times of the ovarian tissue that is transplanted in each transplantation site are equal. Furthermore, we could use alternative delivery methods to administrate AMH other than IP injection such as administration of AMH by osmotic pump subcutaneously transplanted into mice. Osmotic pump has been demonstrated to produce steadily delivery of bioactive AMH in mice for up to one week and has been used in previous studies (Kano *et al*., 2017; Detti *et al*., 2018).

9.2.2 Evaluation of the development competence of the primordial follicles after AMH and DXR treatments

Simultaneously, as an emerging tool to protect fertility, it is important to know whether the primordial follicles preserved by a novel treatment would be healthy and capable of development. In human ovarian xenografts in our studies, after exposure to DXR and AMH, there were primordial follicles that seemed to be morphologically healthy. Even though studies have shown the inhibitory effect of AMH on primordial follicle activation is reversible in mice *in vivo* (Kano *et al*., 2017), there is no evidence to show AMH preserved primordial follicles in human is reversible. In addition, whether the primordial follicles preserved by AMH after exposure to DXR in mice or in human are functional has not been examined, which could be determined by prolonged grafting or *in vitro* culture following short-term xenotransplantation.

The quality of stromal cells and blood vessels in the ovarian tissue following AMH and DXR treatments would be worth examining in the future. Whether DXR-induced primordial follicle loss is due to the direct effect on primordial follicle activation or indirectly after damage to the tissue surrounded the primordial follicles still remains unclear.

9.2.3 Exploring the role of Foxl2 in DXR induced follicular damage

In this project, we observed early growing follicles in mouse ovaries surrounded by a few layers of flattened granulosa cells at 8 days after DXR injection (Chapter 8). Most of these follicles are atretic. In mice, it could take as short as 7 days for primordial follicles to grow to the primary stage *in vivo* (Zheng *et al*., 2013). These abnormal follicles had been exposed to DXR. Interestingly, these follicles were similar in morphology to Forkhead box L2 (Foxl2) mutant mice follicles (Schmidt *et al*., 2004).

As introduced in Chapter 1, Foxl2 is a gene which is expressed in the pre-granulosa cells, and is also suggested to regulate primordial follicle activation although it is also expressed in growing follicles. In mice with an interrupted Foxl2, squamous pre-granulosa cells failed to differentiate into cuboidal granulosa cells during primordial follicle activation, resulting in the absence of secondary follicles (Schmidt *et al*., 2004).

Thus, we speculate that DXR might damage pre-granulosa cells via mediation of Foxl2. Since we are the first group to propose this notion, clearly more studies are warranted to convert it into a formal hypothesis.

9.2.4 Analyse potential mechanism of AMH to determine there is no conflict with chemotherapy

Even though there has been no evidence of a protective effect of AMH against chemotherapy in human ovarian tissue thus far, it is still important to elucidate the underlying mechanisms as to how AMH rescues chemotherapy-induced primordial follicle loss in mice (Kano *et al*., 2017; Sonigo *et al*., 2019). The exploration of these mechanisms could provide a great insight into human fertility preservation in the future through direct manipulation of the pathways involved. Current possible mechanisms involved in AMH has been discussed in Chapter 1.

AMHR2 has been detected in the human brain, and also the pituitary. There is a possibility that AMH exerts an effect via the hypothalamic-pituitary-gonadal axis. One study has demonstrated that in pituitary gonadotrope cell culture, exposure to AMH at a dose of 2.5 μg/ml for 4 or 24 hours results in activation of the Smad signalling pathways and increased expression of Fshβ within the gonadotrope cells (Garrel *et al*., 2016). Therefore, in order to gain further insight on AMH-induced effect on reproduction, it might be worth evaluating pituitary function following treatment with AMH.

9.2.5 Developing a new model based on the established protocols

Currently, several potential molecules have been investigated to protect against chemotherapy induced ovarian damage. However, most of them, such as imatinib, rapamycin, melatonin and sphingosine-1-phosphate are involved in cell death programmes (*e.g.* apoptosis) which might interfere with the effects of chemotherapy on cancer patients (Roness *et al*., 2014; Zhou *et al*., 2017). The technique of xenotransplantation into the mouse subcutaneous pocket developed in this study could be a useful tool to examine the effects of various protectant and chemotherapeutic agents on human ovarian function.

To investigate the effect of potential oncofertility protective substances, it is ideal to use a mouse model with cancer. Using a cancer mouse model enables us to simultaneously determine if the effect of chemotherapeutic agents is influenced while administering ovarian protective substances. For these studies, mouse syngeneic models (genetically modified) or tumour xenograft mouse models (immunocompromised) can be used (Jacoby *et al*., 2014). To investigate potential ovarian protective substances on human ovarian tissue, immunocompromised mouse models need to be used to avoid immunological rejection of human ovarian xenografts. Thus, before or at the time of human ovarian tissue grafting, tumour cells from common childhood cancers such as leukaemia could be xenografted into the same immunocompromised mouse host. Currently, fertility preservation using ovarian tissue cryopreservation is limited for paediatric leukaemia patients because reimplanting ovarian tissue from a leukaemia patient carries a risk of reintroducing cancer cells (Rosendahl *et al*., 2013). Specifically, mouse hosts could be xenografted with leukaemia cells such as commercial leukaemia cancer cell lines (*e.g.* AML-193) or paediatric leukaemia patient samples (Jacoby *et al*., 2014). Once the model is established, it can be

used to determine if potential ovary protective substances can protect ovaries from the chemotherapy-induced gonadotoxic effects without interfering in the chemotherapy effect.

9.3 Conclusion

In this project, DXR administration at our specific dose resulted in primordial follicle loss in mouse ovaries *in vitro* and *in vivo* but did not show an effect on human ovarian tissue xenografted into mouse. There was no effect of AMH on DXR-induced primordial follicle loss in mouse ovaries. Currently, there is only one study that has demonstrated that AMH rescued DXR-induced primordial follicle loss in mouse ovaries. Clearly, many further studies are warranted to verify this effect and investigate whether AMH or not has a similar effect against DXR in human ovarian tissue.

References

Abercrombie M. 1946. Estimation of nuclear population from microtome sections. *The Anatomical Record, 94,* pp.239-247.

Adhikari, D. and Liu, K. 2010. mTOR signalling in the control of activation of primordial follicles. *Cell Cycle*, *9*(9), pp.1673-1674.

Adhikari, D., Zheng, W., Shen, Y., Gorre, N., Hämäläinen, T., Cooney, A.J., Huhtaniemi, I., Lan, Z.J. and Liu, K. 2009. Tsc/mTORC1 signalling in oocytes governs the quiescence and activation of primordial follicles. *Human Molecular Genetics*, *19*(3), pp.397-410.

Akar, M. and Oktay, K. 2005. Restoration of ovarian endocrine function by ovarian transplantation. *Trends in Endocrinology and Metabolism*, *16*(8), pp.374-380.

Albani, E., Bracone, G., Di Biccari, S., Vitobello, D., Fattizzi, N. and Levi-Setti, P.E. 2012. Human ovarian tissue cryopreservation as fertility reserve. *Topics in cancer survivorship.* Prof. Ravinder Mohan (Ed.). *InTech*, ISBN: 978-953-307-894-6, pp.213-224.

Almeida, F. R., Costermans, N. G., Soede, N. M., Bunschoten, A., Keijer, J., Kemp, B. and Teerds, K. J. 2018. Presence of Anti-Müllerian Hormone (AMH) during follicular development in the porcine ovary. *PLOS One*, *13*(7), pp.e0197894.

Anderson, R.A., McLaughlin, M., Wallace, W.H.B., Albertini, D.F. and Telfer, E.E. 2014. The immature human ovary shows loss of abnormal follicles and increasing follicle developmental competence through childhood and adolescence. *Human Reproduction*, *29*(1), pp.97-106.

Ankarberg-Lindgren, C., Kriström, B. and Norjavaara, E. 2014. Physiological estrogen replacement therapy for puberty induction in girls: a clinical observational study. *Hormone Research in Paediatrics*, *81*(4), pp.239-244.

Arcamone, F., Franceschi, G., Penco, S. and Selva, A. 1969. Adriamycin (14-hydroxydaunomycin), a novel antitumor antibiotic. *Tetrahedron Letters*, *10*(13), pp.1007-1010.

Aston, W.J., Hope, D.E., Nowak, A.K., Robinson, B.W., Lake, R.A. and Lesterhuis, W.J. 2017. A systematic investigation of the maximum tolerated dose of cytotoxic chemotherapy with and without supportive care in mice. *BMC Cancer*, *17*(1), pp.684.

Ayuandari, S., Winkler-Crepaz, K., Paulitsch, M., Wagner, C., Zavadil, C., Manzl, C., Ziehr, S.C., Wildt, L. and Hofer-Tollinger, S. 2016. Follicular growth after xenotransplantation of cryopreserved/thawed human ovarian tissue in SCID mice: dynamics and molecular aspects. *Journal of Assisted Reproduction and Genetics*, *33*(12), pp.1585-1593.

Baker, T.G. 1963. A quantitative and cytological study of germ cells in human ovaries. *Proceedings of the royal society of London. Series b, Biological Sciences*, *158*, pp.417-433.

Bar-Joseph, H., Ben-Aharon, I., Rizel, S., Stemmer, S. M., Tzabari, M., and Shalgi, R. 2010. Doxorubicin-induced apoptosis in germinal vesicle (GV) oocytes. *Reproductive Toxicology, 30*(4), pp.566-572.

Barpe, D.R., Rosa, D.D. and Froehlich, P.E. 2010. Pharmacokinetic evaluation of doxorubicin plasma levels in normal and overweight patients with breast cancer and simulation of dose adjustment by different indexes of body mass. *European Journal of Pharmaceutical Sciences*, *41*(3-4), pp.458-463.

Bastings, L., Liebenthron, J., Westphal, J.R., Beerendonk, C.C.M., Van der Ven, H., Meinecke, B., Montag, M., Braat, D.D.M. and Peek, R. 2014. Efficacy of ovarian tissue cryopreservation in a major European center. *Journal of Assisted Reproduction and Genetics*, *31*(8), pp.1003-1012.

Bédécarrats, G. Y., O'Neill, F. H., Norwitz, E. R., Kaiser, U. B. and Teixeira, J. 2003. Regulation of gonadotropin gene expression by Müllerian inhibiting substance. *Proceedings of the National Academy of Sciences*, *100*(16), pp.9348-9353.

Belville, Corinne, Herman Van Vlijmen, Christian Ehrenfels, Blake Pepinsky, Alireza R. Rezaie, Jean-Yves Picard, Nathalie Josso, Nathalie di Clemente, and Richard L. Cate. 2004. Mutations of the anti-Mullerian hormone gene in patients with persistent Mullerian duct syndrome: biosynthesis, secretion, and processing of the abnormal proteins and analysis using a three-dimensional model. *Molecular Endocrinology*, *18*(3), pp.708-721.

Ben-Aharon, I., Bar-Joseph, H., Tzarfaty, G., Kuchinsky, L., Rizel, S., Stemmer, S.M. and Shalgi, R. 2010. Doxorubicin-induced ovarian toxicity. *Reproductive Biology and Endocrinology*, 8(20), pp.1-7.

Bertoldo, M.J., Bernard, J., Duffard, N., Tsikis, G., Alves, S., Calais, L., Uzbekova, S., Monniaux, D., Mermillod, P. and Locatelli, Y., 2016. Inhibitors of c-Jun phosphorylation impede ovine primordial follicle activation. *MHR: Basic Science of Reproductive Medicine*, *22*(5), pp.338-349.

Blanchard, M.G. and Josso, N. 1974. Source of the anti-Müllerian hormone synthesized by the fetal testis: Müllerian-inhibiting activity of fetal bovine Sertoli cells in tissue culture. *Pediatric Research*, *8*(12), pp.968-971.

Blumenfeld, Z. 2012. Chemotherapy and fertility. *Best Practice and Research Clinical Obstetrics and Gynaecology*, *26*(3), pp.379-390.

Bonadonna, G., Monfardini, S., De Lena, M., Fossati-Bellani, F. and Beretta, G. 1970. Phase I and preliminary phase II evaluation of adriamycin (NSC 123127). *Cancer Research*, *30*(10), pp.2572-2582.

Bristol-Gould, S.K., Kreeger, P.K., Selkirk, C.G., Kilen, S.M., Cook, R.W., Kipp, J.L., Shea, L.D., Mayo, K.E. and Woodruff, T.K. 2006. Postnatal regulation of germ cells by activin: the establishment of the initial follicle pool. *Developmental Biology*, *298*(1), pp. 132-148.

Cantley, L.C. 2002. The phosphoinositide 3-kinase pathway. *Science*, 296(5573), pp.1655-1657.

Cantley, L.C. and Neel, B.G., 1999. New insights into tumor suppression: PTEN suppresses tumor formation by restraining the phosphoinositide 3-kinase/AKT pathway. *Proceedings of the National Academy of Sciences*, *96*(8), pp.4240-4245.

Carlsson, I.B., Scott, J.E., Visser, J.A., Ritvos, O., Themmen, A.P. and Hovatta, O. 2006. Anti-Müllerian hormone inhibits initiation of growth of human primordial ovarian follicles *in vitro*. *Human Reproduction. 21*(9), pp.2223-2227.

Casida, L. E., Woody, C. O. and Pope, A. L. 1966. Inequality in function of the right and left ovaries and uterine horns of the ewe. *Journal of Animal Science*, *25*(4), pp.1169-1171.

Castrillon, D.H., Miao, L., Kollipara, R., Horner, J.W. and DePinho, R.A. 2003. Suppression of ovarian follicle activation in mice by the transcription factor Foxo3a. *Science*, *301*(5630), pp.215-218.

Cate, R.L., Mattaliano, R.J., Hession, C., Tizard, R., Farber, N.M., Cheung, A., Ninfa, E.G., Frey, A.Z., Gash, D.J., Chow, E.P. and Fisher, R.A. 1986. Isolation of the bovine and human genes for Müllerian inhibiting substance and expression of the human gene in animal cells. *Cell*, *45*(5), pp.685-698.

Chen, N. T., Wu, C. Y., Chung, C. Y., Hwu, Y., Cheng, S. H., Mou, C. Y., and Lo, L. W. 2012. Probing the dynamics of doxorubicin-DNA intercalation during the initial activation of apoptosis by fluorescence lifetime imaging microscope. *PLOS One*, ***7***(9)**,** pp.e44947.

Chiarelli, A.M., Marrett, L.D. and Darlington, G. 1999. Early menopause and infertility in females after treatment for childhood cancer diagnosed in 1964-1988 in Ontario, Canada. *American Journal of Epidemiology*, *150*(3), pp.245-254.

Childs, A.J., Kinnell, H.L., He, J. and Anderson, R.A. 2012. LIN28 is selectively expressed by primordial and pre-meiotic germ cells in the human fetal ovary. *Stem Cells and Development*, *21*(13), pp.2343-2349.

Choy, H., MacRae, R. and Story, M. 2008. Chapter 29: Basic concepts of chemotherapy and irradiation interaction. *Principles and Practice of Radiation Oncology*, 5th Edition, pp.669-679.

Clementi, M.E., Giardina, B., Di, E.S., Mordente, A. and Misiti, F. 2003. Doxorubicin-derived metabolites induce release of cytochrome C and inhibition of respiration on cardiac isolated mitochondria. *Anticancer Research*, *23*(3B), pp.2445-2450.

Cohen-Haguenauer, O., Picard, J.Y., Mattei, M.G., Serero, S., Van Cong, N., De Tand, M.F., Guerrier, D., Hors-Cayla, M.C., Josso, N. and Frezal, J. 1987. Mapping of the gene for anti-Müllerian hormone to the short arm of human chromosome 19. *Cytogenetic and Genome Research*, *44*(1), pp.2-6.

Cordeiro, M.H., Kim, S.Y. and Woodruff, T.K. 2015. Ovarian Follicle Biology and the Basis for Gonadotoxicity. *Cancer Treatment and the Ovary, Chapter 1*, pp.3-20.

Dath, C., Van Eyck, A. S., Dolmans, M. M., Romeu, L., Delle Vigne, L., Donnez, J. and Van Langendonckt, A. 2010. Xenotransplantation of human ovarian tissue to nude mice: comparison between four grafting sites. *Human Reproduction*, *25*(7), pp.1734-1743.

Davis, J.N., Courtney, C.L., Superak, H. and Taylor, D.K. 2014. Behavioral, clinical and pathological effects of multiple daily intraperitoneal injections on female mice. *Lab Animal*, 43(4), pp.131-139.

Day, F.R., Elks, C.E., Murray, A., Ong, K.K. and Perry, J.R. 2015. Puberty timing associated with diabetes, cardiovascular disease and also diverse health outcomes in men and women: the UK Biobank study. *Scientific Reports*, *5*(11208), pp.1-12.

De Vos, M., Devroey, P. and Fauser, B.C. 2010. Primary ovarian insufficiency. *The Lancet*, *376*(9744), pp.911-921.

Del Mastro, L., Boni, L., Michelotti, A., Gamucci, T., Olmeo, N., Gori, S., Giordano, M., Garrone, O., Pronzato, P., Bighin, C. and Levaggi, A. 2011. Effect of the gonadotropin-releasing hormone analogue triptorelin on the occurrence of chemotherapy-induced early menopause in premenopausal women with breast cancer: a randomized trial. *Jama*, 306(3), pp.269-276.

Demeestere, I., Simon, P., Dedeken, L., Moffa, F., Tsépélidis, S., Brachet, C., Delbaere, A., Devreker, F. and Ferster, A. 2015. Live birth after autograft of ovarian tissue cryopreserved during childhood. *Human Reproduction*, *30*(9), pp.2107-2109.

Denard, B., Pavia-Jimenez, A., Chen, W., Williams, N.S., Naina, H., Collins, R., Brugarolas, J. and Ye, J. 2015. Identification of CREB3L1 as a biomarker predicting doxorubicin treatment outcome. *PLOS One*, *10*(6), pp.e0129233.

Detti, L., Fletcher, N.M., Saed, G.M., Sweatman, T.W., Uhlmann, R.A., Pappo, A. and Peregrin-Alvarez, I. 2018. Xenotransplantation of pre-pubertal ovarian cortex and prevention of follicle depletion with anti-Müllerian hormone (AMH). *Journal of Assisted Reproduction and Genetics*, *35*(10), pp.1831-1841.

Di Clemente, N., Josso, N., Gouedard, L. and Belville, C. 2003. Components of the anti-Müllerian hormone signaling pathway in gonads. *Molecular and Cellular Endocrinology*, *211*(1-2), pp.9-14.

Dissen, G.A., Lara, H.E., Fahrenbach, W.H., Costa, M.E. and Ojeda, S.R. 1994. Immature rat ovaries become revascularized rapidly after autotransplantation and show a gonadotropin-dependent increase in angiogenic factor gene expression. *Endocrinology*, *134*(3), pp.1146-1154.

Dolmans, M.M., Martinez-Madrid, B., Gadisseux, E., Guiot, Y., Yuan, W.Y., Torre, A., Camboni, A., Van Langendonckt, A. and Donnez, J. 2007. Short-term transplantation of isolated human ovarian follicles and cortical tissue into nude mice. *Reproduction*, *134*(2), pp.253-262.

Donnez, J. and Dolmans, M.M. 2010. Cryopreservation and transplantation of ovarian tissue. *Clinical Obstetrics and Gynecology*, *53*(4), pp.787-796.

Donnez, J., Dolmans, M.M., Pellicer, A., Diaz-Garcia, C., Serrano, M.S., Schmidt, K.T., Ernst, E., Luyckx, V. and Andersen, C.Y. 2013. Restoration of ovarian activity and pregnancy after transplantation of cryopreserved ovarian tissue: a review of 60 cases of reimplantation. *Fertility and Sterility*, *99*(6), pp.1503-1513.

Donnez, J., Jadoul, P., Squifflet, J., Van Langendonckt, A., Donnez, O., Van Eyck, A.S., Marinescu, C. and Dolmans, M.M. 2010. Ovarian tissue cryopreservation and transplantation in cancer patients. *Best Practice and Research Clinical Obstetrics and Gynaecology*, *24*(1), pp.87-100.

Drummond AE. 2005. TGF beta signalling in the development of ovarian function. *Cell and Tissue Research*. *322*(1), pp.107-115.

Durlinger, A.L., Gruijters, M.J., Kramer, P., Karels, B., Ingraham, H.A., Nachtigal, M.W., Uilenbroek, J.T.J., Grootegoed, J.A. and Themmen, A.P. 2002. Anti-Mullerian hormone inhibits initiation of primordial follicle growth in the mouse ovary. *Endocrinology*, *143*(3), pp.1076-1084.

Durlinger, A.L., Kramer, P., Karels, B., de Jong, F.H., Uilenbroek, J.T.J., Grootegoed, J.A. and Themmen, A.P. 1999. Control of primordial follicle recruitment by anti-Mullerian hormone in the mouse ovary. *Endocrinology*, *140*(12), pp.5789-5796.

Engelman, J.A., Luo, J. and Cantley, L.C. 2006. The evolution of phosphatidylinositol 3-kinases as regulators of growth and metabolism. *Nature Reviews Genetics*, *7*(8), pp.606-619.

Faddy, M.J. and Gosden, R.G. 1996. Ovary and ovulation: a model conforming the decline in follicle numbers to the age of menopause in women. *Human Reproduction*, *11*(7), pp.1484-1486.

Faddy, M.J., Gosden, R.G., Gougeon, A., Richardson, S.J. and Nelson, J.F. 1992. Accelerated disappearance of ovarian follicles in mid-life: implications for forecasting menopause. *Human Reproduction*, *7*(10), pp.1342-1346.

Fleischer, R. T., Vollenhoven, B. J. and Weston, G. C. 2011. The effects of chemotherapy and radiotherapy on fertility in premenopausal women. *Obstetrical and Gynecological Survey*, *66*(4), 248-254.

Frost, B.M., Eksborg, S., Björk, O., Abrahamsson, J., Behrendtz, M., Castor, A., Forestier, E. and Lönnerholm, G. 2002. Pharmacokinetics of doxorubicin in children with acute lymphoblastic leukemia: Multi-institutional collaborative study. *Medical and Pediatric Oncology: The Official Journal of SIOP-International Society of Pediatric Oncology (Societé Internationale d'Oncologie Pédiatrique)*, *38*(5), pp.329-337.

Garrel, G., Racine, C., L'Hôte, D., Denoyelle, C., Guigon, C.J., Di Clemente, N. and Cohen-Tannoudji, J. 2016. Anti-Müllerian hormone: A new actor of sexual dimorphism in pituitary gonadotrope activity before puberty. *Scientific Reports*, *6*, pp.23790.

Gewirtz, D. 1999. A critical evaluation of the mechanisms of action proposed for the antitumor effects of the anthracycline antibiotics adriamycin and daunorubicin. *Biochemical Pharmacology*, *57*(7), pp.727-741.

Gigli, I., Cushman, R.A., Wahl, C.M. and Fortune, J.E. 2005. Evidence for a role for Anti-Müllerian Hormone in the suppression of follicle activation in mouse ovaries and bovine ovarian cortex grafted beneath the chick chorioallantoic membrane. *Molecular Reproduction and Development*, *71*(4), pp.480-488.

Gook, D.A., Edgar, D.H., Borg, J., Archer, J. and McBain, J.C. 2005. Diagnostic assessment of the developmental potential of human cryopreserved ovarian tissue from multiple patients using xenografting. *Human Reproduction*, *20*(1), pp.72-78.

Gosden RG, Boulton MI, Grant K and Webb R. 1994. Follicular development from ovarian xenografts in SCID mice. *Journal of Reproduction and Fertility. 101*(3), pp.619-623.

Green, D. M., Sklar, C. A., Boice, J. D., Mulvihill, J. J., Whitton, J. A., Stovall, M. and Yasui, Y. 2009. Ovarian failure and reproductive outcomes after childhood cancer treatment: results from the Childhood Cancer Survivor Study. *Journal of Clinical Oncology*, *27*(14), 2374-2381.

Greene, R.F., Collins, J.M., Jenkins, J.F., Speyer, J.L. and Myers, C.E. 1983. Plasma pharmacokinetics of Adriamycin and Adriamycinol: implications for the design of *in vitro* experiments and treatment protocols. *Cancer Research*, *43*(7), pp.3417-3421.

Griffin, I.J., Cole, T.J., Duncan, K.A., Hollman, A.S. and Donaldson, M.D.C. 1995. Pelvic ultrasound measurements in normal girls. *Acta Paediatrica*, *84*(5), pp.536-543.

Grosbois, J. and Demeestere, I. 2018. Dynamics of PI3K and Hippo signaling pathways during *in vitro* human follicle activation. *Human Reproduction*, *33*(9), pp.1705-1714.

Guerreiro, D.D., Lima, L.F.D., Rodrigues, G.Q., Carvalho, A.D.A., Castro, S.V., Campello, C.C., Pessoa, C.D.Ó., Gadelha, C.R.F., Figueiredo, J.R.D., Bordignon, V. and Rodrigues, A.P.R. 2016. In situ cultured preantral follicles is a useful model to evaluate the effect of anticancer drugs on caprine folliculogenesis. *Microscopy Research and Technique*, *79*(8), pp.773-781.

Hardy, K., Mora, J.M., Dunlop, C., Carzaniga, R., Franks, S. and Fenwick, M.A. 2018. Nuclear exclusion of SMAD2/3 in granulosa cells is associated with primordial follicle activation in the mouse ovary. *Journal of Cell Science*, *131*(17), pp.jcs-218123.

Hayer, P., Günzel-Apel, A.R., Lüerssen, D. and Hoppen, H.O. 1993. Ultrasonographic monitoring of follicular development, ovulation and the early luteal phase in the bitch. *Journal of Reproduction and Fertility, Supplement (47)*, pp.93-100.

Hayes, E., Kushnir, V., Ma, X., Biswas, A., Prizant, H., Gleicher, N. and Sen, A. 2016. Intra-cellular mechanism of Anti-Müllerian hormone (AMH) in regulation of follicular development. *Molecular and Cellular Endocrinology*, *433*, pp.56-65.

Hernandez-Fonseca, H., Bosch, P., Sirisathien, S., Wininger, J.D., Massey, J.B. and Brackett, B.G. 2004. Effect of site of transplantation on follicular development of human ovarian tissue transplanted into intact or castrated immunodeficient mice. *Fertility and Sterility*, *81*, pp.888-892.

Hirshfield, A.N. 1991. Development of follicles in the mammalian ovary. *International Review of Cytology*, *124*, pp.43-101.

Hsueh, A.J., Kawamura, K., Cheng, Y. and Fauser, B.C. 2015. Intraovarian control of early folliculogenesis. *Endocrine Reviews*, *36*(1), pp.1-24.

Huang, P., Westmoreland, S.V., Jain, R.K. and Fukumura, D. 2011. Spontaneous nonthymic tumors in SCID mice. *Comparative Medicine*, *61*(3), pp.227-234.

Huang, Y., Hua, K., Zhou, X., Jin, H., Chen, X., Lu, X., Yu, Y., Zha, X. and Feng, Y. 2008. Activation of the PI3K/AKT pathway mediates FSH-stimulated VEGF expression in ovarian serous cystadenocarcinoma. *Cell Research*, *18*(7), pp.780-791.

Hudson, M. M. 2010. Reproductive outcomes for survivors of childhood cancer. *Obstetrics and Gynecology*, *116*(5), pp.1171-1183.

Imai, A., Sugiyama, M., Furui, T., Tamaya, T. and Ohno, T. 2007. Direct protection by a gonadotropin-releasing hormone analog from doxorubicin-induced granulosa cell damage. *Gynecologic and Obstetric Investigation*, *63*(2), pp.102-106.

Jacoby, E., Chien, C.D. and Fry, T.J. 2014. Murine models of acute leukemia: important tools in current pediatric leukemia research. *Frontiers in Oncology*, *4*(95), pp.1-14.

Jafarian, Z., Eimani, H., Azarnia, M., Shahverdi, A.H., Eftekhari-Yazdi, P. and Kamalinejad, M. 2013. The effect of intra-peritoneal administration of Papaver bracteatum

Lindl. extract on development of NMRI mice oocytes treated with Doxorubicin. *Reproductive Medicine and Biology*, *12*(2), pp.57-63.

Jagarlamudi, K., Liu, L., Adhikari, D., Reddy, P., Idahl, A., Ottander, U., Lundin, E. and Liu, K. 2009. Oocyte-specific deletion of Pten in mice reveals a stage-specific function of PTEN/PI3K signaling in oocytes in controlling follicular activation. *PLOS One*, *4*(7), pp.e6186.

Jassem, W. and Heaton, N.D. 2004. The role of mitochondria in ischemia/reperfusion injury in organ transplantation. *Kidney International*, *66*(2), pp.514-517.

John, G.B., Gallardo, T.D., Shirley, L.J. and Castrillon, D.H. 2008. Foxo3 is a PI3K-dependent molecular switch controlling the initiation of oocyte growth. *Developmental Biology*, *321*(1), pp.197-204.

Josso, N. and di Clemente, N. 2003. Transduction pathway of anti-Müllerian hormone, a sex-specific member of the TGF-β family. *Trends in Endocrinology and Metabolism*, *14*(2), pp.91-97.

Jost, A. 1953. Problems of fetal endocrinology: the gonadal and hypophyseal hormones. *Recent Progress in Hormone Research*, *8*, pp.379-413.

Juengel, J.L., Sawyer, H.R., Smith, P.R., Quirke, L.D., Heath, D.A., Lun, S. and McNatty, K.P. 2002. Origins of follicular cells and ontogeny of steroidogenesis in ovine fetal ovaries. *Molecular and Cellular Endocrinology*, *191*(1), pp.1-10.

Kalich-Philosoph, L., Roness, H., Carmely, A., Fishel-Bartal, M., Ligumsky, H., Paglin, S., Wolf, I., Kanety, H., Sredni, B., and Meirow, D. 2013. Cyclophosphamide triggers follicle activation and "burnout"; AS101 prevents follicle loss and preserves fertility. *Science Translational Medicine*, *5*(185), pp.185ra62.

Kano, M., Sosulski, A.E., Zhang, L., Saatcioglu, H.D., Wang, D., Nagykery, N., Sabatini, M.E., Gao, G., Donahoe, P.K. and Pépin, D. 2017. AMH/MIS as a contraceptive that protects the ovarian reserve during chemotherapy. *Proceedings of the National Academy of Sciences*, *114*(9), pp.e1688-e1697.

Karl, T., Pabst, R. and von Hörsten, S. 2003. Behavioral phenotyping of mice in pharmacological and toxicological research. *Experimental and Toxicologic Pathology*, *55*(1), pp.69-83.

Kaur, A., Kaur, M., Sharma, R. and Kumar, S. 2012. Doxorubicin: a critical review on toxicity. *Journal of Pharmacy Research*, *5*, pp.2890-2894.

Kawamura, K., Cheng, Y., Suzuki, N., Deguchi, M., Sato, Y., Takae, S., Ho, C.H., Kawamura, N., Tamura, M., Hashimoto, S. and Sugishita, Y. 2013. Hippo signaling disruption and Akt stimulation of ovarian follicles for infertility treatment. *Proceedings of the National Academy of Sciences*, *110*(43), pp.17474-17479.

Kim, J. H., MacLaughlin, D. T. and Donahoe, P. K. 2014. Müllerian inhibiting substance/anti-Müllerian hormone: A novel treatment for gynecologic tumors. *Obstetrics and Gynecology Science*, *57*(5), pp.343-357.

Kim, J.Y. 2012. Control of ovarian primordial follicle activation. *Clinical and Experimental Reproductive Medicine*, *39*(1), pp.10-14.

King, T.R., Lee, B.K., Behringer, R.R. and Eicher, E.M. 1991. Mapping Anti-Müllerian Hormone (AMH) and related sequences in the mouse: identification of a new region of homology between MMU10 and HSA19p. *Genomics*, *11*(2), pp.273-283.

Knight, P.G. and Glister, C. 2001. Potential local regulatory functions of inhibins, activins and follistatin in the ovary. *Reproduction*, *121*(4), pp.503-512.

Knight, P.G. and Glister, C. 2006. TGF-β superfamily members and ovarian follicle development. *Reproduction*, *132*(2), pp.191-206.

Kong, H.S., Kim, S.K., Lee, J., Youm, H.W., Lee, J.R., Suh, C.S. and Kim, S.H. 2016. Effect of exogenous Anti-Müllerian Hormone treatment on cryopreserved and transplanted mouse ovaries. *Reproductive Sciences*, *23*(1), pp.51-60.

Korsholm AS, Hvidman HW, Bentzen JG, Nyboe Andersen A. and Birch Petersen K. 2017. Left-right differences in ovarian volume and antral follicle count in 1423 women of reproductive age. *Gynecological Endocrinology*, *33*(4), pp.320-323.

Kristensen, S.G., Rasmussen, A., Byskov, A.G. and Andersen, C.Y. 2010. Isolation of pre-antral follicles from human ovarian medulla tissue. *Human Reproduction*, *26*(1), pp.157-166.

Kropp, J., Roti, E.C.R., Ringelstetter, A., Khatib, H., Abbott, D.H. and Salih, S.M. 2015. Dexrazoxane diminishes doxorubicin-induced acute ovarian damage and preserves ovarian function and fecundity in mice. *PLOS One*, *10*(11), pp.e0142588.

Kumar, A., Kalra, B., Patel, A., McDavid, L. and Roudebush, W. E. 2010. Development of a second generation Anti-Müllerian Hormone (AMH) ELISA. *Journal of Immunological Methods*, *362*(1), pp.51-59.

La Marca, A., De Leo, V., Giulini, S., Orvieto, R., Malmusi, S., Giannella, L. and Volpe, A. 2005. Anti-Mullerian Hormone in premenopausal women and after spontaneous or surgically induced menopause. *Journal of the Society for Gynecologic Investigation*, *12*(7), 545-548.

Lahoti, T. S., Patel, D., Thekkemadom, V., Beckett, R., and Ray, S. D. 2012. Doxorubicininduced *in vivo* nephrotoxicity involves oxidative stress- mediated multiple pro- and anti-apoptotic signalling pathways. *Current Neurovascular Research*, *9*(4), pp.282-295.

Lass, A. and Brinsden, P. 1999. The role of ovarian volume in reproductive medicine. *Human Reproduction Update*, 5(3), pp.256-266.

Lawson, K. A. and Hage, W. J. 1994. Clonal analysis of the origin of primordial germ cells in the mouse. *Germline Development*, *182*, pp.68-84.

Lee, S.J., Schover, L.R., Partridge, A.H., Patrizio, P., Wallace, W.H., Hagerty, K., Beck, L.N., Brennan, L.V. and Oktay, K. 2006. American Society of Clinical Oncology recommendations on fertility preservation in cancer patients. *Journal of Clinical Oncology*, *24*(18), pp.2917-2931.

Lei, L. and Spradling, A.C. 2013. Female mice lack adult germ-line stem cells but sustain oogenesis using stable primordial follicles. *Proceedings of the National Academy of Sciences*, *110*(21), pp.8585-8590.

Li, F., Turan, V., Lierman, S., Cuvelier, C., De Sutter, P. and Oktay, K. 2013. Sphingosine-1-phosphate prevents chemotherapy-induced human primordial follicle death. *Human Reproduction*, *29*(1), pp.107-113.

Li, J., Kawamura, K., Cheng, Y., Liu, S., Klein, C., Liu, S., Duan, E.K. and Hsueh, A.J. 2010. Activation of dormant ovarian follicles to generate mature eggs. *Proceedings of the National Academy of Sciences*, *107*(22), pp.10280-10284.

Lichtman, S.M. and Villani, G. 2000. Chemotherapy in the elderly: pharmacologic considerations. *Cancer Control*, *7*(6), pp.548-556.

Ling, Y.H., El-Naggar, A.K., Priebe, W. and Perez-Soler, R. 1996. Cell cycle-dependent cytotoxicity, G2/M phase arrest, and disruption of p34cdc2/cyclin B1 activity induced by doxorubicin in synchronized P388 cells. *Molecular pharmacology*, *49*(5), pp.832-841.

Lotz, L., Liebenthron, J., Nichols-Burns, S.M., Montag, M., Hoffmann, I., Beckmann, M.W., van der Ven, H., Töpfer, D. and Dittrich, R. 2014. Spontaneous antral follicle formation and metaphase II oocyte from a non-stimulated prepubertal ovarian tissue xenotransplant. *Reproductive Biology and Endocrinology*, *12*(41), pp.1-5.

Ma, W.Z., Zheng, X.M., Hei, C.C., Zhao, C.J., Xie, S.S., Chang, Q., Cai, Y.F., Jia, H., Pei, X.Y. and Wang, Y.R. 2017. Optimal FSH usage in revascularization of allotransplanted ovarian tissue in mice. *Journal of ovarian research*, *10*(1), pp.5.

MacLaughlin, D.T. and Donahoe, P.K. 2010. Müllerian inhibiting substance/anti-Müllerian hormone: a potential therapeutic agent for human ovarian and other cancers. *Future Oncology*, *6*(3), pp.391-405.

Magnelli, L., Cinelli, M. and Chiarugi, V. 1995. Phorbol esters attenuate the expression of p53 in cells treated with doxorubicin and protect TS-P53/K562 from apoptosis. *Biochemical and Biophysical Research Communications*, *215*(2), 641-645.

Maheshwari, A. and Fowler, P.A. 2008. Primordial follicular assembly in humans–revisited. *Zygote*, 16(4), pp.285-296.

Maltaris, T., Beckmann, M.W., Binder, H., Mueller, A., Hoffmann, I., Koelbl, H. and Dittrich, R. 2007. The effect of a GnRH agonist on cryopreserved human ovarian grafts in severe combined immunodeficient mice. *Reproduction*, *133*(2), pp.503-509.

Maltaris, T., Koelbl, H., Fischl, F., Seufert, R., Schmidt, M., Kohl, J., Beckmann, M.W., Binder, H., Hoffmann, I., Mueller, A. and Dittrich, R. 2006. Xenotransplantation of human ovarian tissue pieces in gonadotropin-stimulated SCID mice: the effect of ovariectomy. *Anticancer Research*, *26*(6B), pp.4171-4176.

Man, L., Bodine, R., Park, L., Zaninovic, N., Rosenwaks, Z., Schattman, G.L. and James, D. 2016. Co-transplantation of human ovarian tissue with AMH-producing endothelial cells inhibits recruitment of primordial follicles. *Fertility and Sterility*, *106*(3), pp.e3-e4.

Man, L., Bodine, R., Park, L., Zaninovic, N., Shatmann, G.L., Rosenwaks, Z. and James, D. 2017. Long term co-transplantation of human ovarian tissue with AMH-producing endothelial cells increase productivity and longevity of the graft. *Fertility and Sterility*, *108*(3), pp.e179.

Marca, A. L. and Volpe, A. 2007. The Anti-Mullerian hormone and ovarian cancer. *Human Reproduction Update*, *13*(3), pp.265-273.

Margolskee, A. and Selgrade, J.F. 2013. A lifelong model for the female reproductive cycle with an antimüllerian hormone treatment to delay menopause. *Journal of Theoretical Biology*, *326*, pp.21-35.

Mark-Kappeler, C.J., Sen, N., Keating, A.F., Sipes, I.G. and Hoyer, P.B. 2010. Distribution and responsiveness of rat anti-Müllerian hormone during ovarian development and VCD-induced ovotoxicity. *Toxicology and Applied Pharmacology*, *249*(1), pp.1-7.

McGee, E.A. and Hsueh, A.J. 2000. Initial and cyclic recruitment of ovarian follicles. *Endocrine Reviews*, 21(2), pp.200-214.

McLennan, I. S. and Pankhurst, M. W. 2015. Anti-Müllerian hormone is a gonadal cytokine with two circulating forms and cryptic actions. *Journal of Endocrinology*, *226*(3), pp.R45-R57.

Meirelles, K., Benedict, L.A., Dombkowski, D., Pepin, D., Preffer, F.I., Teixeira, J., Tanwar, P.S., Young, R.H., MacLaughlin, D.T., Donahoe, P.K. and Wei, X. 2012. Human ovarian cancer stem/progenitor cells are stimulated by doxorubicin but inhibited by Müllerian inhibiting substance. *Proceedings of the National Academy of Sciences*, *109*(7), pp.2358-2363.

Meirow, D., Hardan, I., Dor, J., Fridman, E., Elizur, S., Ra'anani, H., Slyusarevsky, E., Amariglio, N., Schiff, E., Rechavi, G. and Nagler, A. 2008. Searching for evidence of disease and malignant cell contamination in ovarian tissue stored from hematologic cancer patients. *Human Reproduction*, *23*(5), pp.1007-1013.

Meirow, D., Lewis, H., Nugent, D. and Epstein, M. 1999. Subclinical depletion of primordial follicular reserve in mice treated with cyclophosphamide: clinical importance and proposed accurate investigative tool. *Human Reproduction*, *14*(7), pp.1903-1907.

Messinis, I.E. 2006. Ovarian feedback, mechanism of action and possible clinical implications. *Human Reproduction Update*, *12*(5), pp.557-571.

Molyneux, G., Andrews, M., Sones, W., York, M., Barnett, A., Quirk, E., Yeung, W. and Turton, J. 2011. Haemotoxicity of busulphan, doxorubicin, cisplatin and cyclophosphamide in the female BALB/c mouse using a brief regimen of drug administration. *Cell Biology and Toxicology*, 27(1), pp.13-40.

Morgan, S., Anderson, R. A., Gourley, C., Wallace, W. H. B., and Spears, N. 2012. How do chemotherapeutic agents damage the ovary? *Human Reproduction Update*, *18*(5), pp.525-535.

Morgan, S., Lopes, F., Gourley, C., Anderson, R. A., and Spears, N. 2013. Cisplatin and Doxorubicin Induce Distinct Mechanisms of Ovarian Follicle Loss; Imatinib Provides Selective Protection Only against Cisplatin. *PLOS One*, *8*(7), pp.e70117.

Mullen, R.D. and Behringer, R.R. 2014. Molecular genetics of Müllerian duct formation, regression and differentiation. *Sexual Development*, *8*(5), pp.281-296.

Munster, P.N., Moore, A.P., Ismail-Khan, R., Cox, C.E., Lacevic, M., Gross-King, M., Xu, P., Carter, W.B. and Minton, S.E. 2012. Randomized trial using gonadotropin-releasing hormone agonist triptorelin for the preservation of ovarian function during (neo) adjuvant chemotherapy for breast cancer. *Journal of Clinical Oncology*, *30*(5), pp.533-538.

Newton H, Aubard Y, Rutherford A, Sharma V, Gosden R. 1996. Low temperature storage and grafting of human ovarian tissue. *Human Reproduction*, *11*(7), pp. 1487-1491.

Nilsson, E., Rogers, N. and Skinner, M.K. 2007. Actions of Anti-Müllerian Hormone on the ovarian transcriptome to inhibit primordial to primary follicle transition. *Reproduction*, *134*(2), pp.209-221.

Nilsson, E.E., Schindler, R., Savenkova, M.I. and Skinner, M.K. 2011. Inhibitory actions of Anti-Müllerian Hormone (AMH) on ovarian primordial follicle assembly. *PLOS One*, *6*(5), pp.e20087.

Notarianni, E. 2011. Reinterpretation of evidence advanced for neo-oogenesis in mammals, in terms of a finite oocyte reserve. *Journal of Ovarian Research*, *4*(1), pp.1-20.

Nottola, S.A., Camboni, A., Van Langendonckt, A., Demylle, D., Macchiarelli, G., Dolmans, M.M., Martinez-Madrid, B., Correr, S. and Donnez, J. 2008. Cryopreservation and xenotransplantation of human ovarian tissue: an ultrastructural study. *Fertility and Sterility*, *90*(1), pp.23-32

Ojeda, S.R., Roth, C., Mungenast, A., Heger, S., Mastronardi, C., Parent, A.S., Lomniczi, A. and Jung, H. 2006. Neuroendocrine mechanisms controlling female puberty: New approaches, new concepts. *International Journal of Andrology, 29*(1), 256-263.

Oktay, K., Bedoschi, G., Pacheco, F., Turan, V. and Emirdar, V. 2016. First pregnancies, live birth, and *in vitro* fertilization outcomes after transplantation of frozen-banked ovarian tissue with a human extracellular matrix scaffold using robot-assisted minimally invasive surgery. *American Journal of Obstetrics and Gynecology*, *214*(1), pp.94e1-94e9.

Pangas, S.A. and Rajkovic, A. 2015. Chapter 21-Follicular Development: Mouse, Sheep, and Human Models. *Knobil and Neill's Physiology of Reproduction*, 4th Edition, pp.947-995.

Papakostas, T.D., Pieretti-Vanmarcke, R., Nicolaou, F., Thanos, A., Trichonas, G., Koufomichali, X., Anago, K., Donahoe, P.K., Teixeira, J., MacLaughlin, D.T. and Vavvas, D., 2010. Development of an efficiently cleaved, bioactive, highly pure FLAG-tagged recombinant human Müllerian inhibiting substance. *Protein Expression and Purification*, *70*(1), pp.32-38.

Park, M., Suh, D.S., Lee, K. and Bae, J. 2014. Positive cross talk between FOXL2 and Anti-Müllerian Hormone regulates ovarian reserve. *Fertility and Sterility*, *102*(3), pp.847-855.

Pépin, D., Hoang, M., Nicolaou, F., Hendren, K., Benedict, L. A., Al-Moujahed, A., Sosulski, A., Marmalidou, A., Vavvas, D. and Donahoe, P. K. 2013. An albumin leader sequence coupled with a cleavage site modification enhances the yield of recombinant C-terminal Müllerian Inhibiting Substance. *Technology*, *1*(1), pp. 63-71.

Pepling, M.E. 2006. From primordial germ cell to primordial follicle: mammalian female germ cell development. *Genesis*, *44*(12), pp.622-632.

Pepling, M.E. and Spradling, A.C. 2001. Mouse ovarian germ cell cysts undergo programmed breakdown to form primordial follicles. *Developmental Biology*, *234*(2), pp.339-351.

Perez, G. I., Knudson, C. M., Leykin, L., Korsmeyer, S. J., and Tilly, J. L. 1997. Apoptosis-associated signalling pathways are required for chemotherapy-mediated female germ cell destruction. *Nature Medicine*, *3*(11), pp.1228-1232.

Picard, J.Y., Benarous, R., Guerrier, D., Josso, N. and Kahn, A. 1986. Cloning and expression of cDNA for Anti-Müllerian Hormone. *Proceedings of the National Academy of Sciences*, *83*(15), pp.5464-5468.

Picard, J.Y., Tran, D. and Josso, N. 1978. Biosynthesis of labelled Anti-Müllerian Hormone by fetal testes: evidence for the glycoprotein nature of the hormone and for its disulfide-bonded structure. *Molecular and Cellular Endocrinology, 12*(1), pp.17-30.

Pieretti-Vanmarcke, R., Donahoe, P. K., Pearsall, L. A., Dinulescu, D. M., Connolly, D. C., Halpern, E. F., Seiden, M.V. and MacLaughlin, D. T. 2006. Müllerian Inhibiting Substance enhances subclinical doses of chemotherapeutic agents to inhibit human and mouse ovarian cancer. *Proceedings of the National Academy of Sciences*, *103*(46), 17426-17431.

Praet, M., Pollakis, G., Goormaghtigh, E., and Ruysschaert, J. M. 1984. Damages of the mitochondrial membrane in Adriamycin treated mice. *Cancer Letters*, *25*(1), pp.89-96.

Prentice, P. and Viner, R.M. 2013. Pubertal timing and adult obesity and cardiometabolic risk in women and men: a systematic review and meta-analysis. *International Journal of Obesity*, *37*(8), pp.1036.

Ramirez, V.D. and Sawyer, C.H. 1965. Advancement of puberty in the female rat by estrogen. *Endocrinology*, *76*(6), pp.1158-1168.

Reddy, P., Adhikari, D., Zheng, W., Liang, S., Hämäläinen, T., Tohonen, V., Ogawa, W., Noda, T., Volarevic, S., Huhtaniemi, I. and Liu, K. 2009. PDK1 signaling in oocytes controls reproductive aging and lifespan by manipulating the survival of primordial follicles. *Human Molecular Genetics*, *18*(15), pp.2813-2824.

Reddy, P., Liu, L., Adhikari, D., Jagarlamudi, K., Rajareddy, S., Shen, Y., Du, C., Tang, W., Hämäläinen, T., Peng, S.L. and Lan, Z.J. 2008. Oocyte-specific deletion of Pten causes premature activation of the primordial follicle pool. *Science*, *319*(5863), pp.611-613.

Reddy, P., Zheng, W. and Liu, K. 2010. Mechanisms maintaining the dormancy and survival of mammalian primordial follicles. *Trends in Endocrinology and Metabolism*, *21*(2), pp.96-103.

Revel, A., Koler, M., Simon, A., Lewin, A., Laufer, N. and Safran, A., 2003. Oocyte collection during cryopreservation of the ovarian cortex. *Fertility and Sterility*, *79*(5), pp.1237-1239.

Revel, A., Laufer, N., Ben Meir, A., Lebovich, M. and Mitrani, E. 2011. Micro-organ ovarian transplantation enables pregnancy: a case report. *Human Reproduction*, *26*(5), pp.1097-1103.

Rey, R. 2005. Anti-Müllerian hormone in disorders of sex determination and differentiation. *Arquivos Brasileiros de Endocrinologia and Metabologia, 49*(1), pp.26-36.

Richards, J.S. and Pangas, S.A. 2010. The ovary: basic biology and clinical implications. *The Journal of Clinical Investigation*, *120*(4), pp.963-972.

Richardson, M.C., Guo, M., Fauser, B.C.J.M. and Macklon, N.S. 2013. Environmental and developmental origins of ovarian reserve. *Human Reproduction Update*, *20*(3), pp.353-369.

Rocha, R.M.P., Lima, L.F., Carvalho, A.A., Chaves, R.N., Bernuci, M.P., Rosa-e-Silva, A.C.J.S., Rodrigues, A.P.R., Campello, C.C. and Figueiredo, J.R. 2016. Immunolocalization of the Anti-Müllerian Hormone (AMH) in Caprine Follicles and the

Effects of AMH on In Vitro Culture of Caprine Pre-antral Follicles Enclosed in Ovarian Tissue. *Reproduction in Domestic Animals*, *51*(2), pp.212-219.

Rodriguez-Wallberg, K.A. and Oktay, K. 2012. Recent advances in oocyte and ovarian tissue cryopreservation and transplantation. *Best Practice and Research Clinical Obstetrics and Gynaecology*, *26*(3), pp.391-405.

Roness, H., Derech-Haim, S., Gavish, Z. and Meirow, D. 2015. Anti-Mullerian c-treatment to prevent chemotherapy-induced activation and loss. ESHRE Annual Meeting, Lisbon, Portugal, June 14-17.

Roness, H., Gavish, Z., Cohen, Y. and Meirow, D. 2013. Ovarian follicle burnout: a universal phenomenon? *Cell Cycle*, *12*(20), pp.3245-3246.

Roness, H., Kalich-Philosoph, L. and Meirow, D. 2014. Prevention of chemotherapy-induced ovarian damage: possible roles for hormonal and non-hormonal attenuating agents. *Human Reproduction Update*, *20*(5), pp.759-774.

Roness, H., Kashi, O. and Meirow, D. 2016. Prevention of chemotherapy-induced ovarian damage. *Fertility and Sterility*, *105*(1), pp.20-29.

Rosendahl, M., Ernst, E., Rasmussen, P.E. and Andersen, C.Y. 2010. True ovarian volume is underestimated by two-dimensional transvaginal ultrasound measurement. *Fertility and Sterility*, *93*(3), pp.995-998.

Rosendahl, M., Greve, T. and Andersen, C.Y. 2013. The safety of transplanting cryopreserved ovarian tissue in cancer patients: a review of the literature. *Journal of Assisted Reproduction and Genetics*, *30*(1), pp.11-24.

Rothschild, M.A., Oratz, M. and Schreiber, S.S. 1988. Serum albumin. *Hepatology*, *8*, pp.385-401.

Roti Roti, E. C., and Salih, S. M. 2012. Dextrazoxane Ameliorates Doxorubicin-Induced Injury in Mouse Ovarian Cells. *Biology of Reproduction*, *86*(3), pp.1-11.

Roti, E.C.R., Leisman, S.K., Abbott, D.H. and Salih, S.M. 2012. Acute doxorubicin insult in the mouse ovary is cell-and follicle-type dependent. *PLOS One*, *7*(8), pp.e42293.

Roti, E.C.R., Ringelstetter, A.K., Kropp, J., Abbott, D.H. and Salih, S.M. 2014. Bortezomib prevents acute doxorubicin ovarian insult and follicle demise, improving the fertility window and pup birth weight in mice. *PLOS One*, *9*(9), pp.e108174.

Rzeczkowska, P.A. 2012. Regulation of the Timing of Puberty: Exploration of the Role of Epigenetics. MSc dissertation. University of Toronto.

Sacchi, S., Marinaro, F., Xella, S., Marsella, T., Tagliasacchi, D. and La Marca, A. 2017. The anti-Müllerian hormone (AMH) induces Forkhead box L2 (Foxl2) expression in primary culture of human granulosa cells *in vitro*. *Journal of Assisted Reproduction and Genetics*, *34*(9), pp.1131-1136.

Salih, S.M. 2011. Retrovirus-mediated multidrug resistance gene (MDR1) overexpression inhibits chemotherapy-induced toxicity of granulosa cells. *Fertility and Sterility*, *95*(4), pp.1390-1396.

Sanchez, A.M., Giorgione, V., Viganò, P., Papaleo, E., Candiani, M., Mangili, G. and Panina-Bordignon, P. 2013. Treatment with anticancer agents induces dysregulation of specific Wnt signalling pathways in human ovarian luteinized granulosa cells *in vitro*. *Toxicological Sciences*, *136*(1), pp.183-192.

Sawyer, H.R., Smith, P., Heath, D.A., Juengel, J.L., Wakefield, S.J. and McNatty, K.P. 2002. Formation of ovarian follicles during fetal development in sheep. *Biology of Reproduction*, *66*(4), pp.1134-1150.

Schmidt, D., Ovitt, C.E., Anlag, K., Fehsenfeld, S., Gredsted, L., Treier, A.C. and Treier, M. 2004. The murine winged-helix transcription factor Foxl2 is required for granulosa cell differentiation and ovary maintenance. *Development*, *131*(4), pp.933-942.

Schmidt, K.L.T., Byskov, A.G., Nyboe Andersen, A., Muller, J. and Yding Andersen, C. 2003. Density and distribution of primordial follicles in single pieces of cortex from 21 patients and in individual pieces of cortex from three entire human ovaries. *Human Reproduction*, *18*(6), pp.1158-1164.

Schmidt, K.L.T., Kryger-Baggesen, N., Byskov, A.G. and Andersen, C.Y. 2005. Anti-Müllerian hormone initiates growth of human primordial follicles *in vitro*. *Molecular and Cellular Endocrinology*, *234*(1-2), pp.87-93.

Schott, B., and Robert, J. 1989. Comparative cytotoxicity, DNA synthesis inhibition and drug incorporation of eight anthracyclines in a model of doxorubicin-sensitive and -resistant rat glioblastoma cells. *Biochemical Pharmacology*, *38*(1), pp.167-172.

Schubert, B., Canis, M., Darcha, C., Artonne, C., Smitz, J. and Grizard, G. 2008. Follicular growth and estradiol follow-up after subcutaneous xenografting of fresh and cryopreserved human ovarian tissue. *Fertility and Sterility*, *89*(6), pp.1787-1794.

Sherwood, L. 1989. Urinary systems. *Human Physiology from Cells to Systems*, 3rd Edition, pp 468-514.

Shimasaki S, Moore RK, Otsuka F, Erickson GF. 2004. The bone morphogenetic protein system in mammalian reproduction. *Endocrine Reviews*, *25*(1), pp.72–101.

Shin, J.W., Seol, I.C. and Son, C.G. 2010. Interpretation of animal dose and human equivalent dose for drug development. *The Journal of Korean Oriental Medicine*, *31*(3), pp.1-7.

Siegel, R.L., Miller, K.D. and Jemal, A. 2015. Cancer statistics, 2015. *CA: a Cancer Journal for Clinicians*, *65*(1), pp.5-29.

Silber, S. 2016. Ovarian tissue cryopreservation and transplantation: scientific implications. *Journal of Assisted Reproduction and Genetics*, *33*(12), pp.1595-1603.

Sirotkin, A.V., Florkovičová, I., Schaeffer, H.J., Laurincik, J. and Harrath, A.H. 2017. Interrelationships between ovarian follicles grown in culture and possible mediators. *Reproductive Biology*, *17*(1), pp.97-104.

Sklar, C. A., Mertens, A. C., Mitby, P., Whitton, J., Stovall, M., Kasper, C., Mulder, J., Green, D., Nicholson, H.S., Yasui, Y. and Robison, L. L. 2006. Premature menopause in survivors of childhood cancer: a report from the childhood cancer survivor study. *Journal of the National Cancer Institute*, 98(13), pp.890-896.

Smith, M. A., Seibel, N. L., Altekruse, S. F., Ries, L. A., Melbert, D. L., O'Leary, M., Smith, F.O. and Reaman, G. H. 2010. Outcomes for children and adolescents with cancer: challenges for the twenty-first century. *Journal of Clinical Oncology*, 28(15), pp.2625-2634.

Soleimani, R., Heytens, E., Darzynkiewicz, Z. and Oktay, K. 2011. Mechanisms of chemotherapy-induced human ovarian aging: double strand DNA breaks and microvascular compromise. *Aging*, *3*(8), pp.782-793.

Soleimani, R., Heytens, E., Van den Broecke, R., Rottiers, I. S. A. B. E. L. L. E., Dhont, M. A. R. C., Cuvelier, C. A. and De Sutter, P. 2010. Xenotransplantation of cryopreserved human ovarian tissue into murine back muscle. *Human Reproduction*, *25*(6), pp.1458-1470.

Soleimani, R., Van der Elst, J., Heytens, E., Van den Broecke, R., Gerris, J., Dhont, M., Cuvelier, C. and De Sutter, P. 2008. Back muscle as a promising site for ovarian tissue transplantation, an animal model. *Human Reproduction*, *23*(3), pp.619-626.

Sonigo, C., Beau, I., Grynberg, M. and Binart, N. 2019. AMH prevents primordial ovarian follicle loss and fertility alteration in cyclophosphamide-treated mice. *The FASEB Journal*, *33*(1), pp.1278-1287.

Sonmezer, M. and Oktay, K. 2010. Orthotopic and heterotopic ovarian tissue transplantation. *Best Practice and Research Clinical Obstetrics and Gynaecology*, *24*(1), pp.113-126.

Sonmezer, M., Shamonki, M.I. and Oktay, K. 2005. Ovarian tissue cryopreservation: benefits and risks. *Cell and Tissue Research*, *322*(1), pp.125-132.

Sonowal, H., Pal, P.B., Wen, J.J., Awasthi, S., Ramana, K.V. and Srivastava, S.K. 2017. Aldose reductase inhibitor increases doxorubicin-sensitivity of colon cancer cells and decreases cardiotoxicity. *Scientific Reports*, *7*(1), pp.(3182)1-(3182)14.

Stubbs, S. A., Hardy, K., Da Silva-Buttkus, P., Stark, J., Webber, L. J., Flanagan, A. M., Themmen, A.P., Visser, J.A., Groome, N.P. and Franks, S. 2005. Anti-mullerian hormone protein expression is reduced during the initial stages of follicle development in human polycystic ovaries. *The Journal of Clinical Endocrinology and Metabolism*. *90*(10), pp.5536-5543.

Swain SM, Whaley FS, Gerber MC, Ewer MS, Bianchine JR, Gams RA. 1997. Delayed administration of dexrazoxane provides cardioprotection for patients with advanced breast cancer treated with doxorubicin-containing therapy. *Journal of Clinical Oncology*, *15*(4), pp.1333-1340.

Terada, Y., Terunuma-Sato, Y., Kakoi-Yoshimoto, T., Hasegawa, H., Ugajin, T., Koyanagi, Y., Ito, M., Murakami, T., Sasano, H., Yaegashi, N. and Okamura, K. 2008. Development of Human Graafian Follicles Following Transplantation of Human Ovarian Tissue into NOD/SCID/γcnull Mice. *American Journal of Reproductive Immunology*, *60*(6), pp.534-540.

Tewey, K.M., Rowe, T.C., Yang, L., Halligan, B.D. and Liu, L.F. 1984. Adriamycin-induced DNA damage mediated by mammalian DNA topoisomerase II. *Science*, *226*(4673), pp.466-468.

Tomic, D., Frech, M.S., Babus, J.K., Gupta, R.K., Furth, P.A., Koos, R.D. and Flaws, J.A. 2006. Methoxychlor induces atresia of antral follicles in ERα-overexpressing mice. *Toxicological Sciences*, *93*(1), pp.196-204.

Troussard, A. A., Mawji, N. N., Ong, C., Mui, A., St Arnaud, R. and Dedhar, S. 2003. Conditional knock-out of integrin-linked kinase (ILK) demonstrates an essential role in PKB/Akt activation. *Journal of Biological Chemistry*, *278*(25), 22374-22378.

Tsutsumi, R. and Webster, N.J. 2009. GnRH pulsatility, the pituitary response and reproductive dysfunction. *Endocrine Journal*, *56*(6), pp.729-737.

Uda, M., Ottolenghi, C., Crisponi, L., Garcia, J.E., Deiana, M., Kimber, W., Forabosco, A., Cao, A., Schlessinger, D. and Pilia, G. 2004. Foxl2 disruption causes mouse ovarian failure by pervasive blockage of follicle development. *Human Molecular Genetics*, *13*(11), pp.1171-1181.

Van den Hurk, R., Bevers, M.M. and Beckers, J.F. 1997. In-vivo and in-vitro development of preantral follicles. *Theriogenology*, *47*(1), pp.73-82.

Van Eyck, A.S., Jordan, B.F., Gallez, B., Heilier, J.F., Van Langendonckt, A. and Donnez, J. 2009. Electron paramagnetic resonance as a tool to evaluate human ovarian tissue reoxygenation after xenografting. *Fertility and Sterility*, *92*(1), pp.374-381.

Visser, J.A., Durlinger, A.L., Peters, I.J., van den Heuvel, E.R., Rose, U.M., Kramer, P., de Jong, F.H. and Themmen, A.P. 2007. Increased oocyte degeneration and follicular atresia during the estrous cycle in anti-Mullerian hormone null mice. *Endocrinology*, *148*(5), pp.2301-2308.

Wartenberg H. 1981. Differentiation and development of the testes. *The Testis*, 2nd Edition, pp.67-118.

Weenen, C., Laven, J.S., von Bergh, A.R., Cranfield, M., Groome, N.P., Visser, J.A., Kramer, P., Fauser, B.C. and Themmen, A.P. 2004. Anti-Müllerian hormone expression pattern in the human ovary: potential implications for initial and cyclic follicle recruitment. *MHR: Basic Science of Reproductive Medicine*, *10*(2), pp.77-83.

Weissman, A., Gotlieb, L., Colgan, T., Jurisicova, A., Greenblatt, E.M. and Casper, R.F. 1999. Preliminary experience with subcutaneous human ovarian cortex transplantation in the NOD-SCID mouse. *Biology of Reproduction*, *60*(6), pp.1462-1467.

Wiebold, J.L. and Becker, W.C. 1987. Inequality in function of the right and left ovaries and uterine horns of the mouse. *Journal of Reproduction and Fertility*, *79*(1), pp.125-134.

Wilhelm, D., Palmer, S. and Koopman, P. 2007. Sex determination and gonadal development in mammals. *Physiological Reviews*, *87*(1), pp.1-28.

Williams, C. J. and Erickson, G. F. 2012. Morphology and physiology of the ovary. *Endotext [Internet]*. Available from: http://www.ncbi.nlm.nih.gov/books/NBK278951/

Wilson, C.A., di Clemente, N., Ehrenfels, C., Pepinsky, R.B., Josso, N., Vigier, B. and Cate, R.L. 1993. Mullerian inhibiting substance requires its N-terminal domain for maintenance of biological activity, a novel finding within the transforming growth factor-beta superfamily. *Molecular Endocrinology*, *7*(2), pp.247-257.

Wolterink-Donselaar, I.G., Meerding, J.M. and Fernandes, C. 2009. A method for gender determination in newborn dark pigmented mice. *Lab Animal*, *38*(1), pp.35-38.

Wong, H.L., Bendayan, R., Rauth, A.M., Li, Y. and Wu, X.Y. 2007. Chemotherapy with anticancer drugs encapsulated in solid lipid nanoparticles. *Advanced Drug Delivery Reviews*, *59*(6), pp.491-504.

Xiao, S., Zhang, J., Liu, M., Iwahata, H., Rogers, H.B. and Woodruff, T.K. 2017. Doxorubicin has dose-dependent toxicity on mouse ovarian follicle development, hormone secretion, and oocyte maturation. *Toxicological Sciences*, *157*(2), pp.320-329.

Xu, J., Bishop, C.V., Lawson, M.S., Park, B.S. and Xu, F. 2016. Anti-Müllerian Hormone promotes pre-antral follicle growth, but inhibits antral follicle maturation and dominant follicle selection in primates. *Human Reproduction*, *31*(7), pp.1522-1530.

Yamamoto, A., Omotehara, T., Miura, Y., Takada, T., Yoneda, N., Hirano, T., Mantani, Y., Kitagawa, H., Yokoyama, T. and Hoshi, N. 2018. The mechanisms underlying the effects of AMH on Müllerian duct regression in male mice. *Journal of Veterinary Medical Science*, *80*(4), pp.557-567.

Yang, M.Y., Cushman, R.A. and Fortune, J.E. 2017. Anti-Müllerian hormone inhibits activation and growth of bovine ovarian follicles *in vitro* and is localized to growing follicles. *MHR: Basic Science of Reproductive Medicine*, *23*(5), pp.282-291.

Yuan, J., Zhang, D., Wang, L., Liu, M., Mao, J., Yin, Y., Ye, X., Liu, N., Han, J., Gao, Y. and Cheng, T. 2013. No evidence for neo-oogenesis may link to ovarian senescence in adult monkey. *Stem Cells*, *31*(11), pp.2538-2550.

Zhang, H., Zhang, Y., Zhao, H., Zhang, Y., Chen, Q., Peng, H., Lei, L., Qiao, J., Shi, J., Cao, Z. and Duan, E. 2013. Hormonal regulation of ovarian bursa fluid in mice and involvement of aquaporins. *PLOS one*, *8*(5), pp.e63823.

Zhang, T., He, W.H., Feng, L.L. and Huang, H.G. 2017. Effect of doxorubicin-induced ovarian toxicity on mouse ovarian granulosa cells. *Regulatory Toxicology and Pharmacology*, *86*, pp.1-10.

Zheng, W., Zhang, H., Gorre, N., Risal, S., Shen, Y. and Liu, K. 2013. Two classes of ovarian primordial follicles exhibit distinct developmental dynamics and physiological functions. *Human Molecular Genetics*, *23*(4), pp.920-928.

Zhou, L., Xie, Y., Li, S., Liang, Y., Qiu, Q., Lin, H. and Zhang, Q. 2017. Rapamycin Prevents cyclophosphamide-induced Over-activation of Primordial Follicle pool through PI3K/Akt/mTOR Signalling Pathway *in vivo*. *Journal of Ovarian Research*, *10*(1), pp.(56)1-(56)11.